EXPERIMENTAL STUDIES ON BIOGAS PRODUCTION AND ITS UTILIZATION IN A DIRECT INJECTION DIESEL ENGINE RUN ON DUAL FUEL MODE

A THESIS

Submitted by

DEBABRATA BARIK

(Roll No: 511ME120)

In Partial Fulfilment of the Requirement for the Degree of

DOCTOR OF PHILOSOPHY

DEPARTMENT OF MECHANICAL ENGINEERING

NATIONAL INSTITUTE OF TECHNOLOGY ROURKELA

ROURKELA-769008 (INDIA)

NOVEMBER 2016

EXPERIMENTAL STUDIES ON BIOGAS PRODUCTION AND ITS UTILIZATION IN A DIRECT INJECTION DIESEL ENGINE RUN ON DUAL FUEL MODE

A THESIS

Submitted by

DEBABRATA BARIK

(Roll No: 511ME120)

In Partial Fulfilment of the Requirement for the Degree of

DOCTOR OF PHILOSOPHY

Under the Supervision of

PROF. S. MURUGAN

DEPARTMENT OF MECHANICAL ENGINEERING

NATIONAL INSTITUTE OF TECHNOLOGY ROURKELA

ROURKELA-769008 (INDIA)

NOVEMBER 2016

Department of Mechanical Engineering
National Institute of Technology Rourkela
Rourkela-769008
India

CERTIFICATE

This is to certify that the thesis entitled "**Experimental studies on biogas production and its utilization in a direct injection diesel engine run on dual fuel mode**" being submitted by **Mr. Debabrata Barik** for the award of Ph.D. degree is a record of bonafide research carried out by him in the Department of Mechanical Engineering, National Institute of Technology, Rourkela, under my supervision. It is also certified that to the best of my knowledge the work reported here in, does not form a part of any other thesis or dissertation on the basis of which a degree or award was conferred on an earlier occasion for this or any other candidate.

Place: NIT Rourkela
Date:

Supervisor
(Prof. S. Murugan)
Associate Professor
Department of Mechanical Engineering
National Institute of Technology Rourkela
Rourkela- 769008, India

Dedicated to

My Beloved Parents

And

My Wife Susmita (Gelhi)

ACKNOWLEDGEMENT

Completion of work with a lot of hurdles put off all joys of life, because it brings the real ecstasy in the life. This may not happen without a continuous support of my supervisor. I would like to take the opportunity to express my humble gratitude and deep regards to my supervisor, Prof. S. Murugan, Associate Professor, Department of Mechanical Engineering, for his flawless guidance, monitoring and continuous motivation for the completion of the thesis. The regular counselling, and lessons for life given by him shall help me to proceed properly in a long journey of my life.

I take this opportunity to express my deep sense of gratitude to Prof. Animesh Biswas, Director, NIT Rourkela for providing required infrastructural facilities. I would also like to express my heartfelt thanks to Prof. S.K. Sarangi, Ex-Director, NIT Rourkela for his indirect support by providing a good ambience and necessary facilities for carrying out the research.

I express my sincere thanks to Prof. S.S. Mohapatra, HOD, Department of Mechanical Engineering, NIT Rourkela for providing me the necessary facilities in the department. I take this opportunity to express my deep sense of gratitude to my Doctoral Scrutiny Committee members, Prof. S.S. Mohapatra (Chairman) and Prof. A. Satapathy, Department of Mechanical Engineering, Prof. R.K. Singh and Prof. A. Kumar, Department of Chemical Engineering, for their constant encouragement and valuable suggestions while carrying out my research.

The completion of this research work could not have been accomplished without the support of my research colleagues, Dr. R. Prakash, Dr. Pritinika Behera, Dr. Dulari Hansdah, Dr. Arun Kumar Wamankar, Mr. Abhishek Sharma, Mr. Harishankar Bendu, and Mrs. Kapura Tudu. I express my appreciation for their in debt help and useful ideas related to the improvement and completion of the research work.

I am also thankful to Mr. N.P. Barik, Mr. Ramakrishna Mandal and Mr. N.K. Bisoi for their timely help and cooperation in completing the experimental work.

This work is also the outcome of the blessing guidance and support of my father Mr. Charchil Kumar Barik, mother Mrs. Urmila Barik, my wife Mrs. Susmita Samal, brother Mr. Satyabrata Barik, and sister Mrs. Pradiptyimayi Barik. I would like to thank them for their great support, patience and unconditional love and care during my good and bad times.

Last but not the least, there may be many who remain unacknowledged in this humble note of gratitude and there are none who remain unappreciated. Above all, I owe it all to Almighty God for granting me the wisdom, health and strength to undertake this research work and enabling me to its completion.

(Debabrata Barik)

ABSTRACT

Biodiesel is considered as one of the potential liquid alternative fuels in many countries in the world. It is produced from edible and non-edible oils, animal fat, and algae by the transesterification process. In India, Karanja (Pongamia pinnata) a non-edible oil seed is considered as a potential feedstock for biodiesel production. The de-oiled cakes of Karanja seed obtained from expeller units are of no use, and are disposed in the open. The disposal of such non edible oil cake in the open and land fill generates various anthropogenic gases, and may increase the global warming potential (GWP). The organic matters contained in these de-oiled cakes can be converted to useful energy by adopting a proper waste-to-energy conversion process.

Hence, an attempt was made in this investigation to use the Karanja seed cake (SCK) as a potential feedstock for producing biogas by anaerobic digestion, and the produced biogas was proposed as an alternative fuel for CI engines. Initially, biogas was produced from four different proportions of SCK mixed with cattle dung (CD) in small scale rectors, to study the different parameters effecting the biogas production. The SCK-CD was mixed in the proportion of 75:25, 50:50, 25:75, and 0:100 in percentage on a mass basis, and the mixtures were denoted as S_1, S_2, S_3, and S_4 respectively. Important parameters, such as the pH, temperature, hydraulic retention time (HRT), and carbon/nitrogen ratio (C/N) were evaluated and analyzed. The results indicated that the sample S_3 gave the best result, in comparison with the other samples, and the methane (CH_4) and carbon dioxide (CO_2) contents in the biogas were found to be about 73% and 17% respectively. The sample S_3 was chosen for producing biogas in a large scale floating drum digester. The biogas obtained from the floating drum digester was stored in a gas bag and then characterized for its physiochemical properties, to ensure its application as a gaseous alternative fuel for CI engine.

For ensuring its usage as an alternative fuel in a CI engine, it was tested in a single cylinder, four stroke, air cooled, direct injection (DI) diesel engine developing a power of 4.4 kW at a rated speed of 1500 rpm. The engine was modified to operate on the dual fuel mode. In the first module, the experimental results obtained from the diesel, KME, and dual fuel engine operated with diesel/biodiesel-biogas were validated by a three zone modeling using MATLAB. Combustion parameters, such as peak cylinder pressure, and ignition delay, and emission parameters, such as NO and smoke emission were validated. The validation

indicated that there was a deviation of only about 2-3% between the theoretical and experimental results.

After the modeling work experimental investigation on the engine was performed. Two groups (A and B) of experimental modules were proposed to assess the dual fuel engine's behavior. In group A, two experimental modules were proposed with diesel-biogas dual fuel. In the first module, diesel was used as an injected fuel (pilot) for initiating combustion, and biogas was inducted at four different flow rates in the suction of the engine, varying from 0.3 kg/h to 1.2 kg/h in steps of 0.3 kg/h. The combustion, performance and emission parameters of the engine were evaluated, analyzed and compared with those of diesel operation of the same engine. It was observed that the engine exhibited a drop in brake thermal efficiency and increase in CO and HC emissions throughout the load spectrum. Further, tests were conducted to determine the optimum injection timing of the pilot fuel in the diesel-biogas dual fuel mode, when the engine was operated at the optimum biogas flow rate of 0.9 kg/h. The injection timing of diesel (pilot fuel) was advanced to a maximum of 4.5 ^{o}CA in steps of 1.5 ^{o}CA, from the original injection timing of the engine. The engine behavior in terms of the combustion, performance and emissions was determined, and compared with those of the diesel-biogas dual fuel operation. Based on the experimental results, the advanced injection timing of 26 ^{o}CA was chosen as the optimum injection timing for the pilot injection. The data obtained with the diesel-biogas dual operation with the injection timing of 26 ^{o}CA were considered as reference data for further investigations in this study.

After conducting experiments with the diesel-biogas, a few attempts were made in group B to run the engine only on two different renewable fuels (biodiesel and biogas) that were obtained from a single source of feedstock. In group B, as the first module, biodiesel was used as an injected (pilot) fuel instead of diesel and biogas was used as an inducted fuel. In this operation, biogas was inducted at different flow rates varying from 0.3 kg/h to 1.2 kg/h at regular intervals of 0.3 kg/h in the suction of the engine. From the results, it was observed that the ignition delay was reduced by about 2-4 ^{o}CA for the biodiesel-biogas dual fuel operation from that of the optimized diesel-biogas operation (26 ^{o}CA pilot fuel injection timing with biogas at 0.9 kg/h) at full load. In the second module, the injection timing of the pilot fuel (biodiesel) was advanced to a maximum of 4.5 ^{o}CA at regular intervals of 1.5 ^{o}CA and retarded to 1.5 ^{o}CA, from that of the original injection timing. The results revealed that the injection timing of 24.5 ^{o}CA bTDC gave better performance and lower emissions than those of the original injection timing of the biodiesel-biogas dual fuel operation, as a result of

more oxygen blend in the biodiesel. However, the brake thermal efficiency of the biodiesel-biogas operation was still lower than that of the diesel-biogas dual fuel operation at full load. Therefore, as the third module in group B, diethyl ether (DEE)-an ignition improver was injected along with biodiesel, using an electronic injector in the intake manifold of the engine. Three different quantities of DEE 2%, 4%, and 6% on a mass basis, were injected into the intake manifold along with the air-biogas stream. The results of the biodiesel-biogas-DEE operation were compared with those of the biodiesel-biogas with the injection timing of 24.5 ^{o}CA. The DEE injection of 4% gave an increase in brake thermal efficiency of about 2.3% at the cost of higher NO emission at full load. This is because of the improved combustion as a result of DEE injection. The smoke emission was also reduced by about 5.7% for biodiesel-biogas-DEE injection of 4%, at full load than that of biodiesel-biogas with injection timing of 24.5 ^{o}CA bTDC.

In the fourth module, in order to obtain better performance and lower emissions, the biogas was purified, and the CO_2 and H_2S percentages were reduced by using a vertical packed bed scrubber. The purified biogas was admitted in the suction of the engine at a flow rate of 0.9 kg/h, while the DEE injection was varied from 2% to 6% in steps of 2% in the biodiesel-biogas dual fuel operation. By using the purified biogas, the brake thermal efficiency of the engine was increased by about 4.1%, than that of raw biogas operation with the DEE injection, at an optimum injection timing of the pilot fuel, at full load. The NO emission increased by about 4.9% and smoke was reduced by about 16.7%.

In the fifth module, the effects of the compression ratio on the biodiesel-biogas dual fuel engine were studied, by increasing and decreasing the compression ratio. The results indicated that by increasing the compression ratio, the brake thermal efficiency of the biodiesel-biogas dual fuel mode was found to be close to that of diesel operation and the CO, HC, and smoke emissions were also decreased.

Finally, a short term endurance test was carried out for the biodiesel-biogas dual fuel operation with the optimum injection timing, optimum DEE injection and optimum compression ratio, to study the change in the lubricating oil properties, and the engine wear and tear. Traces of metal and contaminated engine oil were observed after the endurance test, because of the lower lubricity offered by biogas, increased oxidation of biodiesel, and metal corrosion due to moisture in biogas. Overall, it is concluded that, although it was possible to operate the engine only with two renewable fuels on the dual fuel mode, long term durability

is a major concern. Hence, it is suggested that a high grade lubricating oil is essential for improving the lubrication properties of the biodiesel-biogas dual fuel operation.

Keywords: Karanja seed cake, Anaerobic digestion, Biogas, Upgraded biogas, Karanja methyl ester, DEE injection, Dual fuel diesel engine, MATLAB program, Endurance test, Lubricating oil analysis.

CONTENTS

LIST OF FIGURES

LIST OF TABLES

NOMENCLATURE

English symbols

$\frac{dQ_h}{d\theta}$	Rate of heat transfer from gases to walls, kJ/degree crank angle
$\frac{dQ_r}{d\theta}$	Rate of heat release during combustion period, kJ/degree crank angle
$\acute{m}_{finj}$	Fuel injection rate per jet (kg/°CA)
a_s	Speed of sound (m/s)
$\frac{d(mu)}{d\theta}$	Rate of change of internal energy of the system of mass
$\frac{dW}{d\theta}$	Rate of mechanical work done by the system on the boundary
L_p	Connecting pipe length (m)
Δp	Pressure difference (Pa)
AF	Mass ratio of air to liquid and evaporated fuel
C_p	Specific heat capacity under constant pressure (kJ/kg K)
D	Cylinder bore (m)
D_n	Injector nozzle hole (each) diameter (m)
D_{SM}	Sauter mean diameter (m)
h	Convective heat transfer coefficient (W/m^2K)
i	Axial zone number
j	Radial zone number
K_{ac}	Optical absorption co-efficient of the obscuring matter per unit length
K_{bm}	Bulk modulus of elasticity (Pa)
$K_{pr(vap)}$	Preparation (evaporation) constant
m	Mass (kg)
N	Engine rotational speed (rpm)
n	Number of soot particles per unit volume
N_{drop}	Number of fuel droplets in a zone
P	Pressure (Pa)
Qp	Volumetric product productivity
R_{mol}	Universal gas constant, 8.314 kJ/kmol K

S	Spray penetration (m)
T	Absolute temperature (K)
u	Spray velocity (m/s)
x	Space cartesian coordinate (m)
X	Microbial biomass concentration
y	Space cartesian coordinate (m)
z	Number of nozzle holes (jets)

Greek symbols

$\Delta\varphi_{inj}$	Duration of fuel injection (^{o}CA)
$\Delta\varphi$	Computational step (^{o}CA)
a	Connecting rod length
ab	Number of moles of burning zone at the start of times step
afr	Air to fuel ratio
au	Number of moles of air at the start of time step
bb	Number of moles of burning zone at the end of times step
bu	Number of moles of air at the end of time step
c	3.4e-8
ca	Crank angle
D	Cylinder bore diameter
dQ	Heat transfer
dW	Work done
Injmf	Mass fraction of fuel injected
l	Crank radius
lhc	Lower heat of combustion
ma_j	Mass of air
M_f	Molecular Mass of fuel
p	Pressure
q	Heat transfer rate
R	Universal gas constant
T_b	Temperature of burning zone
t_{un}	Temp of unburned zone
M_a	Molecular mass of air

V	Volume
vcl	Clearance volume
Vu	Volume of unburned zone
W	Wiebe function
Watot	Total number of moles of air in the system
Wftot	Total no of moles of fuel in the system
wloss	Number of moles of air lost to combustion
γ	Gamma of the used fuel
θ	Initial spray angle (rad)
λ	Ratio of length of connecting road to stroke length
ρ	Density (kg/m^3)
Φ	Equivalence ratio (fuel to air)
φ	Crank angle (degree)
ψ	Specific absorption per particle

Abbreviations

AAS	Atomic absorption spectroscopy
ADC	Analog to digital converter
Al	Aluminum
ASTM	American society for testing material
aTDC	After top dead center
ATP	Adenosine triphosphate
AW	Agricultural waste
BDC	Bottom dead center
BFG	Blast furnace gas
BSFC	Brake specific fuel consumption
bTDC	Before top dead centre
BTE	Brake thermal efficiency
C	Carbon
C/N	Carbon nitrogen ratio
C_2H_4	Ethylene
CA	Crank angle

CD	Cattle dung
CFC	Chlorofluorocarbon
CH_4	Methane
CI	Compression ignition
Cl	Chlorine
CN	Cetane number
CNG	Compressed natural gas
CO	Carbon monoxide
CO_2	Carbon dioxide
COPD	Chronic obstructive pulmonary disorder
CR	Crop residue
CV	Calorific value
DA	Digital to analog
DAS	Data acquisition system
DEE	Diethyl ether
DI	Direct injection
DNA	Deoxyribonucleic acid
EC	External combustion
EGR	Exhaust gas recirculation
EGT	Exhaust gas temperature
EPA	European Pollution Agency
FFA	Free fatty acid
FID	Flame ionization detector
FT	Fischer-Tropsch
FTIR	Fourier transform infrared spectroscopy
FW	Food waste
GHGs	Greenhouse gases
GWP	Global warming potential
H	Hydrogen
H_2S	Hydrogen sulphide
HC	Hydrocarbon
HCCI	Homogeneous charge compression ignition
HCl	Hydrochloric acid

HRR	Heat release rate
HRT	Hydraulic retention time
HSU	Hatridge smoke units
HW	Hard wood
IC	Internal combustion
ID	Ignition delay
IDI	Indirect injection
IEA	International energy agency
JSC	Jatropha seed cake
KME	Karanja methyl ester
KO	Karanja oil
KOH	Potassium hydroxide
kW	Kilowatts
kWh	Kilowatt hour
LHV	Lower heating value
LNG	Liquefied natural gas
LPG	Liquefied petroleum gas
LTC	Low temperature combustion
MEA	Mono-ethanolamine
MSW	Municipal solid waste
MW	Mega watt
N	Nitrogen
N_2O	Nitrous oxide
NaOH	Sodium hydroxide
NDIR	Non-dispersive infrared
NH_3	Ammonia
NO	Nitric oxide
NO_2	Nitrogen dioxide
NO_x	Oxides of nitrogen
O	Oxygen
O_3	Ozone
OLR	Organic loading rate
PAH	Polycyclic aromatic hydrocarbon

Pb	Lead
PC	Personal computer
PM	Particulate matter
ppm	Parts per million
PPME	Pongamia pinnata methyl ester
PSA	Pressure swing adsorption
PVC	Polyvinyl chloride
PWM	Pulse width modulation
RME	Rapeseed methyl ester
rpm	Revolution per minute
RT	Retention time
S	Sulfur
SCK	Karanja seed cake
SI	Spark ignition
SO_2	Sulfur dioxide
SOC	Start of combustion
SOF	Soluble organic fraction
SOI	Start of injection
SO_x	Oxides of sulfur
STP	Standard temperature and pressure
SW	Soft wood
TBN	Total base number
TDC	Top dead centre
THC	Total hydrocarbon
TS	Total solid
UHC	Unburned hydrocarbon
UO_2	Uranium dioxide
VFA	Volatile fatty acid
VOC	Volatile organic compound
VS	Volatile solid
WR	Wood residue

Unit and description

%	Percentage
°C	Temperature in degree Celsius
°F	Temperature in degree Fahrenheit
bar	Unit of pressure
cc	Cubic centimeter
cm	Centimeter
cSt	Centistoke
eV	Electron volt
g	Gram
hp	Horse power
kg	Kilogram
kHz	Kilo hertz
kPa	Kilo pascal
L	Liter
L/t	Liter/ton
Lha	Liter-hectare
m	Meter
m^3	Cubic meter
mg	Milligram
min	Minute
MJ	Mega joule
ml	Milliliter
mm	Millimeter
mV	Millivolt
Nm	Newton-meter
^oCA	Crank angle in degree
V	Voltage
v/v	Volume/volume
wt %	Percentage by weight

CHAPTER 1

INTRODUCTION

1.1 General

Many developed and developing countries in the world including India, are currently facing three important problems; (i) meeting the energy demand, (ii) environmental degradation and (iii) waste disposal. Due to the increase in population, technology development, industrialization and improvement in the lifestyle, the demand for energy always increases. The supply and use of affordable and clean energies are the major tasks of all countries. As a result, there is a tremendous pressure being mounted on the scientific community to invest more funds in the field of research and development for introducing cleaner and greener fuels, which can either be derived from renewable energy sources or organic waste substances. There has been a significant development in utilizing renewable energy sources such as solar, wind, hydro and biomass for power generation and transportation. However, still there is much scope for harvesting energy from a variety of sources. This chapter discusses the sources of electricity generation, of environmental pollution, and the potentially cleaner and greener fuels that are available currently and the need for the present research work.

1.2 Sources of power generation and pollutants

Currently, electrical power generation in the world is mainly achieved through thermal power plants, followed by hydroelectric, nuclear, and renewable energy sources such as solar, wind, biomass, tidal, and geothermal. In 2012, the world primary energy supply was about 155,505 terawatt-hour (TWh) [1], while the world energy consumption was 104,426 TWh, which was about 32% less than the total supply. Figure 1.1 depicts the world electricity generation by different fossil fuels and renewables.

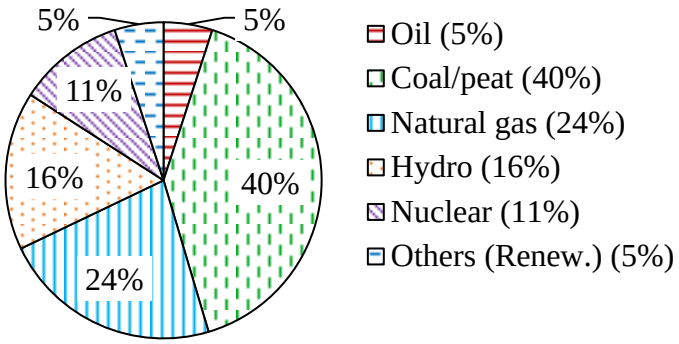

Figure 1.1 World electricity generations by different fossil and renewable fuels [2].

Recently, there has been a large increase in international agreements and national Energy Action Plans, such as the EU 2009 Renewable Energy Directive, to increase the use of renewable energy sources due to the growing concerns about the pollution from the use of fossil fuels [3,4]. One such initiative was the United Nations Development Programme's World Energy Assessment in 2000, which highlighted that many challenges would have to be overcome in order to shift from fossil fuels to renewable energy sources [4]. From 2000 - 2012 renewable energy grew at a rate higher than any other point in history, with a consumption increase of 176.5 million tonnes of oil. During this period of time the oil, coal, and natural gas consumption also grew and had increased much higher than the renewable energies. Figure 1.2 illustrates the growth in consumption of fossil fuels such as oil, coal, and natural gas as well as renewable sources of energy [5]. The world's electrical power generation by means of power plants is shown in Figure 1.3.

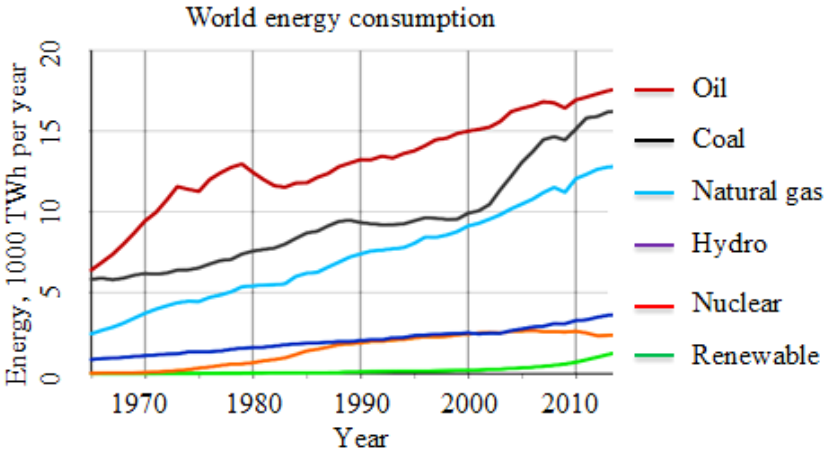

Figure 1.2 Growth in consumption of oil, coal, and natural gas as well as renewable sources [5].

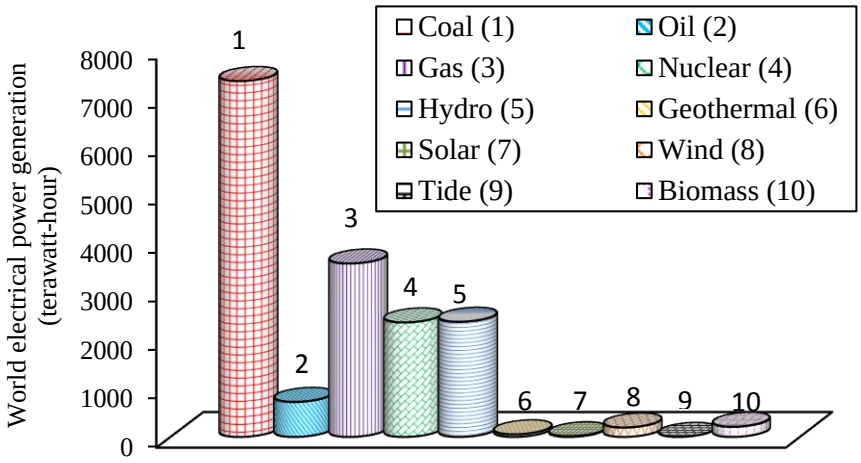

Figure 1.3 World's electrical power generation by means of power plants.

Sustainable energy development strategies typically involve three major technological challenges: (a) energy savings on the demand side, (b) efficiency improvements in energy production, and (c) replacement of fossil fuels by various sources of renewable energy. Table 1.1 gives information on the type of power plants, the fuel used, pollutants, and their causes.

1.3 Anthropogenic gasses

Air pollutants are substances that adversely affect the environment by interfering with the climate, the physiology of plants, animal species, entire ecosystems, as well as human property in the form of crops or man-made structures. The global climate change has been recognized as one of the most important environmental challenges to be faced by humanity in the 21st century.

Air pollutants can originate from natural or anthropogenic (man-made) sources, or both. Examples of natural sources of pollution include volcanic eruptions or wind erosion. Some sources of pollution, such as forest fires, can be related to both natural phenomena and human activities. Emissions from heat engines are an exemplary source of anthropogenic pollution. In this context, the world's most important air pollutants and climate changing agents such as carbon dioxide (CO_2), oxides of nitrogen (NO_x), and oxides of sulfur (SO_x) are considered, and their respective sources, and environmental effects are discussed. Comparisons of anthropogenic CO_2 emissions of different countries are depicted in Figure 1.4. Different pollutants, their sources and environmental effects are given in Table 1.2.

Table 1.1 Information on the type of power plant, fuel used, pollutants and their causes.

Sl. No.	Power plant	Prime mover used	Fuel/energy used	Pollutants formed	Results	Indication/symption	Consequences of pollutant
1	Steam	Steam turbine	Coal, Coke	NO, NO_2, N_2O, CO_2, SO_2, smoke, lead, Hg	Global warming, acid rain	Rise in temperature, rising sea level, change in weather, change in ecosystems	Asthma, Chronic obstructive pulmonary disorder (COPD), lung cancer, pulmonary cancer, mesothelioma, neurobehavioral disorders
2	Diesel	Reciprocating engine	Diesel	NO_x, CO, HC, CO_2, SO_2, soot, PM,	The formation of ozone, aerosols, peroxyacetyl nitrates, and acids	Eye irritation, global temperature rise, difficulty in breathing, acid rain	Nerve damage, headache, cardiovascular illness, irritation of eyes, nose, mouth and throat, Headaches and dizziness, memory loss for kids
3	Gas	Turbine	Natural gas	NO_x, CO, HC, CO_2, SO_2	Global warming, acid rain	Raise in global temperature, acid rain	Lung cancer, pulmonary cancer, mesothelioma, cardiovascular illness
4	Hydro	Turbine	Water current	-	-	-	-

Continued in the next page……

Sl. No	Power plant	Prime mover used	Fuel/energy used	Pollutants formed	Results	Indication/symption	Consequences of pollutant
5	Nuclear	-	Radioactive materials	Radioactive radiation, H_2O_2, UO_2	Unhealthy agriculture, Low fertility in plants	Skin irritation, bone bends	Damage DNA- lead to cancers, birth defects, leukemia, tumors, lung cancer, skin cancer, bone cancer, Ulcer
6	Solar	PV cell	Solar radiation	-	-	-	-
7	Wind	Rotor fan	Wind velocity	-	-	-	-
8	Geothermal	Steam turbine	Geo heat	CO_2, H_2S, CH_4, NH_3,	Global warming, acid rain		-
9	Tidal	Turbine	Wave/ tide current	-	-	-	-
10	Biomass	Turbine/ heat engine	Alcohol, biodiesel, biogas, producer gas, Pyro-gas	NO_x, CO, HC, CO_2, SO_2, soot, PM	Global warming, acid rain	Rise in temperature, rising sea level, change in weather, change in ecosystems	Asthma, Chronic obstructive pulmonary disorder, sleepiness, headache

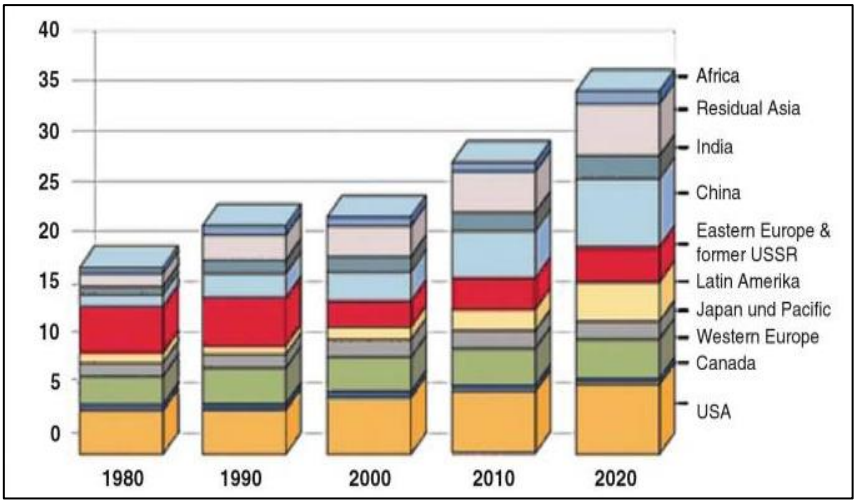

Figure 1.4 Comparisons of anthropogenic CO_2 emissions of different countries.

The emissions from combustion devices and power plants contain numerous compounds that are present in smaller quantities, but may still be posing health hazards to humans. The most important substances in this group include polynuclear aromatic hydrocarbons (PAH), Nitro-PAHs, aldehydes, and other hydrocarbon derivatives. In their pure form, these species have been classified as human carcinogens, e.g., benzo-anthracene, benzo-pyrene, benzo-fluoranthene, benzo-Florentine, dibenzo-anthracene, and indeno-pyrene. Major emission components that have adverse health or environmental effects are listed in Table 1.2.

1.4 Biomass

Biomass contributes about 12% of today's world primary energy supply, while, in many developing countries, its contribution ranges from 40% to 50% [6]. The world's production of biomass is estimated to be 146 billion metric tons in a year, and consists mostly of wild/forest plants. Some farm crops and trees can produce up to 20 metric tons per acre of biomass per year. Different types of algae and grasses produce 50 metric tons of biomass per year [7].

1.5 Types of biomass

Biomass comprises of high contents of cellulose, proteins, hemicellulose, lignin and extractives, thus forming a natural, renewable resource for an eco-friendly, inexpensive and sustainable material. These materials of biomass are readily available in the form of municipal solid waste (MSW), food waste (FW), crop residue (CR), agricultural waste (AW), and wood residues (WR). In biomass, the cellulose $(C_6H_{10}O_5)_x$ fraction is about 40 to 50% of the total biomass by weight, whereas hemicellulose $(C_5H_8O_4)_m$ is usually in the range of 20 to

40% by weight and lignin $(C_9H_{10}O_3(OCH_3)_{0.9\text{-}1.7})_n$ is in the range of 5 to 30% by weight, depending on the nature of the plant, whether it is herbaceous or woody [8]. In general, the majority of bioenergy produced from biomass is from agricultural or plant based waste, having a maximum share of about 64%, followed by MSW 24%, landfill gases 5%, and the remaining are the other biomass wastes [9,10].

1.6 Energy conversion from biomass

A variety of biomass feedstock is available for obtaining energy or fuels in the form of solids, gases, and liquids, which can be used for heat and power generation applications. In view of this, a variety of processes exists for biomass conversions, namely, (i) physical/chemical conversion, (ii) biological/bio-chemical conversion, (iii) thermos chemical conversion and (iv) direct combustion. Figure 1.5 illustrates the pathway of the conversion of biomass into biofuels.

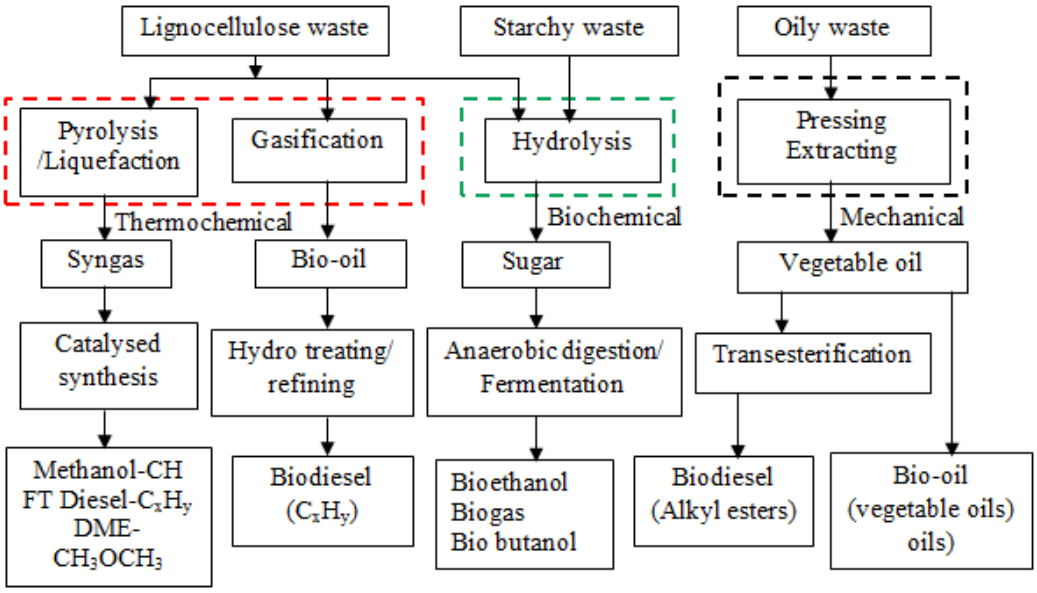

Figure 1.5 Pathways for conversion of biomass to liquid biofuels. (FT = Fischer-Tropsch).

1.6.1 Physical/chemical conversion process

This subsection presents a detailed description of the energy conversion processes for biomass energy (B2E).

Table 1.2 Different pollutants, their sources and environmental effects [11,12].

Pollutant		Natural source	Anthropogenic sources	Environmental Effect
Nitrogen oxides ($NO + NO_2$)	Heat engines	Lightning, soil bacteria	High-temperature fuel combustion, motor vehicles, industrial, and utility	Primary pollutants that produce photochemical smog, acid rain, and nitrate particulates. Destruction of stratospheric ozone. Human health impact
Sulfur dioxide		Volcanic eruptions and decay	Coal combustion, ore smelters, petroleum refineries, diesel engines burning high-sulfur fuels	Acid rain. Human health impact
Particulates		Forest fires, wind erosion, volcanic eruption	Combustion of biofuels such as wood, and fossil fuels such as coal or diesel	Reduced atmospheric visibility. Human health impact. Black carbon particulates contribute to global warming
Ozone		Lightning, photochemical reactions in the troposphere	Secondary pollutant produced in photochemical smog	Damage to plants, crops, and man-made products. Human health impact
Carbon monoxide (CO).		Unnoticeable	Rich & stoichiometric combustion, mainly from motor vehicles	Human health impact
Carbon dioxide (CO_2).		Animal respiration, decay, release from oceans	Fossil fuel and wood combustion	Most common greenhouse gas

Continued in the next page……

Pollutant		Natural source	Anthropogenic sources	Environmental Effect
Non-methane hydrocarbons (VOC)	Others	Biological processes	Incomplete combustion, solvent utilization	Primary pollutants that produce photochemical smog
Methane (CH_4)		Anaerobic decay, cud-chewing animals, oil wells	Natural gas leak and combustion	Greenhouse gas
Chlorofluorocarbons (CFC)		None	Solvents, aerosol propellants, refrigerants	Destruction of stratospheric ozone

1.6.1.1 Transesterification

Biodiesel or methyl ester of vegetable oil is the end product of the transesterification process. Biodiesel is an environmentally friendly fuel and can be used in diesel engines without any modifications. The superior qualities of biodiesel are its lower sulfur content, high flash point, lower aromatic content, dissolved oxygen, origin from biomass, renewable and biodegradable in nature. Due to these benefits, the value of biodiesel in the automotive fuel market is growing fast [13].

1.6.1.2 Mechanism of transesterification

Transesterification is a kind of organic reaction, where the alcohol group in the ester is substituted to give a methyl ester and glycerol. In the transesterification process, a triglyceride reacts with three molecules of alcohol in the presence of a catalyst, producing a mixture of fatty acids, alkyl esters, and glycerol. The overall process is a sequence of three consecutive reactions, in which tri and mono glycerides are formed as intermediates [14]. Transesterification is a reversible reaction thus; excess alcohol is used to increase the yields of the alkyl esters and to allow its phase separation from the glycerol formed. In transesterification, two types of catalysts of acid and base are used.

In the acid catalyst transesterification process, the raw material is catalyzed by Bronsted acids, and/ or H_2SO_4. These catalysts give very high yields of alkyl esters, but the rate of reaction is slow, requiring temperatures above 100 ^oC and a time of more than 3 hours to complete the reaction. Base catalyst esterification of vegetable oil proceeds faster than an acid catalyst, and base catalysts are less corrosive in nature. Industrial esterification processes usually use base catalysts such as alkaline metal alkoxides and hydroxides as well as sodium or potassium carbonates. Alkaline metal alkoxides are the most active catalysts since they give very high yields in short reaction times, even if applied at low molar concentrations. However, they require the absence of water, which is inappropriate for typical industrial processes. Alkaline metal hydroxides (KOH and NaOH) are cheaper than metal alkoxides, but less active [14]. The reaction mechanism for alkali catalyst esterification is a three step process and represented by the following [15,16].

$$\text{Fatty acid } (R_1COOH) + \text{Alcohol } (ROH) \leftrightarrows \text{Ester } (R_1COOR) + \text{Water } (H_2O) \quad (1.1)$$

$$\text{Triglyceride} + ROH \leftrightarrows \text{Diglyceride} + RCOOR_1 \quad (1.2)$$

$$\text{Diglyceride} + ROH \leftrightarrows \text{Monoglyceride} + RCOOR_2 \quad (1.3)$$

$$\text{Monoglyceride} + \text{ROH} \leftrightarrows \text{Glycerol} + \text{RCOOR}_3 \quad (1.4)$$

At the end of the esterification reaction, the products obtained are biodiesel (methyl ester) and glycerin. The glycerin, a by-product, can be further purified for its use in the pharmaceutical and cosmetic industries. The biodiesel obtained from the esterification reaction contains about 10-25% oxygen by weight [17]. Biodiesel gives a lower volumetric heating value of about 12% than diesel, but it gives a high cetane index and flash point. The high flash point contributes to its lower volatility characteristics [18]. The physical and chemical characterization of biodiesel follows the ASTM (American Society for Testing of Materials) standards [19]. The comparison between the different catalytic mechanisms for transesterification is given in Table 1.3.

Table 1.3 Catalytic mechanisms for biodiesel production [16].

Variables	Alkali catalysis	Lipase catalysis	Supercritical alcohol	Acid catalysis
Reaction temperature (^{o}C)	60-70	30-40	239-385	55-80
FFA in raw material	Saponified products	Methyl esters	Esters	Esters
Water in raw material	Interference with reaction	No influence	-	Interference with reaction
Yield of methyl esters	Normal	Higher	Good	Normal
Recovery of glycerol	Difficult	Easy	-	Difficult
Purification	Repeated washing	None	-	Repeated washing
Production cost of catalyst	Cheap	Expensive	Medium	Cheap

1.6.2 Biological/Biochemical conversion process

Biomass can be converted into different types of biofuels such as alcohols, methane, hydrogen, etc., through various biochemical processes. Biomass contains a higher percentage of moisture and ash contents. Hence, it is more suitable for a wet conversion process, such as fermentation, and anaerobic digestion, in which biochemically mediated reaction occurs. Some of the bioenergy conversion processes are found to be very successful and efficient, whereas the other processes are still facing technological challenges such as low energy yield,

water pollution, low conversion efficiency, high capital investment, etc. Anaerobic digestion and fermentation are found to be more advantageous than the other processes.

1.6.2.1 Anaerobic digestion

Anaerobic digestion is a biological degradation process, in which biodegradable organic matters are decomposed in the absence of air, with the help of bacteria, creating biogas as a by-product. The biogas consists of methane (CH_4), carbon dioxide (CO_2), and traces of other gases. Figure 1.6 depicts the pathway for the stages of anaerobic digestion.

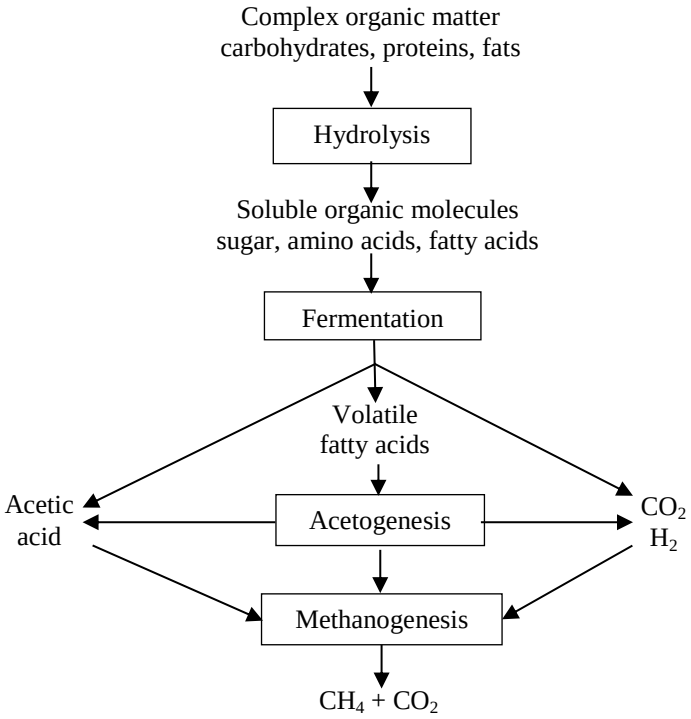

Figure 1.6 Pathway for the stages of anaerobic digestion.

1.6.2.1.1 Mechanism of anaerobic digestion

Anaerobic digestion is a complex process, which can be divided into four stages: (i) hydrolysis, (ii) acidogenesis, (iii) acetogenesis or dehydrogenation, and (iv) methanation. In the first stage, the hydrolyzing microorganisms convert the polymers and monomers into acetate, hydrogen, and some amount of VFA (volatile fatty acids), such as butyrate and propionate. Then, a complex consortium of hydrolytic microorganisms excretes the elements of the organic materials, such as cellulose, cellobiose, xylanase, lipase, protease and amylase into amino acids, and long chain fatty acids [20]. The higher VFA that are formed by the hydrolyzing microorganisms are again converted into acetate and hydrogen, by obligate hydrogen producing acetogenic bacteria. These bacteria, typically characterized as homo

acetogenicare, are named as Acetobacterium woodii and Clostridium asceticism. The metabolism of the acetogenic bacteria is inhibited rapidly by the hydrogen accumulation. Therefore, it is essential to maintain an extremely low partial pressure of hydrogen inside the digester, for the survival of the acetogenic and hydrogen-producing bacteria. The daily biogas production can also be increased by adding hydrogen producing bacteria to the digester feed slurry [20]. At the end of the biochemical degradation process, two groups of bacteria produce CH_4, CO_2 and hydrogen from acetate. Moreover, only a few species, e.g., Methanosarcinabarkeri, Metanonococcusmazei, and Methanotrixsoehngenii can degrade acetate into CH_4 and CO_2, whereas all other bacteria use the hydrogen to form CH_4.

1.6.2.1.2 Parameters and problems associated with anaerobic digestion

Several mechanical, thermal, chemical and biological pretreatment methods have been developed by researchers, to improve the anaerobic digestion performance. However, the stability and performance of the anaerobic digestion process and the rate of gas production are dependent upon the organic feed rates (OFR) [21]. Optimizing the rate of decomposition will optimize the rate of methane production. Temperature, pH, digestion time, and rate of feedstock input to the digester affect the rate of digestion and quality of biogas. For obtaining a higher percentage of methane in biogas, the temperature of the digester should be in the mesophilic range of 36.6 ^{o}C, or in the thermophilic range of 54.4 ^{o}C [13].

1.6.2.2 Fermentation

The process by which complex organic compounds, such as glucose, are broken down by the action of enzymes (usually yeast) into simpler compounds without the use of oxygen is called as fermentation. Fermentation results in the production of fuel in the form of two adenosine triphosphate (ATP) molecules that has a less energy content. In yeast fermentation the end products are basically ethyl alcohol, carbon dioxide and water [22].

1.6.2.2.1 Mechanism of fermentation

Ethanol is derived from the alcoholic fermentation of sucrose or sugar cane and corn (60-70% starch), and other starchy feedstocks [23]. There are two types of processes such as acid hydrolysis and enzymatic hydrolysis to ferment the cellulosic biomass. The chemical reactions involved in fermentation are the enzymatic hydrolysis of sucrose followed by the fermentation of sugar. The invertase enzyme in the yeast catalyzes the hydrolyzed sucrose to convert in to glucose and fructose. The Zymase enzyme present in the yeast converts the glucose and the fructose into ethanol. Finally, distillation and dehydration of the fermented

slurry gives anhydrous ethanol. Figure 1.7 illustrates the path way to ethanol production from biomass. In acid hydrolysis the sugars are converted in to furfural and acetic acid, which is a major disadvantage. Enzyme hydrolysis is usually conducted in mild conditions, i.e. a pH of 4.8 and temperature 318K to 323K, and it does not have the corrosion problem; so, the utility cost of enzyme hydrolysis is low compared to that of acid or alkaline hydrolysis. The chemical reaction involved in fermentation is as follows:

$$C_{12}H_{22}O_{11}(\text{Sucrose}) \rightarrow C_6H_{12}O_6(\text{Glucose}) + C_6H_{12}O_6(\text{Fructose}) \quad (1.5)$$

$$C_6H_{12}O_6\left(\text{Glucose}\right) \rightarrow 2C_2H_5OH(\text{Ethyl alcohol}) + 2CO_2 + \text{energy} \quad (1.6)$$

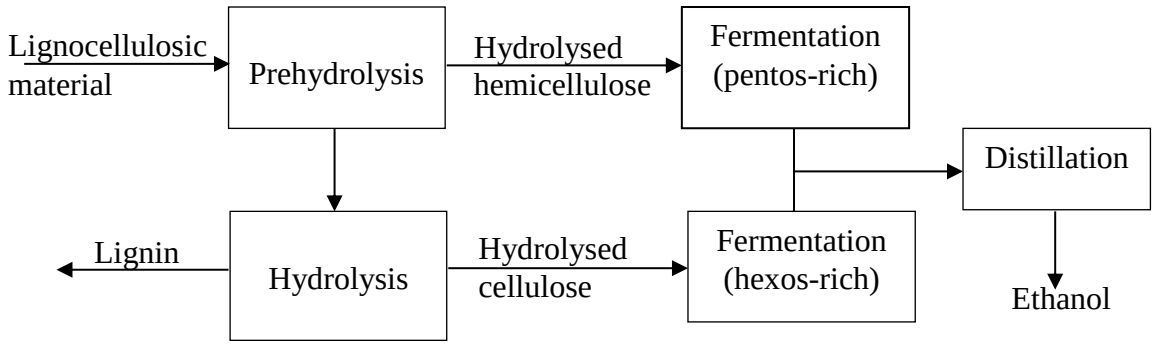

Figure 1.7 Flow chart of ethanol production from biomass.

1.6.3 Thermochemical energy conversion process

Thermal degradation can take place when the biomass burns (i.e. flaming mode) or when it is exposed to elevated temperatures without burning (i.e. non-flaming mode). All combustible materials, whether synthetic or man-made, generally produce toxic products when burned [24]. Thermochemical energy conversion processes include pyrolysis, liquefaction, gasification, and direct combustion. When biomass is heated under oxygen deficient conditions, it generates syngas, which consists primarily of hydrogen (H_2) and carbon monoxide (CO). This syngas can be directly burnt or further processed for gaseous or liquid products, such as producer gas and pyro oil. Low moisture content biomasses are more suitable for conversion processes such as combustion, pyrolysis and gasification.

1.6.3.1 Pyrolysis

Pyrolysis is the thermal degradation of biomass by heat in the absence of oxygen, and results in the production of charcoal (solid), bio-oil (liquid), and fuel gases.

1.6.3.1.1 Pyrolysis mechanism

Depending on the operating conditions, pyrolysis can be divided into three subclasses: conventional pyrolysis (slow), fast pyrolysis and flash pyrolysis.

(i) Conventional pyrolysis

Conventional pyrolysis occurs under a slow heating rate 0.1 K/s to1 K/s and resistance time of 45s to 550s with a massive quantity of biomass as feedstock. In the first stage of pyrolysis, the biomass decomposition starts at 277 ^{o}C to 677 ^{o}C , called as pre-pyrolysis, which involves water elimination, bond breakage, appearance of free radicals, and formation of carbonyl, carboxyl and hydroperoxide groups. In the second stage, the solid biomass decomposition starts at a higher rate and leads to the formation of pyrolytic products. During third stage, char decomposes at a very slow rate and it forms carbon- rich solid residues [25].

(ii) Fast pyrolysis

Fast pyrolysis is a process in which biomass is rapidly heated to high temperatures in the absence of air (specifically oxygen) [26]. It occurs in a high temperature range of 300 ^{o}C to 700 ^{o}C at a faster heating rate of 10 ^{o}C/s to 200 ^{o}C/s, with a short solid resistance time of 0.5s to 10s and with fine particle size (<1 mm) feedstock. In the fast pyrolytic process, biomass decomposes to generate vapours, aerosol, and some charcoal like char. After cooling and condensation of vapours and aerosol, dark brown liquid oil is formed [27]. Fast pyrolysis is recommended when the desired output is mainly liquid and gaseous products. Fast pyrolytic processes produce 60-75 wt.% of liquid bio-oil, 15-25 wt.% of solid char, and 10-20 wt.% of non-condensable gases, depending on the feedstock used [28].

(iii) Flash pyrolysis

Flash pyrolysis occurs in a very high temperature range of 750 ^{o}C to 1000 ^{o}C at a faster heating rate > 1000 ^{o}C/s with a short resistance time < 0.5 second and with very fine particles < 0.2 mm. Biomass conversion to crude oil can have efficiency up to 70% in the flash pyrolysis process [29]. Pyrolysis oil differs greatly from petroleum base fuels and as a result presents some difficulties, if it is used as a replacement for petroleum fuels. Major issues to be tackled are high water content, high oxygen content and viscosity, and acidic nature [30].

1.6.3.2 Gasification

Biomass gasification is the conversion of an organically derived carbonaceous feedstock by partial oxidation into a gaseous product i.e. syngas, consisting primarily of hydrogen (H_2) and

carbon monoxide (CO), with lesser amounts of carbon dioxide (CO_2), water (H_2O), methane (CH_4), higher hydrocarbons, and nitrogen (N_2). In a gasifier, the reactions are carried out at elevated temperatures, 500-1400^oC, and atmospheric or elevated pressures of up to 33 bar. The oxidant used can be air, pure oxygen, or a mixture of these gases. Air based gasifiers typically produce a gas containing a relatively high concentration of nitrogen with a low heating value between 4 and 6 MJ/m^3. Oxygen and steam based gasifiers produce a product gas containing a relatively high concentration of hydrogen and CO with a heating value between 10 MJ/m^3 and 20 MJ/m^3 [31].

1.7 Present scenario of biofuel production

Biomass has the greatest potential as a renewable energy source, in both developing and developed countries. 35% of primary energy from biomass is consumed in developing countries, raising the world's total primary energy consumption from biomass to 14% [32,33]. As far as the environment is concerned, biofuel provides eco-friendly emissions. Plant based biomass absorbs CO_2 during growth and emits it during combustion, forming an atmospheric recycling of CO_2 that leads to the reduction of the greenhouse effect. Also, biomass is a CO_2-neutral fuel as it reduces the overall CO_2 emission [34].

The fuels derived from biomass sources offer distinct advantages; they are; (i) renewable in nature, (ii) abundantly available, (iii) derivable from natural sources, (iv) eco-friendly, and (v) cheaper in price. Recently, biofuels were categorized into four generation groups; they are; (a) first generation biofuels (FGBFs), (b) second generation biofuels (SGBFs), (c) third generation biofuels (TGBFs) and (d) fourth generation biofuels (FoGBFs) fuels. There are no strict technical definitions for these terms. The main distinction between them is the feedstock used. Table 1.4 Provides details of the different categories of biofuels. The advantages and problems associated with biomass energy conversion are given in Table 1.5.

Table 1.4 Classification of biofuel generation based on the feedstock [34].

Generation	Feedstock	Products
First generation biofuels	Sugar, starch, vegetable oils, or animal fats	Bioalcohol, vegetable oil, syngas, biogas
Second generation biofuels	Non-food crops, wheat straw, corn, wood, solid waste, energy crop	Bioalcohols, bio-oil, biohydrogen, bio-Fischer-Trop such diesel, wood diesel
Third generation biofuels	Algae	Biodiesel, vegetable oil
Fourth generation biofuels	Biodiesel, vegetable oil	Bio-gasoline

Table 1.5 Advantages and problems associated with the biomass energy conversion [21].

Sl. No.	Biomass	Problems	Advantages
1.	Food crop (e.g., corn or sugar cane) to ethanol (C_2H_5OH).	Very low net energy yield, competition with food crops, water pollution, inherently low yield per unit area	Strong political lobbies; can be used for gasoline
2.	Food crop (e.g., corn or sugar cane) to butanol (C_4H_9OH)	Low net energy yield, competition with food crops, water pollution, inherently low yield per unit area	Better net energy yield than ethanol
3.	Cellulosic (e.g., switchgrass or Miscanthus) to ethanol or butanol	Unproven at large scale; low net energy yield	Higher yield per unit area, less severe competition with food crops, and less water pollution than with food crops.
4.	Complex biomass (e.g., animal waste) to methane (CH_4)	Conversion efficiency is not yet high enough; unit cost is higher than from natural gas deposits today	Mature technology; can use residues and wastes, turning a pollution problem into an energy resource; CH_4 infrastructure is in place
5.	Complex biomass (e.g., animal waste) to hydrogen (H_2)	Technology is immature; conversion efficiency today is very low	Can use residues and wastes, turning a pollution problem into an energy resource; H_2 can be used in fuel cells

Continued in the next page……

Sl. No.	Biomass	Problems	Advantages
6.	Complex biomass (e.g., animal waste) to electricity (e^-) via the microbial fuel cell (MFC)	Technology is nascent; conversion efficiency is not established	Electricity infrastructure is in place; an MFC is a combustion less, pollution-free fuel cell technology that uses renewable organic fuel directly
7.	Plants (e.g., Jatropha, Soybeans, or sunflowers) to biodiesel (mainly C-16 and C-18 aliphatic)	Technology is immature; yield per unit area is inherently low; competes with food crops	Biodiesel is a high-density fuel that is an ideal substitute for petroleum
8.	Phototrophic microorganisms (algae or cyanobacteria) to biodiesel	Technology is at an early stage; may require a significant capital investment	Biodiesel is a high-density fuel that substitutes ideally for petroleum; possible to have very high yield per unit area, allowing TW output; does not compete with food crops.

1.8 Power generation through biofuels-At a glance

Agricultural, industrial, and urban wastes are cheap sources of biomass. Energy crops can also be grown and used as a power plant fuel, but this often competes with the land used for food production, and can be controversial. Other methods of using it include co-firing biomass with coal in a coal-fired power station, power generation in IC engines with the help of running the IC engines on biodiesel, alcohol and biogas. Some animal wastes can be turned into a combustible gas using anaerobic digestion. A biomass power plant can provide power when required, unlike intermittent renewable sources such as the wind and the sun.

1.9 Need for the present study

Nowadays, biodiesel production from non-edible seeds such as Jatropha curcas (Jatropha), Pongamia pinnata (Karanja), Scheleichera oleosa (Kusum), Shorea robusta (Sal) and Madhuca indica (Mahua) is receiving more attention worldwide [35]. The oil extracted from these seeds is about 25%, and the remaining 75% is the seed cake, a waste by-product. The de-oiled cakes of non-edible nature are of no use, and disposed in the open , because these can neither be used as cattle feed nor directly in agricultural farming, due to their toxic nature (i.e. presence of crucin, saponins). So, if these cakes are kept in an open environment, they would create environmental problems, by generating various gases, such as CH_4 (methane), N_2O (nitrous oxide), H_2S (hydrogen sulfide), NH_3 (ammonia), CO_2 (carbon dioxide) and VOCs (volatile organic compounds), by the action of various microorganisms. The utilization of such de-oiled cakes is a challenge today. In recent years, anaerobic digestion technology has gained importance, especially for biomass wastes [36]. The production of biogas from de-oiled cakes may be a better solution for its effective utilization. Biogas is a carbon neutral gaseous fuel because it can be derived from nature's photosynthetic products, giving zero addition of greenhouse gases (GHGs) to the environment [37,38].

As the biogas is in a gaseous form and is a low cetane fuel, it can be used in compression-ignition (CI) engines in the dual fuel mode for power, heat and electricity generation [39]. Biogas technology also provides the benefit of bio fertilizer; the social and ecological benefits include sanitation, reduction of deforestation and reduction in the use of fossil fuels. In developing countries with agriculture-based economies, this technology can help to decrease the use of wood-based fuels and can improve the electricity infrastructure via internal combustion (IC) engines.

The present investigation is basically focused on the extraction of energy from solid organic waste (i.e. Karanja de-oiled seed cake) to produce biogas by the anaerobic digestion process. Also an attempt has been made towards the viable application of the end product (i.e. biogas) as a gaseous fuel, in a diesel engine for power generation. A floating dome biogas digester was designed and fabricated to carry out the digestion. The generated biogas was used to run a direct injection (DI) diesel engine in the dual fuel mode, offering a solution of partially substituting diesel fuel.

1.10 Organization of Thesis

Chapter 1 Introduction

This chapter describes the sources of electricity generation, and the emissions from power plants and from internal combustion (IC) engines. This chapter also discusses the energy extraction from biomass, biofuels and their production processes, and their suitable application.

Chapter 2 Literature review

This chapter deals with the literature survey on biogas production from various biomass sources, adopting different anaerobic technologies. Also, literatures that deal with the utilization of gaseous fuels on in diesel engine on dual fuel mode are reviewed. Especially focusing on the biogas utilization in diesel engines with diesel and biodiesel as pilot fuels, are surveyed.

Chapter 3 Fuel production and characterization

This chapter deals with the collection and characterization of Karanja de-oiled seed cake (SCK), the design and fabrication of a floating dome biogas digester, biogas characterization, characterization of Karanja methyl ester (KME) and diethyl ether (DEE), and the fabrication of a vertical two-stage biogas scrubber.

Chapter 4 Experimental setup and methodologies

This chapter describes the details of the experimental engine setup, modification to the engine components for the dual fuel operation, step by step method of experiment, and the data acquisition technique for the combustion, performance and emission analysis. The scrubbing/upgrading mechanism for biogas and a detailed discussion on the instrumentation is given. An uncertainty analysis for the instruments is also presented.

Chapter 5 Results and discussion

In this chapter, the results of the combustion, performance and emission obtained from running a single cylinder, four stroke, air cooled, DI diesel engine on the dual fuel mode, following a few fuel and engine modifications, are discussed in comparison with those of the reference data. The validation of the experimental results along with the theoretical analysis of the engine behavior run in the dual fuel mode, in terms of the combustion, performance and emissions, is also given.

Chapter 6 Conclusions and scope for future research

This chapter presents a module wise conclusion of the findings from the experimental investigation carried out in this study. It also mentions the scope for future work.

CHAPTER 2

LITERATURE REVIEW

2.1 General

Gaseous fuels are superior to solid and liquid fuels as they have better mixing quality, less density, and are easily combustible and transportable. Therefore, shifting from the use of solid and liquid fuels to the gaseous fuels is more attractive nowadays. Although liquefied petroleum gas (LPG), and compressed natural gas (CNG) are used for transportation and power generation in many countries, biogas is also considered to be a potential alternative fuel in many developing and underdeveloped countries, because of the abundantly available feedstock for its production. This chapter presents the compression ignition (CI) engine concepts with respect to engine operation, combustion and emissions. Further, it presents the research works that were carried out related to the production and utilization of biogas obtained from various organic feedstocks, using the anaerobic digestion technique. This chapter also includes the review of the biogas utilization in DI diesel engines operated on the dual fuel mode with biodiesel or diesel as a pilot fuel and biogas as the primary fuel. The challenges associated with the biogas dual fuel operation for the combustion, performance and emission issues are also reviewed and presented in this chapter.

2.2 CI engine concepts

Compression ignition (CI) engines give higher thermal efficiency in comparison with spark ignition (SI) engines. The diesel engine, a popular CI engine which was invented by Dr. Rudolf Diesel [40], can run on a variety of fuels. In the beginning, diesel engines were used in industrial, marine and railway installations in isolated locations across the world. The CI engine usually operates on two and four stroke cycles. As the investigation was carried out in a four stroke diesel engine the basics of the diesel combustion, of a four stroke engine are briefly explained as follows.

2.2.1 Principle of operation

In a CI engine, the air is inducted into the combustion chamber during the suction stroke through the intake manifold, and the exhaust valve remains closed. The inducted air quantity is dependent on the cylinder swept volume and engine speed. During the compression stroke, the piston compresses the air, and both the intake and exhaust valves remain closed. The compressed air in the cylinder becomes hotter due to the inter-molecular collision and friction. At the end of the compression stroke, the fuel is injected with the help of a fuel injector actuated by a high-pressure fuel pump. Though the injector has a very small nozzle hole, the fuel passes with a high velocity and gets atomized. The high pressure and high temperature of the compressed air now mixes with the atomized fuel and makes it vapor. The vaporized fuel mixes with the air and when, the air-fuel mixture temperature is higher than the fuel's self-ignition temperature, a series of spontaneous chemical reactions occur leading to a rapid combustion [41]. Moreover, after combustion the piston reaches the bottom dead center (BDC), and the burnt gases are swept out of the cylinder through the exhaust manifold, by the upward movement of the piston towards the top dead center (TDC).

2.2.2 Combustion process in a CI engine

The overall combustion process in a CI engine includes four phases (i) ignition delay or delay period, (ii) premixed or uncontrolled combustion phase, (iii) controlled or diffusion combustion and, (iv) late combustion. All these combustion phases are depicted in Figure 2.1 in association with the rate of heat release.

Delay period is the time lag between the start of fuel injection (SOI) and the start of ignition [42]. This phase is affected by in-cylinder conditions such as temperature, pressure, concentration of the charge, and oxygen availability. Also, the chemical composition and physical characteristics of the fuel play a dominant role in affecting the ignition delay [42]. The uncontrolled or premixed combustion phase is identified by the rapid increase in the heat release rate in the cylinder, due to the combustion of the premixed air-fuel mixture, within the flammability zone of the fuel [41]. The combustion diffusion phase or the controlled combustion phase proceeds at the rate at which, the fuel-air mixture becomes available for burning in the combustion chamber. The last phase is late combustion, which occurs in the expansion stroke

and is determined by the remaining unburned fuel. The heat released during this phase is lower due to the scarcity of the fuel-air mixture and the in-cylinder temperature drops.

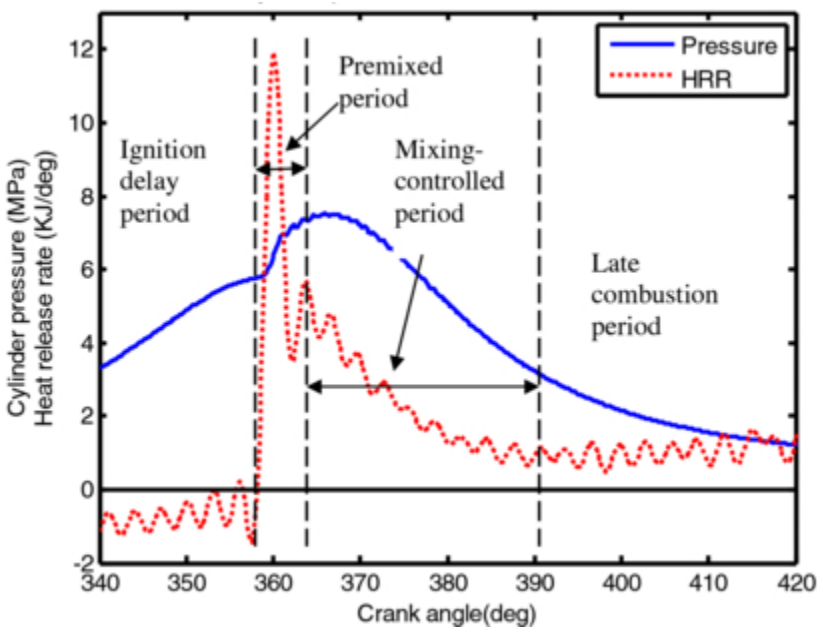

Figure 2.1 Combustion phases in a diesel engine [41].

2.3 Diesel Engine-Exhaust Emissions

One of the major sources of air pollutants is the combustion of fossil fuels in diesel engines. The concentration of the harmful combustion by-products from a diesel engine depends on factors such as engine speed and load, the fuel's physical and chemical properties, the air-fuel ratio, injection timing, and engine design. An understanding of the oxidation mechanism of the CI engine emissions is important, as it can lead towards finding solutions to control them. The emissions from CI engines are categorized into two types; (i) regulated emissions and (ii) unregulated emissions. The formations of the regulated and unregulated emissions are described in the following sub sections.

2.3.1 Regulated emissions

Emissions from CI engines cause adverse health and environmental effects. Most of these pollutants originate from various non-ideal processes during combustion, such as incomplete combustion of fuel, reactions between the mixture components under high temperature and pressure, combustion of the engine lubricating oil and oil additives as well as combustion of non-hydrocarbon components of diesel fuel, such as sulfur compounds and fuel additives [42].

Common pollutants from CI engines include unburned hydrocarbons (HC), carbon monoxide (CO), carbon dioxide (CO_2), nitrogen oxides (NO_x), and particulate matter (PM). These emissions can be controlled or regulated by adopting either engine or fuel modifications. Emission after treatment devices, such as a catalytic converter can be used to decrease the pollution density.

2.3.1.1 Carbon dioxide emission (CO_2)

It is the main product of the carbon combustion contained in the fuel. It is one of the primary elements of greenhouse gases (GHGs) with NO_x, CH_4, perfluorocarbons, sulfur hexafluoride and hydrofluorocarbons. Indeed, CO_2 is already present in the atmosphere, but in a very low concentration. Unfortunately, the amount has increased over the years at an alarming rate. According to the International Energy Agency (IEA) report, in 1870 the total CO_2 concentration from the combustion of fuel was almost zero, but in 2009 it was measured to be around 29 Gt CO_2. Human activities have changed the balance and cannot compensate the natural ability of the forest (plants) to remove CO_2. Globally, the massive utilization of fossil fuels (i.e. natural gas, coal and crude oil), intensified by deforestation and long lifetime of CO_2 in the atmosphere, impacts adversely on the climate and is of serious concern to all nations.

The majority of the CO_2 emission released to the atmosphere is contributed by sectors which heavily use carbon-contained fossil fuels. Those sectors are electricity and heat generation, transportation, and the process industry. All these sectors account for more than three-quarters of the global CO_2 concentration as described in Figure 2.2. The increase in population and economic growth of many nations has led to the increased concentration of CO_2.

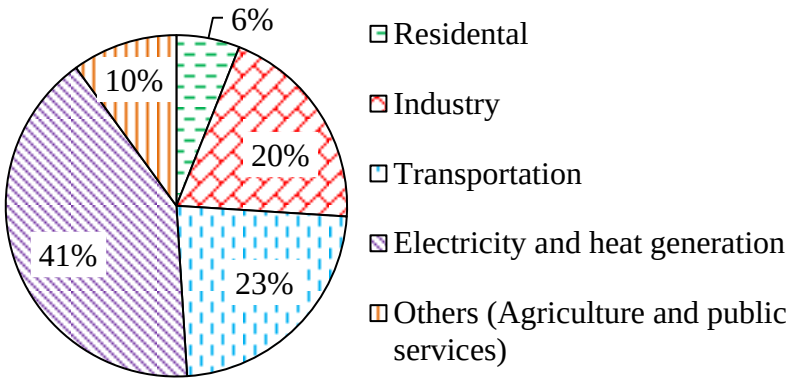

Figure 2.2 Sources of CO_2 emissions [43].

2.3.1.2 Unburned hydrocarbon emission (UHC)

It is produced from the incomplete combustion of the hydrocarbon fuel in the engine. The concentration level is related to misfire and poor charge mixture due to insufficient mixing of fuel and air [42]. The main sources of the formation of HC emissions are oil film layers, wall flame quenching, deposits and crevices in the combustion chamber, liquid fuel, and exhaust-valve leakage. However, the most influential HC sources in fully warmed conditions are the combustion chamber crevices (about 38%) whereas, under cold start or cold conditions the main HC sources are wall flame quenching, lubricating oil films and fuel preparation [44].

2.3.1.3 Carbon monoxide emission (CO)

It is an odorless, tasteless colorless and non-corrosive gas that can be poisonous to humans. It is an intermediate product from the incomplete combustion of carbon contained fuels. The formation process of CO is started by the reaction between oxygen and gaseous or liquid hydrocarbon fuel. The CO produced then can react either with oxygen or hydroxyl (OH) radicals to produce carbon dioxide. However, the oxidation rate of CO is slower than those of the hydrocarbon species, because CO can be produced even if there is not enough oxygen. Therefore, appropriate in-cylinder conditions are required to minimize the CO formation. In diesel engines, there are two main sources of CO formation: over mixing and under mixing of the air and fuel [45].

2.3.1.4 Oxides of nitrogen emission (NO_x)

It is one of the important air pollutants and one of the major diesel emissions, which mainly consist of NO and NO_2. However, NO is the major compound. The propensity of NO_x formation in the combustion chamber can generally be described by three methods. The first method is thermal NO_x, where the formation depends on the molar concentration of nitrogen and oxygen and high temperature in the combustion chamber. The second is NO_x formed from the nitrogen of the fuel, where high nitrogen containing fuels are considered to contribute the NO_x although the current nitrogen levels in diesel are not significant. The third is prompt NO_x formation, where NO_x is produced by the reaction between the radicals of hydrocarbon and nitrogen to form HCN in the combustion chamber. When the equivalence ratio is increased, the amount of HC radicals also increases. In addition, the more HC radicals in the combustion process, the more likely they are to produce NO_x.

2.3.1.5 Particulate matter (PM)

It is a typical emission of diesel engines and is much higher than in SI engines. This is caused by a non-homogeneous combustion process in the cylinder. The PM concentration increases in line as the engine load increases. If the combustion temperature is high then the PM will be smaller. A high fuel concentration in the combustion chamber generates more PM emission. In addition, the scarcity of oxygen also influences the PM formation. Therefore, the air-fuel ratio is considered as an important parameter for PM formation. The aromatic content in the fuel also contributes to the PM. Therefore, a low aromatic content in the fuel potentially reduces the PM concentration [46].

2.3.2 Unregulated emissions

Apart from the major engine pollutants such as HC, CO, $NO_{x,}$ and PM, CI engines also emit various other emissions, which are not yet regulated. Some of the unregulated emissions that come from diesel engines are as follows.

2.3.2.1 Aldehydes emission

Aldehyde, a member of the carbonyl group is a simple compound, which can be identified by a carbon-oxygen double bond with an R-CHO structure. Zhu et al. [47] reported that acetaldehyde and formaldehyde are the two main aldehyde species emitted from motor vehicles. Aldehydes are intermediate compounds which mainly originate from the incomplete combustion of saturated aliphatic hydrocarbons [48,49]. With biodiesel combustion the aldehyde emission increases [50-52].

2.3.2.2 Alkyl compounds emission

They are organic chemical compounds that contain only hydrogen and carbon, either in straight or cyclic chains. Based on the structure, the compounds can be classified into two classes: aliphatic and aromatic. Moreover, aliphatic hydrocarbons are divided into paraffins, cycloparaffins, olefins and acetylenes (Heywood, 1988). Paraffins (C_nH_{2n}+2): saturated hydrocarbon molecules with a single bond open-chain. Examples of the paraffin group are methane (CH_4), ethane (C_2H_6), and 2,2,4-trimethylpentana (C_8H_{18}). Cycloparaffin (C_nH_{2n}): unsaturated hydrocarbon molecules with a single bond ring chain. Examples of the cycloparaffin group are cyclopropane (C_3H_6), cyclobutane (C_4H_8), and cyclopentane (C_5H_{10}). Olefins (C_nH_{2n}):

unsaturated open-chain hydrocarbons containing a double bond. Examples of the group are ethylene (C_2H_4), propylene (C_3H_6), and butylene (C_4H_8). Acetylenes (C_nH_{2n-2}): unsaturated open-chain hydrocarbons containing one C-C triple bond. Examples of the group are acetylene (C_2H_2) and 3,3 dimethyl-1-butyne (C_6H_{10}). Meanwhile, aromatics are hydrocarbons that contain one or more benzene rings.

2.3.2.3 Benzene, toluene, and ethyl benzene emission

These emissions are characterized by a highly flammable range and strong odor. These are volatile organic compounds (VOCs), which are emitted by petrol and diesel engines and potentially contribute to ozone formation. Takada et al. [49], and Nelson et al. [53] reported that the formation of benzene, toluene, and ethylbenzene emissions in a diesel engine is affected by combustion at high temperature and local stoichiometric condition, which improves the fuel evaporation. Moreover, the major source of the production of benzene and toluene is fuel fragments, which are produced by the oxidative pyrolysis of fuel; meanwhile, xylene formation is associated with the aromatic content in the fuel Nelson et al. [53], and Zhu et al. [47].

2.3.2.4 Soluble organic fraction (SOF)

SOF is a part of PM, which is formed by the unburned fuel, which then undergoes the phase change from gas to particulates, and is converted into soot. Stanmore et al. [54] documented that the concentration of SOF is related to various factors such as engine operating conditions, and type of fuel. At a high engine load, the total mass of SOF is lower compared to that of low engine load or even much higher in the idle condition. Moreover, in a HCCI or dual fuel engine operation the SOF would be relatively higher compared to that of conventional CI engines. This is caused by an unburned low volatile component in the fuel, which can be adhered on the cylinder wall Kawano et al. [55]. It is also widely accepted that biodiesel combustion gives a higher SOF. It is mainly due to its lower volatility and higher viscosity, which has a high propensity to be condensed and adsorbed onto the particles surface, which is more obvious in the cold conditions or low engine load Lapuerta et al. [56]. SOF contains polycyclic aromatic hydrocarbons (PAH) which are toxic and harmful to humans and the environment.

2.4 Gaseous fuels

As mentioned in the Introduction, gaseous fuels can easily mix with air and are easily transportable. Therefore, (i) gaseous fuels can be utilized more in internal combustion (IC) engines even though there may be a slight loss in the power output; (ii) gaseous fuels generally have higher octane ratings than gasoline, (iii) the combustion efficiency of an engine fueled with gaseous fuels may be increased by increasing the compression ratio, (iv) the compression ratio of an engine is limited by the type of fuel used. Generally, natural gas, LPG, methane, biogas, and producer gas allow higher compression ratios. The following section gives a brief description of the different gaseous fuels that are commonly available.

2.4.1 Petroleum based fuels

2.4.1.1 LPG

LPG is mainly used in SI engines as it has a high octane number. However, researchers are still trying to use it in CI engines efficiently. LPG refers to a group of hydrocarbon-based gaseous fuel obtained mostly from gas wells and is the by-product of crude oil refining processes. The main constituents of LPG are butane and propane, but the actual composition of commercially available LPG varies widely among countries and depends on the season, properties of the crude oil/gas supply unit, refining process and cost [57]. In cold countries such as the UK, propane is the most abundant component of LPG, in order to provide adequate vapor pressure in winter, whilst in the warmer countries butane has a higher percentage [58].

The emissions from the LPG-driven vehicles are low and LPG is commercially available in most places. It has been proven that, the LPG-operated vehicles have a benefit in reducing emissions compared to those of gasoline. A decrease in the main emissions such as HC, CO, NO_x, PM and CO_2 is obtained mainly due to a high hydrogen-carbon ratio and no aromatic hydrocarbons of LPG. This is supposed to encourage its utilization for transportation. However, its utilization both for domestic cooking and heating applications and in automobiles is still limited.

2.4.1.2 CNG

Compressed natural gas (CNG) consists mostly of methane and is drawn from gas wells or in conjunction with crude oil production. CNG can be stored in cylinders by compressing at a pressure of 200 bar - 250 bar. It also contains hydrocarbons such as ethane and propane, as well

as other gases such as nitrogen, helium, carbon dioxide, sulphur compounds, and water vapor. A sulphur-based odorant is normally added to CNG to facilitate leak detection. Natural gas is lighter than air and thus will normally dissipate in the case of a leak, giving it a significant safety advantage over gasoline and LPG.

2.4.2 Renewable fuels

2.4.2.1 Hydrogen

It is a highly flammable gas and can burn at a concentration of as low as 4% H_2 in air. For automotive applications, hydrogen is generally used in two forms: internal combustion or fuel cell conversion. In the internal combustion process, it burns similar to conventional gaseous fuels, whereas, in the fuel cell technique, hydrogen is used to generate electricity, which in turn is used to power the electric motors of the vehicle. It holds the promise of very low vehicle emissions and has a flexible energy storage. It can be obtained through various thermochemical methods, utilizing methane (natural gas), coal, liquefied petroleum gas, or biomass (biomass gasification), from the electrolysis of water, or by a process called thermolysis. Each of these methods is expensive and poses with its own challenges. However, the technical challenge to the safe application of hydrogen in combustion devices and automobiles has delayed its widespread implementation, for several decades.

2.4.2.2 Biogas

Biogas typically refers to a mixture of different gases produced by the breakdown of organic matter in the absence of oxygen. Biogas can be produced from the feedstocks such as agricultural waste, manure, municipal waste, plant material, sewage, green waste or food waste. The composition of biogas varies depending upon the origin of the anaerobic digestion process and feedstock used.

2.4.3 Other gaseous fuels

2.4.3.1 Producer gas

A gasifier is a chemical reactor in which a solid fuel (biomass/ charcoal) is partially burnt in a controlled oxidation zone. The admission of air is controlled at a certain equivalence ratio. The gasification process in a gasifier, results to a gas called producer gas, which is more suitable for boilers, IC engines, and turbines to generate heat and power. The downdraft gasifier gives

advantages over other type of gasifiers, in terms of tar free gas with a higher hydrogen (H_2) content of about 20% [59]. Air-based gasifiers typically generate a producer gas containing a relatively high concentration of nitrogen with a low heating value between 4 and 6 MJ/m^3. Oxygen and steam based gasifiers produce gas containing a relatively high concentration of hydrogen and CO with a heating value between 10 and 20 MJ/m^3. Therefore, the quality of producer gas can be increased by supplementing the gasification process with steam. The energy required to convert steam into hydrogen is supplied by the exothermic oxidation of carbon to carbon monoxide.

2.4.3.2 Syngas

Syngas (synthesis gas) is a mixture of carbon monoxide and hydrogen, which is the product of high temperature steam or oxygen gasification of organic material such as biomass. After cleaning, the syngas can be used to produce organic molecules, such as synthetic natural gas (SNG) or liquid biofuels such as synthetic diesel (via Fischer-Tropsch synthesis).

2.4.3.3 Blast furnace gas (BFG)

It originates from blast furnaces, and is generated when the iron ore is melted by burning coke. This gas has a very low heating value, about 3465 kJ/kg, because it consists of about 60 percent nitrogen, 18-20% carbon dioxide, 2-4% hydrogen, the remainder being CO. It may be mixed with natural gas or coke oven gas before its use as a fuel, to support and sustain the flame. Blast furnace gas is generated at higher pressure and at about 100-150 °C in a modern blast furnace. This gives it the merit for its application in a top gas pressure recovery turbine (TRT). TRT can generate electrical energy up to 35 kwh/t of pig iron with the help of a high pressure gas flow, without burning any fuel. Dry type TRTs can generate more power than wet type TRTs. The auto ignition point of the blast furnace gas is approximately 630-650 °C, and it has a lower explosive limit of 27% in an air-gas mixture at normal temperature and pressure.

2.4.3.4 Coal gas

Coal gas is a by-product obtained from the destructive distillation of coal. It is also called town gas. The contents of coal gas are hydrogen, carbon monoxide and a few hydrocarbons. Since it is a product from the distillation of coals, the quality of it depends on the coal and the process temperature. The calorific value is an average of about 24000 kJ/m^3.

The chemical compositions of different gaseous fuels are given in Table 2.1. The physical properties of different gaseous fuels are given in Table 2.2.

Table 2.1 Chemical composition of different gaseous fuels.

Gas	CH_4	CO	CO_2	H_2	N_2	C_nH_m
Natural gas	85	0-0.45	0-0.8	0-1.8	0.5-8.4	-
Coal gas	35	8	2	45	6	4
Producer gas	4	23	5	6	62	-
Blast furnace gas	3	30	2	2	52	-

Table 2.2 Physical properties of different gaseous fuels.

Property	CNG	LPG (propane)	Hydrogen	Producer gas	Coal gas	Biogas	BFG
Chemical formula	CH_4	C_3H_8	H_2	$CO+H_2$	CH_4+CO_2	-	-
Molecular weight	16.04	44.1	2.02	-	-	16.56	-
C:H:N, %	75:25:0	82:18:0	0:100:0	15-20:10-15:45-55	32:17:51	20-40:1-3:5-40	42:2:56
Density, kg/m^3	0.72	0.51	-	1.07	0.58	0.65-0.91	1.250
Flash point, ^oC	-184.4	-73.33 to -101.11	-	-	-	>230	-

2.5 Gaseous fuels in CI engines

2.5.1 Dual fuel engine technology

The simultaneous use of two different fuels in an engine is termed as a dual fuel mode. The fuels used may be either two different liquid fuels (it should not be blended or emulsified) or one liquid fuel and one gaseous fuel. The dual fuel technology is an attractive one, because various alternative fuels can be used, which typically have a lower cost than that of conventional fossil fuels, and require no major engine modifications. It can also be operated on various

combinations of gaseous and liquid fuels. Moreover, the engine operation can be switched to a normal operation, when the availability of gaseous fuel runs out. Generally, gaseous fuels have a high octane number, which is appropriate for engines with a higher compression ratio. This is particularly advantageous because it can resist knock.

Saravanan and Nagarajan [60] reported various techniques for the admission of gaseous fuels in a dual fuel diesel engine. The different methods are carburetion, intake manifold injection, intake port injection, and direct in-cylinder injection. The adoption of all these techniques will increase the mixing strength of the air and gaseous fuel. In the dual fuel mode, the air- fuel mixture cannot auto-ignite, because of its low cetane number, and therefore a small amount of liquid fuel (i.e. a high cetane fuel called as pilot fuel) is injected at the end of the compression stroke [61]. The heat released in the combustion chamber during the dual fuel operation can be categorized into three basic phases. Firstly, the premixed combustion of the pilot fuel and some part of the gaseous fuel-air mixture. Secondly, the combustion of the gaseous fuel-air mixture close to the pilot fuel spray zone and diffusive burning of the pilot fuel. Thirdly, the gaseous fuel-air mixture combustion due to the flame propagation from the pilot spray zone [62].

2.5.2 Fuels used in CI engines

2.5.2.1 LPG

LPG is a viable alternative gaseous fuel produced form the petroleum reefing process and primarily consists of propane, propylene, butane and other hydrocarbons [63,64]. It can be liquefied in low pressure range of 0.7-0.8 Mpa at atmospheric temperature. So the storage and transport of LPG is easier than that of other gaseous fuels.

Johnson [65], and Tira et al. [66] reported that the overall emissions from the LPG operated engines and vehicles are lower than that of diesel. The decrease in emissions such as HC, CO, NO_x, PM and CO_2 is mainly due to a high hydrogen-carbon ratio and the absence of aromatic hydrocarbons in LPG.

Boretti [67] investigated the LPG-diesel dual fuel operation in a heavy duty diesel truck engine and concluded that, apart from the emissions benefit, the LPG operated dual fuel engines also have low maintenance, low operational cost, and high thermal efficiency. The higher thermal efficiency observed in a LPG-diesel mode is mainly due to the LPG, which has a high flame

speed and high octane number, and thus enhances the combustion efficiency. The low liquefaction pressure and temperature of LPG allows it for storage stability.

Research works on the utilization of LPG in a diesel engine in the dual fuel mode, with various liquid fuels have been carried out by many researchers. Also, various engine and fuel modifications were employed to increase the thermal efficiency and reduce tail pipe emissions from the engines. The results of some of the proposed techniques for using LPG as an alternative fuel in a diesel engine are summarized briefly in Table 2.3.

Table 2.3 Summary of the research work carried out on LPG application in a diesel engine on dual fuel mode.

Sl. No.	Author Name	Reference	Type of fuel used	Engine type and capacity	Test results and engine behavior compared with diesel
1.	Lata et al.	[68]	Diesel as a primary fuel. Hydrogen, Liquefied petroleum gas (LPG) and mixture of LPG-hydrogen as secondary fuels.	Four stroke, CI, constant speed, vertical, water-cooled, DI, turbo charger, intercooler, Gen-Set with a rated power of 62.5 kW at 1500 rpm	• A maximum enhancement in the brake thermal efficiency of about 6% was obtained with 40% of LPG induction. • Compared to the diesel operation, the HC and CO emissions increased, while the NO_x and smoke emissions reduced. • 40% of the mixture of LPG and hydrogen was used (in the ratio 70:30) as secondary fuel, brake thermal efficiency enhanced by 27% and HC emission reduced by 68%. Further, the shortcoming of low efficiency at a lower load in a dual fuel operation was removed when a mixture of hydrogen and LPG was used as the secondary fuel at a higher than 10% load condition.
2.	Kumaraswamy and Prasad	[69]	Diesel, Diesel-LPG with EGR	Single cylinder, four stroke, DI diesel engine at 1500 rpm	• Reduced NO_x emissions. • High CO, HC and BSFC under low operating loads.

Continued in the next page……

Sl. No.	Author Name	Reference	Type of fuel used	Engine type and capacity	Test results and engine behavior compared with diesel
3.	Renald and Somasundaram	[70]	Diesel, Diesel-LPG	Single cylinder four stroke, DI diesel engine	• The BTE increased by about 5% when 60% of diesel and 40% of LPG used. • The brake specific fuel consumption (BSFC) was reduced by about 33%. • NO_x was reduced by about 35% for 60% LPG and 40% diesel combination. • CO_2 emission reduced by about 67% for 60% LPG and 40% diesel combination.
4.	Selim et al.	[71]	Jojoba methyl ester, LPG, CNG dual fuel	Single cylinder, four stroke, variable compression ratio, IDI diesel engine with a rated power of 9 kW at 3000 rpm.	• Torque increased with the increase in LPG • Knock started at earlier torque. • Increased ignition delay with the increase in LPG percentage. • A higher rate of pressure rise with LPG dual fuel operation.

Continued in the next page……

Sl. No.	Author Name	Reference	Type of fuel used	Engine type and capacity	Test results and engine behavior compared with diesel
5.	Elnajjar et al.	[72]	Different percentages of Propane and Butane. The propane: butane ratios are given below: LPG_1: 100:0 LPG_2: 70:30 LPG_3: 55:45 LPG_4: 25:75 LPG_5: 0:100	Single cylinder, naturally aspirated, four stroke, indirect injection (IDI), water cooled diesel engine.	• For the same fuel mixture, increasing the engine speed reduced the levels of combustion noise. • LPG_1 and LPG_3 gave the highest levels of noise compared to the other fuel blends. • By advancing the pilot fuel injection timing the overall efficiency decreased; at the same time the level of noise increased. • LPG_4 gave the best performance among the other fuel types with the highest level of efficiency. • At 45 BTDC injection timing LPG_3 gave knocking. • Compression ratio of 20 seems to be the best among all those tested.
6.	Qi et al.	[73]	Diesel, LPG-Diesel	Single cylinder, four stroke, DI diesel engine with a rated power of 11.03 kW at 2000 rpm.	• Increase in the LPG mass fraction gave a lower cylinder peak pressure. • The LPG-diesel operation gave a longer ignition delay and extended combustion duration. • Lower NO_x and smoke emissions. • Higher CO and HC emissions at both 1500 and 2000 rpm.

Continued in the next page……

Sl. No.	Author Name	Reference	Type of fuel used	Engine type and capacity	Test results and engine behavior compared with diesel
7.	Jothi et al.	[74]	Diesel, Diesel-LPG, Diesel-LPG-DEE with 5%,10%,15%, and 20% EGR	Stationary four stroke, single cylinder, DI diesel engine with a rated power 3.7 kW at 1500 rpm	• BTE increased by about 2.5% at part loads. • 5% EGR gave improved performance throughout the load spectrum and about 2.2% increase in BTE at full load. • 20% lower NO emission was observed. • Peak pressures were higher at 20% EGR at part loads, whereas for 20% EGR at full load the peak pressure was lower than that of LPG operation without EGR.
8.	Vijayabalan and Nagarajan	[75]	Diesel, Diesel-LPG (glow plug introduced inside the combustion chamber)	Single cylinder, vertical air-cooled diesel engine with a rated power of 3.7 kW at 1500 rpm.	• BTE increased by about 3%. • HC, CO and smoke emissions reduced by about 69%, 50%, and 9% respectively. • Presence of glow plug did not affect the NO emission.

Continued in the next page……

Sl. No.	Author Name	Reference	Type of fuel used	Engine type and capacity	Test results and engine behavior compared with diesel
9.	Lata et al.	[76]	LPG and hydrogen	Four stroke, compression ignition, constant speed, vertical, water-cooled, DI, turbo charger, intercooler, Gen-Set with a rated power of 62.5 kW at 1500 rpm	• Ignition delay with 30% LPG substation raised by about 5 ^{o}CA. • For 30% and 50% LPG substation, the peak cylinder pressure was 10.6 % and 14.4 % lower than that of diesel. • There was an increase in the combustion duration at a lower operating load. • Combustion duration was 12.5% and 8.3% higher for 30% and 50% of LPG substation at 10% of operating load.
10.	Surawski et al.	[77]	Diesel, Diesel-LPG with fumigation	Six cylinder, four stroke, Turbocharged diesel engine with a maximum power of 162 kW at 2500 rpm.	• BTE was lower than that of diesel except at full load operation. • There was an increase in the ignition delay due to the low cetane index of LPG. • Lower PM emissions observed for no load and part load operations, but PM was higher at full load. • The LPG dual fuel operation gave higher HC and CO emissions compared to those of diesel throughout the load spectrum.

2.5.2.2 CNG

The main component of natural gas is methane, which is the simplest hydrocarbon. The combustion of natural gas is clean and emits less CO_2 than almost all other petroleum-derivate fuels. Natural gas has been used to fuel vehicles since the 1930s.

Selim [78] experimentally investigated the effect of a series of parameters on the in-cylinder pressure and rate of pressure rise in a natural gas fueled Ricardo E6 single cylinder, indirect injection (IDI) diesel engine. He observed that, the maximum rate of pressure rise decreased with the increase of engine speed, but increased with the diesel injection timing advanced for both the normal diesel and dual fuel modes. The reductions of the maximum rate of pressure rise for the normal diesel and dual fuel modes were 2.57 bar/°CA and 3.65 bar/°CA respectively, when the engine speed increased by 900 rpm. The peak in-cylinder pressure for the natural gas dual fuel mode was higher than that for the normal diesel mode at all loads. He also observed that as the diesel mass increased; the maximum pressure rise rate of the dual fuel mode first decreased, and then started to increase. In general, the dual fuel mode exhibited a higher pressure rise rate compared to that of the normal diesel engine, and the maximum increase could reach up to about 11.5 bar/°CA.

Abdelaal and Hegab [79] compared the combustion characteristics of the diesel and natural gas-diesel dual fuel modes in a single cylinder diesel engine at 52% and 87% engine loads of 1600 rpm. The diesel injection was kept constant at 20% and the percentage of the natural gas was varied with load. They reported that, the in-cylinder pressure in the natural gas-diesel dual fuel mode was about 6.7 bar and 6.2 bar lower, the ignition delay was 2.8°CA and 5.5°CA longer, and the maximum pressure rise rate was about 0.39 bar/°CA and 1.14 bar/°CA lower for 52% and 87% of the engine loads respectively, in comparison with the conventional diesel mode. In addition, the dual fuel mode exhibited a lower heat release rate. They also reported that applying exhaust gas recirculation (EGR) to the dual-fuel mode additionally decreased the in-cylinder pressure and increased the ignition delay.

Liu et al. [80] also observed that the natural gas induction in diesel engine in the dual fuel mode with diesel as a pilot fuel gave a lower in-cylinder pressure and lower maximum rate of pressure rise. They reported that the in-cylinder pressure and the rate of pressure rise were reduced by about 10 bar and 2.3 bar/°CA.

Papagiannakis and Hountalas [81] experimentally studied the effect of the natural gas mass ratio on the combustion characteristics at three different engine loads and three engine speeds. The natural gas mass ratio in the tests was varied from 0 to 80%. The results showed that, the ignition delay and combustion duration were longer and the cylinder peak pressure was lower in the dual fuel operation compared to that of diesel operation for all test cases. As the natural gas mass ratio increased, the cylinder peak pressure decreased significantly, and the ignition delay and combustion duration increased.

The results of some of the techniques adopted/ proposed for using CNG in a diesel engine are summarized briefly in Table 2.4.

Table 2.4 Summary of the research work carried out on CNG application in a diesel engine on the dual fuel mode.

Sl. No.	Author Name	Reference	Type of fuel used	Engine type and capacity	Test results and engine behavior compared with diesel
1.	Papagiannakis et al.	[82]	Diesel-natural gas	Single cylinder, four-stroke, DI diesel engine with a maximum rated power of 6.7 kW at 3000 rpm.	• BTE decreased in the dual fuel mode than that of diesel. • 45% decrease in NO emission at BMEP of 3.7 bar. • Diesel-natural gas dual fuel operation gave higher CO and HC emissions. • Soot emission decreased in the dual fuel mode.
2.	Carlucci et al.	[83]	Diesel-natural gas	Single cylinder, four valve, four stroke diesel engine with an electronic control common rail injector.	• NO decreased. • CO increased. • Increased pilot injection pressure gave a higher heat release rate. • Lower PM emission.

Continued in the next page……

Sl. No.	Author Name	Reference	Type of fuel used	Engine type and capacity	Test results and engine behavior compared with diesel
3.	Liu et al.	[84]	CNG-diesel	Six cylinder, direct injection, turbocharged, common rail diesel engine with a rated power of 247 kW at 2200 rpm	• The CO and HC emissions were considerably higher, and 90% of the HC emission was the unburned methane. • NO_x emission reduced by about 30%. • PM emission reduced. • At full load, ignition delay decreased with a retarded injection timing.
4.	Paul et al.	[85]	CNG with blends of Diesel-ethanol-biodiesel	Single cylinder, four stroke, water cooled, DI diesel engine with a rated power of 3.6 kW.	• Increasing the percentages of ethanol and biodiesel in the blend increased the BTE. • NO_x emission decreased with an increase in ethanol and biodiesel in the diesel blend. • BSFC was higher than that of diesel. • Increased CNG injection quantity gave higher CO and HC emission.

Continued in the next page……

Sl. No.	Author Name	Reference	Type of fuel used	Engine type and capacity	Test results and engine behavior compared with diesel
5.	Paul et al.	[86]	Diesel, Diesel-ethanol, diesel-CNG, Diesel-Ethanol blends with CNG	Single cylinder, four stroke, water cooled, DI diesel engine with a rated power of 3.6 kW.	• The ethanol addition gave a lower NO_x, BSEC and smoke opacity. • Diesel-CNG gave higher CO and HC emissions than those of diesel-ethanol.
6.	Gharehghani et al.	[87]	Diesel, fish oil biodiesel, diesel-CNG, biodiesel-CNG	Single-cylinder variable compression ratio direct injection diesel engine.	• The CNG-biodiesel dual fuel mode gave about 1.6% increase in BTE than that of CNG-diesel. • The HC reduced by about 32% for CNG-biodiesel dual fuel mode than that of CNG-diesel, but the NO_x emission increased by about 36%. • All the dual fuel operations gave lower NO_x than diesel.

Continued in the next page……

Sl. No.	Author Name	Reference	Type of fuel used	Engine type and capacity	Test results and engine behavior compared with diesel
7.	Paul et al.	[88]	Diesel, Pongamia pinnata methyl ester (PPME), Diesel-CNG PPME-CNG	Single cylinder, four stroke, water cooled DI diesel engine with a rated power of 5.2 kW at 1500 rpm	• PPME-CNG gave a higher energy share than that of diesel-CNG. • PPME-CNG gave a significant reduction in CO, smoke and HC emissions. • NO_x emission increased for the PPME-CNG operation.
8.	Cheenkachorn et al.	[89]	Diesel, diesel-LNG dual fuel	Hyundai D6CA, direct injection diesel engine, with a rated power of 440 kW at rpm1800.	• 3.50% drop in BTE was observed in dual fuel operation. • SFC for the dual fuel operation was slightly lower than that of diesel. • Volumetric efficiency of diesel was higher than that of the dual operations. • The dual fuel operation gave higher HC and CO emissions, but lower NO_x and CO_2 emission.

Continued in the next page……

Sl. No.	Author Name	Reference	Type of fuel used	Engine type and capacity	Test results and engine behavior compared with diesel
9.	Papagiannakis et al.	[90]	Natural gas-diesel dual fuel	Single cylinder, four stroke, DI, diesel engine with a rated power of 6.7 kW at 3000 rpm.	• Increase in the pilot fuel quantity and air inlet temperature gave lower BSFC and higher BTE. • The CO decreased with the preheated air, but this affects adversely the NO emission.
10.	Papagiannakis and Hountalas	[91]	Diesel, Diesel-natural gas	Single cylinder, four stroke, DI diesel engine.	• Lower peak cylinder pressure. • Longer combustion duration. • There was an increase in BSFC and decrease in BTE. • Decrease in NO_x and soot emissions. • Higher CO and HC emissions.

Continued in the next page……

Sl. No.	Author Name	Reference	Type of fuel used	Engine type and capacity	Test results and engine behavior compared with diesel
11.	Ryu	[92]	Diesel, diesel-CNG, biodiesel, biodiesel-CNG. (biodiesel from used vegetable oil)	Single-cylinder, water-cooled, 4-stroke, DI diesel engine with rated power of 9.69 kW at 2400 rpm. (pilot fuel injection timing varied)	• Longer ignition delay of 1.6-4.4 ^{o}CA for the biodiesel-CNG operation. • There was a drop in BTE and increase in BSFC. • BSEC of biodiesel-CNG improved with advanced pilot injection timing at a low load. • Smoke decreased and NO_x was increased with the advanced injection. • The biodiesel-CNG operation resulted in relatively high CO and HC emissions.
12.	Ryu	[93]	Diesel, biodiesel-CNG. (biodiesel from edible frying oil)	Single cylinder, water cooled, four stroke, DI diesel engine with a rated power of 9.69 kW at 2400 rpm. (pilot fuel injection pressure varied)	• The biodiesel-CNG operation gave a longer ignition delay of 1.2-2.6 ^{o}CA. • Ignition delay decreased with the increase in injection pressure. • Smoke and NO_x reduced. • Higher HC and CO emissions for the biodiesel-CNG dual fuel mode. • HC and CO decreased with the increase in the pilot fuel injection pressure.

2.5.2.3 Biogas

Biogas, a combustible gaseous fuel, is produced by the anaerobic digestion of organic matter by a consortium of microorganisms. Biogas can be used for the generation of heat, power and electricity. Lantz et al. [94] documented various influential factors that affect the efficient utilization of biogas in diesel engines such as, drop in efficiency and volumetric efficiency, longer delay period, higher CO and HC emissions, and a poorly developed commercial market for biogas technology, low quality of biogas (i.e. low concentration of methane), limited biogas fueling stations, poor biogas distribution system, and relatively higher cost of dual-fuel vehicles compared to those running on diesel or biodiesel.

Biogas is mainly composed of methane, and its application in dual fuel engines is relatively easy to form a homogeneous air-fuel mixture, and it produces a low CO_2 emission due to its high hydrogen-carbon ratio [95]. It has a good property for preventing engine knock due to methane, which has a high research octane number (about 120-130) [78]. However, the presence of CO_2 potentially reduces the flammability range, resulting in the deterioration of the combustion process by increasing the cyclic combustion variation, lowering the flame temperature, and prolonging the ignition delay. In addition, the presence of CO_2 in biogas leads to a lower volumetric energy density and fuel conversion efficiency, and the combustion enthalpy is reduced.

Roubaud and Favrat [96] observed in their investigation that, the high self-ignition temperature of biogas resisted auto-ignition; however, with the use of improved engine design, such as pre-chamber ignition, optimization of injection timing, injection of high cetane pilot fuel, and adoption of a higher compression ratio, the engine efficiency can be improved with the reduced HC and CO emissions, without sacrificing the rate of fuel consumption. Reducing the content of CO_2 and other inert gases from biogas can improve its combustion quality and calorific value.

Research works on the utilization of biogas in a diesel engine on the dual fuel mode, with diesel-biogas, and biodiesel-biogas have been carried out by many researchers. They also adopted various engine and fuel modifications to improve the thermal efficiency and to reduce the emissions. A review of the research works that have been carried out in the last three decades on biogas utilization of biogas in CI engines are summarized and given in Table 2.5.

Table 2.5 Summary of the research work carried out on biogas application in a diesel engine on the dual fuel mode.

Sl. No.	Author Name	Reference	Type of fuel used	Engine type and capacity	Test results and engine behavior compared with diesel
1.	Bedoya et al.	[97]	Diesel, diesel-biogas, and palm oil biodiesel-biogas. Biogas composition: 60% CH_4, 40% CO_2	Two cylinder, four stroke, naturally aspirated, air cooled diesel engine with a rated power of 20 kW at 3000 rpm.	• Full diesel substitution was possible with palm oil biodiesel as a pilot fuel. • The supercharger and mixer (Kenics type) in the inlet system gave a higher thermal efficiency and reduced HC, and CO emissions than that of natural aspiration. • The part load emission was reduced with the use of a supercharger.
2.	Duc and Wattanavichien	[98]	Diesel-premixed biogas Biogas composition: 73% CH_4, 17% CO_2	Single cylinder, four stroke, naturally aspirated, water cooled, DI diesel engine with a rated power of 7.73 kW at 2400 rpm.	• 3% drop in BTE in the dual fuel mode than that of diesel. • Higher HC, CO and lower soot emissions observed at low/medium loads. • Lower exhaust gas temperature. • Diesel substitution of about 43-49% at full load.

Continued in the next page……

Sl. No.	Author Name	Reference	Type of fuel used	Engine type and capacity	Test results and engine behavior compared with diesel
3.	Makareviciene et al.	[99]	Diesel-biogas. Three grades of biogas used: 1. M95: 95% CH_4, 5% CO_2 2. M85: 85% CH_4, 15% CO_2 3. M65: 65% CH_4, 35% CO_2	Four cylinder, four stroke, turbocharged, DI diesel engine with an electronic injector and distributor type pump, with rated power of 66 kW	• Total fuel consumption increased, BTE dropped, HC, CO increased, but NO decreased. • Advanced injection timing of the pilot fuel gave reduced HC, CO emissions and increased BTE. • 50% reduction in the diesel consumption was observed with a biogas induction, at the advanced injection timing of 22 ^{o}CA bTDC.
4.	Chandra et al.	[100]	Diesel-CNG. Diesel-methane enriched biogas (95% CH_4, 3% CO_2). Diesel-raw biogas (65% CH_4, 32% CO_2)	Single cylinder, four stroke, stationary diesel engine, with a rated power of 5.9 kW converted to operate as a gas engine	• Injection advance of 35 ^{o}CA bTDC gave a maximum BTE of 22.2%, 26.2%, and 23.3% for CNG, methane enriched biogas, and raw biogas respectively. • Raw biogas gave increase in BSFC at full load.

Continued in the next page……

Sl. No.	Author Name	Reference	Type of fuel used	Engine type and capacity	Test results and engine behavior compared with diesel
5.	Cacua et al.	[101]	Diesel-biogas with oxygen enrichment. Biogas composition: 60% CH_4, 40% CO_2	Two cylinder, four stroke, air cooled, naturally aspirated, air cooled DI diesel engine with a rated power of 20 kW at 3000 rpm.	• Efficiency increased to 28% at 40% load condition with 27% oxygen in the inducted air. • Peak cylinder pressure increased by 25%. • Shorter ignition delay and earlier start of premixed combustion were noticed. • CO decreased by 19.5% with 25% O_2 compared to 21% O_2 in air. • Methane emission decreased by about 35%.
6.	Bora et al.	[102]	Diesel, diesel-biogas dual fuel with compression ratio	Single cylinder, four stroke, water cooled, DI diesel engine with a rated power of 3.5 kW at 1500 rpm.	• BTE was lower than that of diesel. • Lower volumetric efficiency. • BSEC decreased by about 19.3% for CR 18. • Longer ignition delay. • CO_2 increased with the increase in CR. • 26.2% reduction in CO for CR 18 than CR 16, but higher than that of diesel. • NO for diesel was high. CR 16 gave the lowest NO, and CR 18 gave 66.6% increase in NO.

Continued in the next page……

Sl. No.	Author Name	Reference	Type of fuel used	Engine type and capacity	Test results and engine behavior compared with diesel
7.	Yoon and Lee	[103]	Diesel-biogas, biodiesel (soybean methyl ester)-biogas	Four cylinders, four stroke, water cooled, turbocharged CI engine with a rated power of 46 kW at 4000 rpm.	• Lower peak pressure at low and intermediate loads. • High HRR and IMEP at 60% load. • Shorter ignition delay. • Lower NO_x emissions. • Lower soot emission. • Higher CO and HC emissions.
8.	Luijten and Kerkhof	[104]	Jatropha oil-biogas	Single cylinder, four stroke, naturally aspirated, DI diesel engine with a rated power of 12 kW	• For low and intermediate loads, biogas addition gave a decrease in BTE up to 10%. • A drop in volumetric efficiency and air-excess ratio was noticed.
9.	Mustafi et al.	[105]	Natural gas (NG)-diesel, biogas-diesel	Single cylinder, four stroke, water cooled, DI diesel engine with a rated torque of 32.6 Nm at 1800 rpm.	• A high peak cylinder pressure was observed for biogas-diesel dual fuel operation. • Longer ignition delay for biogas dual fuel operation • Biogas dual fuel operation gave lower BSFC • NO_x emission reduced by about 9-12%. • Biogas dual fuel operation gave higher CO emission, and the PM emission was lower by about 70%.

Continued in the next page……

Sl. No.	Author Name	Reference	Type of fuel used	Engine type and capacity	Test results and engine behavior compared with diesel
10.	Bari	[106]	Biogas in diesel engine with various CH_4 and CO_2 concentrations	Two cylinder, four stroke, naturally aspirated, water cooled DI diesel engine with swirl combustion chamber, with a rated power of 16.8 kW at 1500 rpm.	• Higher CO_2 percentage in biogas gave a higher BSFC than that of diesel. • Presence of CO_2 deteriorated the BTE and increased the HC emission. • Low burning speed of biogas
11.	Tippayawong et al.	[107]	Diesel-biogas dual fuel	Single cylinder, four stroke, naturally aspirated, water cooled DI diesel engine with a rated power of 5.5 kW at 2400 rpm.	• 90% substitution of diesel was possible with biogas • 7% higher power output than that of diesel • Unusual wear on the critical components was detected • Little carbon deposit inside the combustion chamber.

2.5.3 Other fuels

2.5.3.1 Producer gas for diesel engines

Banapurmath et al. [108] experimentally investigated the use of producer gas in a DI diesel engine, with diesel/vegetable oil/biodiesel as pilot fuels in the dual fuel mode. They reported that, a higher peak pressure, and higher rate of pressure rise were observed for the diesel-producer gas operation than for vegetable oil/biodiesel-producer gas operation.

Roy et al. [109] investigated the effect of the hydrogen content in producer gas on the performance and exhaust emissions of a supercharged dual fuel (producer gas-diesel) engine. They studied the engine performance with a producer gas induction having 20% H_2 and 13.7% hydrogen. From the results, they concluded that based on the cyclic variation; there was 2% less COV in stable combustion. But, a severe problem was observed when the IMEP exceeded 10%. They also observed that, at an equivalence ratio of 0.42 the cylinder pressure and heat release rate increased drastically.

Devakumar and Reddy [110] modified a DI diesel engine to operate on the diesel-producer gas dual fuel mode. They reported that, the use of producer gas in a diesel engine caused 10% reduction in the maximum torque compared to that of diesel operation. It was suggested that, the performance of the engine could be improved, if better engine design and controls are used. However, it was possible to achieve a cost saving of fuel up to 18-25% than in the normal diesel mode.

An experimental investigation was carried out by Parikh et al. [111] to examine the effect of producer gas on the combustion and the pollutant emissions of a DI and IDI engine run on the dual fuel mode. They studied the variation of the CO_2 and oxygen (O_2) contents of the exhaust from the dual fuel operation with both the DI and IDI engines. Increased CO_2 content and decreased O_2 content on the performance and emissions for all the loads have been reported. They indicated that, there was a better air utilization in the dual-fuel mode. However, for the maximum diesel replacement and full load conditions, the air utilization was extremely unstable. A slight increase in the producer gas resulted in instantaneous heavy smoke in the exhaust, with the engine tending to stop.

Sombatwong et al. [112] investigated the effect of the producer gas quantity on the cylinder pressure and the heat release rate in the dual fuel operation, at a constant speed of 1500 rpm and pilot diesel consumption of 0.22 kg/h. They found that combustion started later for a higher producer gas amount compared to that of diesel operation. The slow burning nature of the producer gas during the ignition delay period was the reason for this result. The knocking characteristic of different compositions of producer gas was studied by Arunachalam and Olsen [113]. They reported that the knocking tendency of a fuel is important for an engine manufacturer, as it limits the compression ratio of engine operation.

2.6 Production of biogas from different feedstocks

Since this investigation is related to the use of biogas obtained from an organic agricultural as well as industrial waste in a CI engine, firstly the selection of feedstock was considered. Therefore, the research works related to the production of biogas using different feedstocks were reviewed and they are presented below.

2.6.1 Anaerobic digestion

Anaerobic digestion is a biological process in which biodegradable organic substrates are decomposed by bacteria in the absence of air, forming gaseous byproducts. The gaseous byproducts consist of methane (CH_4), carbon dioxide (CO_2), and traces of other gases [114,115]. Hydrolysis is the first step in anaerobic digestion. In this, the enzyme mediated transformation of insoluble organic materials and higher molecular mass compounds such as lipids, polysaccharides, proteins, fats, nucleic acids into soluble organic materials takes place. These soluble organic materials are the compounds suitable for use as sources of energy. Hydrolysis is carried out by anaerobes such as *Bactericides, and Clostridia* and facultative bacteria such as *Streptococci* [116]. The second step is acidogenesis in which, microorganisms digest the soluble organic materials, and break down the products in to acetic acid, hydrogen, CO_2 and low weight simple volatile organic acids like propionic acid and butyric acid. These acids are again converted to acetic acid by acetogenesis bacteria [117]. Lastly, the acetic acid, hydrogen and carbon dioxide are converted into a mixture of CH_4 and CO_2 by methanogenic bacteria [118,119]. Anaerobic digestion is a slow process; hence it requires a large hydraulic retention time (HRT) of 10-20 days for conventional biogas plants. This leads to a large volume of the digester, and hence the high cost of the system. The decrease in gas production during the winter

season poses a problem in the practical application of the plant. It is reported that biogas production reduced from around 1700 L/day in May-July to around 99 L/day in January-February [120]. Thus, there is a need to improve the overall efficiency of the anaerobic digestion process. Attempts have been made to either reduce the HRT, or enhance the biogas production for the same HRT by incorporating fixed film matrices in the reactors [121].

Several mechanical, thermal, chemical and biological pre-treatment methods have been investigated to improve the performance by easy accessible of intermolecular matters to anaerobic micro bacteria. Farland [122] reported that, the stability of the anaerobic process and the rate of gas production depend upon the organic feed rates. Deublein and Steinhauser [123] documented that, the optimized methane gas production is dependent on the rate of optimized decomposition.

2.6.2 Biogas from biomass a feasibility issue

Weiland [124] documented that biomass is comprised of a high content of cellulose, proteins, hemicellulose, lignin and extractives, thus forming a natural renewable resource for an eco-friendly inexpensive and sustainable material. These materials of biomass are readily available in municipal solid waste (MSW), food waste (FW), crop residue (CR), agricultural waste (AW), and wood residues (WR).

Saxena et al. [125], and Balat and Demirbas [126] reported that, in the biomass, the cellulose fraction is about 40-50% by weight, whereas hemicellulose is usually in the range of 20-40% by weight, and lignin in the range of 5-30% by weight depending on the nature of the plant, whether it is herbaceous or woody. All types of biomass consist of three polymers, which are basically of cellulose $(C_6H_{10}O_5)_x$, hemicellulose such as xylan $(C_5H_8O_4)_m$, and lignin $[C_9H_{10}O_3(OCH_3)_{0.9\text{-}1.7}]_n$. The proportion of these polymers constitutes the difference between species, such as herbaceous wood or soft wood (SW) and hard wood (HW). In general, soft wood contains about 40-44% cellulose, 25-29% hemicellulose, 25-31% lignin and 1-5% extractives, while hard wood contains 43-47% cellulose, 25-35% hemicellulose, 16-24% lignin and 2-8% extractives. The cellulose, hemicellulose and lignin contents in common agricultural residues and wastes are given in Table 2.6.

Saxena et al. [125] reported that the maximum energy produced from biomass waste is mainly from wood waste 64%, followed by municipal solid waste (MSW) 24%, agriculture waste (AW)

5%, and landfill gases 5% [127]. Cellulosic biomass, sometimes referred to as lignocellulosic biomass, is a heterogeneous complex of carbohydrate polymers and lignin (complex polymer of the phenylpropanoid unit) [128]. Lignocellulosic biomass typically contains 55-75% carbohydrates by dry weight. Cellulose, like starch, is a polymer of glucose. However, unlike starch, the specific structure of cellulose favours the ordering of the polymer chains into tightly packed, highly crystalline structures that are water insoluble and resistant to depolymerisation [129]. Crystalline cellulose comprises the major proportion of cellulose, whereas a small percentage of unorganized cellulose chains forms amorphous cellulose. Cellulose is more susceptible to enzymatic degradation in its amorphous form [130].

Table 2.6 Cellulose, hemicellulose and lignin contents in common agricultural residues and wastes [125,130].

Lignocellulosic material	Cellulose (%)	Hemicellulose (%)	Lignin (%)
HW Stems	40-55	24-40	18-25
SW Stems	45-50	25-35	25-35
Nut shells	25-30	25-30	30-40
Corn cobs	45	35	15
Grasses	25-40	35-50	10-30
Paper	85-99	0	0-15
Wheat straw	30	50	15
Sorted refuse	60	20	20
Leaves	15-20	80-85	0
Cotton seed hairs	80-95	5-20	0
Newspaper	40-55	25-40	18-30
Waste paper from chemical pulps	60-70	10-20	5-10
Solid cattle manure	1.6-4.7	1.4-3.3	2.7-5.7
Coastal Bermuda grass	25	35.7	6.4
Switch grass	45	31.4	12
Swine waste	6.0	28	NA

Zheng et al. [131], and Hashem et al. [132] documented their research work on the biogas production from a biomass based feedstock, and the removal of heavy metal from agricultural waste. They have indicated that, hemicelluloses were mainly derived from the chains of pentose sugar, and acted as the cement material holding together the cellulose micells and fibre. The backbone of the chains of hemicelluloses can be a homopolymer (generally consisting of a single sugar repeat unit) or a heteropolymer (mixture of different sugars). Among the most important sugars of the hemicellulose's component is xylose. In hard wood xylan, the backbone chain consists of xylose units which were linked by β-(1→4)-glycosidic bonds and branched by α-(1→2)-glycosidic bonds with 4-O-methylglucuronic acid groups [132]. In addition, O-acetyl groups sometime replaced the OH groups in position C_2 and C_3.

Demirbas [133] have reported that for the soft biomass, the acetyl groups were fewer in the backbone chain. However, soft biomass xylan has additional branches consisting of arabinofuranose units linked by α-(1→3)-glycosidic bonds to the backbone. Hemicelluloses are largely soluble in alkali and, as such, are more easily hydrolysed. Lignin is covalently linked with xylans in the case of hard organic biomass and with galactoglucomannans in soft biomass. The basic chemical phenyl propane units of lignin (primarily syringyl, guaiacyl, and p-hydroxy phenol) are bonded together by a set of linkages to form a very complex matrix. This matrix comprises a variety of functional groups, such as hydroxyl, methoxyl, and carbonyl, which impart a high polarity to the lignin macromolecule [134]. These functional groups and different types of sugars with carbon in the form of cellulose, xylan, and lignin are the main base for quality biogas production and stimulating anaerobic digestion.

2.6.3 Factors that influence biogas production

2.6.3.1 Operating parameters

Factors such as temperature, pH balance, carbon/nitrogen ratio, retention time and feedstock input rate to the digester affect the rate of decomposition and amount of gas production. Bacteria are more effective in a limited range of temperatures. Any change in these properties can adversely affect the biogas production.

2.6.3.1.1 Temperature

The research work reported by Takizawa et al. [135] reveals that there are different temperature ranges at which anaerobic digestion can be carried out, such as psychrophilic (<30 ^{o}C), mesophilic (30-40 ^{o}C) and thermophilic (50-60 ^{o}C). Mesophilic and thermophilic are the two types of anaerobic bacteria most commonly found in the digesters. Mesophilic bacteria have the optimum output at temperatures of 25-40 ^{o}C and thermophilic bacteria survive best at 50-65 ^{o}C [136,137].

Angelidaki and Ahring [138] have mentioned in their research that the length of the digestion period is dependent on temperature. Angelidaki and Ahring [138], and Garba [139] have also reported that, the increase in biogas yield and reduced concentration of slurry was observed at 55 ^{o}C of digester temperature when ammonia (NH_3) was in a high concentration. Methanogens are very sensitive to sudden thermal changes; therefore any drastic change in temperature must be avoided.

2.6.3.1.2 Pre-treatment

Pre-treatment is a process that breaks the complex organic structures of biomass into simpler molecules, which are then more susceptible to microbial degradation. Dar and Tandon [140], Singh et al. [141], and Wang et al. [142] reported several pre-treatment processes of biomass feedstock, such as alkali or acid treatment, pre-digestion of fresh substrate, thermochemical pre-treatment, and ultrasonic pre-treatment.

Dar and Tandon [140] observed an improvement of about 31-42% microbial digestibility and an increase in biogas production, when alkali treated (1% NaOH for 7 days) biomass was added as a supplement to the digestible feedstock.

Singh et al. [141] reported on their investigation that, the pre-digestion of fresh slurry in a batch reactor at temperatures of 30-35 ^{o}C for two days, and using the same slurry as the feedstock for anaerobic digestion, could increase the biogas production by 17-19% having a methane content of 68-86%. Wang et al. [142] reported that, when they adopted an ultrasonic pre-treatment to treat the waste activated sludge for 30 minutes, it increased the methane production up to 64%.

2.6.3.1.3 C/N ratio

It is necessary to maintain a proper composition of the feedstock for an efficient operation of the biogas plant, so that the C/N ratio in the feed remains within the desired range. Klassen et al. [143] reported that microorganisms utilize the carbon present in feedstock, 25-30 times faster than nitrogen. Hence, to meet a favorable requirement for the microbes, the C to N ratio must be in the range of 20-30:1. A higher C/N ratio than that of the acceptable range, gives an indication of the rapid consumption of nitrogen by methanogens and results in a lower gas production. On the other hand, a lower C/N ratio causes ammonia accumulation and the pH value exceeds 8.5, which is toxic to methanogenic bacteria. Optimum C/N ratios of the feed materials can be achieved by mixing materials of high and low C/N ratios. For example, a solid organic waste can be mixed with sewage or animal manure [144]. Table 2.7 gives the carbon nitrogen ratios of some of the common digestible materials used for biogas production.

Table 2.7 Carbon nitrogen ratios of some common digestible materials [144].

Materials	C %	N %	C/N ratio
Dry wheat straw	46	0.53	86:1
Dry rice straw	42	0.53	79:1
Corn stalks	40	0.75	53:1
Fallen leaves	41	1.00	41:1
Soybean stalks	41	1.30	31:1
Wild grass	14	0.54	26:1
Peanut stems and leaves	11	0.59	19:1
Fresh sheep droppings	16	0.55	29:1
Fresh cattle dung	7.3	0.29	25:1
Fresh horse droppings	10	0.42	24:1
Fresh pig manure	7.8	0.60	13:1
Fresh human wastes	2.5	0.85	3:1

2.6.3.1.4 pH

The pH of a digester is one of the most important parameters affecting its performance. The pH of an anaerobic digester initially falls because of the production of volatile acids, but as the

methanogenic bacteria consume the volatile acids and alkalinity is produced, the digester stabilizes itself.

Chandra [145], and Gupta et al. [146] investigated the biogas production from non-edible seed cakes. They reported that, most of the anaerobic bacteria, including methane forming bacteria, perform well within a pH range of 6.8-7.2. A pH range of 6.5-7.5 is generally considered desirable for optimum biogas production. Therefore, it is often necessary to periodically monitor the pH of digester to keep track of the changes in alkalinity throughout the anaerobic digestion process.

Gupta et al. [146] investigated the biogas production in batch reactors, with detoxified Mahua seed cake as feedstock. They observed that the digester containing cattle dung and water in the ratio 1:1 gives a pH range between 6.4 and 7.2. On the other hand, the digesters containing cake mixtures showed an initial decrease in the pH (5.9-6.1) for about 6-9 days, indicating a fast hydrolytic and acetogenic phase, and then moved towards the alkaline range.

Desai and Madamwar [147] reported that, the amount of CO_2 and volatile fatty acids produced during anaerobic digestion affect the pH of the digester slurry. For a smoother anaerobic digestion, the concentration of volatile fatty acids and acetic acid in the feedstock should be below 2000 mg/lit.

2.6.3.1.5 Hydraulic retention time (HRT)

It is the average time consumed by the input feedstock inside the digester before it comes out after digestion. Generally, the HRT depends upon the tropical climate condition. A shorter retention time is likely to face the risk of less active bacterial action, while a longer retention time requires a larger volume of the digester, and hence, a higher capital investment.

Baserja [148] observed a maximum gas production of 2.2 lit/day (CH_4=62%) at an HRT of 10 days having a loading rate of 6 gTS/lit, while treating a mixture of cattle dung, poultry waste, and cheese with ratio of 2:1:3. The retention time ranges between 30-60 days, and only about 1/3 of the tank volume is used for active digestion. If anaerobic digestion is to be completed with other MSW (municipal solid waste) disposal options, then the retention time must be lower than the current standard of 20 days. Garba [139] indicated that for mesophilic digestion the

temperature range varies from 25 ^{o}C to 40 ^{o}C and the HRT may be longer than 20 days. Table 2.8 gives the biogas production rate and the methane yield of some digestible materials.

2.6.3.1.6 Solid concentration

The amount of raw materials fed into the digester depends upon the solid concentration. Desai and Madamwar [147] documented their investigation results related to biogas production from cheese whey, poultry waste and cattle dung. They observed that, the best acceptable solid concentration for a faster anaerobic digestion was in the range of 7-9%. The total solid level below 7% was unstable, and it was overloaded when it was more than 10% [148]. When a proper solid concentration between 7-10% was maintained then, the biogas yield increased to 0.46 m^3/day at 37 ^{o}C and 0.68 m^3/day at 55 ^{o}C respectively [148].

Table 2.8 Rate of biogas production and methane yield for some digestible materials.

Feedstock	Biogas yield (m^3/kg TS)	CH_4 %
Animal barnyard manure	0.260 - 0.280	50 - 60
Pig manure	0.561	45 - 68
Horse droppings	0.200 - 0.300	55 - 65
Green grass	0.630	70
Flax straw	0.359	55
Wheat straw	0.432	59
Leaves	0.210 - 0.294	58
Sludge	0.640	50
Brewery liquid waste	0.300 - 0.600	58
Carbohydrate	0.750	49
Lipid	1.440	72
Protein	0.980	50

2.6.3.1.7 Agitation

Rubia et al. [149] investigated the effect of the particle size of sunflower oil cake and agitation on biogas production in a batch type digester. They have also observed that, for an ultimate improvement in biogas production, stirring of digester slurry was essential. Stirring of the slurry improves the contact between the microorganism and the substrate. Hence, the microorganisms

can yield more quantity and quality biogas. The stirring can be done by installing several mixing devices like stirrer, blower etc. Also, the agitation can be increased by flushing the slurry from the digester by inserting the nozzle again into it.

2.6.3.1.8 Seeding of the biogas plant

It is often necessary to introduce enriched seeding bacteria into the digester for starting up the anaerobic digestion process. Generally, the digested slurry from a running biogas plant or material from well-rotted manure pit, or cattle dung slurry was used as the seed. If the volatile fatty acids were accumulated during the operation due to overloading, then these fatty acids could be used by reseeding or temporarily stopping the feed to the digester or by adding lime in a requisite quantity [129].

2.6.3.1.9 Particle size of feedstock

Although the particle size is not as much an important parameter as the temperature and pH of the digester, it still has some influence on the biogas production. The particle size of the feedstock should not be too large; otherwise, it would result in the clogging of the digester, and also it would be difficult for microbes to carry out its digestion. On the other hand, smaller particles would provide a larger surface area for adsorbing the substrate, that would result in increased microbial activity, and hence, increased gas production.

Gollakota and Meher [150] experimentally investigated the particle size, temperature, loading rate and stirring on the biogas production potential from castor seed cakes. They reported that five particle sizes of 0.088, 0.40, 1.0, 6.0 and 30.0 mm gave the maximum quantity of biogas. They also documented that, a physical treatment of feedstock like grinding, may significantly enhance biogas production.

2.6.3.1.10 Use of additives

Gunaseelan [151], and Vervaeren et al. [152] have made attempts to increase the biogas production from cattle manure and maize by stimulating the microbial activity using various biological and chemical additives under different operating conditions. Gunaseelan [151] have used Parthenium hysterophorus a wild grass weed as an additive in a batch reactor. 10% Parthenium hysterophorus was mixed with cattle manure and allowed for anaerobic digestion at room temperature of 30± 1°C in 3-litre batch digesters. The chemical changes during the course

of digestion and the effect of the digested slurry on biogas production were investigated. He observed that, the methane content in the biogas increased from 60% to 70% with the addition of an additive. Some of the commonly available biological additives are green plants, weeds crop residues, and microbial cultures. According to a study by Vervaeren et al. [152] methane production was increased to almost 11% by adding biological ensilage as additives to maize.

2.6.3.1.11 Microbial strains

Strains of some bacteria and fungi have also been found to enhance gas production by stimulating the activity of particular enzymes. Tirumale and Nand [153] have investigated the addition of cellulolytic strains of bacteria like actinomycetes and mixed consortia for enhanced biogas production in a floating dome digester. They observed that, the biogas production was increased in the range of 8.4-44% from cattle dung. Also they reported that, all the strains exhibited a range of activity of all the enzymes involved in cellulose degradation, viz. C_1 enzyme, exoglycanase, endoglucanase, and β-glucosidase. It seemed that, the endoglucanase activity was of central importance for the hydrolysis of cellulose. The improvement of CH_4 yield from thickened activated sludge ranged from 8.1% to 86.4%, while in the case of a mixture of thickened activated sludge, and primary sludge it was found to vary from 0% to 24% [154].

2.6.3.1.12 Green biomass addition with feedstock

Sichuan and Spobd [155], and Chowdhry et al. [156] investigated the biogas production potential of tree leaves. They observed that the powdered leaves of plants and legumes like *Gulmohar, Leucacena leucocephala, Acacia auriculiformis, Dalbergia sisoo and Eucalyptus tereticonius* have been found to stimulate biogas production ranging from 18% to 40%. The additives were useful to maintain favorable conditions for rapid gas production in the reactor, such as pH, inhibition/promotion of acetogenesis and methanogenesis for the best yield, etc. Alkali treated (1% NaOH for 7 days) plant residues such as lantana, wheat straw, apple leaf litter and peach leaf litter, when used as a supplement to cattle dung resulted in almost twofold increase in biogas quantity and methane production [140]. Kalia et al. [157] experimentally investigated the addition of green biomass for an enhanced biogas production from ageratum. They observed that partially decomposed ageratum produced 43% and *Euphorbia tirucalli L.* produced 14% more gas as compared to pure cattle dung.

2.6.3.1.13 Digested slurry recycling

The recirculation of the digested slurry back into the reactor can improve the gas production marginally, since the microbes that wear washed away are reintroduced into the reactor, thereby providing an additional microbial population. Malik et al. [158], and Kanwar et al. [159] recycled the digested slurry along with the feedstock to conserve water and to increase biogas production. They observed that, about 60-65% more biogas can be obtained by simply recycling the digested slurry in 1 m^3 plug flow type pilot plants. The liquefaction of cellulose and hemicellulose that are present in the feedstocks was low at the start of recirculation (3%-20%) and was not affected by carrying out digestion in a plant of 1 cm^3 capacity.

Santosh et al. [160] investigated water conservation during the anaerobic digestion of a feedstock in a large scale biogas digester. They observed that, the recycling of the digested slurry into the digester saved about 50% of water consumption. They also reported that, recycling of 50% fresh slurry along with 10% digested slurry can give about 50% water conservation, and 10% increase in biogas production.

A review of the different types of feedstock and digester, the catalysts used for biogas production, and the product yield etc., are listed in Table 2.9. A review of the different techniques that can be adopted to enhance biogas production is summarized in Table 2.10.

Table 2.9 Summary of the research work carried out for biogas production from different feedstocks.

Sl. No	Feedstock	HRT (in days)	Temperature	Digester type	Reference
1.	Rice straw, triticale straw, soft wood	42	130 ^{o}C	Batch type, co- anaerobic digestion	[161]
2.	Plant organic waste	36	70, 90, 110 ^{o}C	Full scale vaxt kraft biogas plant	[162]
3.	Saw dust, cattle dung, banana stem, rice bran, paper waste	45	30 ^{o}C	Mini-pilot and co-digester	[163]
5.	Jatropha seed cake	40	29 and15 ^{o}C	Batch type, anaerobic digestion	[37]
6.	Cattle slurry, cheese whey	42	35 ^{o}C	Anaerobic co-digestion	[164]
7.	Municipal biomass waste (food waste, fruit - vegetable waste, dewatered sewage)	20	35±2 ^{o}C	Pilot scale anaerobic co-digestion	[165]
8.	Padauk angsana leaves,	54	-	Laboratory scale, anaerobic digestion	[166]
9.	Cattle manure, crude glycerin		35-55 ^{o}C	Batch type, anaerobic digestion	[167]
10.	Corn straw	15	20 ^{o}C	Laboratory scale, anaerobic digestion	[168]
11.	Grass silage liquor	42	35-55 ^{o}C	Batch and continuous type anaerobic digestion	[169]
12.	Spent wash	60	27-36 ^{o}C	Laboratory scale, anaerobic digestion	[170]

Table 2.10 Summary of the different techniques adopted to enhance the biogas production.

Sl. No.	Raw material	Biogas yield	Methane	Biogas after treatment of feedstock	Pre-treatment method use	Methane in after treated biogas	Reference
1.	Rice straw, triticale straw, soft wood (co-digestion)	-	30 Nml CH_4/g	Increase	N-methylmorpholine- N-Oxide (NMMO)	-	[161]
2.	Plant organic waste	-	82 Nm^3 CH_4/ton	30% more	Mechanical and electroporation pre-treatment of lay crop, membrane filtration of process.	Increase	[162]
3.	Saw dust, cattle dung, banana stem, rice bran, paper waste (co-digestion)	10144 ml	-	Increase	Co-substrates	Increase	[163]
4.	Slaughter house effluent	-	-	Increase	Substrate digestion with bacterial population evolution	Increase	[171]
5.	Jatropha seed cake	0.145m^3/kg of TS	-	-	C:N ratio in between 22:1 to 27:1, JSC slurry with 20% TS at dilution rate (JSC:water-1:34)	Increase	[37]

Continued in the next page……

Sl. No.	Raw material	Biogas yield	Methane	Biogas after treatment of feedstock	Pre-treatment method use	Methane in after treated biogas	Reference
6.	cattle slurry, cheese whey (co-digestion)	-	155.571 CH_4/kg of VS	Increase	CS:W, 50%:50%, with pH chemical correction	343.43l-CH_4/kg of VS	[164]
7.	Municipal biomass waste (food waste, fruit -vegetable waste, dewatered sewage)	4.25 $m^3/(m^3$ d)	-	-	(Co-digestion) (OLR) 6.0 kg VS/m^3d	Increase	[165]
8.	Padauk angsana leave, waste water (co-digestion)	134 m^3/ton	580 m^3 /ton		Add 2% wt. NaOH aqueous solution, cellulose, 10% TS	78.27% CH_4	[166]
9.	Cattle manure, crude glycerin (co-digestion)	400%	-	Increase	Pre-treatment with ultrasound and added 4%, 6% crude glycerine	-	[167]
10.	Corn straw	-	-	Increase 33.07%	Biological pre-treatment with a complex microbial agent	75.57% CH_4	[168]

Continued in the next page……

Sl. No.	Raw material	Biogas yield	Methane	Biogas after treatment of feedstock	Pre-treatment method use	Methane in after treated biogas	Reference
11.	Diff. Biomass (co-digestion)	-	-	Increase	Hydrothermal heating organic dissolving in to a liquid phase	Increase	[172]
12.	Grass silage liquor	-	-	Increase	Add NaOH	70-80% of CH_4	[169]
13.	Spent wash	-	65-75% methane	Increase	Add 1 M NaOH	Increase CH_4 percentage	[170]

2.6.4 Biogas scrubbing

The main drawback in the composition of biogas is the presence of carbon dioxide (CO_2) and hydrogen sulphide (H_2S). The CO_2 and H_2S can be removed from biogas by scrubbing. Selection of the upgrading technology for biogas is site-specific, case-sensitive, and dependent on the biogas utilization and local circumstances. Therefore, matching the technology selected for use to the specific requirements is significantly important. The detailed reviews on the state-of-the-art of biogas cleaning and upgrading technology are presented in the following subsections.

2.6.4.1 Scrubbing of CO_2 from biogas

A variety of techniques is used for removing CO_2 from biogas. These may include physical or chemical absorption, adsorption on a solid surface, membrane separation, cryogenic separation and chemical conversion.

2.6.4.1.1 Physical absorption of CO_2

The physical absorption method is less complicated, requires fewer infrastructures and is cost effective. Pressurized water scrubbing is one example of physical absorption. In this process, pressurized water acts as an absorbent. In pressurized water scrubbing, pressurized water is sprayed from the top of a packed bed column to the bottom, and biogas is allowed to pass through the spray of water from the bottom to the top. Thus, the absorption process is of a counter-current type. The CO_2 in biogas dissolves in the water and the methane comes out from the scrubber.

Bhattacharya et al. [173] developed one such water scrubbing system. This provides 100% pure methane, but depends upon factors like the dimensions of the scrubbing tower, gas pressure, composition of raw biogas, water flow rates, and purity of water used. Vijay [174] developed a packed bed type scrubbing system, using locally available packing materials and removing 30-40% more CO_2 by volume compared with the scrubbing systems without a packed bed. Khapre [175] designed a continuous counter-current type scrubber with gas a flow rate of 1.8 m^3/h at 0.48 bar pressure and water inflow rate of 0.465 m^3/h. It continuously reduced the CO_2 content from 30% intake to 2% outlet by volume.

Dubey [176] examined three water scrubbers having diameters of 150 mm (height: 1.5 m), 100 mm (height: 10 m) and 75 mm (height: 10 m) to absorb the available CO_2 of 37-41% in the raw

biogas. He found that, the CO_2 absorption was influenced by the intake flow rates of biogas and water rather than the different diameters of the scrubbers.

2.6.4.1.2 Chemical absorption of CO_2

Chemical absorption involves the formation of reversible chemical bonds between the solute and the solvent. Chemical solvents generally employ either aqueous solutions of amines, i.e. mono, di or tri-ethanolamine or aqueous solution of alkaline salts, i.e. sodium, potassium and calcium hydroxides.

Tippayawong and Thanompongchart [177] used aqueous solutions of sodium hydroxide (NaOH), calcium hydroxide ($Ca(OH)_2$) and mono-ethanolamine (MEA) as chemical absorbents for scrubbing CO_2 in biogas. They passed these absorbents in a packed bed scrubber in a counter current direction. Their test results revealed that, the aqueous solutions used were effective in reacting with the CO_2 in the biogas, and a maximum of 90% removal efficiency was observed, giving a high CH_4 enriched fuel. They also reported that, the absorption capability of the solvent was transient in nature with time. Absorption saturation was reached in about 50 min for $Ca(OH)_2$, and 100 min for NaOH and MEA, respectively. They have recommended that, with a regular replacement or regeneration of used solutions, biogas upgradation could be achieved.

Biswas et al. [178] have reported that, by bubbling biogas through 10% aqueous solution of mono-ethanolamine (MEA), the CO_2 content of the biogas was reduced from 40 to 0.5-1.0% by volume. The MEA solution can be completely regenerated by boiling for 5 min, and thus can be reused. Another study was carried out by Baciocchi et al. [179] for scrubbing CO_2 in biogas using a NaOH aqueous solution, where the initial CO_2 percentage in biogas was 42%. They have followed a three stage absorption process and about 90% CO_2 removal efficiency was observed, using 9 L of a 3.8 mol/ L of NaOH solution per m^3 of biogas, under standard conditions of 273 K and 100 kPa. They have recommended adjusting the liquid to gas flow ratio, for achieving a higher CO_2 removal efficiency, depending the specific composition of the inlet biogas and on the required CH_4 content in the outlet stream.

Savery and Cruzon [180] have suggested that, the three agents NaOH, KOH and $Ca(OH)_2$ could be used in the chemical scrubbing of biogas. The absorption of CO_2 in alkaline solution was assisted by agitation. The turbulence in the liquid aids the diffusion of the molecule in the body of the liquid, and extends the contact time between the liquid and the gas. Another factor

governing the rate of absorption was the concentration of the solution. The rate of absorption was most rapid with NaOH at normalities of 2.5-3.0.

2.6.4.1.3 CO_2 adsorption using a solid surface

This adsorption process involves the transfer of the solute in the gas stream to the surface of a solid material, where it concentrates mainly as a result of physical or Vander Waals forces. Commercial adsorbents are generally granular solids with a large surface area per unit volume. Wise [181] indicated that by a proper choice of the adsorbent, CO_2 can be efficiently removed from biogas. Biogas purification can be carried out using some form of silica, alumina, activated carbon or silicates, which are also known as molecular sieves.

Schomaker et al. [182] have examined the possibility of removing CO_2 from biogas by pressure swing adsorption (PSA). PSA consisted of three active carbon beds. One of the beds was fed with biogas under a pressure of about 6 bar, and the CO_2 was smoothly adsorbed. When there was a saturation of CO_2 in the adsorption bed, the process was shifted to the second bed, and the saturated bed was depressurized to ambient pressure. The efficiency of this CO_2 absorption process was almost 98%. A continuous monitoring of a small-scale installation of 26 m^3/h of biogas plant, in Sweden using the PSA technique through carbon molecular sieves, gave excellent results in terms of CH_4 enriching.

Pandey and Fabian [183] have used naturally occurring zeolite-Neopoliton Yellow Tuff (NYT) for the adsorption of CO_2. They have observed that, the active component for CO_2 adsorption was chabazite, which has an adsorption capacity of 0.4 kg CO_2 per kg of chabazite at 1.50 bar and 22.8 ^oC.

2.6.4.1.4 Membrane technology for CO_2 separation

The principle of membrane separation is one in which some of the components of the raw biogas were passed through a thin membrane (<1 mm), while the others were retained. The passing of each component is triggered by the differences in the partial pressure over the membrane, and this is highly dependent on the permeability of the membrane material. For high methane purity, permeability must be high. Hagen and Polman [184] reported that a solid membrane constructed from an acetate-cellulose polymer has permeability for CO_2 that is 20-60 times higher than that of CH_4. However, a pressure of about 25-40 bar is required for the membrane separation process.

Wellinger and Lindberg [185] described two basic techniques for scrubbing biogas with the help of membranes: one was a high pressure gas separation with gas phases on both sides of the membrane, and the other was a low pressure gas liquid absorption separation, where a liquid absorbed the molecules diffusing through the membrane. The high pressure gas separation membranes effectively worked up to 3 years, which was compared to the life time of the membranes used for natural gas purification which typically worked effectively for 2-5 years.

Deng and Hägg [186] investigated biogas upgradation by a membrane separation process using a highly efficient CO_2-selective polyvinyl amine/ polyvinyl alcohol (PVAm/PVA) blend membrane. The blend membrane gave a unique CO_2 facilitated membrane from PVAm and the robust mechanical properties from PVA, which exhibited both high CO_2/CH_4 separation efficiency and very good stability. CO_2/CH_4 selectivity up to 40 and CO_2 permeance up to 0.55 m^3 (STP)/m^2 h at 2 bar were documented with synthesized biogas (35% CO_2 and 65% CH_4).

Rautenbach et al. [187] designed a pilot plant for the removal of CO_2 from biogas using a membrane separation technique. They reported that monsanto and acetate cellulose membranes were more permeable to CO_2, O_2 and H_2S than CH_4. The best separation occurred at 25 ^oC temperature and 5.50 bar pressure.

Glub and Diaz [188] used the high gas flux across the membrane, and the flux increased proportionally with a partial pressure difference. Thus, the higher the pressure difference, the smaller the membrane area required for scrubbing. However, the maximum pressure which the membrane can withstand must be taken into consideration.

Stern et al. [189] used a bench-scale membrane pilot plant, for upgrading biogas generated from a municipal wastewater treatment plant. The membrane separation plant was tested with two identical hollow-fiber modules for periods of over 1000h. First, the hollow-fiber module was tested at an average pressure of about 36 bar and at stage-cuts of 0.34±0.41, and then the second hollow-fiber module was operated at about 29 bar and at stage-cuts of 0.36±0.39. The CH_4 concentration in biogas enhanced from 62±63 mol% to as much as 97 mol%.

2.6.4.1.5 Cryogenic separation of CO_2

CO_2 removal from biogas by a cryogenic separation method involves the separation of gas mixtures by fractional condensation and distillation at low temperature. Hagen and Polman [184]

used a cryogenic separation technique to remove the CO_2 in biogas. They compressed the biogas with the help of a multi stage compressor up to a pressure of about 80 bar and then cooled it with chillers maintained at about -45 ^oC. The CO_2 in the biogas condenses and a purity of 97% CH_4 in biogas was obtained.

2.6.5 Scrubbing of H_2S from biogas

H_2S is a corrosive gas and its concentration varies with the feedstock. It is necessary to remove in order to avoid corrosion in compressors, gas storage tanks and engines. H_2S is poisonous as well as environmentally hazardous, since it is converted to sulfur dioxide after combustion. H_2S can be removed either in the digester, from the crude biogas or in a upgrading process. The most commonly used H_2S removal process can be classified into two general categories, namely: (i) dry oxidation process and (ii) liquid phase oxidation process.

2.6.5.1 Dry oxidation process

The dry oxidation process can be used for the removal of H_2S from gas streams by converting it either into sulfur or oxides of sulfur. This process is used, where the sulfur content of gas is relatively low and a very high purity of biogas cleaning is required. Some of these methods are described below.

2.6.5.1.1 Introduction of air/oxygen into the biogas system

A small amount of oxygen of about 2-6%, if introduced into the biogas storage system by using a positive displacement pump can reduce the H_2S percentage; as a result, the sulphide in the biogas oxidizes into sulfur and the H_2S concentration decreases. This is a very simple and low cost process. No special chemicals or equipment are required. Concentrating on the parameters, such as temperature, reaction time and position where the oxygen to be added, should be determined. Oxygen induction can reduced the H_2S concentration by about 95%. However, care should be taken to avoid overdosing of oxygen, as biogas in air is explosive in the range of 6-12%, depending on the methane concentration of 67-73% [185].

2.6.5.1.2 Adsorption using iron oxide

H_2S reacts with iron hydroxides or iron oxides to form iron sulphide. Hagen and Polman [184] passed biogas through iron oxide pellets, to remove H_2S. When the pellets were completely covered with sulfur, they were removed from the tube for the regeneration of sulfur. This process

is notably simple, but during the regeneration reaction it generates a huge amount of heat. Also they observed that, the packings used in the reactor became toxic. Further, the authors tried to use wood chips to cover the iron oxide, which had somewhat a larger surface to volume ratio than plain steel. It was observed that approximately 20 g of H_2S was bound per 100 g of iron oxide chips. The application of wood chips is very popular particularly in the USA. It is a low cost process; however, particular care has to be taken that the temperature does not rise too high during the regeneration of the iron filter [185].

Hagen and Polman [184] have also reported that the H_2S in biogas can be adsorbed in the activated carbon. This process is a catalytic reaction, and carbon acts as a catalyst. The sulfur saturated activated carbon can then either be replaced with fresh activated carbon or regenerated.

2.6.5.1.3 Liquid phase oxidation process

The liquid phase oxidation process is primarily used for the treatment of gases containing relatively low concentration of H_2S. It may be either: (a) a physical absorption process or (b) a chemical absorption process. In the physical absorption process the H_2S can be absorbed by the solvents. One of the solvent is water. But, the consumption of water is very high for the absorption of a small amount of H_2S. If some chemicals like NaOH are added to water, the absorption process of H_2S can be enhanced. The chemical absorption of H_2S can take place with iron salt solutions like iron chloride. This method is extremely effective in reducing high H_2S levels. The process is based on the formation of insoluble precipitates. $FeCl_3$ can be added directly to the digested slurry to reduce the H_2S in the biogas. The addition of $FeCl_3$ is more suitable for a small scale anaerobic digester. For large scale biogas production plants, H_2S removal by a scrubber will be more suitable and economic.

From the above literature review, it is understood that biogas can be obtained from different organic substrates that are available in the form of municipal, agricultural and industrial wastes. Some researchers have produced biogas from Jatropha seed cake, but nobody has made attempts to produce biogas from Karanja seed cakes, which is an organic waste obtained from the biodiesel production process; the biogas thus produced, was purified and utilized for heat and power applications. Therefore, this was identified as a problem for this research.

2.7 Objective of research

The main objectives of the research work are as follows;

(i) To produce biogas from the Karanja seed cake (SCK) and cattle dung (CD) mixture by anaerobic digestion, to minimize the solid organic waste originated from biodiesel industries.

(ii) Use of an appropriate method to remove hydrogen sulphide (H_2S) and carbon dioxide (CO_2) from the produced biogas.

(iii) To utilize the unpurified and purified biogas as alternative primary fuels in a single cylinder, four stroke, CI engine, run on the dual fuel mode, using diesel as a pilot fuel. And to study the combustion, performance, and emission characteristics of the engine, and compare the results with those of diesel operation.

(iv) To run a CI engine completely with two different renewable fuels (Karanja biodiesel and biogas) obtained from a single source of energy originated from Karanja seed cake.

(v) To determine the optimum condition of biodiesel-biogas dual fuel operation, by evaluating the engine combustion, performance, and emission characteristics of a CI engine, when it was subjected to a few fuel and engine modifications.

(vi) To carry out a short term endurance test to study the wear of the engine components, and lubricating oil contamination.

CHAPTER 3

FUEL PRODUCTION AND CHARACTERIZATION

3.1 General

The main objective of this investigation was to run a direct injection (DI) diesel engine with only renewable fuels. Two renewable fuels (i) Karanja methyl ester-a biodiesel, and (ii) biogas, were used in the engine adopting dual fuel technology. In the dual fuel mode, Karanja biodiesel was used as a pilot fuel, and biogas was used as a primary fuel. Karanja biodiesel was extracted from Karanja oil (KO), and the biogas was generated from a mixture of Karanja seed cake (SCK) and cattle dung (CD) by anaerobic digestion. Further, the biogas was purified using a vertical two-stage scrubber. The mechanism for biogas production, feedstock characterization for anaerobic digestion, characterization of Karanja biodiesel, biogas, and purified biogas are discussed in the following sections.

3.2 Production of biogas

Initially, to determine the best combination of the SCK and CD mixtures, for the maximum biogas production, four different proportions of SCK and CD mixture were taken and kept for a period of 30 days in the laboratory for analysis. During this observation period, it was observed that the SCK-CD mixing ratio of 25:75 gave the maximum amount of biogas with a higher methane percentage. Considering the optimum mixing ratio of SCK and CD, a large-scale floating dome type biogas plant was also designed and fabricated.

3.3 Laboratory scale biogas digester

3.3.1 Substrates for feedstock

The SCK was collected in the solid form from M/s Sanjay oil crusher unit, Rourkela, India. Fresh cattle dung was collected from a cattle farm near the National Institute of Technology (NIT), Rourkela campus. The cattle dung was diluted with water in a 1:1 ratio stirred at 2000 rpm for 10 minutes, and filtered with a nylon grid of size 0.25 mm. The filtrate was used as the seed for anaerobic digestion. The same procedure was repeated for all the four samples with

different quantities of CD. Also, about 50 gm of powdered dry rice straw with a particle size 0.12-2.2 mm was mixed with the substrate samples, for maintaining the proper C/N ratio. Rice straw was collected from the local farmer and washed with water. Then, the washed rice straw was dried in an electric oven, in the heating range of 20-450 ^{o}C, at 90 ^{o}C for 5 hours at a heating rate of 10 ^{o}C/min. The dried straw was ground in a straw grinding mill of model NBM-36, 3.5 kW power at 1500 rpm to make an amorphous substrate, which can be easily mixed with the SCK-CD samples. About 50g of powdered dry RS of particle size 0.12-2.2 mm was mixed with the substrate samples for maintaining the required C/N ratio. Figure 3.1 shows the block diagram of the step by step energy extraction from Karanja seed.

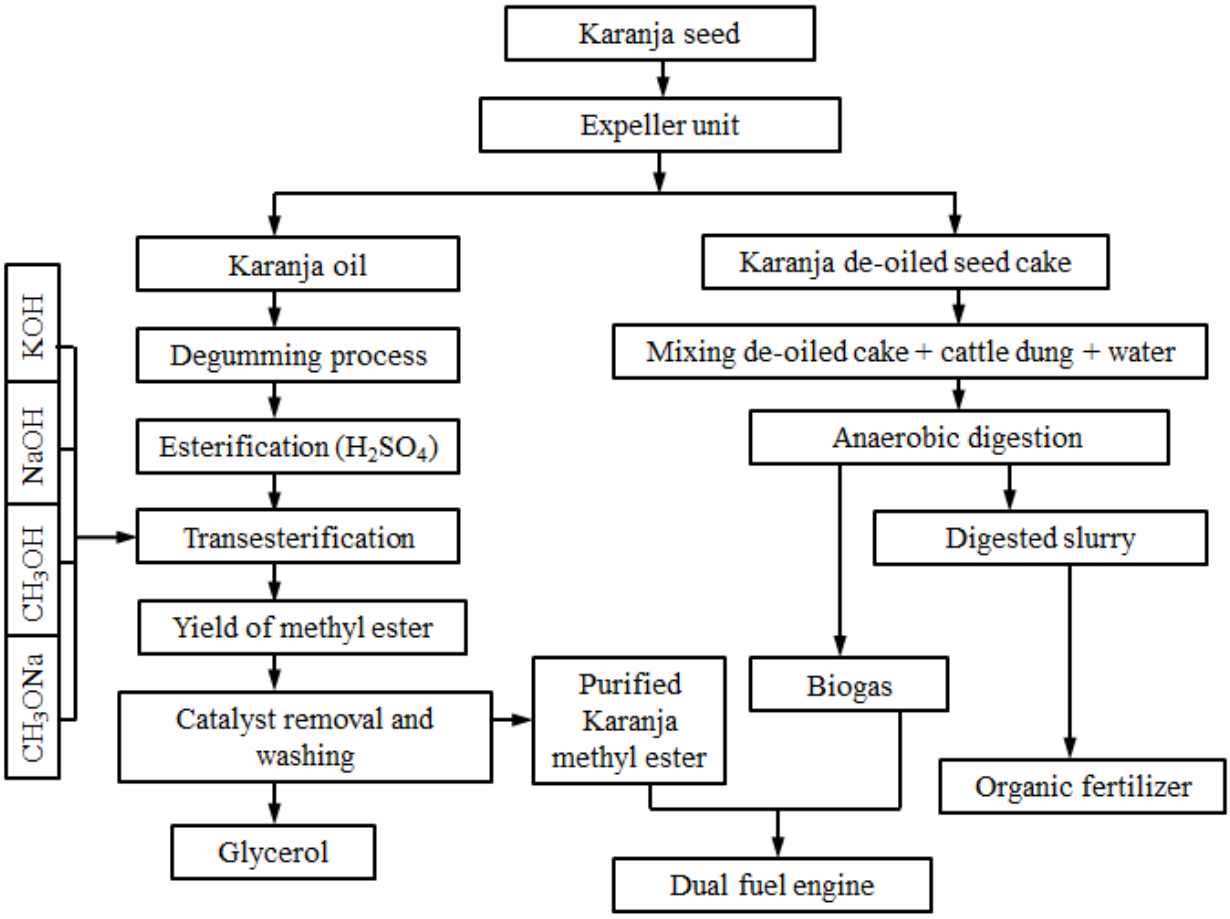

Figure 3.1 Block diagram for energy extraction from Karanja seed.

Figure 3.2 shows the photographs of the energy extraction and a whole part utilization of the whole Karanja seed.

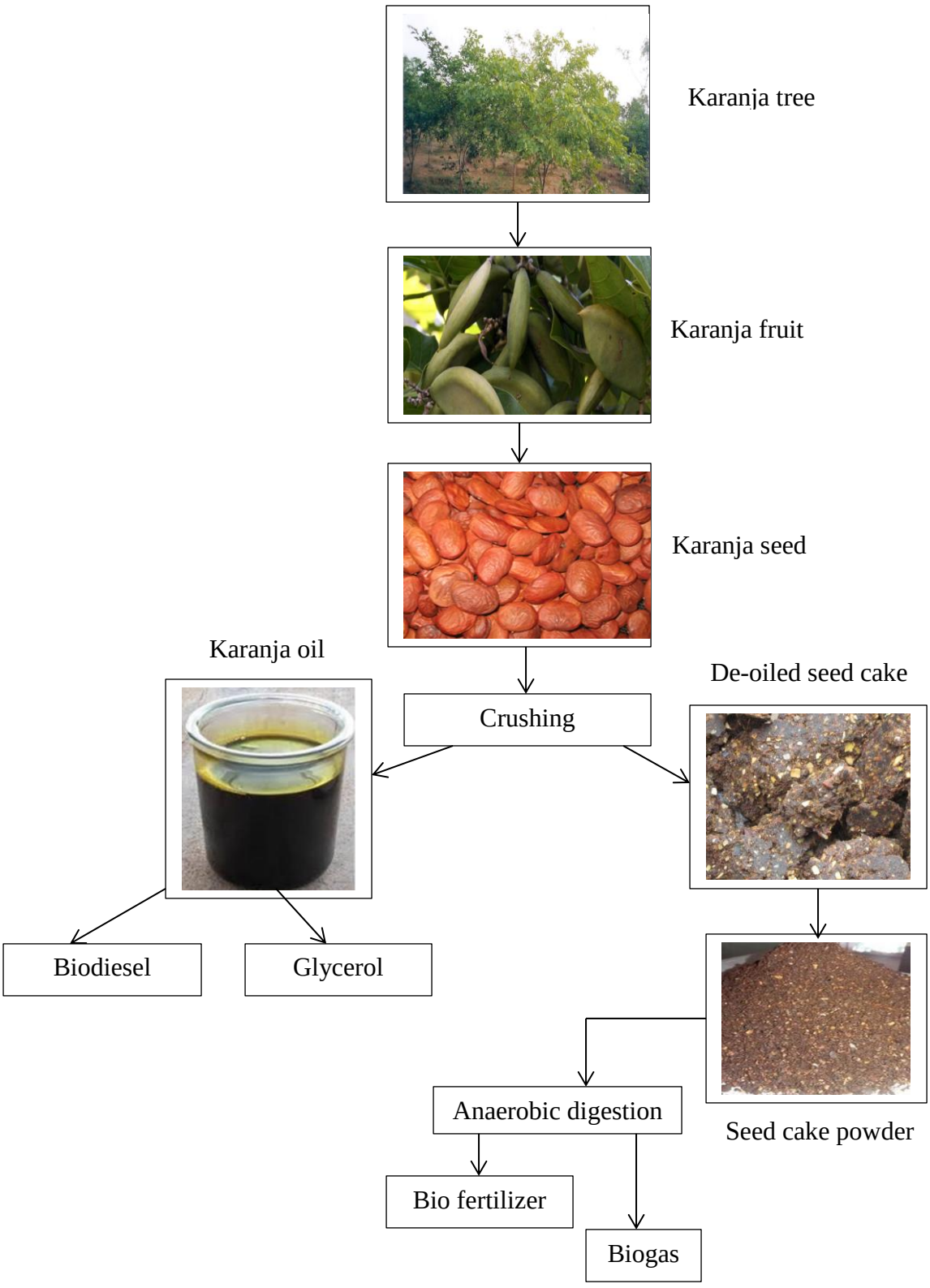

Figure 3.2 Utilization of the whole Karanja seed.

3.3.2 Preparation of the feed material

Experiments were conducted in the laboratory scale reactors, namely A, B, C and D for carrying out the anaerobic digestion of SCK-CD for 30 days of retention time. The reactors were named as S_1, S_2, S_3 and S_4. Three different mixtures of SCK and CD for biogas production were taken as samples, and 75%, 50% and 25% of the SCK on a mass basis were mixed with 25%, 50% and 75% CD to get the mixtures. The dilution ratio of SCK and water was fixed as 1:3.5 on a weight basis at normal pressure and temperature. For comparison, the CD slurry was also taken as one of the samples, as it is commonly used as a feedstock for the production of biogas [190]. The C/N ratio for SCK and CD was found to be 13.82:1 and 21.76:1 as shown in Table 3.1.

Table 3.1 Ultimate analysis of the SCK, CD, and RS.

Feed material	wt. %, dry basis							C/N ratio
	Oil content	C	H	N	S	P	K	
SCK	5.20	55.71	8.48	4.03	0.34	0.90	1.30	13.82:1
CD	-	36.13	4.70	1.66	0.03	0.05	0.06	21.76:1
RS	-	42.00	6.47	0.50	0.12	0.10	0.87	84.00:1

Yadvika et al. [118] reported that for a maximum biogas production, the C/N ratio should be within 20-30:1. Hence, during the sample preparation, RS having a higher C/N ratio of 84:1 was mixed with the samples S_1, S_2, and S_3. The measured quantity of 50 gm ground RS was mixed with the SCK-CD substrate to maintain the C/N ratio of the samples S_1, S_2, and S_3. The C/N ratio for S_4 was found to be 21.76:1; hence, RS was not mixed with this sample. The total solid (TS), volatile solid (VS), fixed carbon (FC) and non-volatile solid present in the SCK, CD and RS are given in Table 3.2.

3.3.3 Design of experiment

Initially, measured quantities of SCK and CD were taken and mixed with water in the proportions of 1:3.5 and 1:1. Powdered RS was added to all the samples except S_4. The ultimate analyses of the samples are given in Table 3.3. It is seen from the table that, the C/N ratios were, 19.74:1, 21.62:1, 24.74:1 and 21.76:1 for S_1, S_2, S_3, and S_4 respectively. The total volume of the inoculum for each sample was measured with a cylindrical measuring tube. The pH of the samples was measured with the help of a pH meter (model Crison 20) for a digestion time of 30

days. The initial pH for the four samples S_1, S_2, S_3, and S_4 were found to be 5.2, 5.5, 5.6 and 6.5 respectively. The microbial analysis of the slurry was performed, and all nine bacterial species were observed from the samples S_1, S_2, S_3, and S_4. Among these species, some were positive, some were negative, and some were motile and non-motile. The habitat diversity of the bacteria showed that seven species were obligate anaerobic, one was obligate aerobic, and another one was facultative anaerobic in nature. The 16S ribosomal RNA sequence (16s rRNA) analysis revealed that the bacterial isolates were *Acetobacter syzygii*, *Bacteroides nordii*, *Clostridium perfringens*, *Methanobacterium formicicum*, *Lactobacillus acidophilus*, *Methanosarcina siciliae*, *Prevotella bivia*, and *Porphyromonas asaccharolytica*, *Ruminococcus gnavus*.

Table 3.2 Proximate analysis of the SCK, CD, and RS.

Feed material	wt. %, dry basis					
	Moisture content	Total solid	Volatile matter	Ash content	Fixed carbon	Non-volatile solids
SCK	9.50	90.5	85.8	5.30	17.48	5.27
CD	81.2	18.8	14.9	4.70	33.13	20.6
RS	16.7	83.3	70.0	15.5	12.67	3.6

The micro-organisms present in the phyla Firmicutes, Bacteroides, Proteobacteria, and Euryarchaeota were observed by the phylogenetic analysis of the representative bacterial clones. Among them, the phyla Firmicutes and Bacteroidetes were a dominant group, and within the phylum Firmicutes and Bacteroidetes, class Clostridia and Bacteroidia were the dominant bacterial community. Microorganisms within the class Clostridia and Bacteroidetes have been frequently reported to be significant throughout various anaerobic habitats, and have the ability to degrade a wide variety of complex organic molecules, including proteins and carbohydrates. The Clostridum and Bacteroides species isolated from the rumen, digesters, and natural habitats hydrolyze cellulose, hemi-cellulose, and protein to produce volatile fatty acids (VFAs), alcohol, CO_2, H_2, and methane. The cell of the gram positive bacteria has a thick peptidoglycan, and it cross-linked with the bacterial enzyme transpeptidase. It acts upon the proteins and peptides and converts them into amino acids, which is part of the hydrolysis phase. Hydrolysis occurs in the presence of oxygen; if the organism is strictly anaerobic, it would use hydrogen as an electron

donor for supporting the hydrolysis phase. Gram-negative bacteria contain a thin peptidoglycan layer lacking enzyme transpeptidase; therefore they depend upon the other bacteria in the anaerobic system.

3.3.4 FTIR analysis of inoculums

Various characteristic functional groups present in the inoculums were identified, by using the Perkin Elmer RX Fourier Transform Infrared spectroscopy (FTIR). On the interaction of an infrared light with the inoculum, the chemical bond will stretch, contract and absorb infrared radiation in a specific wavelength range, regardless of the structure of the rest of the molecules. The FTIR spectra were collected in the range of 400-4000 cm^{-1} with a 8 cm^{-1} resolution. Figure 3.3 depicts the FTIR spectra of the feedstock samples before anaerobic digestion.

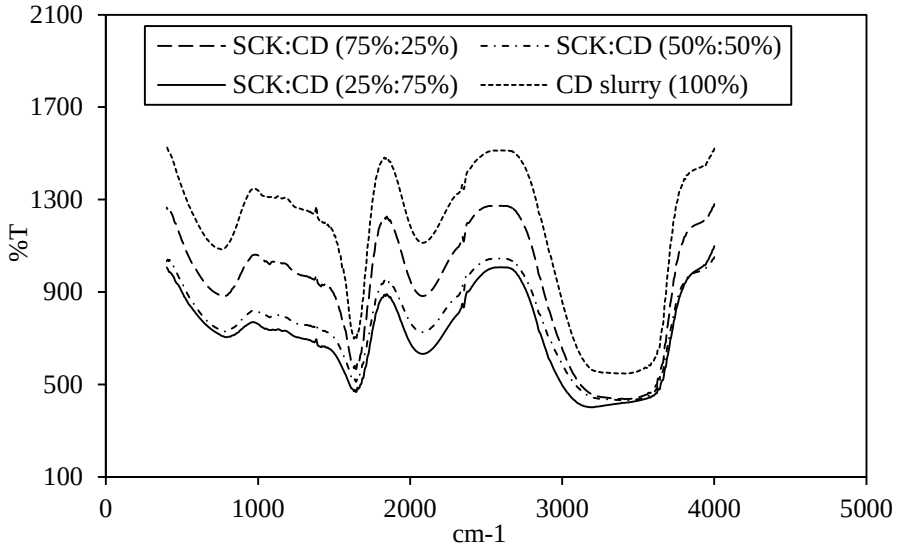

Figure 3.3 FTIR spectra of the substrate before anaerobic digestion.

It can be observed from the figure that, the samples S_1, S_2, S_3, and S_4 have the functional groups at different wavelengths. The N-H weak vibrations at 1631.56 cm^{-1} and 3413.98 cm^{-1} indicated the presence of primary amines. The C=O stretching vibration at 1864.07 cm^{-1} indicated the presence of carboxylic acids. The presence of nitro compounds was detected at 1414.53 cm^{-1} and 1369.78 cm^{-1} with N-O. The C-C and C-N stretching vibrations at 2386.10 cm^{-1} and 2352.22 cm^{-1} indicated the presence of alkynes. The O-H stretching vibration at 3655.25 cm^{-1} indicated the presence of alcohols and phenols. The strong C-H stretching vibration at 1468.97 cm^{-1} detected the alkyl methylene. From the FTIR spectrographic study, it was concluded, that the inoculums

were suitable for anaerobic digestion, as they possessed ingredients for the survival and growth of anaerobic microorganisms.

Then, the prepared samples were kept in four reactors, and air tight sealing was done, using an industrial grade epoxy compound (i.e. M-seal) having the shear, tensile and compressive strengths of 70 kg/cm, 200 kg/cm^2 and 400 kg/cm^2 respectively. Figure 3.4 shows the reactor used for biogas production. The photograph of the laboratory scale biogas digester is shown in Figure 3.5. The daily biogas production was measured by water displacement in U-shaped glass tubes (outer diameter 18 mm, length 1500 mm and 2.5 mm thickness). Experiments were carried out for the different samples simultaneously, to overcome the climatic effect on the biogas production. Regular temperature changes were recorded for a period of 30 days using J-type thermocouples (sensitivity of 55 µV/ °C, accuracy ±0.1 ^{o}C, range -40 to 350 ^{o}C), and were found to be between 32 ^{o}C and 34 ^{o}C.

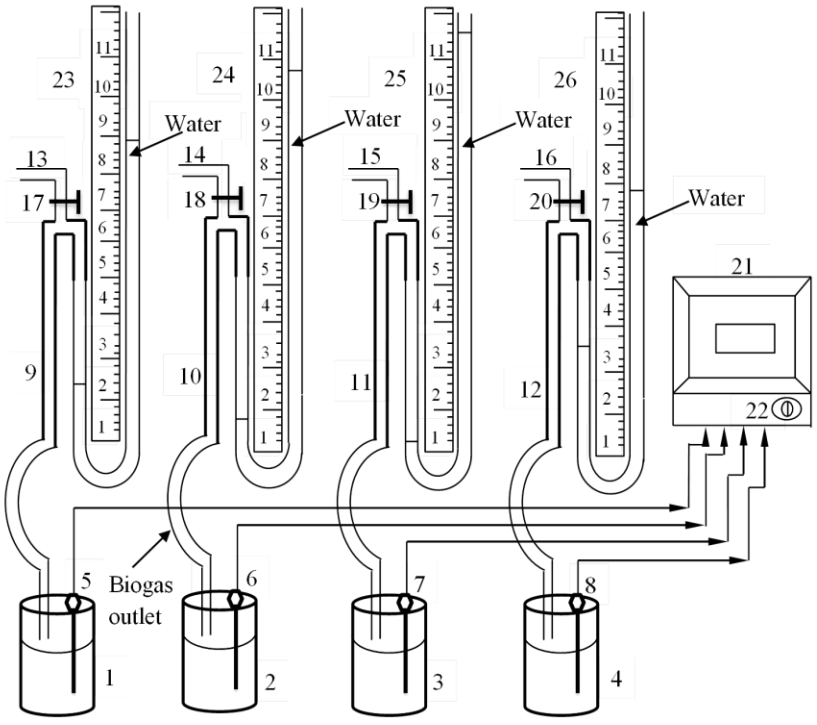

(1-4) Reactors A, B, C, D
(5-8) J-type thermocouples
(9-12) U tube holder
(13-16) Biogas outlet to biogas analyzer
(17-20) Control valve
(21) Temperature indicator
(22) Thermocouple dimmer stat
(23-26) Water level indicator

Figure 3.4 Reactors used for biogas production.

Figure 3.5 Pictorial view of laboratory scale biogas digesters.

3.3.5 Effect of pH

The average pH of the input substrate for the SCK-CD was found to be about 6.29, 6.36, 6.69 and 7.07 for the four samples S_1, S_2, S_3, and S_4 respectively. Most anaerobic bacteria, including methane forming bacteria, perform best when the pH ranges from 5.5 to 8.5 [191]. The pH in the anaerobic reactor initially decreased due to the production of volatile acids. However, as the methane forming bacteria consumed the volatile acids, and alkalinity was produced, the pH of the digester increased, and then stabilized. When the digestion time was more than 5 days, the methane forming bacteria began to consume rapidly the volatile acids. Generally, in a properly operated anaerobic digester, the pH is maintained between 6.8 and 7.2, as the volatile acids are converted into methane (CH_4) and carbon dioxide (CO_2). The pH of an anaerobic digestion process is significantly affected by the CO_2 content of the biogas [190,192,193].

Table 3.3 Feed material properties with different proportions of SCK and CD.

Samples	Composition	Quantity of SCK (gm)	Volume of water (ml)	Quantity of fresh CD (gm)	Quantity of RS (gm)	Quantity of slurry (gm)	Volume of slurry (ml)	TS (%)	VS (%)	C/N ratio
S_1	SCK: CD (75%:25%)	225	750	75	50	1100	1050	77.47	72.27	19.74:1
S_2	SCK: CD (50%:50%)	150	600	150	50	950	910	59.55	54.55	21.62:1
S_3	SCK: CD (25%:75%)	75	450	225	50	800	762	41.62	36.82	24.74:1
S_4	CD slurry (100%)	-	300	300	-	600	565	18.8	14.9	21.76:1

Figure 3.6 shows the variation of pH with five days' average of the total digestion time. It is noticed that, the sample S_4 give the maximum pH compared to the other three samples. For the samples of 75% and 100% CD, initially the pH decreases, because of the formation of volatile acids, and after 10-15 days of digestion time, the pH increases, resulting in the formation of an alkaline. For the samples of 75% and 50% de-oiled cake, the initial pH is 5.2 and 5.5 which is 25% and 18.18% less than that of sample S_4, respectively, because the hydrolytic and acetogenic bacteria are more active during 2-7 days of digestion time, forming acetic acid. During anaerobic digestion, the maximum pH is found to be 6.88 for S_1 with 30 days of digestion time, 6.9 for S_2 with 28 days of digestion time, 6.91 for S_3 with 27 days of digestion time and 7.14 for S_4 with 10 days of digestion time. The methanogenic bacterium starts decomposing after 10-12 days, ends after 25-28 days of digestion time, and forms gaseous products such as CH_4, CO_2, and traces of other gases. Hence, among all the samples, the average maximum and minimum pH is found to be 7.07 and 6.29 for S_4 and S_1 respectively, which was in the suitable range for healthy anaerobic digestion.

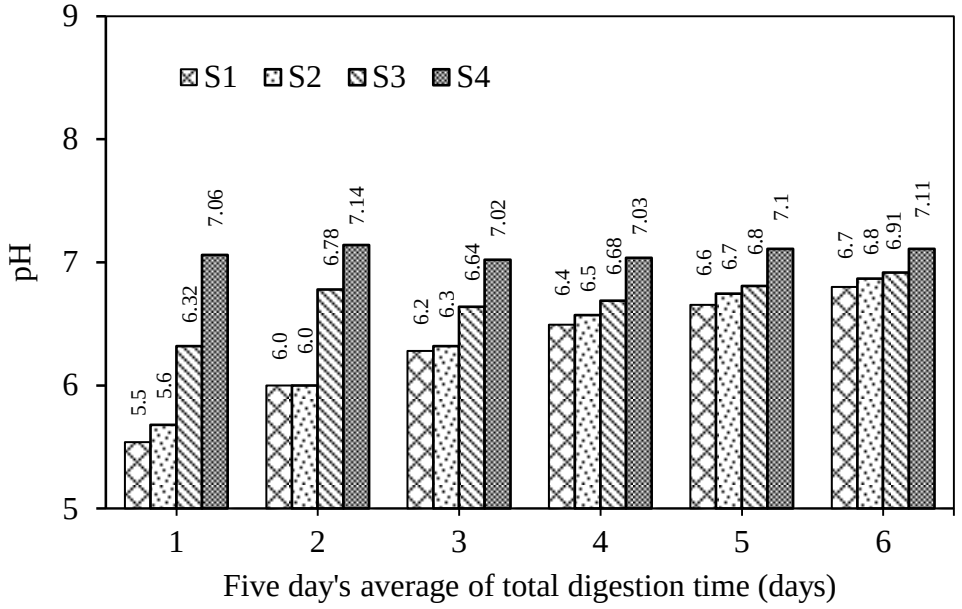

Figure 3.6 Variation of pH with five days' average of the total digestion time.

3.3.6 Effect of digestion time

In this study, experiments were performed to investigate the biogas yield from the different proportions of the SCK and CD slurries, when they were used as a feedstock. Figure 3.7 shows the daily biogas yield with respect to the digestion time. The average daily biogas production

during the 30 days' digestion time is observed to be 35.65 ml/day per kg of TS, 151.91 ml/day per kg of TS, 175.58 ml/day per kg of TS and 17.79 ml/day per kg of TS, for samples S_1, S_2, S_3 and S_4 respectively. It can also be observed that, for samples S_2 and S_3 the biogas production rate becomes stable after a digestion time of 10 days and starts falling after 26 days of digestion time, because of the deficiency of the feed materials in the reactor for the microorganisms. The initial days' (1-9 days) biogas production is found to be low, compared to the later days of the digestion time. Chandra et al. [190] reported that, when the digestion time was more than 5 days, the methanogenic bacteria consumed volatile acids rapidly, and thereby more biogas production occurred.

In this investigation, it is observed that, the SCK mixed with the CD in proportions of 50% and 25% produced 88.2% and 89.86% more biogas than pure CD. This might be due to the presence of more carbon, nitrogen and organic compounds (like $C_6H_{12}O_6$) in the SCK. The typical reactions during anaerobic digestion are given below.

$$C_6H_{12}O_6\left(\text{organic compound}\right) \rightarrow 2C_2H_5OH\left(\text{ethanol}\right) + 2CO_2\left(\text{carbon dioxide}\right) \tag{3.1}$$

$$2C_2H_5OH\left(\text{ethanol}\right) + CO_2\left(\text{carbon dioxide}\right) \rightarrow CH_4\left(\text{methane}\right) + 2CH_3COOH\left(\text{acetic acid}\right) \tag{3.2}$$

$$CH_3COOH\left(\text{acetic acid}\right) \rightarrow CH_4\left(\text{methane}\right) + CO_2\left(\text{carbon dioxide}\right) \tag{3.3}$$

$$CO_2\left(\text{carbon dioxide}\right) + 4H_2\left(\text{hydrogen}\right) \rightarrow CH_4\left(\text{methane}\right) + 2H_2O\left(\text{water}\right) \tag{3.4}$$

Among the two samples S_2 and S_3, more amount of biogas was produced from S_3 because the percentage of the CD is higher, i.e., 75 % CD in the slurry inhibited a rapid anaerobic digestion. It can also be observed that, S_1 continued to produce biogas up to a digestion time of 30 days, whereas for S_2 and S_3 the biogas production fell at the digestion time of 26 days, because sample S_1 contains 75% SCK and 25% CD, wherein the population of microorganism is less for a quicker decomposition of the massive feedstock of the reactor. Sample S_4 gives the least amount of biogas compared to all the others, because of the presence of less organic compounds for microbial growth and survival. The methane content in biogas is found to be about 65.2%, 68.3%, 72.7% and 61.4% by volume, for the mixing ratio of SCK: CD of 75%:25%, 50%:50%, 25%:75% and 0%:100% respectively.

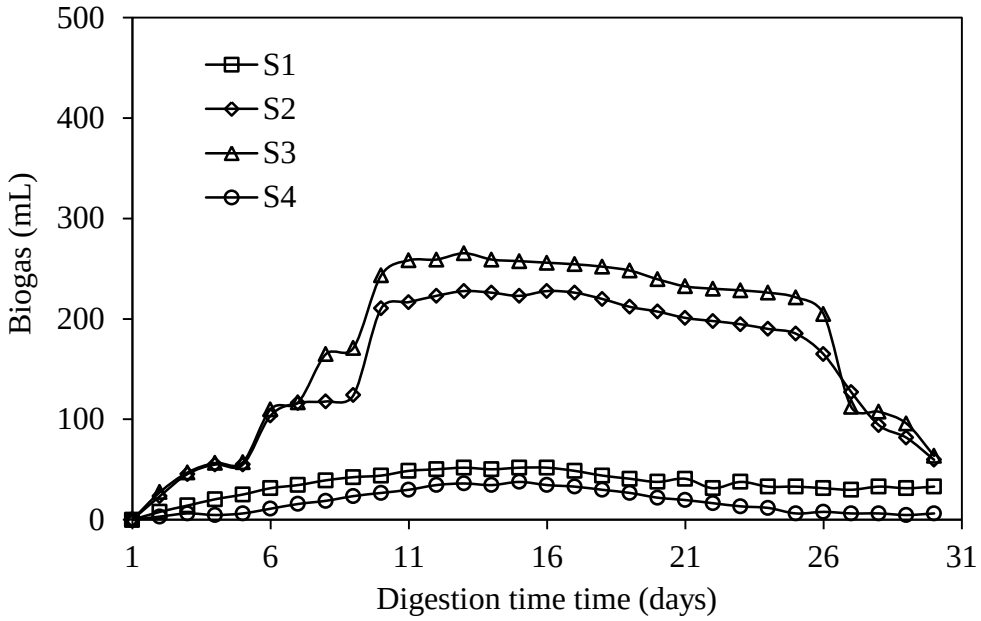

Figure 3.7 Daily biogas yields with respect to the digestion time.

3.3.7 C/N ratio

The C/N ratio of the feedstock is an important parameter for biogas production. The nitrogen present in the feedstock builds up the cell structure of the microorganisms. Also, the presence of nitrogen (protein, nitrates) in the feedstock promotes the synthesis of amino acids, proteins, and nucleic acids. During anaerobic digestion, the nitrogen is converted into ammonia (NH_3) which, as a strong base, neutralizes the volatile acids produced by the methanogenic bacteria, and thus helps in maintaining the neutral pH for rapid biogas production. The excess nitrogen in the feedstock can lead to excess ammonia formation, which increases the toxicity of the feed slurry. It was reported that the optimum C/N ratio for biogas production from the CD slurry must be within the range of 20-30:1 [37,118,194,195]. The carbon present in the feedstock forms the cytoplasm of the microorganisms, and provides the energy for their life activities.

The cumulative biogas production at different C/N ratios for SCK-CD is shown in Figure 3.8. It can be observed from the figure that, the C/N ratio of 24.74:1 gives the maximum yield of 5.26×10^3 ml of biogas per kg of TS, that of 21.62:1 gave 4.55×10^3 ml of biogas per kg of TS, and that of 19.74:1 gives 1.06×10^3 ml of biogas per kg of TS. CD slurry with a C/N ratio of 21.76:1 produced 0.53×10^3 ml of biogas per kg of TS in the digestion time of 30 days cumulative.

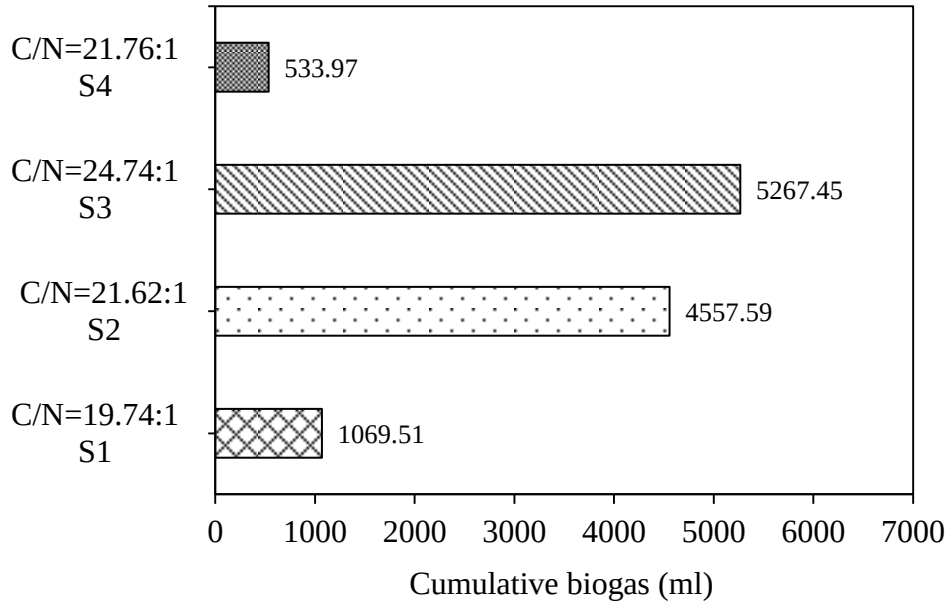

Figure 3.8 Effect of C/N ratios on biogas production.

3.3.8 Cumulative biogas production

Figure 3.9 depicts the cumulative biogas yield over 30 days of the digestion period for S_1, S_2, and S_3 in comparison with S_4.

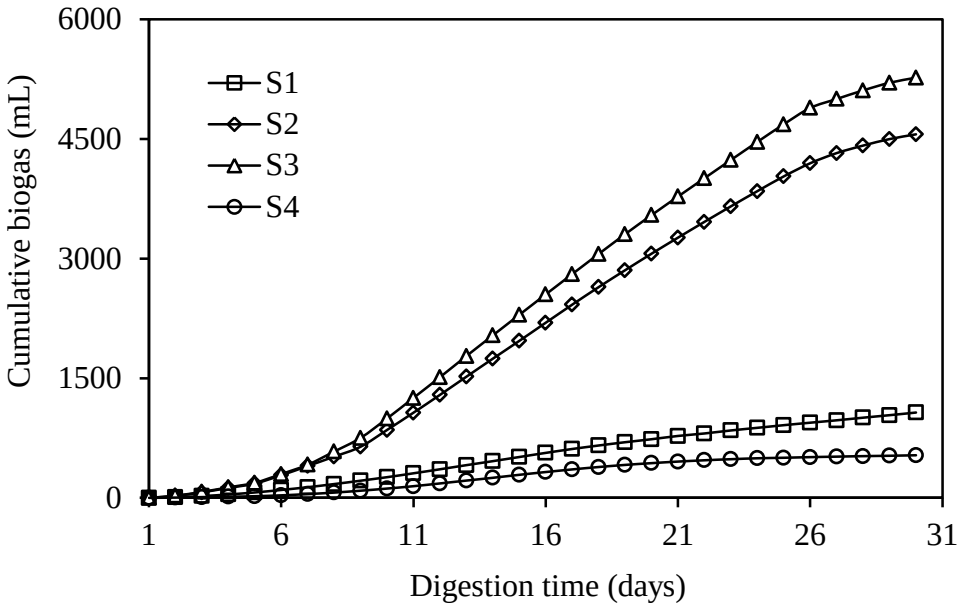

Figure 3.9 Cumulative biogas yield with respect to the digestion time.

The maximum cumulative biogas yield is observed for S_3, followed by S_2. The maximum biogas yield for S_3 is due to the presence of essential nutrients in the correct chemical form and concentrations. In general, carbon and nitrogen are the main nutrients for anaerobic bacteria. Sample S_3 had a maximum C/N ratio of 24.7:1 than that of other samples, which give a maximum biogas yield in the digestion time of 30 days (the detailed discussion for the C/N ratio on cumulative biogas yield has already been given in Section 3.3.7). The cumulative biogas yields for the samples S_1, S_2, S_3, and S_4 are found to be about 1.06×10^3 ml per kg of TS, 4.55×10^3 ml per kg of TS, 5.26×10^3 ml per kg of TS and 0.53×10^3 ml per kg of TS respectively, with an input TS of 77.5%, 59.5%, 41.6 and 18.8%.

3.3.9 Characterization of SCK-CD digested slurry

After anaerobic digestion, there was a little quantity of digested slurry noticed in all the reactors, which could not produce biogas, but in nature it was an organic waste. Hence, the digested slurry was tested for its fertilizer value, which is given in Table 3.4. From the table, it can be observed that after digestion the nitrogen, phosphorus and potassium values of the slurry increases, which is good for the growth of plants. Also, the digested slurry became nontoxic due to the action of anaerobic microorganisms [146]. It is suggested that the digested slurry can be used as an organic fertilizer in the agricultural sector, and the disposal problem of a huge amount of SCK obtained from biodiesel production plants can be eliminated.

Table 3.4 Fertilizer value of bio-digested SCK-CD slurry.

Sample name	Nitrogen, %	Phosphorous, %	Potassium, %	Carbon, %
S_1	5.2	1.8	2.8	55
S_2	6.1	2.7	3.1	48
S_3	6.8	3.1	3.8	45
S_4	2.4	1.2	1.7	34

3.3.10 Characterization of biogas

The biogas obtained from the samples S_1, S_2, S_3 and S_4 was tested to determine its density, heating value, energy content and chemical composition. The properties of biogas produced from samples S_1, S_2, S_3, and S_4 are compared and given in Table 3.5. It can be observed from the table that, the sample S_3 has a higher heating value and lower density than S_1, S_2, and S_4. This

indicates that the biogas obtained from the sample S_3 is a better quality alternative gaseous fuel than that obtained from the other samples. The energy content of S_3 was 6-6.5 kW/m^3, which can allow this to be used as a renewable gas for cooking, if produced on a large scale.

Table 3.5 Properties of biogas produced from S_1, S_2, S_3, and S_4.

Properties	Test method ASTM	S_1	S_2	S_3	S_4
Lower heating value, MJ/kg	D 1945	20.2	23.3	27.53	17.2
Density at 1 atm @ 15 ^{o}C, kg/m^3	D 3588	1.29	1.25	1.2	1.31
Auto-ignition temperature, ^{o}C	-	635-675	610-640	600-650	640-670
Energy content, kW/m^3	D 4868	4.8-5.9	5.2-6.1	6.0-6.5	4.5-5.3
Critical pressure, bar	-	72-86	73-85	75-89	70-85
Critical temperature, ^{o}C	-	-80.2	-81	-82.5	-80.1
Boiling point, ^{o}C	D 1835	-128 to -160	-125 to -170	-120 to -150	-130 to -162

A comparison of the biogas constituents obtained from the samples S_1, S_2, S_3, S_4 and some of the commonly available feedstocks are given in Table 3.6. It can be observed from the table that, the sample S_3 contains the maximum of about 73% methane, which is higher than that of the other samples. The methane in the biogas, obtained from Jatropha curcas, municipal solid waste, and the CD are in the range of 60-68%, 40-60% and 50-70% [190,196]. The biogas obtained from the sample S_3 has about 17% CO_2, which acted as an agent for the reduction of smoke and NO_x emissions, when it is used in an SI (spark ignition), CI (compression ignition), HCCI (homogeneous charge compression ignition) and dual fuel engines [103,105,197-199]. The biogas produced from the co-digestion of SCK-CD mixture is superior in quality than that from the cattle dung sample. The mixing ratio of 25:75 % (SCK: CD) is found to be the optimum, and the cumulative biogas yield is approximately 89.8 % with 73 % methane content.

Table 3.6 Comparison of the gas constituents of biogas obtained from S_1, S_2, S_3 and S_4.

Gas constituents	S_1, % vol.	S_2, % vol.	S_3, % vol.	S_4, % vol.	Jatropha curcas, % vol.	Municipal solid waste, % vol. [196]
CO_2	26.1	23.5	17.37	25-30	20-30	20-40
O_2	1.21	1.14	1.5	0-3	1-2	<1
C_nH_{2n+2}	Nil	Nil	Nil	-	-	<1
CO	Nil	Nil	Nil	-	-	-
H_2	0.6	0.9	1.4	0-1	0-1	-
CH_4	63.6	67.3	73	50-70	60-68	40-60
N_2	8.2	6.9	6.5	0-10	1-15	2-20
H_2S	0.29	0.26	0.23	0-3	0-2	40-100 ppm

3.4 Large-scale biogas digester

The pictorial view of the working model of the floating drum-type biogas digester is shown in Figure 3.10.

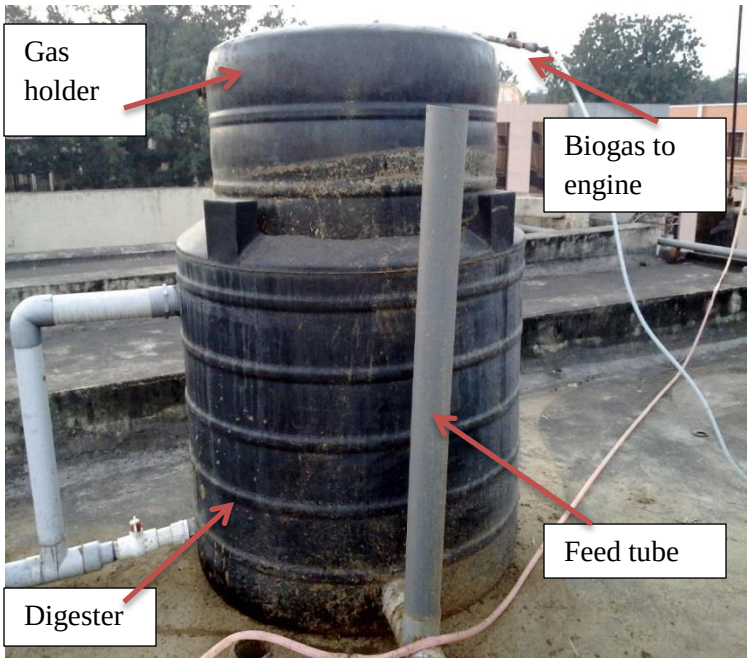

Figure 3.10 Pictorial view of the working model of the floating drum-type biogas digester.

After a successful testing of feedstock in the laboratory scale batch digesters, the optimum ratio of feedstock was used for biogas production in a large scale floating drum type biogas digester. The floating dome biogas plant consisted of two parts; a digester (part A) and a gas holder (part B), and both were made of PVC (polyvinyl chloride) material. The diameter of the digester was 0.25 m more than that of the gas holder (diameter 1.10 m). The detailed specifications of the biogas plant are given in Table 3.7.

Table 3.7 Specifications of a large scale biogas plant.

Specifications	Details
Plant type	Floating dome
Digester diameter, m	1.35
Digester height, m	1.265
Gas holder diameter, m	1.10
Gas holder height, m	1.225
Operating temperature range, ^{o}C	10-59
Total volume of digester, m^3	1.81
Total volume of gasholder, m^3	1.16
Effective volume of digester, m^3	1.35
Effective volume of gas holder, m^3	0.95
HRT, days	Min 4-12

The gas holder was placed inverted over the digester for collecting the biogas from the slurry. The gas holder always floated over the slurry, and a 12 mm hose pipe was connected from the gas holder to the engine experimental setup, for carrying the biogas. The feedstock used for the experiment was Pongamia pinnata de-oiled cake, with cattle dung in the proportion of 25%:75% on a mass basis. The measured quantities of Pongamia pinnata de-oiled cake (3 kg/day) and cattle dung were taken, and mixed with water in the ratio of 1:3.5 and 1:1 for feeding the digester. The total volume of the inoculum formed (de-oiled cake + cattle dung + water) was measured with a cylindrical vertical measuring tube, and poured inside the digester.

The pH of the inoculum was measured with the help of a pH meter (model Crison 20, range 1-14). The initial pH of the inoculum (at day 1) was found to be 5.6, and it was slowly increased up

to a hydraulic retention time (HRT) of 12 days. It was observed that, after the HRT of 12 days the pH of the inoculum increased to 6.9, and then it remained constant. The digester was able to produce biogas after the HRT of 10-12 days, and during the digestion period the ambient temperature was 30-37 ^{o}C. The physical parameters of the feedstock are given in Table 3.8.

Table 3.8 Different physical parameters of the feedstock used in a large scale plant.

Specifications	Details
Feedstock used	Karanja seed cake (25%) + cattle dung (75%)
TS (total solid) in feedstock, %	41.62
VS (volatile solid) in feedstock, %	36.82
C/N ratio of feedstock	24.74:1
Concentration / pH of slurry	5.6-7.3
Seed cake: water ratio	1:3.5
Cattle dung: water ratio	1:1
Pongamia seed cake feed rate, kg/day	3
Cattle dung feed rate, kg/day	9
Daily biogas production, m^3/day	Max 0.48-0.52

3.4.1 Daily biogas production in a large scale plant

The variation of biogas production with time is depicted in Figure 3.11. It can be observed that, the biogas production for the SCK: CD mixture and only CD became stable after HRT of 14 days. In the initial days i.e. 1-9 days, the biogas production is found to be low, compared to the later days of the digestion time. This may be due to the consumption of volatile acids by the methanogenic bacteria rapidly, and thereby more biogas production occurs. Also, it can be observed that the biogas production in the case of SCK: CD is higher than that of CD. This is due to the availability of ingredients in the digester for active digestion by the bacteria, whereas in the CD sample the population of bacteria is high, but the ingredients are low for the survival of the bacterial community.

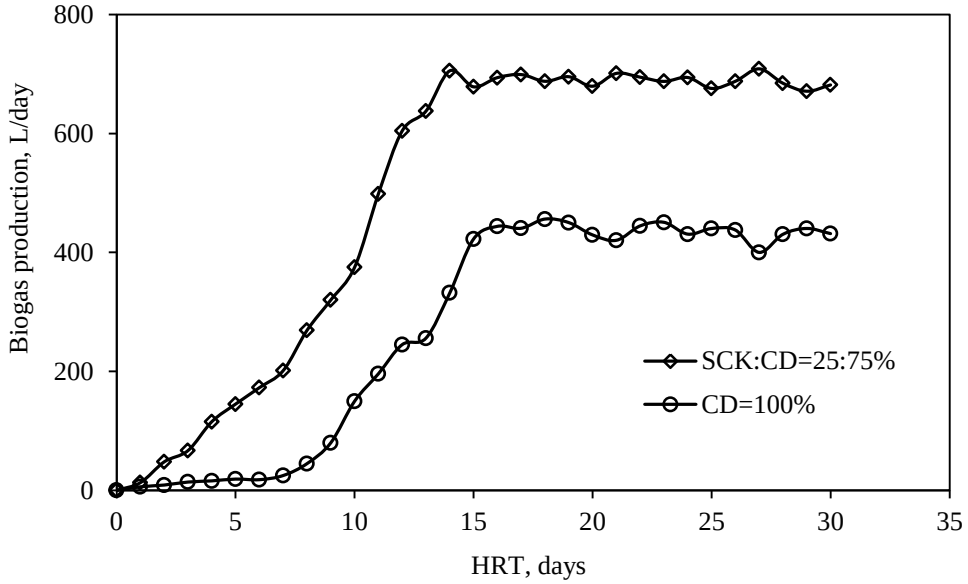

Figure 3.11 Variation of biogas production with time.

3.4.2 Cost analysis

The cost analysis for a biogas plant is an important parameter for calculating biogas production economics. The costs involved in the operation are basically of two types: (A) fixed cost (B) variable cost. The cost analysis of biogas production is given below;

(A) Fixed cost calculation

(i) Cost of digester = ₹ 10,500.00

(ii) The cost of gas holder = ₹ 7,000.00

(iii) Cost of tubes = ₹ 900.00

(iv) Cost of assembly = ₹ 300.00

(v) The total fixed cost = ₹ 10,500.00 + ₹ 7,000.00 + ₹ 900.00 + ₹ 300.00

= ₹ 18,700.00

(B) Variable cost calculation

The SCK and CD feed quantity to the digester were 3 kg/day and 9 kg/day respectively.

(i) The price for per kg of SCK = ₹ 10.00

(ii) The price for per kg of CD = ₹ 2.00

(iii) The cost of the SCK feed per day = 3kg×₹ 10.00 = ₹ 30.00

(iv) The cost of the CD feed per day = 9kg×₹ 2.00 = ₹ 18.00

(v) The total cost of feedstock per day = ₹ 30.00 + ₹ 18.00 = ₹ 48.00

The daily biogas production quantity was 0.5 m^3/day. Hence for producing 1 m^3 of biogas the daily expenditure was ₹ 96.00.

3.4.3 Biogas properties

The biogas obtained from the anaerobic digestion of SCK and CD mixture was characterized to find the physical properties and elemental composition. The properties of the biogas obtained from the SCK and CD are compared with those of biogas produced from cattle dung, and are given in Table 3.9.

Table 3.9 Properties of biogas produced from SCK and CD.

Properties	Test method	SCK + CD	CD
Lower heating value, MJ/kg	ASTM D 1945	27.53	17.2
Density at 1 atm @ 15 ^oC, kg/m^3	ASTM D 3588	1.2	1.31
Flame speed, m/s	ASTM D 7424	25	21
Stoichiometric A/F, kg of air/kg of fuel	ASTM D 4891	11.88	10.12
Flammability limits, vol.% in air	ASTM D 6793	7.5-14	7.5-11.7
Octane number	ASTM D 2699	130	110
Auto-ignition temperature, ^oC	-	600-650	640-670
Energy content, kW/m^3	ASTM D 4868	6.0-6.5	4.5-5.3
Fuel equivalent, L oil/m^3 biogas	-	0.6-0.65	0.42-0.5
Explosion limits, % in air	ASTM E 582	6-12	6-9
Critical pressure, bar	-	75-89	70-85
Critical temperature, ^oC	-	-82.5	-80.1
Boiling point, ^oC	ASTM D 1835	-120 to -150	-130 to -162

A comparison of the gas constituents of the biogas obtained from the Karanja seed cake and some of the commonly available feedstocks is given in Table 3.10.

Table 3.10 Comparison of the gas constituents of biogas obtained from Karanja seed cake and other feedstocks.

Gas constituents	SCK + CD, % vol.	CD, % vol.	Jatropha, % vol.	MSW, % vol.
CO_2	17.37	25-30	20-30	20-40
O_2	1.5	0-3	1-2	<1
C_nH_{2n+2}	Nil	-	-	<1
CO	Nil	-	-	-
H_2	1.4	0-1	0-1	-
CH_4	73	50-70	60-68	40-60
N_2	6.5	0-10	1-15	2-20
H_2S	0.23	0-3	0-2	40-100 ppm

3.5 Liquid fuel properties characterization

In the initial stage of the investigation, the liquid fuels used were diesel and Karanja biodiesel. In a later stage, diethyl ether (DEE) was used for improving the performance of the dual fuel engine. Hence, the properties of diesel, Karanja biodiesel and DEE are given in Table 3.11.

Table 3.11 Properties of diesel, Karanja biodiesel and DEE.

Properties	Test method, ASTM	Diesel	Karanja biodiesel	DEE
Density, kg/m^3	D 4052	830	880	713
Calorific value, MJ/kg	D 4809	43.8	40.96	33.90
Auto-ignition temperature, °C	E 659	210-350	170-320	150-160
Flash point, ^oC	D 93	50	230	-40
Fire point, ^oC	D 93	56	258	44
Cetane number	D 613	50	57.6	125
Oxygen, wt. %	E 385	Nil	24.01	28.2

3.6 Biogas scrubbing

The main drawbacks in the composition of biogas are the presence of carbon dioxide (CO_2) and hydrogen sulphide (H_2S), which affect the storage devices. From the property analysis of the

biogas, it was observed that the raw biogas contained about 17% CO_2 and 0.23% of H_2S. In nature, CO_2 is a combustion arrester, and H_2S is corrosive to metal. For a long term use of biogas, it is essential to remove the CO_2 and H_2S. Due to lack of space and some technical constraints, biogas purification was not done in the initial stages of the research. However, it was done in later parts of the research modules. The raw biogas was further purified using a vertical packed bed two stage scrubber.

3.6.1 Packed-bed scrubber

A scrubber was designed using solid works. For the design, various factors were considered, such as biogas flow quantity, water flow quantity, working pressure, tower packing, and the diameter and height of the packed bed. The schematic representation of the scrubber is shown in Figure 3.12.

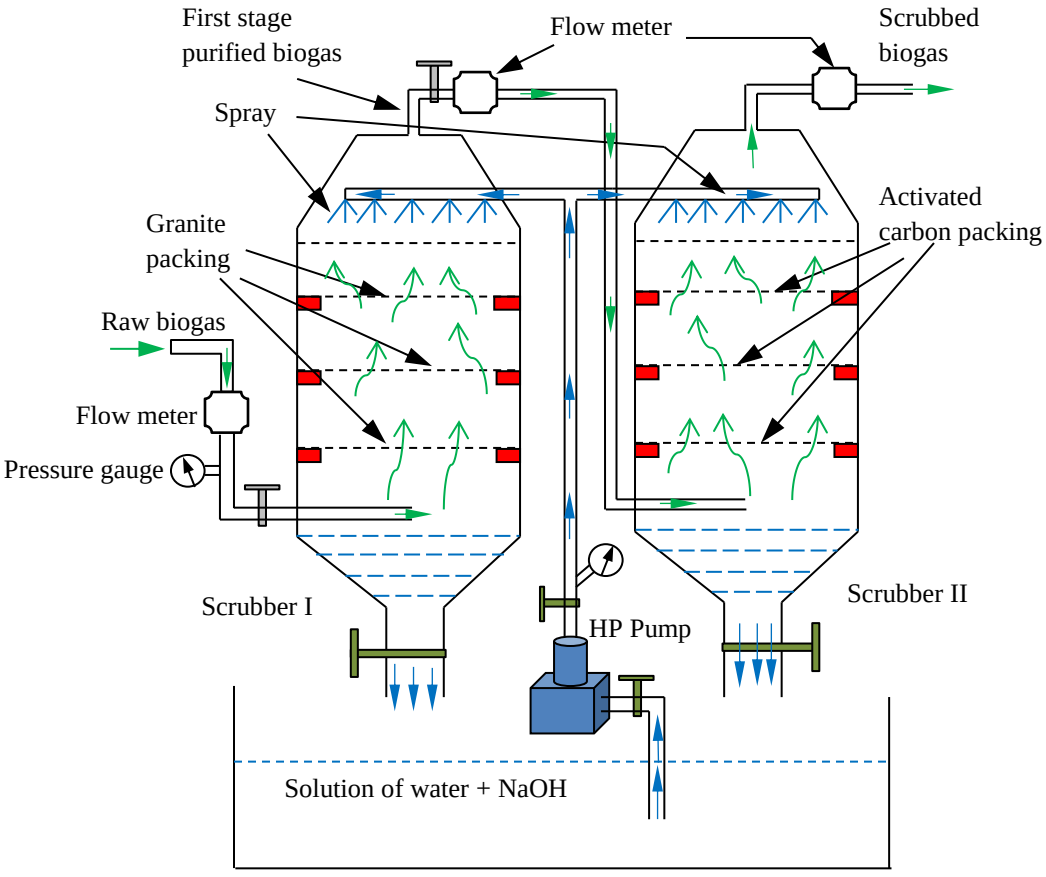

Figure 3.12 Schematic representation of the scrubber.

The designed packed bed scrubber consisted of a cylindrical column, equipped with a biogas gas inlet and out let valve, water inlet, and outlet valve and distributing space at the bottom. The photograph of

the fabricated scrubber is shown in Figure 3.13. The detailed specifications of the scrubber are given in Table 3.12.

Figure 3.13 Photographic view of the scrubber.

Table 3.12 Specifications of the scrubber.

Sl. No.	Parameters	Details
1	Material	Polyvinyl chloride
2	Type	Vertical
3	Stage	2
4	Height, mm	1350
5	Diameter, mm	153
6	Operating temperature, °C	10-80
7	Packing material	Granite (grain size: 15 mm) Activated carbon (grain size: 2 mm)
8	Biogas induction pressure, bar	1.5
9	Biogas induction flow rate, kg/h	1.2
10	Water flow rate, kg/h	700
11	Absorbent used	NaOH + water

3.6.2 Working principle

At the beginning about 30 liters of the liquid solvent (NaOH + water) were prepared and kept in a vessel. The reactors were connected with tubes and sealed properly to avoid any leakage of biogas. To improve the effectiveness of the biogas upgradation system, two scrubbers were set up in series. Biogas from the biogas plant was continuously supplied at a flow rate of 1.2 kg/h, at a pressure of 1.5 bar. A stream of solvent at a flow rate of 700 kg/h was allowed to spray from the top, inside the reactor. The biogas and water flow direction in the reactor were of the counter flow type. Three layers of granite packings were provided in each of the reactors to increase the contact surface of biogas with the solvent. The CO_2 and H_2S in the biogas reacted with the solvent and were absorbed. A pH meter was used to check the pH of the solvent. The pH of the solvent in a range of 7-8 indicated the saturation stage of the solvent. It was also observed that with the increase in time the acidity of the solvent increased and the absorptivity decreased. The typical chemical reaction during the purification process is as follows:

$$CO_2 + 2OH^- \rightarrow {CO_3}^{2-} + H_2O \quad (3.5)$$

$$CO_2 + {CO_3}^{2-} + H_2O \rightarrow 2{HCO_3}^- \quad (3.6)$$

$$CO_2 + R - NH_2 + H_2O \rightarrow R - {NH_3}^+ + {HCO_3}^- \quad (3.7)$$

$$CO_2 + R\acute{R} - NH \rightarrow R\acute{R} - NCOO^- + H^+ \quad (3.8)$$

3.6.3 Characterization of the upgraded biogas

After scrubbing the biogas, the sample was characterized, and the properties were compared with those of raw biogas and natural gas; these are given in Table 3.13. A comparison of the gas constituents of the scrubbed biogas obtained from the SCK, compared with natural gas, is given in Table 3.14.

Table 3.13 Properties of upgraded biogas.

Properties	Test method, ASTM	Raw biogas	Upgraded biogas	Natural gas
Lower heating value, MJ/kg	D 1945	27.53	41.32	49.56
Density at 1 atm @ 15 ^{o}C, kg/m^{3}	D 3588	1.2	0.91	0.72
Flame speed, m/s	D 7424	25	32	34
Stoichiometric A/F, kg of air/kg of fuel	D 4891	11.88	15.75	17.25
Octane number	D 2699	130	132	135
Auto-ignition temperature, ^{o}C	-	600-650	610	540

Table 3.14 Comparison of the gas constituents of raw biogas, upgraded biogas and natural gas.

Gas constituents	Raw biogas, % vol.	Upgraded biogas, % vol.	Natural gas, % vol.
CO_2	17.37	4.26	1.5-4.34
O_2	1.5	0.4	-
Methane (CH_4)	73	90.6	85.1-92.4
Ethane (C_2H_6)	Nil	Nil	6.7-9.3
N_2	6.5	4.7	0.01-1.0
H_2	1.4	-	-
H_2S	0.23	0.04	0.02-0.07

CHAPTER 4

EXPERIMENTAL SETUP AND METHODOLOGIES

4.1 General

Since this investigation relates to an early stage study on the utilization of a gaseous alternative fuel in a dual fuel mode, initially a few minor modifications were done in the hardware of the single cylinder, diesel engine. A complete description of the engine experimental setup, the instruments used, the different experimental methods used in the investigation, the methods of determining the various engine parameters, and the basic test fuels used in the dual fuel mode are also explained in this chapter.

4.2 Engine experimental setup

In this investigation, a constant speed, stationary, single cylinder, four stroke, air cooled, DI diesel engine, with a rated power output of 4.4 kW at 1500 rpm, was modified to operate as a dual fuel engine, using biogas as the primary fuel, and diesel or biodiesel as the injected fuels. A pictorial view of the experimental setup is given in Figure 4.1.

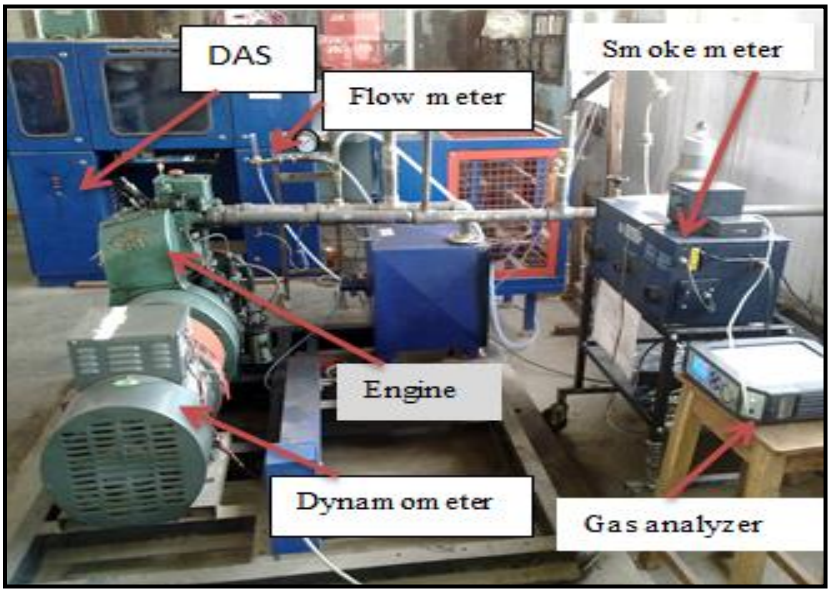

Figure 4.1 Pictorial view of the experimental setup.

The layout of the engine experimental setup is shown in Figure 4.2. A single cylinder engine was employed for the investigation because, it will consume less fuel, and the modifications to be further carried out would be easier than those of the multi-cylinder engine. The detailed specifications of the engine are listed in Annexure I. For loading the engine, an electrical dynamometer (Make: Kirloskar, WHD10075, ACG), with a maximum brake power of 6 kW was coupled with the engine shaft. The dynamometer was loaded with the help of a resistive load bank.

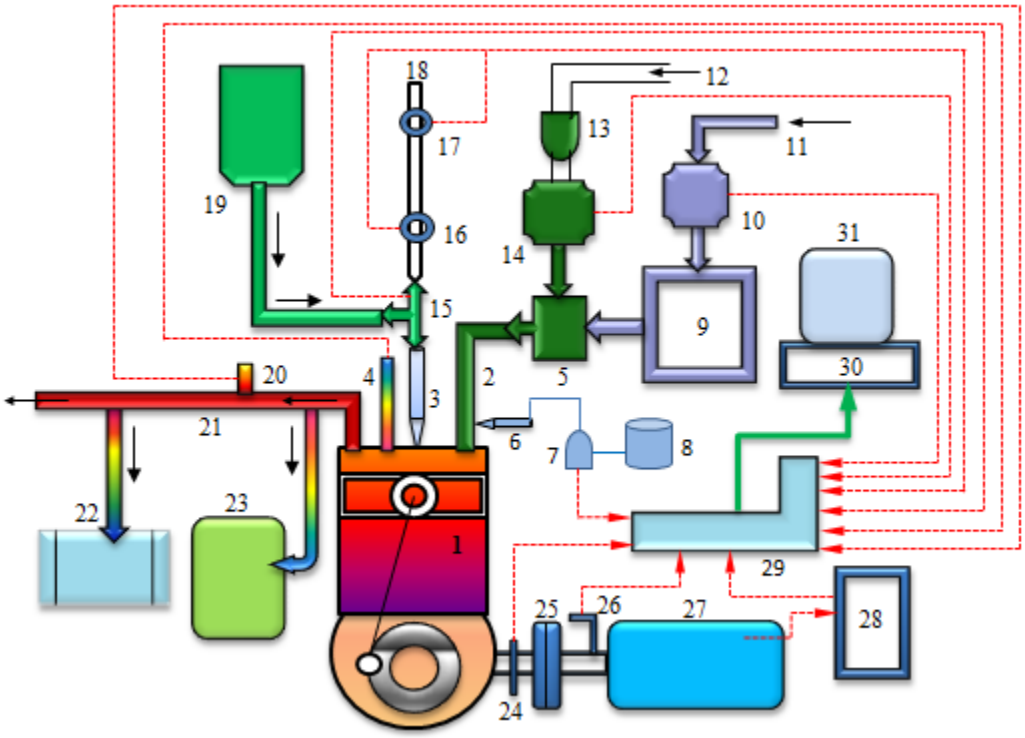

Figure 4.2 Schematic representation of the experimental setup. 1 engine, 2 intake manifold, 3 fuel injector, 4 pressure transducer, 5 biogas-air mixing kit, 6 DEE electronic injector, 7 DEE injection pump, 8 DEE storage tank, 9 air box, 10 air flow meter, 11 air intake, 12 biogas intake, 13 filter, 14 biogas flow meter, 15 solenoid valve, 16 low fuel level optical sensor, 17 high fuel level optical sensor, 18 burette, 19 fuel tank, 20 exhaust gas temperature sensor, 21 exhaust manifold, 22 smoke meter, 23 exhaust gas analyzer, 24 crank angle encoder, 25 coupling, 26 speed sensor, 27 dynamometer, 28 resistive load cell, 29 control panel, 30 data acquisition system, 31 computer.

The air consumption by the engine was measured with the help of a differential pressure sensor connected to the air box. This sensor measured the pressure differences before and after the orifice plate and gave a proportional voltage output with respect to the pressure pulses. From this, the air consumption was measured. A surge tank was used to damp out the pulsations produced by the engine, for ensuring a steady flow of air through the intake manifold. The fuel measuring system consisted of a vertical burette (30 cm^3) fitted with two optical sensors; one was at a higher level, and the other was at a lower level (the higher to lower level effective measurement volume was 20 cm^3). The optical fuel level sensor gave an input to the data acquisition system from which, the time taken for the consumption of fuel for a fixed volume was calculated at a particular load. A solenoid valve was connected between the fuel tank and burette to control the fuel supply to the engine either from the tank or the burette, as per the requirement. The photograph of the solenoid valve is shown in Figure 4.3.

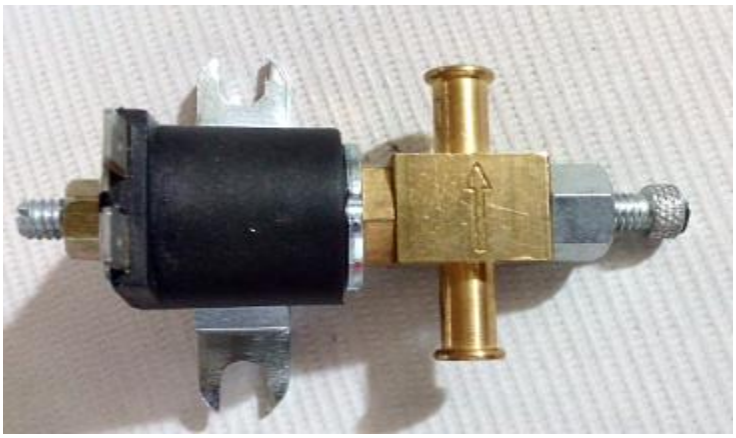

Figure 4.3 Photograph of the solenoid valve.

Three K-type thermocouples were installed at various locations for measuring the exhaust gas temperature, inducted air temperature, and biogas temperature. A non-contact PNP type sensor was connected near the flywheel of the engine to measure the engine speed. The PNP sensor gave the pulse output for each revolution of the crankshaft. The frequency of the pulses was converted into voltage output, and connected to the computer. A stand-alone frequency to a voltage converter was used for signal conditioning. Initially, the combustion, performance, and emission parameters of the engine were studied with diesel at a compression ratio of 17.5 and nozzle opening pressure of 200 bar, which was prescribed by the manufacturer, by maintaining a rated speed of 1500 rpm to get the baseline data for diesel.

4.3 Biogas supply to engine

The biogas generated in the biogas plant was stored in a storage balloon of capacity 3 m^3 (Material: Synthetic rubber, Make: Arjun, Dimension: 2.74 m × 1.21 m × 0.91 m). The collected biogas in the balloon was supplied to the engine by a hosepipe (diameter: 12 mm). The stored biogas from the storage kit was supplied to the engine at a pressure of 1.5 bar. The flow rate of biogas was measured with a gas flow meter. The photograph of the flow meter is shown in Figure 4.4. A gas-air mixing kit (multi-hole type) was connected to the intake manifold of the engine for ensuring proper air-biogas mixture supply to the engine. Figure 4.5 portrays the photographic view of the biogas-air mixing kit. The mixing kit was cylindrical in design, and of a venturi type. Multiple holes (each diameter 3 mm) were provided to the inner periphery of the mixing kit. During the suction stroke of the engine, the pressure reduction in the venturi tends to be proportional to the square of the intake air speed and hence, the biogas flushes into the intake air stream.

Figure 4.4 Photograph of the biogas flow meter.

Figure 4.5 Photographic view of the biogas-air mixing kit.

4.4 Calculation of performance parameters

4.4.1 Brake thermal efficiency

In order to determine the brake thermal efficiency of the engine, three input parameters were measured: (i) time taken for the consumption of 20 cm^3 of fuel, (ii) lower heating value of the test fuel used, and (iii) density of the fuel. The brake thermal efficiency can be calculated as given below:

$$\mathrm{BTE} = \frac{(\text{brake power} \times 3600 \times 100)}{(\text{Volume flow rate of fuel per hour} \times \text{fuel density} \times \text{lower heating value})} \tag{4.1}$$

4.4.2 Brake specific fuel consumption

The formula used to calculate the brake specific fuel consumption is given below:

$$\mathrm{BSFC} = \frac{(\text{volume flow rate of fuel per hour} \times \text{fuel density})}{(\text{brake power})} \tag{4.2}$$

4.5 Emission parameters

The engine exhaust emissions such as CO, HC, NO, CO_2, and O_2 were measured with a five-gas analyzer (AVL 444). The ASTM D6522 standard was followed for the emission measurement. In each module of the experiment, during the steady-state operation of the engine, the exhaust gas was allowed to surge through the probe, and then filtered and made moisture free by a

condensation trap. The moisture free dry exhaust gas was passed through the NDIR (Non-dispersive infrared) sensor for the CO, HC, and CO_2 measurement. The NO emission was measured with the help of an electrochemical sensor.

4.5.1 Exhaust gas analyzer (AVL 444)

The CO, CO_2, O_2 emissions were measured in percentage volume, and the HC and NO emissions were measured in parts per million (ppm) during each run of the engine. The photographic view of the AVL 444 exhaust gas analyzer is shown in Figure 4.6. The complete technical specifications of the AVL 444 exhaust gas analyzer is given in Annexure II.

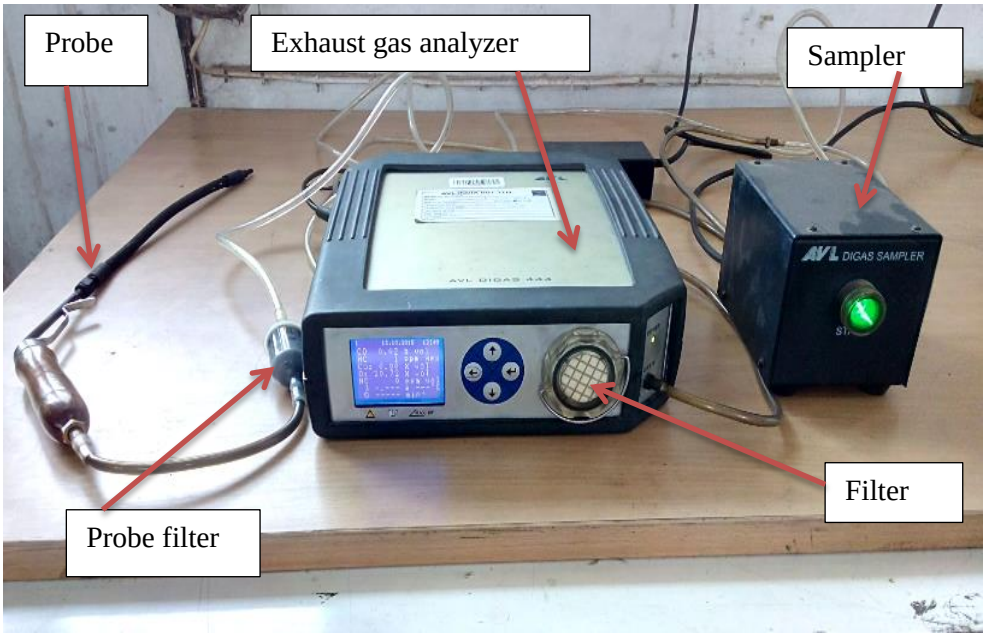

Figure 4.6 Photographic view of the AVL 444 exhaust gas analyzer.

The exhaust gas analyzer was interfaced through a (RS 232C) communication bus to an in-house developed emission data acquisition platform, which recorded the emissions over a span of 120 s in consecutive intervals of 20 s, which was greater than the instrument response time of 15 s, for each cycle of engine operation. The exhaust gases were tapped from the engine exhaust outlet tube. A fine filter was used to remove the adverted particulates, and a condensation trap was incorporated to make the exhaust gas moisture free and cool, so that, the exhaust gas inlet temperature to the analyzer was maintained $\leq 40^{o}$C. Stray condensates, if any, were tackled by the condensate separator inbuilt in the analyzer, which was flushed before every data recording. Leak check, HC residue test, zero adjustments, and condensate purging of the analyzer were

carried out before each set of observations. The analyzer was calibrated with the recommended calibration gas mixture, before the start of the entire range of experiments.

4.5.1.1 NDIR principle

A non-dispersive infrared (IR) measurement was used to determine the concentration of the gaseous pollutants like HC, CO, and CO_2. The schematic layout of the NDIR principle is illustrated in Figure 4.7. Each pollution constituent in the exhaust gas absorbs a specific infra-red at a particular frequency. Two cells are exposed to the IR radiation one is a reference cell containing an inert gas (usually nitrogen), and the other is a cell that allows the sample gas containing the pollutant to be investigated. No IR absorption occurs in the reference cell (1) while the absorption in the sample cell (2) is proportional to the concentration of the component of interest. Beyond the reference and sample cells, there is one detector, which absorbs the IR radiation transmitted. The detector is separated from the sample gases by an optical filter. Because, if more radiation is transmitted through the reference cell, there will be a higher temperature rise in the reference detector chamber than in the sample detector. As a result, the pressure differential is created, which causes the movement of the diaphragm; this can be detected by a capacitance pickup. The resulting signal is amplified, and transmitted to an appropriate readout device [200,201]. The infrared absorption device may be used for continuous monitoring of the combustion products.

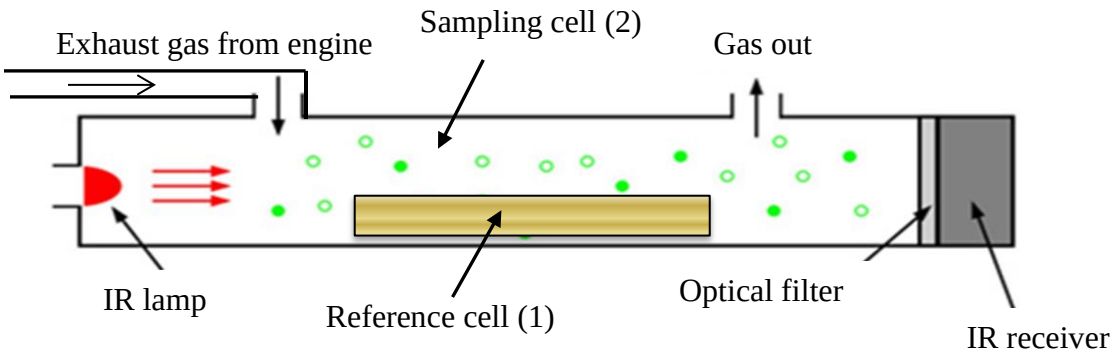

Figure 4.7 Schematic layout of the NDIR principle.

4.5.1.2 Electrochemical sensor

The specific detection of nitric oxide (NO) by the electrochemical sensors is based on a general principle used in electrochemistry. In brief, the NO diffuses across a gas-permeable membrane, and a thin film of electrolyte covering the probe. The NO species are oxidized on the sensor

which consists of a working, and Ag/AgCl reference electrode pair. A potential (approx. 900 mV) is applied to the working/measuring electrode, relative to a reference electrode, and the resulting small redox current due to the oxidation of NO according to the following reaction, is measured by an amplifier system and recorder:

$$NO + 4OH^- \rightarrow NO_3^- + 2H_2O + 3e^- \quad (4.3)$$

4.5.2 Conversion of CO, HC and NO into g/kWh

The brake specific emissions are the mass flow rates of the individual pollutant divided by the engine power. The formulae used to convert the emissions from ppm and % volume to g/kWh are given below:

CO emission in g/kWh:

$$CO\left(\frac{g}{kWh}\right) = \left[\left\{\frac{(m_f+m_a)}{29} \times 10\right\} \times CO \text{ (in \% vol)} \times \frac{28}{\text{brake power}}\right] \quad (4.4)$$

HC emission in g/kWh:

$$HC\left(\frac{g}{kWh}\right) = \left[\left\{\frac{(m_f+m_a)}{29} \times 1000\right\} \times HC \text{ (in ppm)} \times \frac{13}{\text{brake power}}\right] \quad (4.5)$$

HC emission in g/kWh:

$$NO\left(\frac{g}{kWh}\right) = \left[\left\{\frac{(m_f+m_a)}{29} \times 1000\right\} \times NO \text{ (in ppm)} \times \frac{32.4}{\text{brake power}}\right] \quad (4.6)$$

4.5.3 Calibration of the exhaust gas analyzer

4.5.3.1 Pre-test calibration

The gas analyzer was calibrated prior to the emission test with calibration gases certified to ±2% accuracy as per the EPA test methods in 40 CFR 60 and the ISO 3930, 1976 test method. Three calibration gases (zero, mid and high) for CO, NO, and NO_2 can be used. The purified ambient air may be used as the zero gas. The mid-level gas concentration is 40% to 60% of the high-range calibration gas. A high-level gas concentration of the high-range calibration gas shall not be higher than 125% of the expected concentration nor less than 90% of the expected concentration. The high-level gas is equal to the calibration span. The analyzer calibration error shall be not more than ±5% of the calibration span value for the mid and high-range calibration gases, or 5 ppm, whichever is less restrictive. The calibration error can be calculated as follows:

$$\% \text{ difference} = \frac{\text{analyzer response} - \text{gas concentration}}{\text{calibration span}} \times 100 \quad (4.7)$$

For the zero gas, the calibration error shall be no more than 10 ppm:

Difference in ppm = analyzer response – zero gas concentration

The steps involved for calibration are discussed:

As a first step, allow the analyzer to purge the calibration gases prior to beginning the emissions test. Then in second step, conduct a test which consists of three runs, with each run at least 20 minutes in length. In the third step, record the readings for HC, CO and NO at every 2 minute intervals during the 20 minute run.

4.5.3.2 Post-test calibration

After a maximum of three valid 20-minutes of emission tests, conduct a post-test calibration as follows for the HC, CO, and NO calibration gases:

Step 1: Allow the analyzer to purge the gas sample until a stable zero reading is observed. Record the zero reading.

Step 2: Introduce the high-range calibration gas to the analyzer, and allow it to reach a stable reading. Record the analyzer reading.

Step 3: Introduce the mid-range calibration gas into the analyzer and allow it to reach a stable reading. Record the analyzer reading.

Calculate the difference with the pre-test calibration value. If the difference is greater than ±5% or 5 ppm, whichever is less restrictive, the emission test runs are invalid, and must be repeated.

$$\% \text{ difference} = \frac{(\text{post} - \text{test readings}) - (\text{pre} - \text{test readings})}{\text{pre} - \text{test readings}} \quad (4.8)$$

4.5.4 Smoke opacity measurement

The intensity of smoke emission was measured with the help of a diesel smoke meter (AVL 437C). A photographic view of the AVL 437C diesel smoke meter is shown in Figure 4.8. The detailed specification of the AVL 437C diesel smoke meter is given in Annexure III. This smoke meter works on the principle of the Hartridge smoke meter, and measures the smoke opacity of the engine exhaust. The Hartridge smoke meter consists of an optical unit mounted inside a

measuring head and a separate electronic control unit. The measurement principle is based on light extinction detection [202]. The collimated beam from the light source is absorbed, and scattered by the particulate emission. A photodiode determines the light intensity of the attenuated beam, and the corresponding opacity value is transmitted to a separate remote display. A partial flow continuous gas sampling combined with a heated and temperature controlled smoke chamber compensates for changes in pressure, and the test conditions give the most accurate value of the smoke opacity.

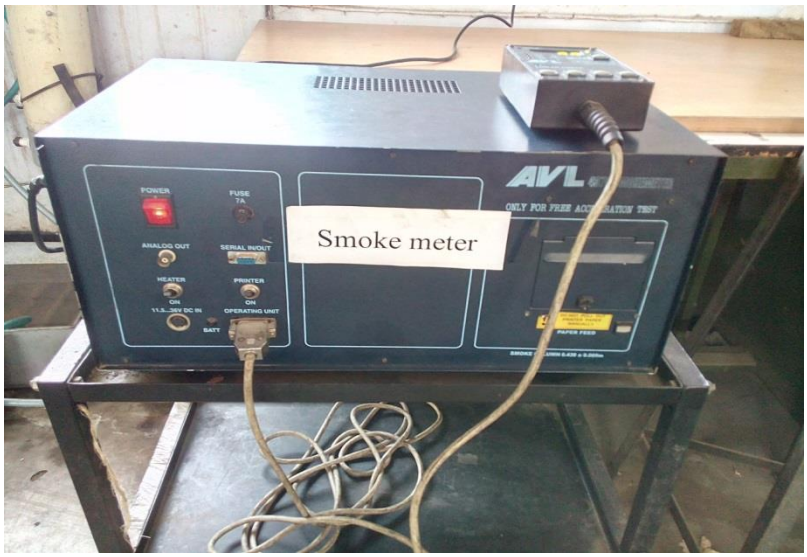

Figure 4.8 Photographic view of the AVL 437C diesel smoke meter.

4.5.4.1 Smoke meter calibration

The smoke meter calibration was done by warming the heating elements up to 70^{o}C. The heating was designed to prevent the temperature falling below the dew point, and thus to avoid measurement error. Fresh air was allowed to enter the measurement chamber which was drawn through the filter paper, underwent measurement and set the zero point of calibration. The halogen bulb current irradiates the column of fresh air volume, and the microprocessor measures the signal from the detector and set as the reference value for 0% opacity. The linearity can be checked by gently pushing the linearity check knob down up to its dead position. The calibration plate was thus measured in front of the detector, and the measured opacity value was indicated, and printed on the protocol print out. The probe of the smoke meter was inserted at the end of the engine exhaust pipe during the smoke opacity measurement. Once the engine reached the stable

operating state, the probe was introduced into the exhaust pipe, and the measurements were taken.

4.6 Combustion parameters

4.6.1 Piezoelectric transducer

The parameters such as in-cylinder pressure, heat release rate, ignition delay, combustion duration, and the rate of pressure rise were determined, to analyze the combustion behavior of the fuel inside the engine combustion chamber, when the engine was operated on the dual fuel mode. In order to analyze these parameters, it is necessary to collect the instantaneous pressure and volume data with respect to the crank angle. This was done by mounting a pressure transducer on the engine cylinder head. The in-cylinder gas pressure during combustion was measured using a Kistler piezoelectric transducer (model 5395A) in conjunction with a Kistler charge amplifier. The pressure transducer was flush mounted in the clearance volume of the engine. A photographic view of the Kistler pressure transducer is shown in Figure 4.9. The cylinder gas pressure data was recorded as the average of 20 cycles of data, with a resolution of 0.6 °CA, using a data acquisition system (DAS).

Figure 4.9 Photographic view of the Kistler pressure transducer.

The quartz sensors can withstand a very high pressure varying from 0 to 250 bar. A hole was drilled on the dummy plug, and the pressure sensor was placed in it. The drilled hole diameter was 5 mm, and an internal thread of pitch 1 mm was made. The piezoelectric sensor was properly sealed, so that there would be no change in the compression ratio and no leakage of gas from the cylinder. The pressure sensor sensed the pressure produced during the combustion of fuel. The measured pressure acts through a diaphragm on the quartz crystal measuring elements,

which transforms the pressure into an electrostatic charge Q in Pico-coulomb. The complete specification of the Kistler make piezo quartz pressure sensor is given in Annexure IV. Figure 4.10 portrays the photographic view of the location at which the pressure transducer is flush mounted.

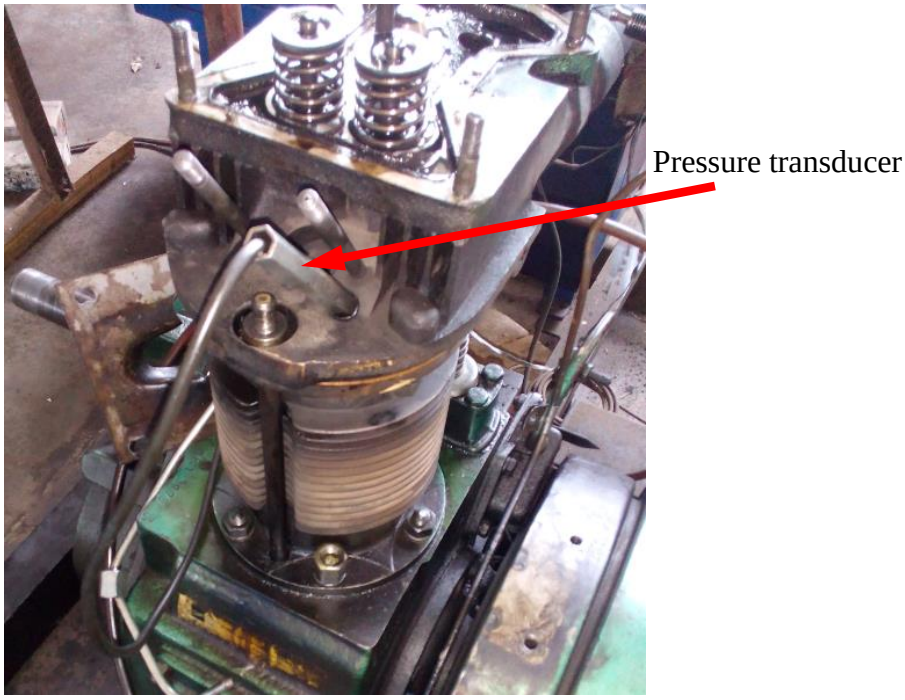

Figure 4.10 Photographic view of the flush mounted transducer on the engine cylinder head.

The TDC marker (Kistler model 5015A1000) was placed near the engine flywheel. At the TDC position, a small metallic deflector was fitted. The photographic view of the TDC marker and metallic deflector is shown in Figure 4.11. The setup was aligned in such a way that the sensor gave an output in the form of a square wave, exactly when the piston was at the TDC.

A TDC marker was fitted on the flywheel to indicate the position of the TDC. The TDC marker provided a voltage pulse, when the piston reached the TDC position. This sensor had a matched pair of an infrared diode and phototransistor, from which the infrared rays emitted, and fell on the phototransistor when it was not interrupted. The flywheel with a small deflector mark at the TDC position with respect to a sensor point was made to get the signal, when the piston reached exactly the TDC. At this point, the output voltage of the phototransistor rose to 5 volts, and at all other points it was approximately zero. Voltage signals from the optical sensor were fed to the data acquisition system along with pressure signals for recording. The engine cylinder pressure,

and the TDC signal were acquired using a digital data acquisition system, and stored on a high-speed computer. A 12 bit analog to digital converter (ADC) was used to convert the analog signals to digital signals. The analog to digital card had both external and internal trigger facility. The pressure and crank angle data were collected in an excel spreadsheet installed in the data acquisition system.

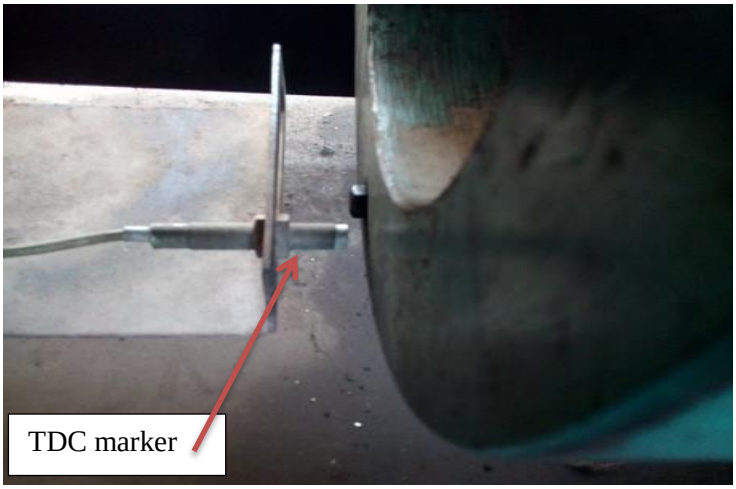

Figure 4.11 Photographic view of the TDC marker and deflector.

4.6.2 Analog to digital converter (ADC)

The analog signals from the sensors fitted at different locations of the engine were fed into an ADC, and then passed to a display unit, through a data acquisition card and microcontroller. Both the pressure and proximity sensors were interfaced with the engine, and the output obtained was an analog signal. Further, the analog signal was converted into digital using the ADC, which was finally fed to a display unit through the data acquisition system. Using the data acquisition system's graphical analysis, evaluating the differential equation, computing the mathematical expression, display, control and recording were done for various engine operating parameters, like instantaneous pressure, crank angle, temperature, and the heat release rate. From this, other combustion parameters such as ignition delay, cumulative heat release rate, mass fraction burned and combustion duration were computed. A computer was used to process and store the data, and store during the investigation.

4.6.3 Calibration of the pressure transducer

The calibration of the pressure transducer was carried out to reduce the error in measurement. The piezoelectric transducer signals naturally decay over time, and are therefore only suitable for dynamic measurements, like engine cylinder pressure measurements. Accordingly, they must be calibrated using a dynamic procedure. The Kistler piezoelectric transducer (model 5395A) used in this investigation was subjected to a dynamic calibration procedure using a standard dead weight tester. The dead weight tester generated the known pressure by hydraulically lifting precise weights with a piston with an accurately known cross-sectional area. The charge output signal of these transducers was used as the input to a charge amplifier via a high impedance cable. The charge amplifier converts the low-level charge (which is of the order of several Pico-Coulombs) to a proportional voltage, which can be recorded with standard data acquisition equipment. In this procedure, a known pressure was applied to the transducer. Then, the output was grounded to zero volts, thereby eliminating signal decay. The pressure was then abruptly dropped to the atmospheric level, by rapidly releasing the hydraulic pressure holding up the weights and allowing them to fall. The resulting voltage change was recorded as a function of time, using a digital oscilloscope programmed to trigger on a voltage drop. The voltage change caused due to the pressure change was determined using a peak-to-peak calculation feature on the scope. Dynamic pressures were taken at intervals of 200 psi from 200 to 1000 psi. Ten measurements were taken at each dynamic pressure. These were then averaged and graphed against the corresponding voltage output. The linearity of the transducer was found to be better than 1%. The repeatability was observed to be about 2 to 3%.

4.6.4 In-cylinder pressure measurement

The in-cylinder pressure at every 0.6 degree crank angle interval was measured with a quartz piezoelectric pressure transducer (KISTLER, Model: 5395A). The pressure transducer was connected to a charge amplifier, and mounted on the cylinder head of the engine, and flushed into the clearance volume, to measure the instantaneous cylinder pressure, and the volume with respect to the crank angle. A crank angle encoder was used to measure the crank angle, and the TDC position of the piston.

For a particular cycle, a total of 1200 data points, for both cylinder pressure and volume were recorded at each load. The heat release rate at a particular load was calculated by considering

twenty cycles. A detailed discussion of the heat release rate calculation is provided in the subsequent sections. Furthermore, the smoothing of the instantaneous pressure data was done by using the following equation:

$$P_n = \frac{[(P_{n-1})+2(P_n)+(P_{n+1})]}{4} \tag{4.9}$$

The change of pressure for unit crank angle was determined by using the equation

$$\frac{dP}{d\theta} = \frac{[(P_{n-2})-8(P_{n-1})+8(P_{n+1})-(P_{n+2})]}{[12(\Delta\theta)]} \tag{4.10}$$

For the in-cylinder combustion analysis, the signals from the crank angle encoder, and the pressure transducer were connected to the charge amplifier. A data acquisition system (DAS) was used for collecting the data, and the acquired data stored in the computer for analysis. The acquired data from the DAS were transferred to an excel sheet, and the heat release rate (HRR), ignition delay (ID), the start of combustion (SOC), and combustion duration (CD) inside the cylinder were calculated. The engine speed was measured with a non-contact type optical sensor mounted near the flywheel.

4.7 Calculation of the parameters for dual fuel operation

4.7.1 Ignition delay calculation

The ignition delay in a compression ignition (CI) engine is defined as the time (or crank angle) interval between the start of injection and start of combustion [203,204]. This delay is due to the physical and chemical processes that take place, before the chemical energy of the injected liquid fuel is released. The physical processes that affect the ignition delay are the atomization of the liquid fuel jet, evaporation of fuel droplets and mixing of the fuel vapor with air. The chemical processes involved are pre-combustion reactions, availability of air, and the presence of residual gas mixtures. All these parameters are modulated and dominated by the engine design, engine speed, engine load, and fuel characteristics. The ignition delay in dual fuel operation is dependent on the availability of oxygen in the intake air and fuel. Considering the oxygen concentration, the ignition delay can be expressed as [42,205]:

$$\theta_d = C(O_{dual})^k \cdot (0.36 + 0.22M_{ps}) \exp\left[E_A\left(\frac{1}{RT_m(r_c)^{n-1}} - \frac{1}{17190}\right) + \left(\frac{21.2}{P_m(r_c)^n - 12.4}\right)^{0.63}\right] \tag{4.11}$$

C, k, O_{dual} are the modified coefficients, M_{ps} is the mean piston speed in m/s, R is the universal gas constant (8.314 kJ/kgK), and E_A is the activation energy.

$$E_A = \left(\frac{618840}{\text{Cetane number}+25}\right) \text{ kJ/kg} \quad (4.12)$$

T_m (K) and P_m (bar) are the mean temperature and mean pressure of air + biogas in the inlet manifold respectively, and n is the polytropic index.

$$O_{dual} = \frac{(O_f)_{\text{dual fuel}}}{(O_f)_{\text{diesel}}} \quad (4.13)$$

where O_f is the oxygen mole fraction, $(O_f)_{\text{dual fuel}}$ is the oxygen mole fraction in biogas and air in the dual fuel mode, and $(O_f)_{\text{diesel}}$ is the oxygen mole fraction in diesel operation. The oxygen mole fraction is given by: $O_f = \frac{M_{air}}{4.76(M_{mixture})}$, where, the mole fraction (M) of the mixture is:

$$M_{mixture} = M_{air} + M_{biogas} + M_{exh.gas} \quad (4.14)$$

4.7.2 Calculation of the heat release rate

The rate of heat release at each crank angle for diesel operation was determined from the following correlation, derived from the first law of thermodynamics [104,206].

$$\frac{dU}{dt} + \dot{W} = \dot{Q} \quad (4.15)$$

where $\dot{W}$ is the rate of work done by the system due to the system boundary displacement (J). $\dot{Q}$ is the net heat release during combustion (J) and $\dot{Q}_{LW}$ is the heat loss across the cylinder wall (J). Considering the ideal gas condition with the unit mass system, Eq. (4.15) can be represented as:

$$\dot{Q} = \left[\frac{C_v}{R} + 1\right] P\frac{dV}{dt} + \frac{C_v}{R} V\frac{dP}{dt} + \dot{Q}_{LW} \quad (4.16)$$

Replacing time (t) with crank angle(θ), and $\frac{C_p}{C_v} = \gamma$, the equation becomes

$$\dot{Q} = \frac{\gamma}{\gamma-1} P\frac{dV}{d\theta} + \frac{1}{\gamma-1} V\frac{dP}{d\theta} + \dot{Q}_{LW} \quad (4.17)$$

where P is the instantaneous cylinder pressure, θ is the crank angle, γ is the ratio of the specific heats, C_p/C_v, and V is the instantaneous cylinder volume (m^3). The instantaneous cylinder volume was obtained from the engine geometry and crank angle values. The heat loss across the cylinder wall, is $\dot{Q}_{LW}$.

The blow-by losses $\dot{Q}_{LW}$ can be calculated by using the well-known correlation described by Rakopoulos [207]. The instantaneous mass m in the cylinder at any crank angle θ (corresponding time t) is calculated from:

$$m(\theta) = m(\theta_{ivc}) - \int_{\theta_{ivc}}^{\theta} \frac{dm_e}{dt}\frac{1}{6N}d\theta \tag{4.18}$$

where, the mass is accomplished at the point of the inlet valve closer, with a known value of pressure and temperature. Consider, $d\theta = 6Ndt$. N is the engine speed in rpm. The gross heat release rate with respect to θ can be as follows:

$$\frac{dQ_g}{d\theta} = \frac{dQ_n}{d\theta} + \frac{dQ_{LW}}{d\theta} \tag{4.19}$$

where, $\frac{dQ_{LW}}{d\theta}$ is the rate of heat transferred to the combustion chamber wall [207].

The specific heat ratio, γ, is a function of temperature, and it influences the magnitude of $\dot{Q}$ and $\dot{Q}_{LW}$. The presence of CO_2 in the biogas lowers the value of γ. However, the authors Luijten and Kerkhof [104] suggested that the change in γ, within a typical range of 1.3-1.35 did not affect the $\dot{Q}$ and $\dot{Q}_{LW}$. Hence, a constant value for γ=1.35 is considered in this study, for analyzing the heat release rate in the dual fuel operation.

The HRR in the dual fuel operation is dependent on the quality of the fuel mixture. Also, it is dependent on the mass flow rate and lower heating value (LHV) of both the liquid and gaseous fuels. The rate of heat release in the dual fuel operation can also be expressed as follows.

$$HRR = \frac{m_f \cdot LHV_f}{m_f \cdot LHV_f + \sigma(1-m_f)\cdot\left[(LHV_{CH_4} + LHV_{H_2})\right]} \tag{4.20}$$

$$= \frac{m_f \cdot LHV_f}{LHV_{f+biogas}} \tag{4.21}$$

where m_f is the mass fraction of fuel in the fuel mixture, and LHV is the lower heating value of the fuel (kJ/kg). Here, in Eq. (4.20), hydrogen (H_2) is considered, because the biogas used for this experiment contains a small amount of hydrogen (H_2=1.4% vol.), which also takes part in the combustion, giving some heat energy. The LHV and m_f were calculated as follows:

$$(LHV)_{biogas} = \sigma\left(LHV_{CH_4} + LHV_{H_2}\right) \tag{4.22}$$

$$m_f = \frac{HRR\cdot\sigma\left(LHV_{CH_4}+LHV_{H_2}\right)}{(1-HRR)\cdot LHV_f + \sigma\left(HRR\left(LHV_{CH_4}+LHV_{H_2}\right)\right)} \tag{4.23}$$

$$= \frac{\dot{m}_{CH_4} + \dot{m}_{H_2}}{\dot{m}_{CH_4} + \dot{m}_{CO_2} + \dot{m}_{H_2}} \quad (4.24)$$

where σ is the quality of the intake mixture to the engine and ṁ is the mass flow rate in kg/h.

4.7.3 Calculation of combustion duration

Combustion duration was calculated as the crank angle interval between the point at which the heat release rate becomes positive, and the point at which 90% of the heat release has taken place [89,208].

4.7.4 Calculation of brake thermal efficiency

The brake thermal efficiency (BTE) of an engine is the efficiency at which the chemical energy of a fuel is converted into useful work. The BTE of an engine operating on diesel/biodiesel, and in the dual fuel mode can be determined, by using the following equations;

$$[\eta_{th}]_{diesel} = \frac{P}{\dot{m}_f \cdot (LHV)_f} \times 100 \quad (4.25)$$

$$[\eta_{th}]_{dual\ fuel} = \frac{P}{(\dot{m}_f + \dot{m}_{biogas}) \cdot (LHV)_{dual}} \times 100 \quad (4.26)$$

$$= \frac{P}{\dot{m}_f \cdot LHV_f + \dot{m}_{biogas} \cdot LHV_{biogas}} \times 100 \quad (4.27)$$

where, η_{th} is the brake thermal efficiency (%), $\dot{m}_f$ is the mass flow rate of fuel (kg/h), and $(LHV)_f$ is the calorific value of fuel used (kJ/kg). P is the brake power (kW) of the engine. In the dual fuel operation, the BTE depends on the fuel consumption of both diesel and biogas, with the calorific value of both.

4.7.5 Calculation of biogas energy share

In a dual fuel operation, the energy share of the primary gaseous fuel is an important parameter for analyzing the lean premixed combustion. In order to generate a certain amount of power, both the primary fuel (biogas) and pilot fuel (diesel/biodiesel) contribute energy. The energy share by a fuel strongly depends on the calorific value and rate of fuel consumption [208]. The energy share in the dual fuel operation is defined as the ratio of energy supplied by the primary fuel, to the sum of the energy supplied by the primary fuel and the pilot fuel. The biogas energy share is quantified as follows:

$$\text{Biogas energy share} = \frac{\text{Energy equivalent of biogas}}{\text{Energy equivalent of (pilot fuel+biogas)}} \times 100 \quad (4.28)$$

$$\text{where the energy equivalent of the pilot fuel} = \frac{\dot{m}_{\text{pilot fuel}} \times CV_{\text{pilot fuel}}}{3600} \quad (4.29)$$

$$\text{and, energy equivalent of biogas} = \frac{\dot{m}_{\text{biogas}} \times CV_{\text{biogas}}}{3600} \quad (4.30)$$

where, $\dot{m}_{\text{pilot fuel}}$ and $\dot{m}_{\text{biogas}}$ are the mass flow rates of the fuels, and CV is the calorific value of the fuel used.

4.8 Experimental methodology

The different methods used in this investigation are illustrated in Figure 4.12, and they are explained in the subsequent subsections.

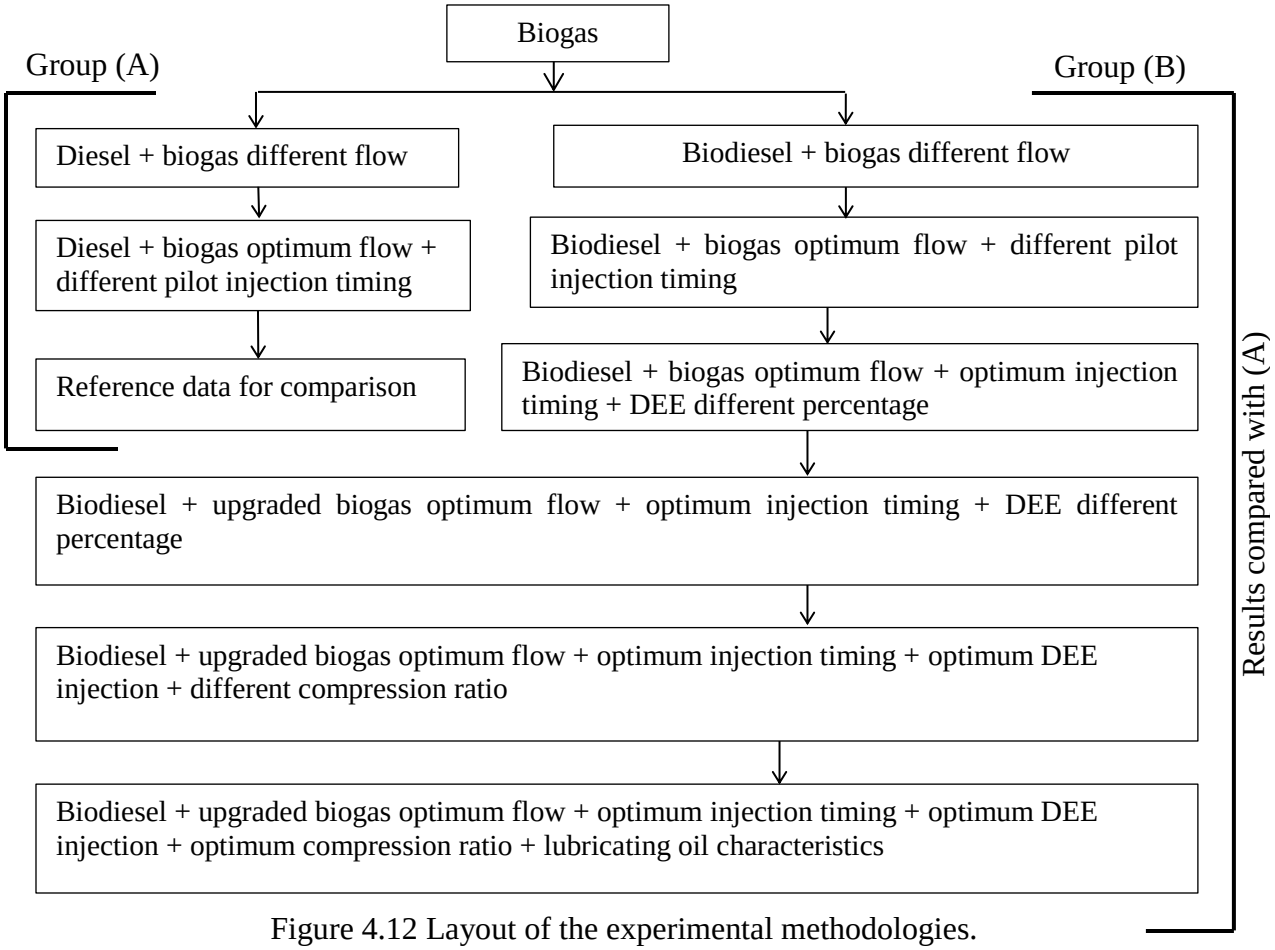

Figure 4.12 Layout of the experimental methodologies.

4.8.1 Engine experiment with diesel and KME

Initially, the engine was operated with diesel for obtaining the baseline reference data of the combustion, performance and emission parameters. The load of the engine was varied from 0% to 100% in steps of 25% each. The brake power produced by the engine at each respective load is 0, 1.14, 2.36, 3.54 kW, and 4.38 kW for loads of 0%, 25%, 50%, 75%, and 100% respectively. For each set of loads, the engine was run for at least 5 min to attain a steady state, after which the data were collected for the analysis. Further, the engine was allowed to run on Karanja methyl ester (KME). The data for diesel and KME were recorded only for comparison purposes with the dual fuel operation of the engine.

4.8.2 Engine experiment in the diesel-biogas dual fuel mode

In the diesel-biogas dual fuel mode, diesel was used as a pilot fuel, while biogas was inducted through the intake manifold of the engine at 0.3 kg/h, 0.6 kg/h, 0.9 kg/h and 1.2 kg/h. In this section the combustion, performance and emission characteristics of the engine were recorded for each fuel with varying loads. Finally, the results obtained in the diesel-biogas dual fuel mode were compared with those of diesel operation, and the optimum flow rate of biogas was observed.

4.8.3 Engine experiment with diesel-biogas and biodiesel-biogas dual fuel mode varying the injection timings

This section presents the results of the combustion, performance, and emission characteristics of the DI diesel engine operated with diesel-biogas, and biodiesel-biogas dual fuel, varying the injection timings.

In order to change the fuel injection timings, it is required to adjust the fuel injection pump settings. By varying the numbers of shims under the fuel injection pump, the fuel injection timing was changed. To advance the fuel injection timing, the shims under the pump were removed and to retard, additional shims were introduced under the fuel injection pump. At standard injection timing, the number of shims placed under the pump was three. The thickness of each shim is 0.3 mm. By removing one shim, about 1.5 ^{o}CA injection timing was advanced, and introducing an additional shim will retard the timing by1.5 ^{o}CA. Figure 4.13 illustrates the

photographic view of the fuel injection pump with shims. Figure 4.14 shows the photograph of the shim used below the fuel injection pump.

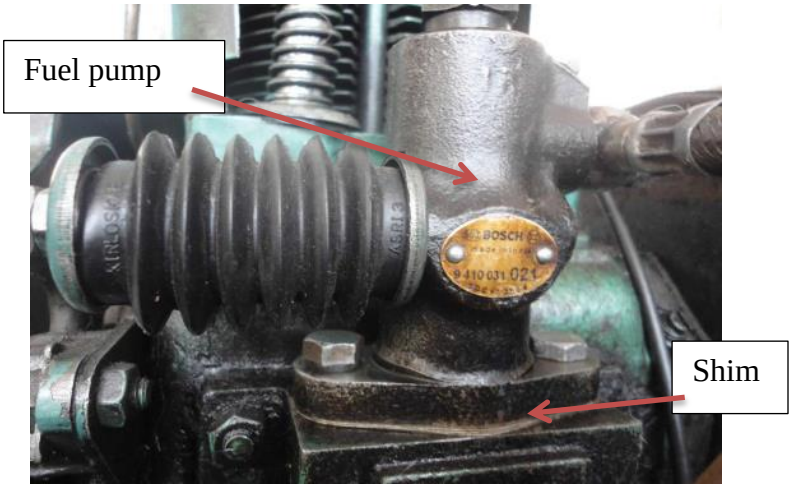

Figure 4.13 Photographic view of the fuel injection pump with shims.

Figure 4.14 Photograph of the shim used below the fuel injection pump.

4.8.4 Experiment with biodiesel-biogas dual fuel mode with variation in DEE injection quantity

4.8.4.1 DEE port injection

The DEE was injected near the intake valve to the air-biogas stream with the help of an electronically controlled injector and pump at a pressure of 3 bar, using a five-hole solenoid based electronic injector. A photographic view of the electronic injector is shown in Figure 4.15.

Figure 4.15 Photographic view of the electronic injector used for DEE injection.

The injector nozzle hole diameter was 0.126 mm each. The injector and pump were operated at 12 V power supply. A microcontroller (Atmega-328) was used to drive the fuel pump. The microcontroller was programmed to control the injection quantity of DEE, using a pulse width modulation (PWM). The duty cycle of PWM modulates the required injection quantity as set by the user. The excess fuel return system of the injector was modified, to send back the excess DEE, to the storage tank. An adapter (L293D) was used to supply the required current and voltage to the injector, pump, and a microcontroller. The flow chart of the programming used for regulating the pump and injector is shown in Figure 4.16. The algorithm used to operate the DEE electronic injector is given in Annexure VI.

4.8.4.2 DEE injection strategies

The DEE injection strategy and the injection duration were dependent on the engine valve timing position and engine speed. From the valve timing values, it was observed that, the intake valve remained open for 220 ^{o}CA of the crank position (i.e. 4.5 ^{o}CA bTDC + 180 ^{o}CA aTDC + 35.5 ^{o}CA aBDC =220 ^{o}CA). The valve overlap period was 9 ^{o}CA (i.e. 4.5 ^{o}CA bTDC+4.5 ^{o}CA aTDC). The valve overlap duration reduced the effective air-biogas intake duration to 211 ^{o}CA (i.e. 220 ^{o}CA-9 ^{o}CA=211 ^{o}CA). This 211 ^{o}CA effective intake duration was divided into three angular injection durations, and each was of 70.3 ^{o}CA. The programming in the microcontroller was written to inject DEE as per the injection duration of 70.3 ^{o}CA, 140.6 ^{o}CA and 210.9 ^{o}CA, in

each cycle of the experimental module. The injection durations were converted into time scale using the equation: $I_{Duration} = (60 \times \theta \times 10^6)/(N \times 360)$, where $I_{Duration}$ is the injection duration in μ sec., θ is the crank rotation for a specific interval value, deg., and N is the engine speed, rpm.

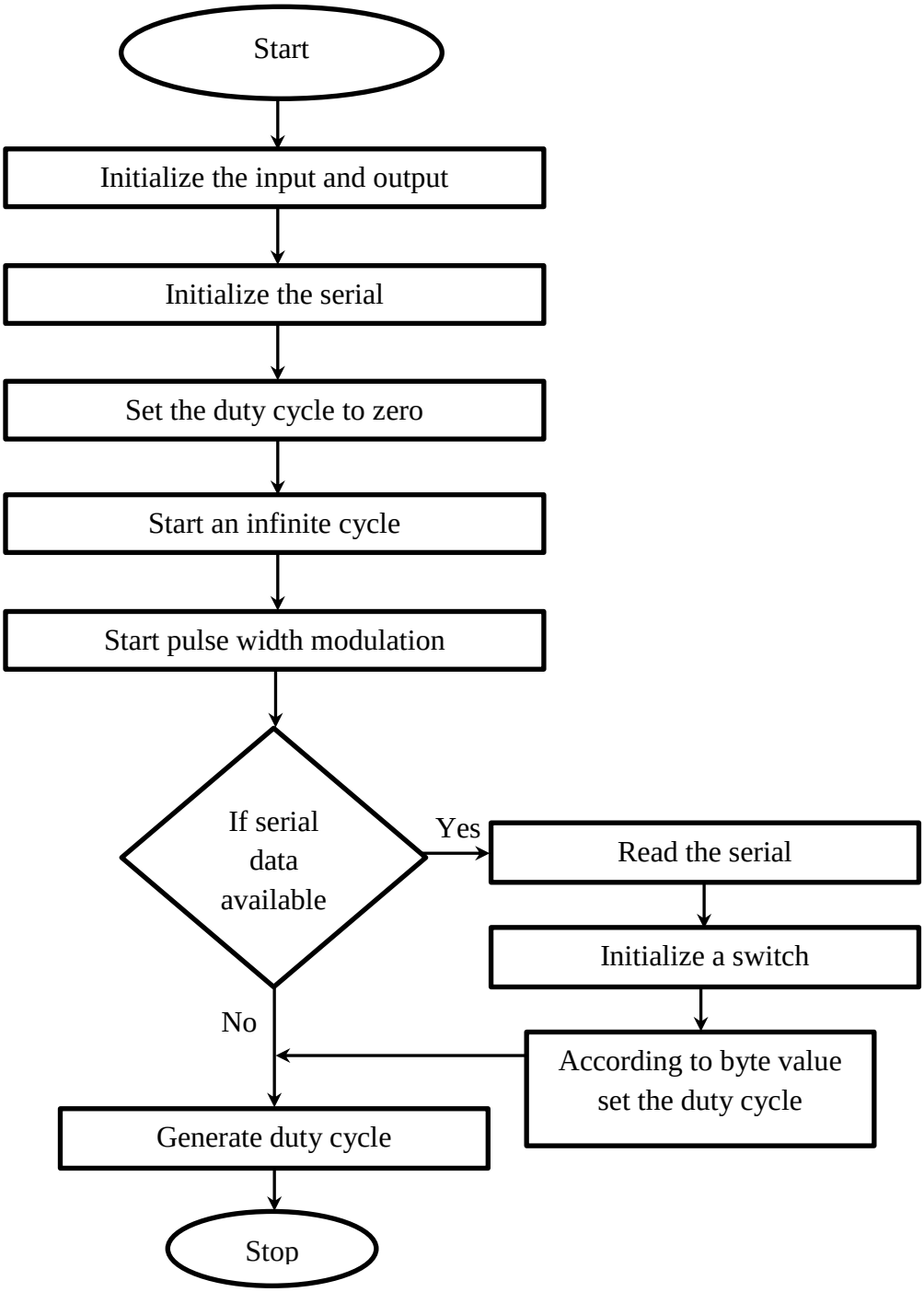

Figure 4.16 Flow chart of the electronic fuel injector.

The engine was first run with diesel up to the warm up condition to ensure the steady state operation. During the steady state condition, the baseline data for diesel and KME were collected. Then, the biogas supply valve was slowly opened, and the flow rate of biogas was set at 0.9 kg/h. In the KME-biogas dual fuel mode, the engine was allowed to run up to the steady state, and the data were collected. Then, the injection timing of KME was varied by changing the thickness of the shims used in the fuel injection pump as explained above. For the diesel and KME operations, the injection timing was set at 23 ^{o}CA bTDC. During the dual fuel operation, the injection timing was varied from 23 ^{o}CA bTDC to 24.5 ^{o}CA bTDC (24.5 ^{o}CA bTDC was found to be the optimum from the previous analysis by the authors). During the KME-biogas dual fuel operation of 24.5 ^{o}CA bTDC, DEE was injected near the intake port with the help of an electronic injector. The DEE injection quantity was varied from 2% to 6% in steps of 2%. During experimentation, the engine was loaded from 0% load (no load) to 100% load (full load) in steps of 25%. Corresponding to the variation in load the brake mean effective pressure (BMEP) values are 0, 1.37, 2.97, 4.55, and 5.63 bar for 0%, 25%, 50%, 75%, and 100% load respectively. During the diesel, KME, KME-biogas, and KME-biogas-DEE operations, the engine was set to run at a constant speed of 1500 rpm, at a pilot injection pressure of 200 bar with a standard compression ratio of 17.5:1. The mass of pilot fuel consumption was regulated by the conventional governor control mechanism, according to the variation in load, speed, and supply of primary fuels (biogas and DEE).

4.8.5 Variation of the compression ratio

In the present investigation, the compression ratio was changed by changing the clearance volume, by inserting gaskets of different thicknesses, between the cylinder and the cylinder head. Figure 4.17 shows the photographic view of the (a) gasket and (b) dismantled engine cylinder and head.

The steps involved in the compression ratio calculation are as follows:

$$\text{Compression ratio} = \frac{\text{Maximum cylinder volume } (V_s+V_c)}{\text{Clearance volume}(V_c)} \quad (4.31)$$

Maximum cylinder volume = swept volume (V_s) + clearance volume (V_c)

$$Vs = \frac{\pi d^2}{4} \times L \quad (4.32)$$

where, d = cylinder bore diameter = 8.75 cm, L = stroke length = 11 cm.

(a) gasket

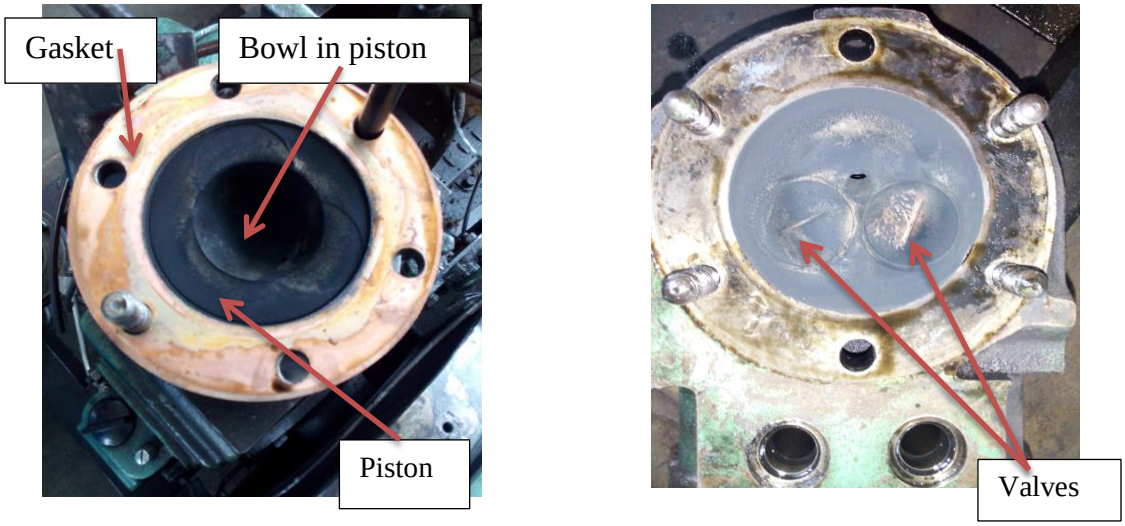

(b) Dismantled engine cylinder and head.

Figure 4.17 Photographic view of the (a) gasket and (b) dismantled engine cylinder and head.

$$CR = 17.5 = \frac{V_s + V_c}{V_c} \quad (4.33)$$

$$17.5 = \frac{V_s}{V_c} + 1 \quad (4.34)$$

$$V_c = \frac{V_s}{16.5} = \frac{661.45}{16.5} = 40.08 \text{ cm}^3$$

Gasket volume = 7.21 cm^3 (d=8.75 cm, t=0.12 cm)

$$\text{For } CR = 18.5, V_c = \frac{V_s}{17.5} = \frac{661.45}{17.5} = 37.79 \text{ cm}^3$$

Clearance volume excluding gasket volume + gasket volume = 37.79

32.87 + gasket volume = 37.79

Gasket volume required for CR 18.5 = 4.92 cm

Gasket thickness required = 0.08 cm

Similarly, the gasket volume and thickness required for CR = 16.5 was calculated.

The calculated gasket volume and thickness corresponding to the different compression ratios are given in Table 4.1.

Table 4.1 Gasket volume and thickness required for different compression ratio.

Compression ratio	Gasket volume (cm^3)	Gasket thickness (cm)
16.5	9.8	0.16
17.5	7.21	0.12
18.5	4.92	0.08

4.9 Instrument uncertainty analysis

Uncertainty is the means for measuring the error of a result or an instrument. Without such measure, it is impossible to judge the fitness value. To estimate the accuracy bounds of an estimated parameter, the uncertainty analysis is highly recommended. The evaluation of uncertainty from some known physical value can be obtained by using the formula described by Coleman et al. [209]. Annexure V lists the uncertainties of the instruments used in the present investigation.

$$U_R = (B_R^2 + P_R^2)^{1/2} \tag{4.35}$$

U_R is the uncertainty of the physical parameter considering 5% significance. B_R and P_R are the systematic and random uncertainties respectively.

$$\frac{B_R}{R} = \left[\sum_{i=1}^{n} \left(\frac{1}{R}\frac{\partial R}{\partial X_i} B_i\right)^2\right]^{1/2} \tag{4.36}$$

$$\frac{P_R}{R} = \left[\sum_{i=1}^{n} \left(\frac{1}{R}\frac{\partial R}{\partial X_i} P_i\right)^2\right]^{1/2} \tag{4.37}$$

In the equation cited, R is the physical parameter that depends on the variable X_i. The symbols P_R and P_i denote the uncertainty in R and the measurement level, respectively. For the uncertainty analysis, 20 sets of observation have been taken in the same engine, and same operating condition, and as a result, the maximum overall uncertainty of the instruments obtained was ± 2.20%.

4.10 Mathematical modeling and validation of experimental results

4.10.1 General description of the model

In a dual fuel mode, biogas was inducted through the intake manifold, and the air-biogas mixture enters to the combustion chamber during the suction stroke. The auto ignition temperature of biogas is too high and it did not self-ignite. Hence, the air-biogas mixture is considered as a non-burning zone. The air-biogas mixture ignites after the injection of pilot fuel, and the burning zone stats. In burning zone, fuel is continuously injected and burns with the available air from the non-burning zone, and the inducted biogas in non-burning zone burns at the periphery of the burning zone. In this present model, the analysis is taken into consideration from the occurrence of compression to the end of the expansion stroke.

It is assumed that, the inlet and exhaust valve are fully closed during the compression and expansion stroke. Practically, in all four stroke DI diesel engines the compression process is a polytropic one, which begins from the moment the inlet valve closes and ends, when the fuel injection starts. Similar assumptions are considered in this analysis. The shape of the combustion chamber and piston in this research engine is hemispherical and bowl in piston type, and the pilot fuel injector nozzle has three holes.

The main calculation is based on the integration of the first law of thermodynamics, and the ideal gas equation. The following assumptions are made for the analysis;

(a) The cylinder contains the non-burning zone and burning zone.

(b) The pressure and temperature in each zone are uniform and vary with the crank angle, and the content of each zone follows the perfect gas laws.

In the theoretical model, the spray of pilot fuel injected into combustion chamber is divided into several zones. The boundaries of these zones are determined from lines of constant equivalence ratios. Applying the first law of thermodynamics, ideal gas equation and other basic relations to

the cylinder charge (i.e. zones), a system of ordinary differential equations for cylinder pressure and zones volumes have been obtained as follows [210]:

$$\frac{dp}{d\theta} =$$

$$\left[\sum_{i=1}^{n} \psi_i \dot{m}_{i,in}\left(\emptyset_i R_i T_i - u_i + h_{i,in}\right) - \sum_{i=1}^{n} \psi_i \dot{m}_{i,out}\left(\emptyset_i R_i T_i - u_i + h_{i,out}\right) + \sum_{i=1}^{n} \psi_i \emptyset_i m_i T_i \frac{\partial R_i}{\partial \emptyset_i}\frac{d\emptyset_i}{d\theta} - \right.$$

$$\left.\sum_{i=1}^{n} \psi_i m_i \frac{\partial u_i}{\partial \emptyset_i}\frac{\partial \emptyset_i}{d\theta} + \sum_{i=1}^{n} \psi_i \dot{Q}_i - \sum_{i=1}^{n} \frac{dV_i}{d\theta}\right] / \left[\sum_{i=1}^{n}\left(\emptyset_i m_i \frac{\partial u_i}{\partial p} + \psi_i \emptyset_i V_i - \psi_i \emptyset_i m_i T_i \frac{\partial R_i}{\partial p}\right)\right] \quad (4.38)$$

Where; $\emptyset_i = m_i \frac{\partial u_i}{\partial T_i}\left(1/\left(m_i R_i + m_i T_i \frac{\partial R_i}{\partial T_i}\right)\right) \psi_i = 1/(\emptyset_i p + p)$ (4.39)

Where i denote an individual control volume and n is the total number of zones in the cylinder. From the above ordinary differential equation the cylinder pressure and zones volumes can be calculated. The zones temperatures can be computed from ideal gas equation by using cylinder pressure and zones volumes.

4.10.2 Energy equations

During the compression stroke, one zone exists; hence, the first law of thermodynamics for a close system is applied together with the ideal gas state equation [210]. The change in internal energy is expressed as follows:

$$\frac{d(mu)}{d\theta} = \frac{dQ_r}{d\theta} - \frac{dQ_h}{d\theta} - \frac{dW}{d\theta} \quad (4.40)$$

By replacing the work transfer term dW/dθ with PdV/dθ or by using the ideal gas law PV = mRT, the above equation (4.38) can be rearranged as:

$$m\frac{du}{d\theta} = \frac{dQ_r}{d\theta} - hA\frac{dT}{d\theta} - RT\frac{dV}{d\theta} \quad (4.41)$$

where, V is the instantaneous cylinder volume with respect to the crank angle, which is given by,

$$V = V_{cl} + (\pi D^2/4)r\left[1 + \lambda^{-1} - \cos\varphi - (\lambda^{-2} - \sin^2\varphi)^{1/2}\right] \quad (4.42)$$

In the above equations, the term dQ is given as the fourth order polynomial expression of the absolute temperature T, including the enthalpy of formation at absolute zero. The internal energy calculation as a function of temperature is:

$$\frac{hi}{R_{mol}T} = ai1 + ai2/2\ T + ai3/3T^2 + ai4/4T^3 + ai5/5T^4 + ai6/3T^5 \quad (4.43)$$

$$ui = hi - RT \quad (4.44)$$

For the surrounding air zone, which only loses the air mass and biogas to the burning zone, the first law of thermodynamics for the unburned zone can be written as:

$$dE = dQ - pdV - h_a dm_a \quad (4.45)$$

In the burning zone there is an enthalpy flow from the fuel, which is ready to be burned in the time step. So, the first law of thermodynamics for the burning zone becomes

$$dE = dQ - pdV + h_a dm_a + h_f dm_f \quad (4.46)$$

The first law of thermodynamics for the combustion in time step dt is:

$$f(E)=E(T_2) - E(T_1) - dQ + dW + dm_f Q_{vs} = 0 \quad (4.47)$$

If f(E) is greater than the accuracy, the required new value of T_2 is calculated using the Newton-Raphson numerical method. The unburned zone temperature is calculated using the equation,

$$T_u = T_{soc}\left(\frac{P}{P_{soc}}\right)^{\gamma-1/\gamma} \quad (4.48)$$

4.10.3 Heat transfer model

The heat transfer between the cylinder trapped mass and the surrounding walls is calculated, using the formula of Anand [211]. The formula to calculate the heat loss from the cylinder, is

$$dQ/dt = a\frac{\lambda_g}{D}(Re)^b\left(T_w - T_g\right) + c.\left({T_w}^4 - {T_g}^4\right) \quad (4.49)$$

In this equation 'T_w' is the cylinder wall temperature which is assumed as 450 K, and a, b, c are constants. The constant values are taken as, a=0.2626, b=0.6, c=5.67×10^{-8} W/m^2/K.

4.10.4 Division of pilot fuel spray into multiple zones its development

The fuel injected inside the combustion chamber breaks up into globules, forming a cone shaped spray corresponding to each one of the nozzle holes. If the kmoles of air trapped in the cylinder in every cycle are $w_{a_{tot}} = m_{a_{tot}}/M_a$, then the phenomenon will continue until each spray penetration reaches a value of $\left(\frac{D}{2} + \frac{\pi D}{z}\right)$.

The mean value of fuel injection rate can be calculated as followes [211]:

$$\bar{m}_{f_{inj_j}} = m_{f_{tot}}/\left(z.\Delta\emptyset_{inj}\right) \quad (4.50)$$

where index j denotes each one of the z sprays and $\Delta\emptyset_{inj}$ is the total duration of fuel injection in degree crank angle. At each crank angle step, the fuel injection rate and the cumulative fuel injected in each spray are, respectively as follows:

$$\dot{m}_{f_{inj_j}} = \dot{m}_{f_{inj}}/z \tag{4.51}$$

Similarly, the velocity and pressure drop across the nozzle are, respectively,

$$u_{inj} = \dot{m}_{f_{inj_j}} 6N/(\rho_l . F) \tag{4.52}$$

$$\Delta P = 0.5\rho_l\left(u_{inj}/c_D\right)^2 \tag{4.53}$$

The mass of air entrained in the zones are

$$m_{a_j} = \frac{\pi}{3}\left(\tan\frac{\theta}{2}\right)^2 . \rho_a . (x - x_{br})^3 \tag{4.54}$$

In the above relations, it is considered that the volume taken by the fuel is negligible against that of the air [212].

For the fuel mass that is effectively inside the spray only after the break-up length is

$$m_{f_j} = m_{f_{inj_j}}(t - t_{brs})/t \tag{4.55}$$

$$m_{f_j} = \frac{m_{f_{inj_j}}}{(\Delta\emptyset_{inj}/6N)}(t - t_{brs}) \tag{4.56}$$

$$m_{f_j} = m_{f_{inj_j}} \text{ for } t > \left(\Delta\emptyset_{inj}/6N\right) + t_{brs} \tag{4.57}$$

The air fuel ratios (AFR) by mass are as followes:

$$AFR_{spr} = \frac{m_{a_j}}{m_{f_j}} \tag{4.58}$$

$$AFR_{spr_s} = \frac{m_{a_{js}}}{m_{f_j}} \tag{4.59}$$

The biogas-pilot fuel to air equivalence ratio of each zone can be calculated based on the evaporated fuel mass of each zone [213]:

$$\Phi_{zvap}(i,j) = \frac{m_{fzvap}(i,j)/m_{az}(i,j)}{(1/AFR_{st})} \tag{4.60}$$

4.10.5 Wiebe's combustion model

The Wiebe function is used to predict the mass fraction burnt and the burn rate in IC engines, operating with different combustion systems and different fuels. Wiebe linked the chain chemical reactions with the fuel reaction rate in IC engines and his approach is based on the premise that a simple one-step rate equation would not be adequate to describe the complex

reacting systems, such as those occurring in an IC engine. The Wiebe functions [212] for the non-dimensional burn fraction x as a function of the degrees of crank angle can be written as

$$x = 1 - \exp\left[-6.908\left(\frac{\theta-\theta o}{\Delta\theta}\right)^{m+1}\right] \quad (4.61)$$

The heat release rate calculated with the help of the Wiebe function is,

$$\frac{dQ_c}{d\theta} = 6.908(m+1)\left(\frac{Q_{av}}{\Delta\theta}\right)\left(\frac{\theta-\theta_o}{\Delta\theta}\right)^{m}\exp\left[-6.908\left(\frac{\theta-\theta o}{\Delta\theta}\right)^{m+1}\right] \quad (4.62)$$

where x is the mass fraction burned, θo is the start of combustion and $\Delta\theta$ is the combustion duration. The parameter m represents the rate of combustion. Q_{av} is the heat released per cycle. The value of m for both the fuels is taken as 3.0.

When calculating the heat release, prior knowledge of the actual overall equivalence ratio is necessary. The term equivalence ratio is defined as the ratio of the actual air-fuel ratio to the stoichiometric air-fuel ratio. This helps in fixing the mass of fuel to be admitted.

4.10.6 Ignition delay

The time delay between the start of injection and the start of combustion is defined as the ignition delay period. The determination of the start of combustion (SOC) by selecting the proper method is a key issue in ignition delay studies. In the combustion model, the ignition delay is also taken into account. The ignition delay period is calculated by integrating Wolfer's relation, using the trapezoidal rule [213].

$$\int_{t_{inj}}^{t_{ign}} \frac{dt}{t(p,T)} = \frac{1}{K_{t_{inj}}}\int_{t_{inj}}^{t_{ign}} \frac{dt}{(p(t))^{-q}\exp(\frac{E}{RT(t)})} = 1 \quad (4.63)$$

The values of various constants corresponding to a DI diesel engine are K =2272; q = -1.19; E/R = 4650.

where, K = thermal conductivity, q = heat losses, E/R=activation energy/universal gas constant.

4.10.7 Chemistry of combustion

In a combustion process, the fuel and the oxidizer react to produce products of different compositions. The theory of combustion is a complex one, and has been the topic of intensive research for many years. Let us represent the chemical formula of a fuel as $C\alpha H\beta O\gamma N\delta$. In the present case, it was considered that 10 species were present in the combustion product, and the combustion equation is given by:

$\epsilon\varphi C\alpha H\beta O\gamma N\delta + 0.21O_2 + 0.79N_2 \rightarrow \nu 1CO_2 + \nu 2H_2O + \nu 3\ N_2 + \nu 4O_2 + \nu 5CO + \nu 6H_2 + \nu 7H + \nu 8O + \nu 9OH + \nu 10NO$ (4.64)

From the atomic balance of each species C- H- O- N the following 4 equations, are obtained.

C $\epsilon\varphi\alpha = (y1+y5)\ N1$ (4.65)

H $\epsilon\varphi\beta = (2y1+2y6+y7+y9)\ N1$ (4.66)

O $\epsilon\varphi\gamma+0.42 = (2y1+y2+2y4+y5+y8+y9+y10)\ N1$ (4.67)

N $\epsilon\varphi\delta +1.58 = (2y3+y10)\ N1$ (4.68)

The chemical reactions considered in equilibrium, are as follows:

$N_2 + O_2 \rightarrow 2NO$ (4.69)

$2H_2O + O_2 \rightarrow 4OH$ (4.70)

$2CO + O_2 \rightarrow 2CO_2$ (4.71)

$2H_2 + O_2 \rightarrow 2H_2O$ (4.72)

$N_2 \rightarrow 2N$ (4.73)

$H_2 \rightarrow 2H$ (4.74)

$O_2 \rightarrow 2O$ (4.75)

The use of the equilibrium constant is identical to maximizing the entropy of the gas. This method is similar, when considering a restricted species list such as the present case [214]. The chemical equilibrium constant can be calculated from the following equations:

$$K_{p1} = \frac{P_{NO}^2}{P_{N_2}.P_{O_2}}, \quad K_{p2} = \frac{P_{OH}^4}{P_{H_2O}^2.P_{O_2}}, \quad K_{p3} = \frac{P_{CO_2}^2}{P_{CO_2}^2.P_{O_2}} \tag{4.76}$$

$$K_{p4} = \frac{P_{H_2O}^2}{P_{H_2}^2.P_{O_2}}, \quad K_{p5} = \frac{P_N^2}{P_{N_2}}, \quad K_{p6} = \frac{P_H^2}{P_{H_2}}, \quad K_{p7} = \frac{P_O^2}{P_{O_2}} \tag{4.77}$$

Once the composition is known, the thermodynamic properties of interest like enthalpy, entropy, specific volume, and internal energy can be computed.

4.10.8 Nitric oxide formation model

The current approach to model the NO_x emissions from diesel engines is, to use the extended Zeldovich thermal NO mechanism, by neglecting other sources of NO_x formation. The extended Zeldovich mechanism consists of the following reactions:

$$O + N_2 \rightarrow NO + N \quad (4.78)$$

$$N + O_2 \rightarrow NO + O \quad (4.79)$$

$$N + OH \rightarrow NO + H \quad (4.80)$$

This mechanism can be written as an explicit expression for the rate of change of the concentration of NO [215]. The change of NO concentration is expressed as follows:

$$(d\,(NO))/dt = 2\,(1-\alpha^2)\,R_1/(1+\alpha R_1/(R_2+R_3)) \quad (4.81)$$

where Ri is the one-way equilibrium rate for the reaction i, defined as:

$$R_1 = k_{1f}\,(N)e(NO)e, \quad R_2 = k_{2f}\,(N)e(O_2)e, \quad (4.82)$$

$$R_3 = k_{3f}\,(N)e(OH)e, \quad \alpha = (NO)/(NO)e \quad (4.83)$$

4.10.9 The net soot formation model

The exhaust gas of the engine contains solid carbon soot particles that are generated in the fuel rich regions inside the cylinder during combustion. Soot particles are clusters of solid carbon spheres, with the HC and traces of other components absorbed on the surface. They are generated in the combustion chamber in the fuel rich zones, where there is not enough oxygen to convert all the carbon to CO_2. Subsequently, as the turbulence motion continues to mix the components, most of these carbon particles find sufficient oxygen to react and form CO_2. Thus, soot particles are formed and consumed simultaneously in the combustion chamber. The net soot formation rate was calculated by using the semi-empirical model proposed by Hiroyasu et al. [216]. According to this model, the soot formation rate (index sf) and soot oxidation rate (index sc) were given by:

$$\frac{dm_{sf}}{dt} = A_{sf}(m_{f.ev} - m_{f.bu})^{0.8} p^{0.5} \exp(-E_{sf}/R_{mol}T) \quad (4.84)$$

$$\frac{dm_{sf}}{dt} = A_{sc} m_{sn} (p_{o2}/p) p^{1.8} \exp(-E_{sc}/R_{mol}T) \quad (4.85)$$

where, the pressures are expressed in bar and d_{mf} is the unburned fuel mass in kg to be burned in time step of dt. Therefore, the net soot formation rate is expressed as:

$$\frac{dm_{sn}}{dt} = \frac{dm_{sf}}{dt} - \frac{dm_{sc}}{dt} \quad (4.86)$$

A program using MATLAB was generated, with all the above mentioned equations and considering all the values of the constants, in order to predict the combustion attributes, like the in- cylinder pressure, ignition delay, and emission such as NO and smoke emissions. The MATLAB program used for this analysis is given in Annexure VII. The comparison of the experimental results and the MATLAB simulation results are discussed in Chapter 5.

4.11 Endurance tests

The main objective of the endurance test was to evaluate the wear characteristics of the engine components, and changes in the lubrication oil properties of the test engine run in the biodiesel-biogas dual fuel mode with the optimum parameters for biogas flow quantity, optimum injection timing, optimum DEE injection quantity, and the optimum compression ratio. A short-term endurance test was conducted as per IS 10000 Part IX - 1980 method for 100 hrs.

Before the start of the test, the existing fuel injection pump, fuel injector, fuel filter and oil filter were replaced with new ones as recommended by the engine manufacturer. Before fitting the engine, the fuel injector, and fuel injection pump were dismantled completely, and photographs were taken in order to compare the wear and deposits on them after the durability test. The used lubricating oil was drained completely, and fresh lubricating oil of SAE 20-40 grade was filled in the oil sump. The engine cylinder head was dismantled and the carbon deposits on the cylinder head, and piston crown were completely cleaned using methanol. The cylinder head gasket was also changed with a new one, and the cylinder head was fitted in the engine block. Once the engine was reassembled, it was allowed to run for 12 hours in the manner recommended by the manufacturer. This test was carried out to take care of any misalignments occurring during dismantling and re-assembling of the engine.

4.11.1 Preliminary run

The purpose of the preliminary run of the engine is to ensure that, the engine should run trouble free. Under the preliminary run, the engine was subjected to a preliminary run of 49 hours at the rated speed and load. The engine was allowed to run repeatedly for a cycle of seven times as per the pattern given in Table 4.2.

Table 4.2 Preliminary run pattern of the engine.

Load on engine, %	Engine run time, hour
25	1.5
50	2
75	1.5
100	2

4.11.2 Long run

The long run endurance test was conducted using biodiesel-biogas, and at the end of each 17-hour cycle, the engine was stopped and minor adjustments were carried out in accordance with the manufacturer's schedule. A total of three cycles were repeated as per the pattern given in Table 4.3. Before starting the next cycle, it was ensured that the engine sump oil had reached the room temperature. During a 100 hour run of the engine, there was no major breakdown noticed. After completion of the endurance test, the engine was completely dismantled, and the deposit formations on the cylinder head, piston top, and injector tip were investigated.

Table 4.3 Test cycle for long-run endurance test.

Load on engine, %	Engine run time, hour
100	4
50	4
100	1.5
No load	0.5
100	3.5
50	3.5

4.12 Measurement method for wear and lubricating oil properties

About 50 ml of the lubricating oil were collected from the engine after every 25 hours (from the preliminary run onwards) for examining the various tribological properties and wear particles. The methodologies used for the measurement of wear, carbon deposits, and lubricating oil properties are described below. The measurement methodologies are given in Table 4.4.

4.12.1 Valve wear

Valve guide wear refers to the increase in the clearance between the valve stem and the valve guide [217]. The excessive friction and extreme heat around the valve may wear down the guide. The method for checking the valve guide wear is as follows: (i) at first the inside diameter of the guide was measured with a small hole gauge. The outside diameter of the valve stem was then measured with a precision micrometer. The difference in the two measurements was taken as the measured clearance, and it was compared with a maximum allowable clearance, and given in terms of the percentage change in clearance.

4.12.2 Carbon deposits

After the run of the engine with biodiesel-biogas in the dual fuel mode, the carbon deposits on the engine components such as the cylinder head, piston crown, and injector tip were studied, as these are directly associated with the fuel properties. Carbon deposits are the unburnt carbon soot deposited on the engine components. These were analyzed by the visual inspection of the various parts, and the amount was measured by weighing the carbon deposits by the weight balance.

Table 4.4 Methods and instruments used for measuring engine wear and the lubricating oil properties.

Measurement type	Test method	Type of analysis	Instrument used
Valve wear	-	-	Precision micrometer
Fuel pump plunger	-	-	Precision weight balance
Piston ring	-	-	Precision weight balance
Carbon deposit on head, and piston	-	Visual inspection	Precision weight balance
Lubricating oil viscosity	ASTM D445-82	-	Viscometer
Lubricating oil flash point	ASTM D92-78	-	Cleveland open cup test
Carbon content	-	-	Fourier transform infrared spectroscopy
Metal wear	-	-	atomic absorption spectroscopy

4.12.3 Analysis of lubricating oil properties

Lubricating oil analysis is required when different fuels are used, and also to know the effect of these fuels on long term applications. The lubricating oil properties of a short-term endurance test can be studied by the fuel dilution method. The lubricating oil properties are affected by fuel dilution which lowers the viscosity and flash point of the lubricating oil.

4.12.4 Ash content measurement

The lubricating oil samples were taken in a silicon crucible, and kept in the furnace at 450°C for 4 hours, and then 600°C for 2 hours to produce ash. The residual ash contains the wear debris of metal primarily. By weighing the crucible before and after the test, the weight percentage of ash was determined.

4.12.5 Atomic absorption spectroscopy (AAS)

The various elements such as Fe, Al, Cu, Zn, Cr, Mg, and Pb in the lubricating oil were analyzed by the atomic absorption spectroscopy. The AAS works on the principle of absorption interaction, where atoms in the vapor state absorb radiation at a certain wavelength that is well defined and show the characteristics of a particular atomic element. In this process, the source of radiation projects a beam of a specific wavelength through a pure flame (air-acetylene) to a sensor and the amount of radiation arriving at the photo sensor is recorded. The fluid sample is introduced into the flame and vaporized. The amount of radiation arriving at the photo sensor is reduced in proportion to the quantity of the specific element present in the sample.

This gives a fair idea about the wear of different parts, and the material compatibility of the new fuel with the existing engines. In this study, the engine used was a reciprocating type and has many sliding components and hence, it was anticipated, that the wear debris originating from different metallic parts would appear in the lubricating oil. The AAS measurement procedure is as follows: (i) approximately 10 grams of oil sample was weighed in a silica crucible and burnt at 450 ^{o}C for 4 hours and at 650 ^{o}C for 2 hours, (ii) The ash was dissolved in concentrated HCl acid, (iii) the mixture was diluted with distilled water to make a 100 ml solution, and (iv) preparation of standard solutions of various metals (concentrations ranging from 5 ppm to 20 ppm).

CHAPTER 5

RESULTS AND DISCUSSION

5.1 Validation of experimental results through mathematical model

5.1.1 General

In this section, a mathematical model was developed to analyze the engine operating parameters and was validated with the experimental results, obtained from a single cylinder, four stroke, air cooled, DI diesel engine modified to operate on dual fuel mode with diesel-biogas, biodiesel-biogas dual fuel. A MATLAB program was developed and coded for a three-zone thermodynamic model and the experimental results were compared and validated. Among the three zones, first zone was consisted of pure air, second zone was consisted of air-biogas mixture and was assumed as the non-burning zone, and the third one consisted of fuel and combustion products, called the burning zone.

The combustion parameters, such as cylinder peak pressure, ignition delay and the chemical equilibrium composition were calculated theoretically, using the three zone model. As the NO and soot emissions are important in a dual fuel CI engine operated on biogas, they were calculated using a semi-empirical model. A comparison of the theoretical and experimental results is analyzed and presented in this section.

5.1.2 Combustion analysis

5.1.2.1 Pressure crank angle diagram

Figure 5.1.1 depicts the variation of simulated and experimental results of the peak cylinder pressure for diesel, KME, DBDFM0.9, and BBDFM0.9 with the variation in crank angle. It can be observed from the figure that, the simulated results of diesel, KME, DBDFM0.9, and BBDFM0.9 give higher values of cylinder pressure compared to the experimental results. The lower cylinder pressure for the experimental results may be due to the measuring instruments' error. This may also depend on the physical conditions during the experiment and the uncertainty of the acquired data. In general, the peak cylinder pressure in a CI engine is predominantly

influenced by the ignition delay, the amount of fuel burnt in the initial stages, and the formation fuel rich region in the combustion chamber during the delay period. The peak cylinder pressure for simulation and experimental results for diesel are about 77.7 bar and 75.7 bar. For KME the peak cylinder pressure for simulation and experimental results are 72.4 bar and 71.3. For DBDFM0.9 it is 76.1 bar and 74.6 bar respectively. Similarly, for BBDFM0.9 the peak cylinder pressure for simulation and experimental results are 74.7 bar and 72.9 bar respectively. For diesel, KME, DBDFM0.9 and BBDFM0.9, the simulated peak cylinder pressure is about 2.6%, 1.5%, 1.9%, and 2.4% higher than that of the experimental result respectively. This marginal deviation in the pressure between simulation and experiment are due to the experimental instrument error.

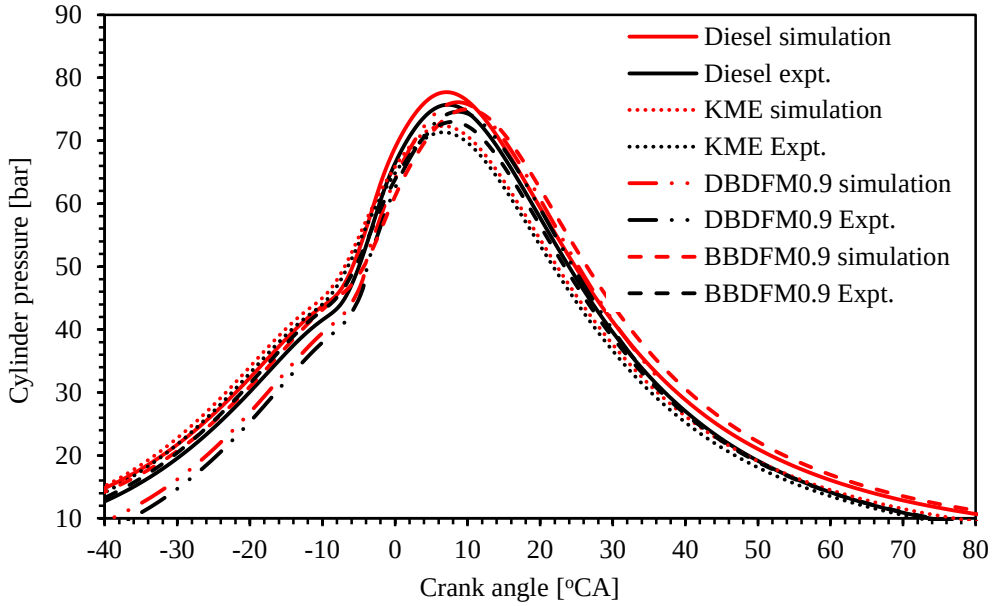

Figure 5.1.1 Comparison of cylinder pressure variation with crank angle for simulated and experimental results.

5.1.2.2 Ignition delay

The comparison of simulated and experimental results of ignition delay at different loads for diesel, KME, DBDFM0.9 and BBDFM0.9 is depicted in Figure 5.1.2. It is evident from the figure that, the ignition delay for simulation and experimental results followed the similar trend for diesel, KME, DBDFM0.9, and BBDFM0.9. The ignition delay decreases with the increase in load as a result of the increase in cylinder gas temperature. The shorter ignition delay for the KME operation than that of diesel and dual fuel operation may be due to the high cetane number

of KME and the presence of oxygen in the fuel improves the start of ignition, and increases the pre-ignition reaction of the fuel. The deviation of ignition delay between the simulated and experimental results for the diesel operation is about 0.4 ^{o}CA, at full load. Similarly, for the KME, DBDFM0.9, and BBDFM0.9 the deviation of ignition delay between simulation and experimental result is about 0.4 ^{o}CA, 0.3 ^{o}CA, and 0.2 ^{o}CA respectively, at full load.

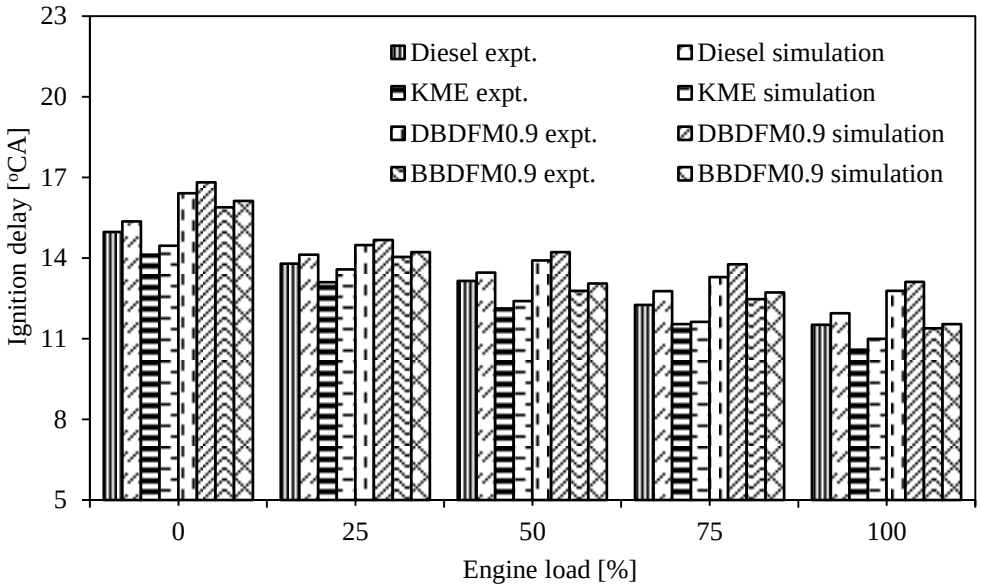

Figure 5.1.2 Comparison of simulated and experimental results of ignition delay at different loads for diesel, KME, DBDFM0.9 and BBDFM0.9.

5.1.3 Emission analysis

5.1.3.1 NO emission

The comparison between the simulation and experimental results of NO emission with load for diesel, KME, DBDFM0.9, and BBDFM0.9 is illustrated in Figure 5.1.3. In a diesel engine, the NO is the predominant pollutant, forms due to the combustion of fuel at high elevated temperature. When the combustion temperature in the range of 1400 ^{o}C to 2000 ^{o}C or more the oxygen reacts with the nitrogen and forms NO_x. In NO_x NO is the major constituent. The deviation of NO emission between the simulation and experimental results is about 2.4%, 3.7%, 5.5%, and 5.4% for diesel, KME, DBDFM0.9 and BBDFM0.9 at full load. This may be due to the change in combustion reaction of the fuel inside the engine when it is operated on a dual fuel mode.

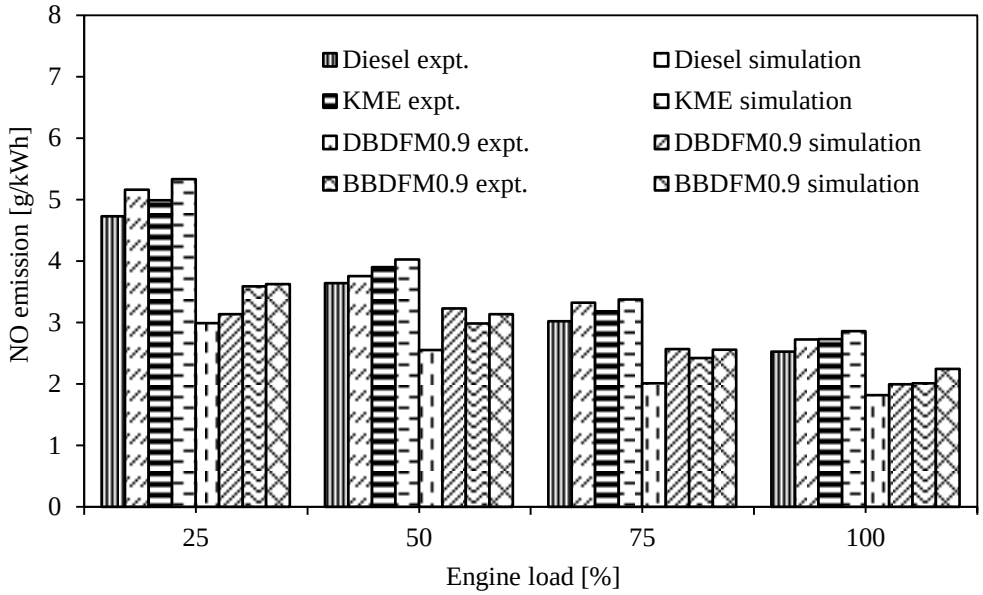

Figure 5.1.3 Comparison between the simulation and experimental results of NO emission with load for diesel, KME, DBDFM0.9, and BBDFM0.9.

5.1.3.2 Smoke emission

The comparison between the simulation and experimental results of smoke emission with load for diesel, KME, DBDFM0.9, and BBDFM0.9 are depicted in Figure 5.1.4. It can be observed from the figure that, the simulated results of smoke are higher than that of experimental results throughout the load spectrum, irrespective of the fuels used. The decrease in smoke for the case of experimental result may be due to the error of the instrument. But, the deviation between the experimental results and simulation is in the acceptable limit. The deviation of smoke emission between the simulation and experimental results is about 1.4%, 2.2%, 2.9%, and 3% for diesel, KME, DBDFM0.9, and BBDFM0.9, at full load respectively. The smoke emission is a result of the oxygen deficiency in the diffusion combustion phase, and the use of a high molecular weight fuel. Diesel has a high carbon to hydrogen ratio, high molecular weight, less oxygen and high aromatic content. Hence, higher smoke emission is observed with the diesel operation compared to that of KME, DBDFM0.9, and BBDFM0.9.

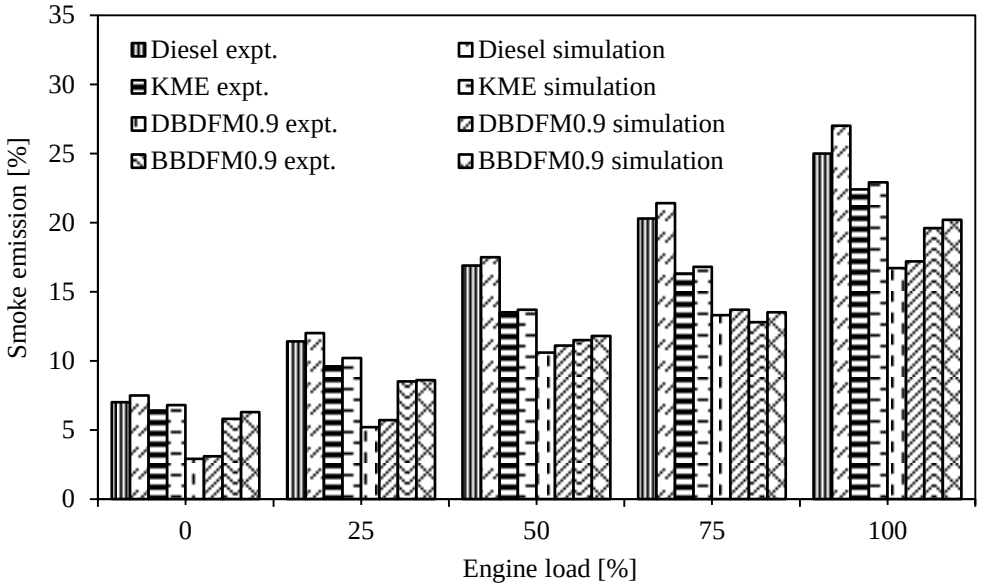

Figure 5.1.4 Comparison between the simulation and experimental results of smoke emission with load for diesel, KME, DBDFM0.9, and BBDFM0.9.

5.1.4 Summary

A comprehensive three zone model is developed to validate the experimental results obtained from a single cylinder, four stroke, air cooled, DI diesel engine modified to operate on dual fuel mode with diesel-biogas and biodiesel-biogas, with minor engine and fuel modifications. The conclusions of the above investigation are as follows:

- For the case of diesel, the simulated peak cylinder pressure is about 2.6% higher than that of the experimental result. But, for the case of KME, DBDFM0.9 and BBDFM0.9 the simulated peak cylinder pressure is about 1.5%, 1.9%, and 2.4% higher than that of the experimental result respectively.
- The deviation of ignition delay between the simulated and experimental results for the diesel operation is about 0.4 ^{o}CA, at full load. For the KME, DBDFM0.9, and BBDFM0.9 the deviation of ignition delay between simulation and experimental result is about 0.4 ^{o}CA, 0.3 ^{o}CA, and 0.2 ^{o}CA respectively, at full load.
- The deviation of NO emission between the simulation and experimental results is about 2.4%, 3.7%, 5.5%, and 5.4% for diesel, KME, DBDFM0.9 and BBDFM0.9 at full load.

- The deviation of smoke emission between the simulation and experimental results is about 1.4%, 2.2%, 2.9%, and 3% for diesel, KME, DBDFM0.9, and BBDFM0.9, at full load respectively.

Table 5.1 provides the summary of the values of the simulation and experimental results for combustion and emission parameters at full load for diesel, KME, DBDFM0.9, and BBDFM0.9.

Table 5.1 Summary of the values of the simulation and experimental results for combustion and emission parameters at full load for diesel, KME, DBDFM0.9, and BBDFM0.9.

Sl. No.	Parameters	Diesel simulation	Diesel expt.	KME simulation	KME expt.	DBDFM0.9 simulation	DBDFM0.9 expt.	BBDFM0.9 simulation	BBDFM0.9 expt.
A. Combustion parameters									
1	Maximum cylinder pressure, bar	77.7	75.4	72.4	71.3	76.1	74.6	74.7	72.9
2	Ignition delay, ^{o}CA	11.9	11.5	10.9	10.5	13.1	12.7	11.5	11.3
B. Emission parameters									
1	NO, g/kWh	2.72	2.523	2.85	2.726	1.99	1.81	2.24	2.007
2	Smoke emission, %	27	25	22.9	22.4	17.2	16.7	20.2	19.6

5.2 Diesel-biogas dual fuel mode with different flow rates of biogas

5.2.1 General

This chapter presents a section wise discussion interpreting the results of the combustion, performance and emissions of a DI diesel engine run on the dual fuel mode, to utilize biogas as an alternative fuel. Initially, the engine was run on a dual fuel mode in which diesel was used as a pilot fuel, while biogas was inducted in different quantities in suction, and the experimental results were obtained. The injection timing of the engine was optimized by assessing the engine behavior in terms of the combustion, performance, and emissions of the diesel-biogas dual fuel mode. The optimized injection timing and the flow rate were used as a reference data. Furthermore, the engine was run on a biodiesel-biogas dual fuel mode, adopting different engine modifications that include varying the biogas flow rate, varying injection timing, varying DEE injection quantity, use of upgraded biogas with DEE injection, varying the compression ratio with the use of upgraded biogas. The results are analyzed, compared with those of the optimized diesel-biogas dual fuel mode and presented in this chapter.

5.2.2 Diesel biogas dual fuel mode

In this section, the experimental results of the combustion, performance and emissions obtained from a single cylinder, four stroke, DI diesel engine, operated on the diesel-biogas dual fuel mode at various load conditions are presented in comparison with those of conventional diesel operation. The results of the investigation have already been published in Energy journal, which is mentioned in the list of publications. The diesel-biogas dual fuel mode is denoted as DBDFMX, where X indicates the flow rate of the biogas in kg/h. The acronyms used in this investigation are as follows:

DBDFM0.3 - diesel + biogas 0.3 kg/h,

DBDFM0.6 - diesel + biogas 0.6 kg/h

DBDFM0.9 - diesel + biogas 0.9 kg/h

DBDFM1.2 - diesel + biogas 1.2 kg/h

5.2.3 Combustion analysis

5.2.3.1 Pressure crank angle diagram

The peak cylinder pressure depends mainly on the rate of combustion in the initial stages, which is influenced by the fuel intake components, in the uncontrolled heat release phase [218]. Figure 5.2.1 portrays the variation of cylinder pressure with the crank angle at full load.

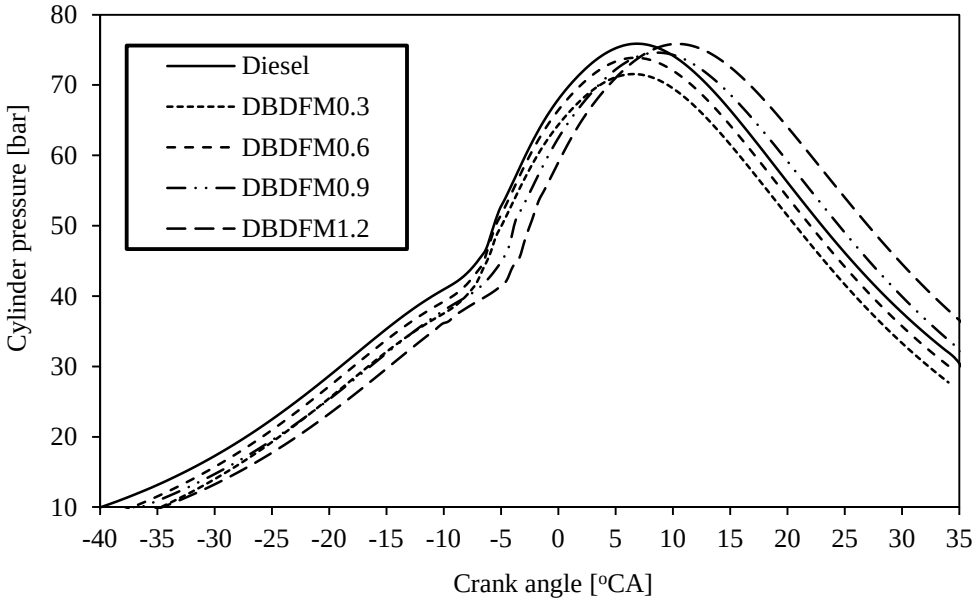

Figure 5.2.1 Variation of cylinder pressure with the crank angle at full load.

It can be observed from the figure that, in the dual fuel mode the start of combustion is overall delayed by about 2-3 ^{o}CA, compared to that of diesel operation at full load. This is due to the presence of CO_2 (17%) in the biogas, and the higher auto-ignition temperature of the biogas. For diesel, the peak cylinder pressure is about 75.7 bar, which occurs at 7.4 ^{o}CA aTDC, whereas, for the dual fuel operation of DBDFM0.3, DBDFM0.6, DBDFM0.9, and DBDFM1.2 the peak cylinder pressures of 71.6 bar, 73.9 bar, 74.6 bar and 75.8 bar occur at 6.4 ^{o}CA aTDC, 6.9 ^{o}CA aTDC, 8.6 ^{o}CA aTDC and 10.6 ^{o}CA aTDC respectively, at full load. The reason for the increase in peak cylinder pressure in the dual fuel operation with the biogas induction is due to the induction of biogas with the intake air charge that brings about a decrease and dilution of the oxygen concentration, which may cause the ignition delay to extend, leading to a higher rate of increase in pressure in the premixed combustion phase. This reason is in good agreement with the ones Duc and Wattanavichien [98] stated from their research on a single cylinder engine. It can also be observed that the presence of CO_2 in the biogas did not significantly affect the

maximum cylinder pressure, but the ignition and peak cylinder pressure occur a little later and shift some degrees toward the expansion process. A similar reason is given by Yoon and Lee [103], and Park et al. [219] in their research works.

5.2.3.2 Ignition delay

Figure 5.2.2 depicts the variation of the ignition delay with engine load. The ignition delay (θ_d) is the time lag in the start of the burning of fuel and start of injection of fuel. This is mainly influenced by parameters, such as fuel type, fuel quality, air-fuel ratio, engine speed, fuel atomization quality, inducted air temperature, compression ratio, and pressure [218].

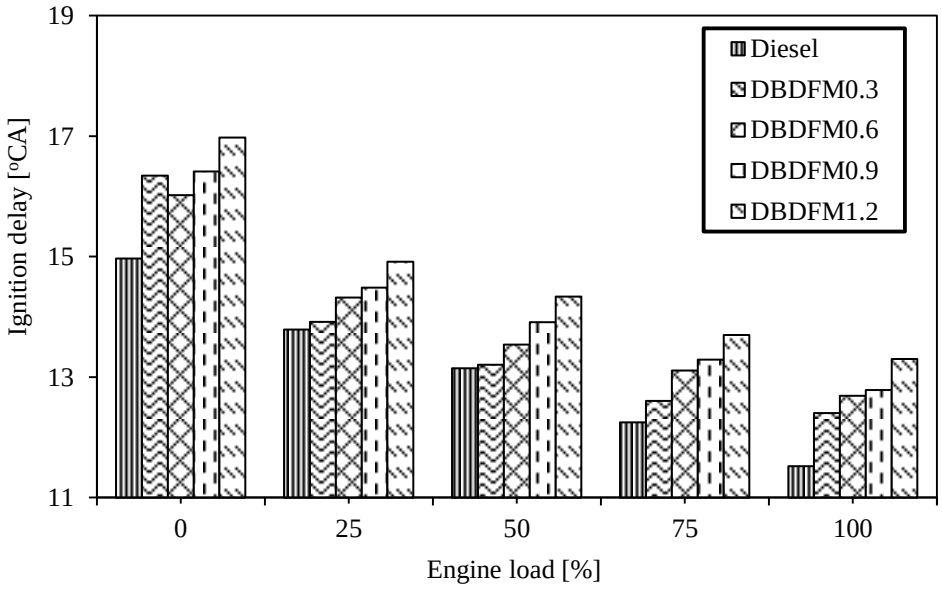

Figure 5.2.2 Variation of ignition delay with the load.

It can be observed that the ignition delay decreases with an increase in the engine load. This is due to the increase in the combustion chamber temperature. This reason matches with the reasons given by Paul et al. [86], and Prakash et al. [206]. The ignition delay for diesel is found to be about 11.5 ^{o}CA, whereas, in dual fuel operation it is longer by about 2-3 ^{o}CA at full load. The longer ignition delay is due to the induction of biogas through the intake manifold, which reduces the oxygen concentration in the air-fuel mixture and alters the pre-ignition property of the charge [205]. In addition to this, the requirement of high stoichiometric air for the biogas causes a prolonged ignition delay in the dual fuel combustion strategy. This reason is also evidenced by the research work documented by Mustafi et al. [105], and Tira [66].

5.2.3.3 Heat release rate

Figure 5.2.3 depicts the variation of the heat release rate with the crank angle for diesel and the dual fuel operations at full load.

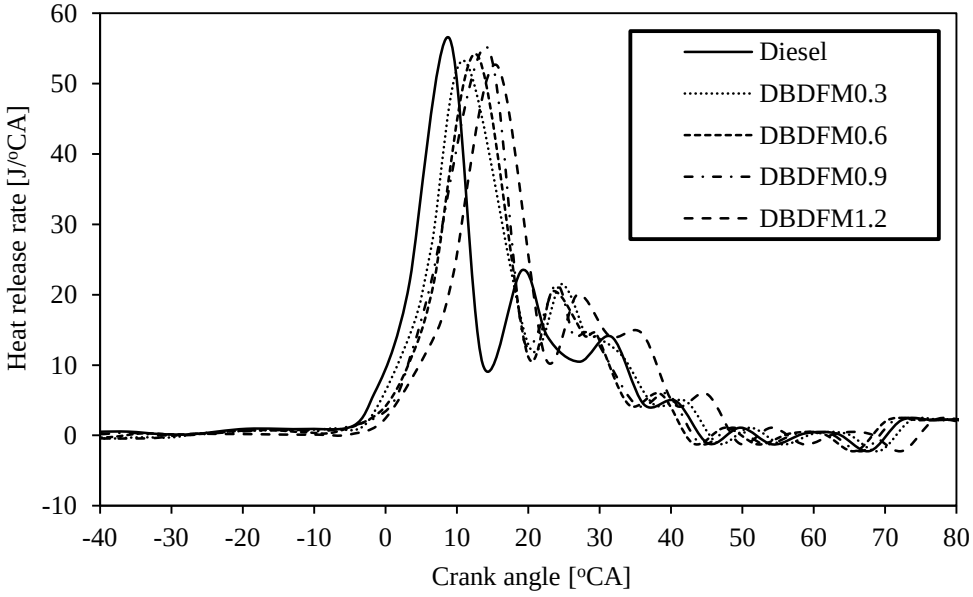

Figure 5.2.3 Variation of heat release rate with the crank angle at full load.

The heat release rate in the premixed combustion phase depends on the ignition delay, mixture formation, and the combustion rate in the initial stages of combustion [41]. It can be observed from the figure that, the maximum rate of heat release is noticed in the diesel operation than in the dual fuel operation. This is due to the higher heating value of diesel. With the increase in biogas quantity the heat release rate increases in the dual fuel operation. This may be due to the increased accumulation of fuel during the relatively longer delay period and the combined effect of the combustion of the pilot fuel and gaseous fuel in the immediate vicinity of the ignition and combustion centers of the pilot fuel, which modifies and extends significantly the flammability zone around the pilot fuel [105,220,221]. The occurrence of the heat release rate is found to be delayed in the dual fuel operation, compared to that of diesel. This is due to the induction of biogas, which has a higher specific heat and presence of 17% CO_2 in it, and causes retarded combustion [86,105]. The maximum heat release for diesel occurs at about 8.9 ^{o}CA aTDC, whereas, for DBDFM0.3, DBDFM0.6, DBDFM0.9, and DBDFM1.2 the maximum heat release occurs at 11.2 ^{o}CA aTDC, 12.7 ^{o}CA aTDC, 14.1 ^{o}CA aTDC and 15.6 ^{o}CA aTDC respectively, at full load.

5.2.3.4 Combustion duration

Figure 5.2.4 illustrates the variation of the combustion duration with load for the diesel and diesel-biogas dual fuel operations.

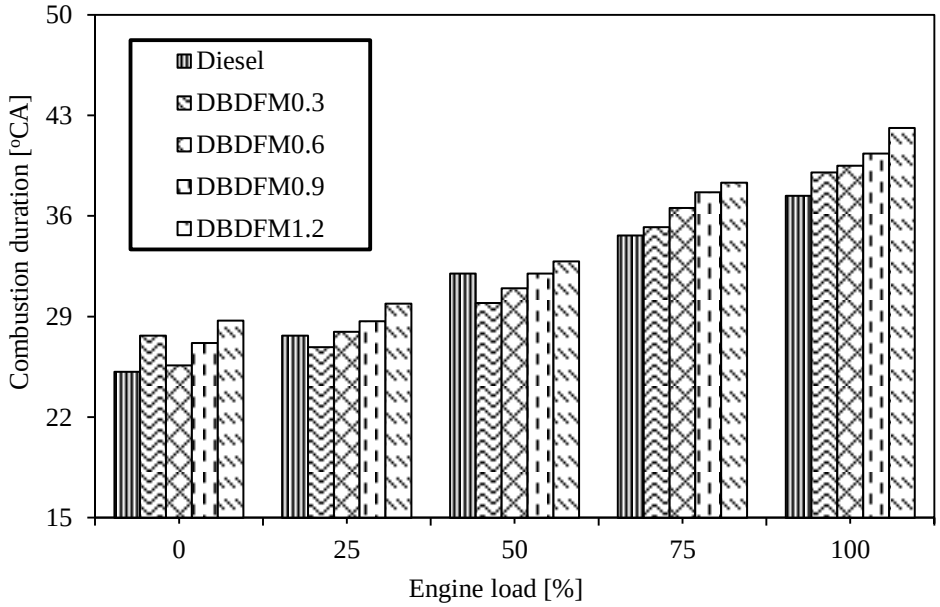

Figure 5.2.4 Variation of the combustion duration with load.

Combustion duration is defined as the interval measured in crank angle between 10% mass burned and 90% mass burned of the accumulated heat release. It can be observed from the figure that, the combustion duration increases with an increase in the engine load, owing to the increase in fuel quantity [208]. The combustion duration for diesel is 37.4 ^{o}CA. In dual fuel operation, the combustion duration of 39 ^{o}CA, 39.5 ^{o}CA, 40.4 ^{o}CA and 42.1 ^{o}CA is observed for DBDFM0.3, DBDFM0.6, DBDFM0.9, and DBDFM1.2 respectively, at full load. The combustion duration in dual fuel operation increases with the increase in the biogas flow rate. This is due to the induced biogas, which alters the physical properties of the charge being compressed, and reduces the oxygen concentration in the charge mixture, causing slower diffusion combustion, which results in a prolonged combustion duration [89]. Also, biogas causes a slower rate of burning of the pilot fuel, as it contains about 17 % CO_2. In both diesel and dual fuel operations, a longer combustion duration is noticed, at full load than at no load, due to the consumption of more fuel at relatively high load. Similar reasons were also stated by Yoon and Lee [103], and Mustafi et al. [105].

5.2.3.5 Maximum cylinder pressure

The variation of the maximum cylinder pressure with load in the diesel-biogas dual fuel mode in comparison with diesel is depicted in Figure 5.2.5. It can be observed from the figure that, the cylinder pressure increases with an increase in the engine load, as expected. The maximum cylinder pressure for diesel is about 75.7 bar and for the dual fuel operation of DBDFM0.3, DBDFM0.6, DBDFM0.9, and DBDFM1.2 it is about 71.6 bar, 73.9 bar, 74.6 bar, and 75.8 bar respectively, at full load. This gradual increase in the maximum cylinder pressure in the dual fuel operation is due to the induction of biogas with the intake air charge that brings about a decrease and dilution of oxygen concentration, which may cause a longer ignition delay, and lead to an increase in cylinder pressure in the premixed combustion phase. Yoon and Lee [103], and Carlucci et al. [83] have reported similar reasons in their research work.

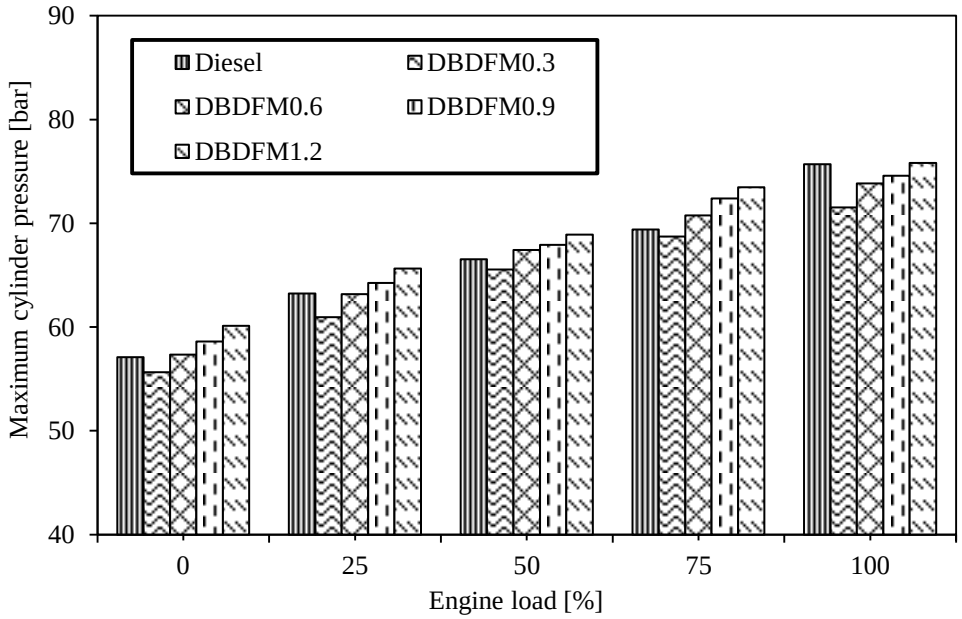

Figure 5.2.5 Variation of the maximum cylinder pressure with load.

5.2.4 Performance analysis

5.2.4.1 Brake specific fuel consumption (BSFC)

Figure 5.2.6 portrays the variation of BSFC with load for diesel and the diesel-biogas dual fuel mode. It can be observed that a higher brake specific fuel consumption (BSFC) is noticed in dual fuel operation than in diesel at part loads. This is due to the lower energy density of biogas, lower cylinder temperature, and the presence of CO_2 in biogas that prevents faster burning [101].

The differences in BSFC between diesel and dual fuel operation are not significantly different at high operating loads. At full load, the dual fuel operation has a similar fuel energy conversion efficiency to that of diesel [91]. This is because, less energy from the fuel is required at full load compared to that of no load, due to the increased cylinder temperature at full load [222,223]. The BSFC for diesel is 0.27 kg/kWh, and for DBDFM0.3, DBDFM0.6, DBDFM0.9, and DBDFM1.2 the BSFC is 0.35 kg/kWh, 0.40 kg/kWh, 0.42 kg/kWh and 0.51 kg/kWh respectively, at full load.

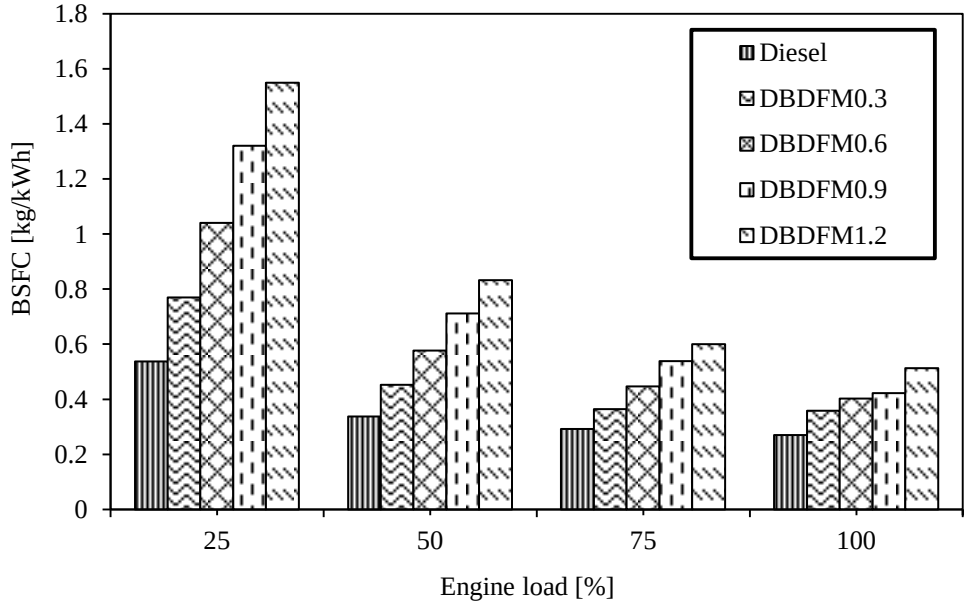

Figure 5.2.6 Variation of BSFC with load.

5.2.4.2 Brake thermal efficiency (BTE)

The variation of BTE with load for diesel and diesel-biogas dual fuel mode is illustrated in Figure 5.2.7. It can be observed that, the BTE of the dual fuel operation is found to be lower than that of diesel operation throughout the load spectrum. At full load, the BTE of diesel is 30.3%, and in dual fuel operation the BTE for DBDFM0.3, DBDFM0.6, DBDFM0.9, and DBDFM1.2 is 28.1%, 27%, 26.1%, and 22.2% respectively. A drop in BTE of 7.2%, 10.8%, 13.8% and 26.7% is observed for DBDFM0.3, DBDFM0.6, DBDFM0.9, and DBDFM1.2 in comparision to that of diesel at full load respectively. This reduction in the BTE is due to the deficiency of oxygen caused by the induction of biogas through the intake manifold. The deficiency of oxygen causes incomplete combustion and subsequent decrease in converting the input fuel energy, and results in a higher total fuel flow rate during the combustion process. Paul et al. [88] have also observed

a similar trend for the drop in BTE. Also, another reason may be the decreased flame propagation speed and increased negative compression work, which in turn, are caused by the induction of a large quantity of air-biogas mixtures. This reason has also been mentioned by Yoon and Lee [103], for the results they have obtained in a dual fuel diesel engine fueled with biodiesel-biogas dual fuel.

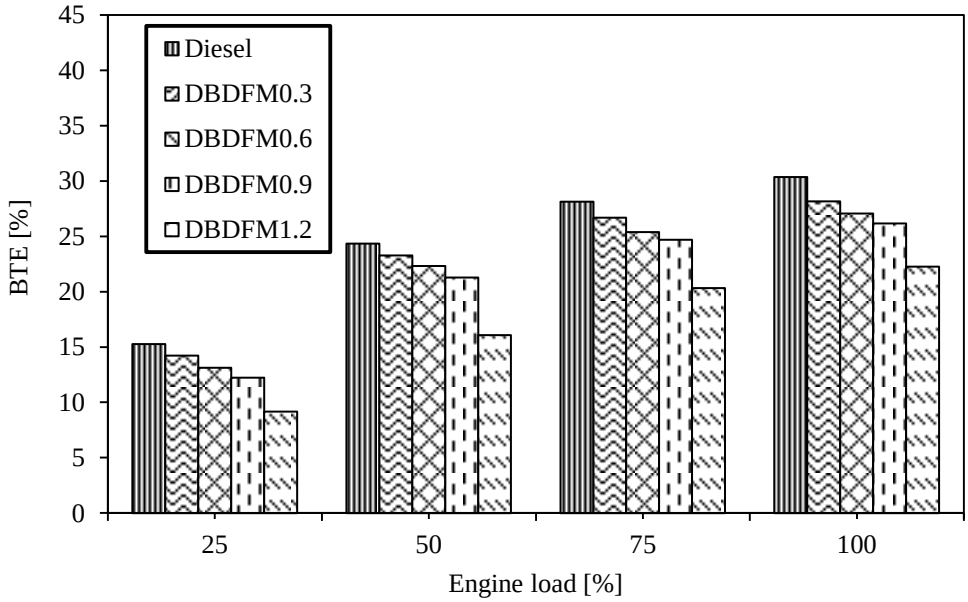

Figure 5.2.7 Variation of BTE with load.

5.2.4.3 Energy share

The variation of the biogas induction quantity with the biogas energy share is depicted in Figure 5.2.8. It can be observed from the figure that, the biogas energy share is low at full load, while the energy share is high at no load, for all the flow rates of biogas in dual fuel operation. This is due to more diesel consumption at relatively high load than at no load. DBDFM1.2 gives the maximum energy share in comparison with DBDFM0.3, DBDFM0.6, and DBDFM0.9 throughout the load spectrum. At full load, DBDFM0.3, DBDFM0.6, DBDFM0.9, and DBDFM1.2 give energy shares of about 14.8%, 26.6%, 36.9% and 43.9% respectively.

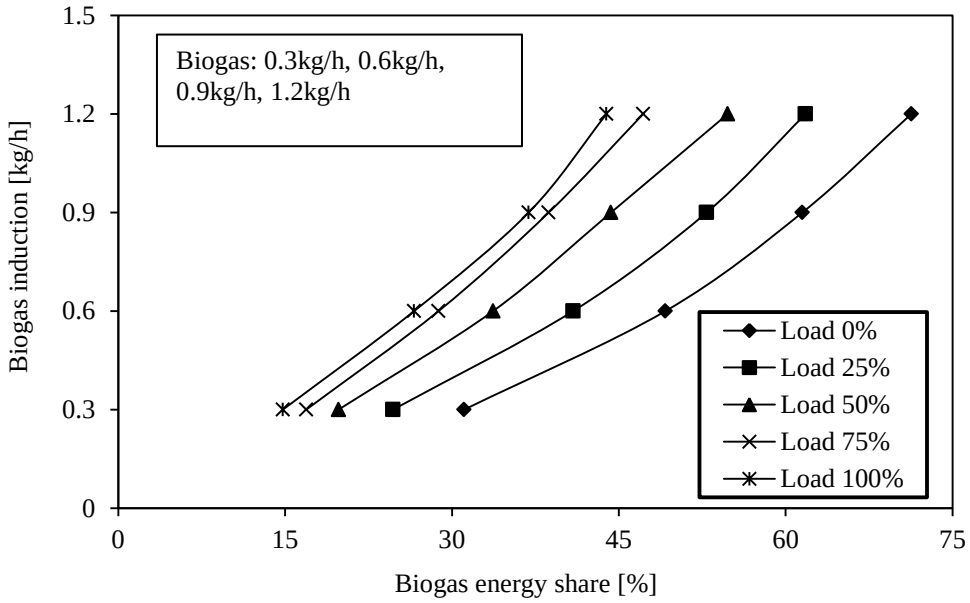

Figure 5.2.8 Variation of biogas induction quantity with biogas energy share.

5.2.4.4 Volumetric efficiency

The variation of volumetric efficiency with load for diesel and diesel-biogas dual fuel operation is depicted in Figure 5.2.9.

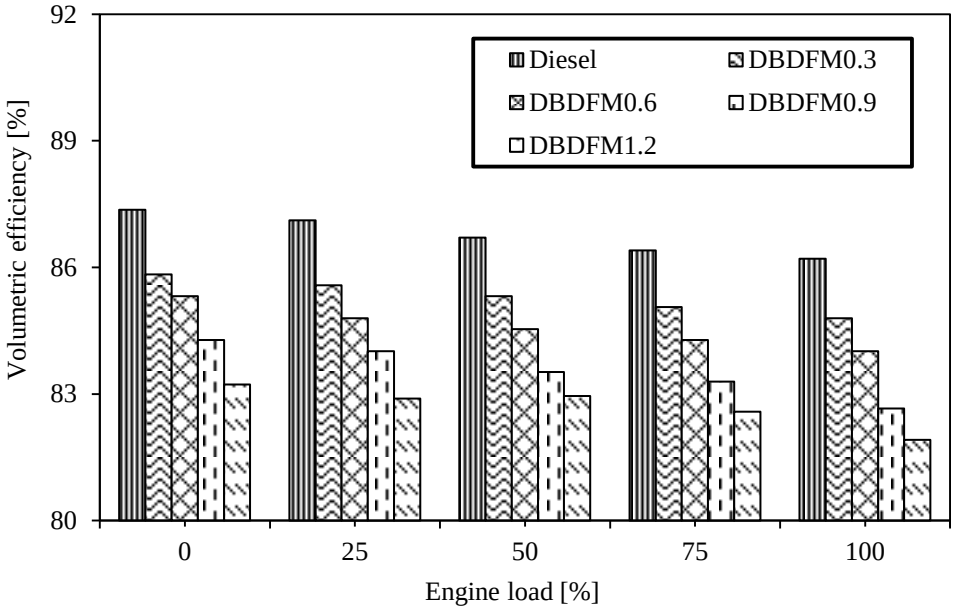

Figure 5.2.9 Variation of volumetric efficiency with load.

The volumetric efficiency of diesel operation is found to be higher than that of the dual fuel operation. The volumetric efficiency of diesel is found to be about 86.2%, whereas, the

volumetric efficiency of DBDFM0.3, DBDFM0.6, DBDFM0.9, and DBDFM1.2 is 84.7%, 84%, 82.6% and 81.9% respectively, at full load. This reduction in volumetric efficiency in the dual fuel operation is due to the induction of biogas with air through the intake manifold, which replaces some amount of fresh air. Also, another reason may be the increase in the induced air temperature, as a result of the hot cylinder wall, that reduces the air density. Abdelaal et al. [100] have also reported similar reasons for their research results, obtained from a diesel-natural gas fueled single cylinder, DI diesel engine with oxygen enriched intake air.

5.2.4.5 Diesel replacement

The variation of diesel replacement quantity with load is depicted in Figure 5.2.10. It is apparent from the figure that, the diesel replacement increases with an increase in the biogas quantity. This is due to the biogas energy conversion into work, leading to a considerable improvement in the heat release. However, as the load increases, the diesel replacement quantity has a declining trend. This is due to the higher thermal load imposed on the engine at higher loads, which inhibits more diesel consumption thereby reducing the replacement quantity. At full load, DBDFM0.3, DBDFM0.6, DBDFM0.9, and DBDFM1.2 give a maximum diesel replacement of about 0.168 kg/h, 0.20 kg/h, 0.263 kg/h and 0.274 kg/h respectively.

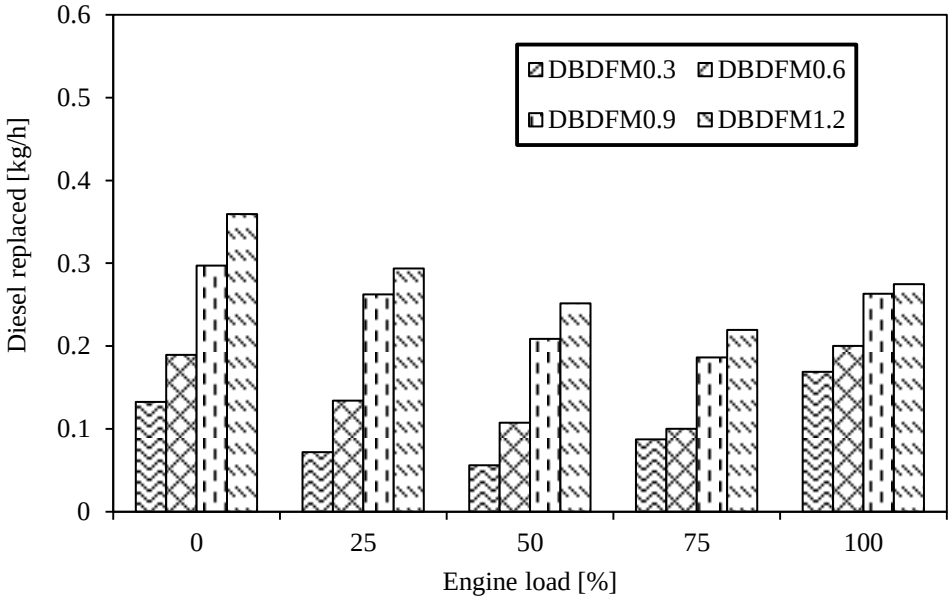

Figure 5.2.10 Variation of diesel replacement quantity with load.

5.2.4.6 Exhaust gas temperature (EGT)

The variation of the EGT with load is depicted in Figure 5.2.11. It can be noticed that diesel shows the highest value of EGT among all the fuels tested in this experiment, throughout the load spectrum. The EGT of diesel at full load is 331.8 ^{o}C. The EGT is marginally lower in the dual fuel operation compared to that of diesel, throughout the load spectrum. This is due to the dilution of charge by the CO_2 present in the biogas, and reduced flame propagation speed of the pilot fuel, causing incomplete combustion that lowers the EGT. This is in good agreement with Mustafi et al. [105]. In addition to this, the inducted biogas gets hot to auto ignite during the combustion process, and absorbs the heat energy, which decreases the local flame temperature, leading to a reduction in the EGT. The dual fuel operation of DBDFM0.3, DBDFM0.6, DBDFM0.9, and DBDFM1.2 gives a reduction in the EGT of 3.4%, 6.4%, 9.5% and 13.8% respectively, than that of diesel at full load.

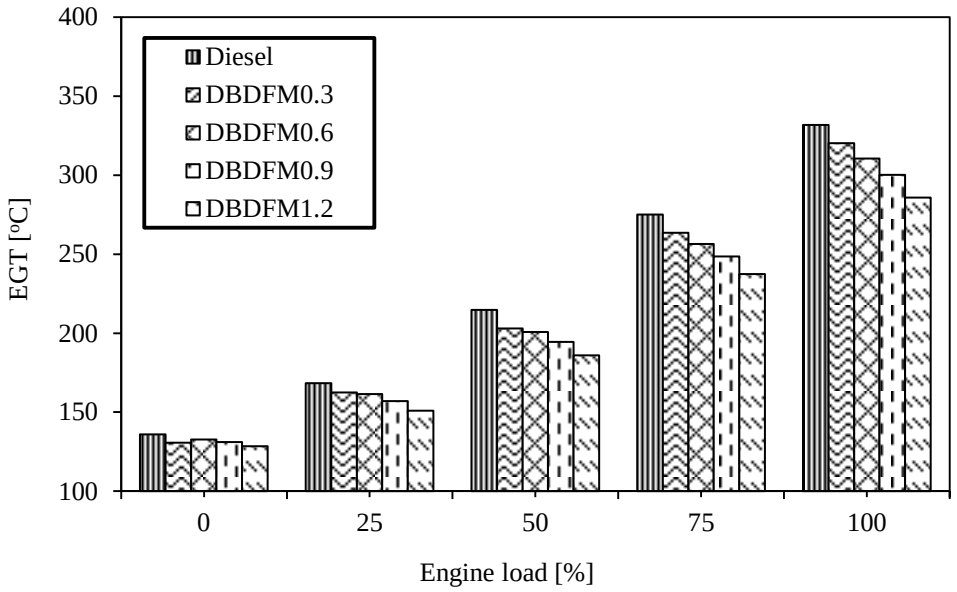

Figure 5.2.11 Variation of EGT with load.

5.2.5 Emission analysis

5.2.5.1 Carbon monoxide (CO) emission

The variation of CO emission with load is depicted in Figure 5.2.12. The CO emission in the dual fuel operation is considerably higher than that of diesel under all test conditions. This is due to incomplete combustion caused by the dilution of charge by the CO_2 present in biogas and the

deficiency of oxygen. Hence, the flame formed in the ignition region of the pilot fuel is normally suppressed and does not proceed until the biogas fuel-air mixture reaches a minimum limiting value for auto ignition. Similar observations and reasons were documented by Abdelaal et al. [224], and Papagiannakis et al. [90] based on the investigations they carried out in a dual fuel engine with oxygen addition to the intake air, and pilot fuel ignited natural gas-diesel dual fuel engine respectively. The CO emission is higher by about 38% for DBDFM1.2 at full load, in comparison with diesel, whereas, only 23.3% increment in CO emission is observed for DBDFM0.9 at full load, incomparison to diesel. The poor mixture formation of gaseous and liquid fuel may also be another reason for the higher CO emission [225].

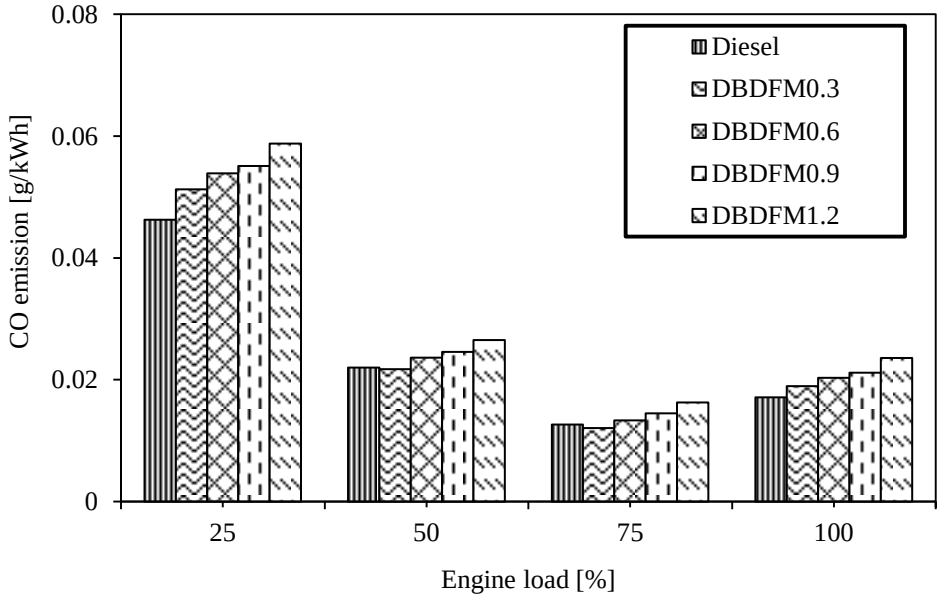

Figure 5.2.12 Variation of CO emission with load.

5.2.5.2 Hydrocarbon (HC) emission

Figure 5.2.13 illustrates the variation of HC emission with the load. The concentration of brake specific HC emissions in dual fuel operation is considerably higher than that of diesel, under all the test conditions. The HC emission is found to be higher by about 41% for DBDFM1.2, whereas, 30% increment in HC emission was observed for DBDFM0.9 in comparison with diesel at full load. This higher HC emission is due to the incomplete combustion of the fuel. The biogas induction through the intake manifold reduces the volume of inducted air; hence, the combustion takes place with less oxygen resulting in a higher HC emission. Papagiannakis et al. [90] had also documented a similar reason when they correlated the results obtained in their

investigation of a natural gas-diesel fueled dual fuel engine. In addition to this, there are contributions from the crevice volumes, in which the gas–air mixture is forced during the compression stroke and then remains unburned. This reason is in good agreement with the results obtained by Karim [226]. The overlapping between the intake and exhaust valves to facilitate scavenging might also cause an increase in HC emissions for dual fuel combustion because the unburned air-biogas mixture leaves the cylinder through the exhaust manifold. Bedoya et al. [97] have also reported a similar reason for what they observed during their investigation on a diesel-biogas dual fuel engine.

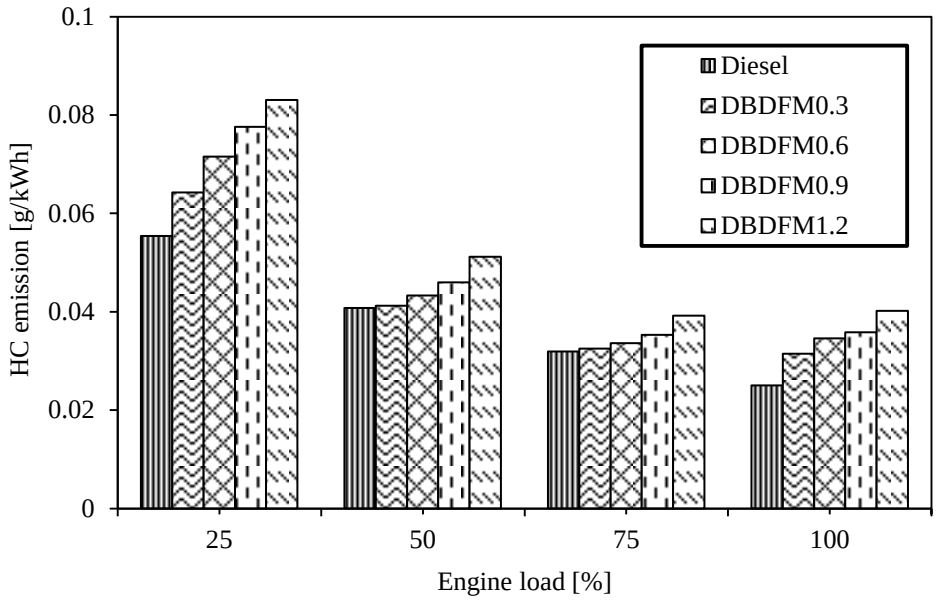

Figure 5.2.13 Variation of HC emission with load.

5.2.5.3 Nitric oxide (NO) emission

Figure 5.2.14 portrays the variation of NO emission with load. The NO formation is highly dependent on the combustion temperature, availability of oxygen, compression ratio and the retention time for the reaction. The concentration of the brake specific NO emission is found to decrease steeply for all the test conditions with an increase in the load. Lower NO emissions are found in the dual fuel operation compared to that of diesel throughout the load spectrum. This is due to the presence of CO_2 having a high molar specific heat, which dilutes the charge and lowers the cycle temperature significantly. In addition, the CO_2 in biogas lowers the oxygen concentration of the charge followed by an overall decrease in the cycle temperature. Hence, the NO formation is suppressed with the combined effect of these phenomena. Similar reasons for

the reduction in thermal NO were given by Saravanan et al. [227] and, Al-Dawody and Bhatti [228], based on their investigation in a diesel engine, fueled with diesel and biodiesel. A reduction in NO emission of about 33.8% is observed for DBDFM1.2 at full load, compared to that of diesel.

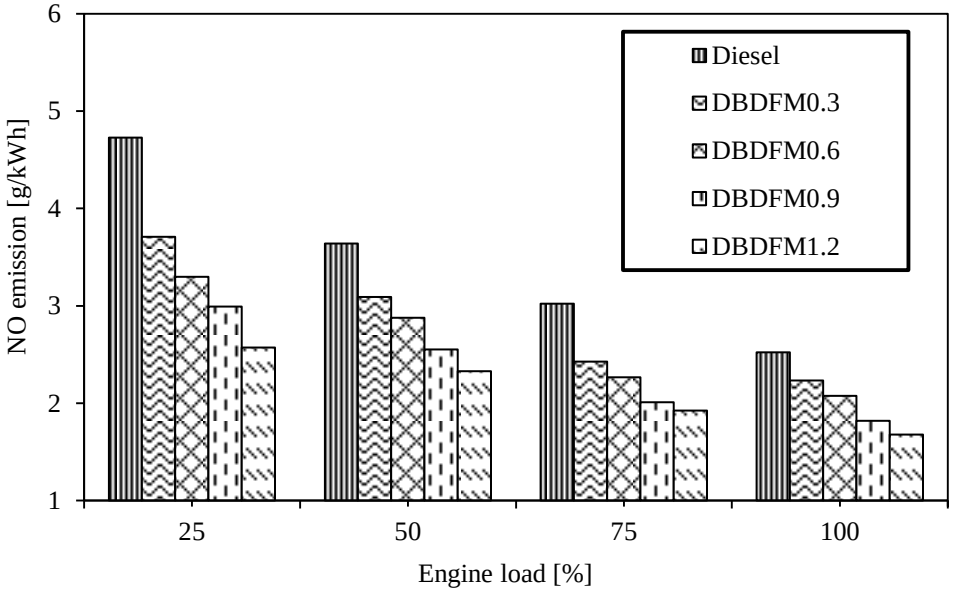

Figure 5.2.14 Variation of NO emission with the load.

5.2.5.4 Smoke emission

The variation of smoke emission with load is depicted in Figure 5.2.15. The smoke emission is higher when a fuel's ratio of hydrogen to carbon is less than two [229]. The smoke emission in the case of dual fuel operation is found to be less than that of diesel operation. This is due to the absence of aromatic compounds in the biogas. Also, the smoke emission is strongly dependent on the amount of air in the cylinder, as well as on the amount of oxygen in the fuel. It is obvious that the fuel composition affects the amount of smoke produced by the engine. In dual fuel operation, some amount of diesel is replaced by the biogas resulting in less smoke emission. In general the reduction of smoke is attributed to flame temperature reduction and increased oxidation of soot precursors in the soot forming region by the enhanced concentration of O and OH around the flame (resulting in high oxidation) produced from the CO_2 in biogas. This reason is in a good agreement with the reason given by Mustafi et al. [105] in their research work carried out using a DI diesel engine fueled with natural gas and biogas. The CO_2 concentration in the fuel causes a decrease in the overall cycle temperature, which has a positive (i.e. reduction)

impact on smoke formation and, at the same time, does not seem to have an adverse (i.e. increase) effect on the NO emissions. This reason is well matched with the reason documented by Papagiannakis et al. [82] and, Karthikeyan and Mahalakshmi [230] for the results obtained from a dual fuel engine operated on diesel-natural gas, and diesel-turpentine on dual fuel modes respectively. The dual fuel operation of DBDFM0.3, DBDFM0.6, DBDFM0.9, and DBDFM1.2 exhibits a reduction in smoke emission by about 8%, 22%, 33% and 49% respectively, at full load, incomparision with diesel.

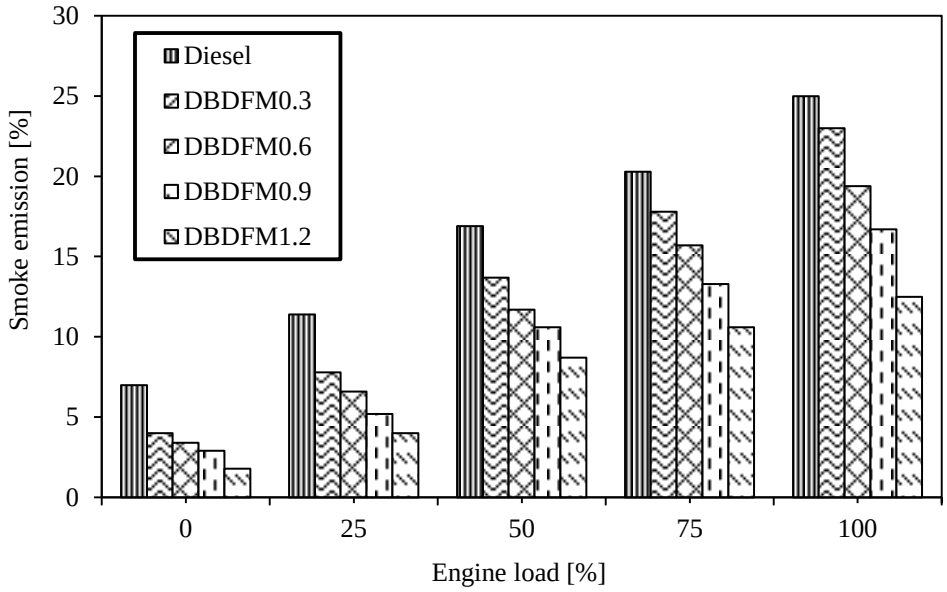

Figure 5.2.15 Variation of smoke emission with load.

5.2.6 Summary

The use of biogas with diesel in a CI engine seems to be desirable to reduce emissions, saving of conventional diesel and to utilize bioenergy from biomass. It is also a promising technique for on-farm electricity generation. This biogas dual fuel engine, not only consumes a wide range of gaseous fuel resources effectively, but also has the potential to avoid much of the current and future problems of diesel engines, including a very significant reduction in its exhaust emission trade-offs. The diesel replacement of 0.263 kg/h is possible with DBDFM0.9 at full load. About 36% increase in the BSFC and 13.8% drop in BTE is noticed in the dual fuel operation of DBDFM0.9 in comparison with diesel, at full load. At full load, 23.3% and 30% increase in the CO and HC emissions is observed for DBDFM0.9, in comparison with diesel. A simultaneous

reduction of 28% and 33% in NO and smoke emissions are observed for DBDFM0.9 in comparison with diesel, at full load respectively.

Table 5.2 provides the values of important parameters of the investigation results obtained for diesel and diesel-biogas dual fuel mode at full load.

Table 5.2 Summary of the values of the combustion, performance and emission parameters at full load for diesel and diesel-biogas dual fuel operation.

Sl. No.	Parameters	Diesel	DBDFM0.3	DBDFM0.6	DBDFM0.9	DBDFM1.2
A. Combustion parameters						
1	Maximum cylinder pressure, bar	75.7	71.6	73.9	74.6	75.8
2	Ignition delay, ^{o}CA	11.5	12.4	12.6	12.7	13.3
3	Maximum heat release rate, J/^{o}CA	56.5	53.1	54.1	55.2	52.6
4	Combustion duration, ^{o}CA	37.4	39.0	39.5	40.4	42.1
B. Performance parameters						
1	BSFC, kg/kWh	0.27	0.35	0.40	0.42	0.51
2	BTE, %	30.3	28.1	27	26.1	22.2
3	Volumetric efficiency, %	86.2	84.7	84	82.6	81.9
4	Diesel replaced, kg/h	-	0.168	0.20	0.263	0.274
5	EGT, ^{o}C	331.8	320.2	310.5	300.1	285.7
C. ***Emission parameters***						
1	CO, g/kWh	0.0171	0.0189	0.0203	0.0211	0.0236
2	HC, g/kWh	0.025	0.031	0.034	0.035	0.0
3	NO, g/kWh	2.523	2.23	2.07	1.81	1.67
4	Smoke emission, %	25	23	19.4	16.7	12.5

5.3 Diesel-biogas dual fuel mode with optimum biogas flow rate and different injection timings of pilot fuel

5.3.1 General

This section presents the experimental results of the combustion, performance and emission characteristics of a single cylinder, four stroke, DI diesel engine, operated on the dual fuel mode with an optimum biogas flow of 0.9 kg/h, and three different advanced pilot fuel injection timings, viz. 24.5, 26, 27.5 ^{o}CA bTDC. The acronyms used for the investigation are as follows:

DBDFM0.9/23.0 – diesel + biogas 0.9 kg/h with diesel injection timing of 23 ^{o}CA bTDC

DBDFM0.9/24.5 – diesel + biogas 0.9 kg/h with diesel injection timing of 24.5 ^{o}CA bTDC

DBDFM0.9/26.0 – diesel + biogas 0.9 kg/h with diesel injection timing of 26 ^{o}CA bTDC

DBDFM0.9/27.5 – diesel + biogas 0.9 kg/h with diesel injection timing of 27.5 ^{o}CA bTDC

The results of the investigation have already been published in Journal of the Energy Institute which is mentioned in the list of publication.

5.3.2 Combustion analysis

5.3.2.1 Pressure crank angle diagram

The peak cylinder pressures with respect to the crank angle at full load for the diesel and dual fuel operations are depicted in Figure 5.3.1.

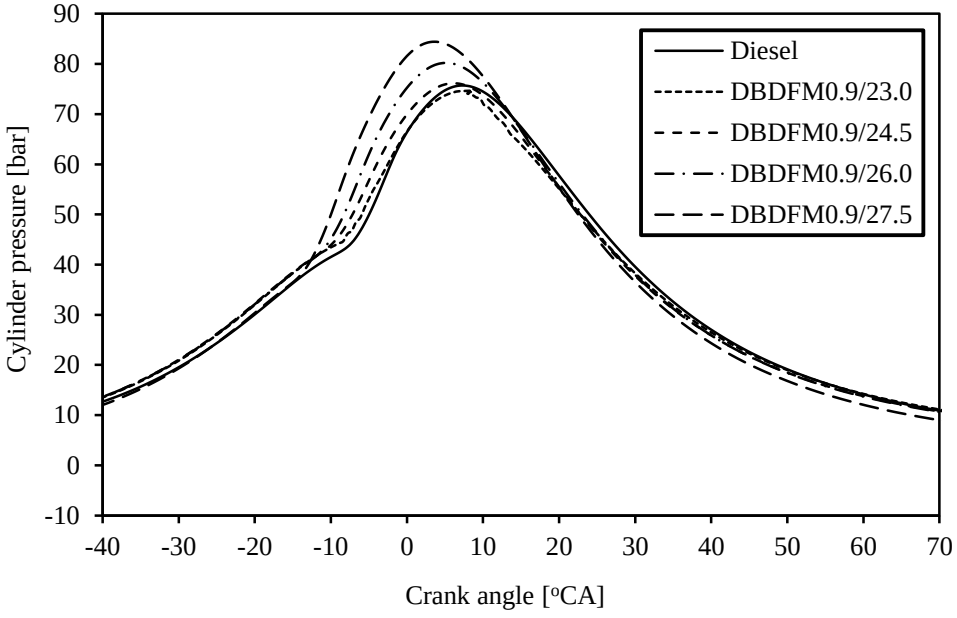

Figure 5.3.1 Variation of cylinder pressure with crank angle at full load.

In diesel operation, the peak cylinder pressure is about 75.7 bar, which occurs at 7.4 ^{o}CA aTDC, whereas for DBDFM0.9/23.0, the peak cylinder pressure of 74.6 bar occurs at about 8.6 ^{o}CA aTDC. This is due to the induction of biogas with the intake-air charge that brings about a decrease and dilution of oxygen concentration, which may cause the ignition delay to extend, leading to a higher rate of increase in pressure in the premixed combustion phase. Similar reasons are given by Duc and Wattanavichien [98], and Behera et al. [231], for the results they obtained from a DI diesel engine operated on acetylene and biogas respectively. DBDFM0.9/24.5, DBDFM0.9/26.0, and DBDFM0.9/27.5 give peak cylinder pressures of 76.1 bar, 80.2 bar, and 84.4 bar, which occur at 6 ^{o}CA aTDC, 5 ^{o}CA aTDC and 3.6 ^{o}CA aTDC respectively, at full load. The reason for the higher peak cylinder pressure in the dual fuel operation with advanced injection timing is due to the formation of a fuel rich mixture inside the combustion chamber. With advanced injection, the combustion occurs in the early crank angles in the cycle, and more rapid burning takes place in the premixed combustion phase. Hence, more amount of fuel burns before the top dead centre (TDC) and the peak cylinder pressure moves closer to TDC. The reason was commonly reported by many researchers for instance; Sahoo et al. [61] and Agarwal et al. [232] have reported it in their studies. Another reason for the increase in the peak cylinder pressure in the dual fuel operation with advanced injection timing is due to the lower in-cylinder air temperature at relatively early injections, which may cause the ignition delay to extend, leading to a higher rate of pressure rise in the premixed combustion phase. This is in good agreement with Ryu [92], and Nwafor [233].

5.3.2.2 Ignition delay

Figure 5.3.2 portrays the variation of ignition delay for the diesel and dual fuel operations at different injection timings. It can be observed from the figure that, as the pilot injection timing is advanced, the ignition delay in the dual fuel operation is found to be longer. It may be due to the low in-cylinder temperature at early injections that delayed the pilot fuel ignition. A similar reason was reported by Ryu [92], Satyanarayana and Muraleedharan [234], and Park et al. [235]. It can also be observed that the ignition delay in the dual fuel operation with the standard injection timing of 23 ^{o}CA bTDC is greater than that of diesel, due to the cooling effect of the inducted biogas. Another reason for the longer ignition delay is due to the induction of biogas through the intake manifold, which reduces the oxygen concentration in the air-fuel mixture, and alters the pre-ignition property of the charge. In addition to this, the influence of a high stoichiometric air requirement for the biogas causes

the prolonged ignition delay in the dual fuel operation. This reason is also evidenced from the research work documented by Mustafi et al. [105] which they carried out on a single cylinder, water cooled, DI diesel engine run on the dual fuel mode. A shorter ignition delay is noticed at full load, than that of no load, which is due to the higher cylinder temperature at full load. The ignition delay for diesel is found to be about 11.8 ^{o}CA, whereas, in the dual fuel operation it is longer by about 2-3 ^{o}CA at full load. The dual fuel operation of DBDFM0.9/23, DBDFM0.9/24.5, DBDFM0.9/26.0, and DBDFM0.9/27.5 gives a longer ignition delay of 12.7 ^{o}CA, 12.9 ^{o}CA, 13.1 ^{o}CA, and 13.6 ^{o}CA, respectively at full load.

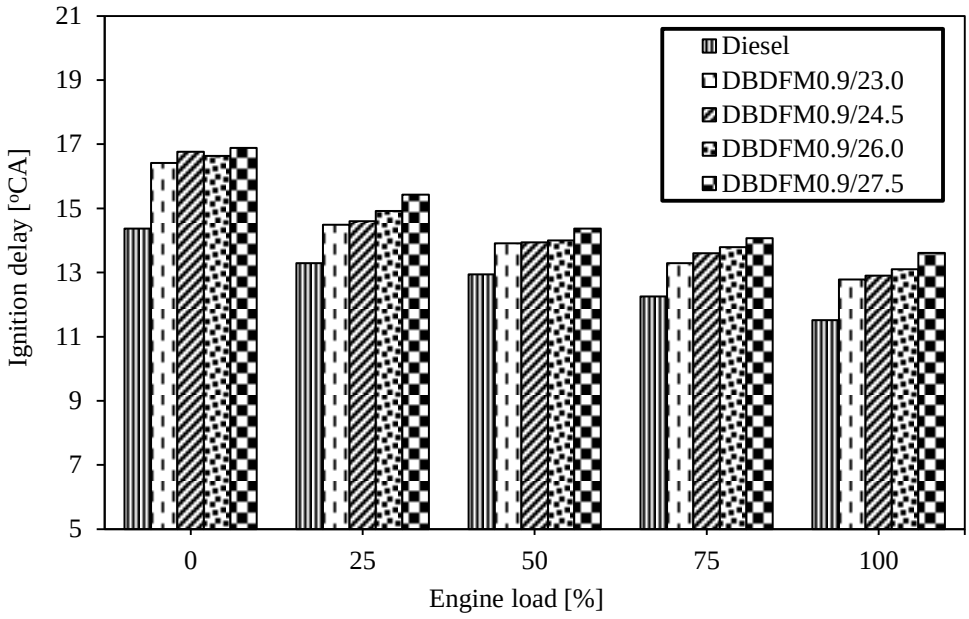

Figure 5.3.2 Variation of ignition delay with load.

5.3.2.3 Heat release rate

The variation of the heat release rate with crank angle for the diesel and dual fuel operations is depicted in Figure 5.3.3. The heat release rate in the dual fuel engine is extremely complex, because it involves two fuels with different characteristics and properties, which are simultaneously burned inside the cylinder. The heat release rate in the dual fuel operation is the result of three combustion processes, namely the combustion of the pilot injected diesel, combustion of the biogas in the immediate vicinity of the ignition kernel, and the pre-ignition activity with the subsequent flame propagation. This reason matched with that of Donateo et al. [236] for the results, which they obtained from a diesel engine operated on methane and diesel. However, the relevance of the third process depends on the amount of biogas. Under idling or no load operations, the air-fuel (biogas+diesel+air) mixture becomes very lean, and consistent flame propagation does not take place from the ignition centers. Hence, the rate of

combustion is mainly influenced by the pilot fuel during the idling condition. The heat release rate in the premixed combustion phase depends on the ignition delay, mixture formation and the combustion rate in the initial stages. Mustafi et al. [105] have reported similar type of results for their experiment with a biogas run DI diesel engine.

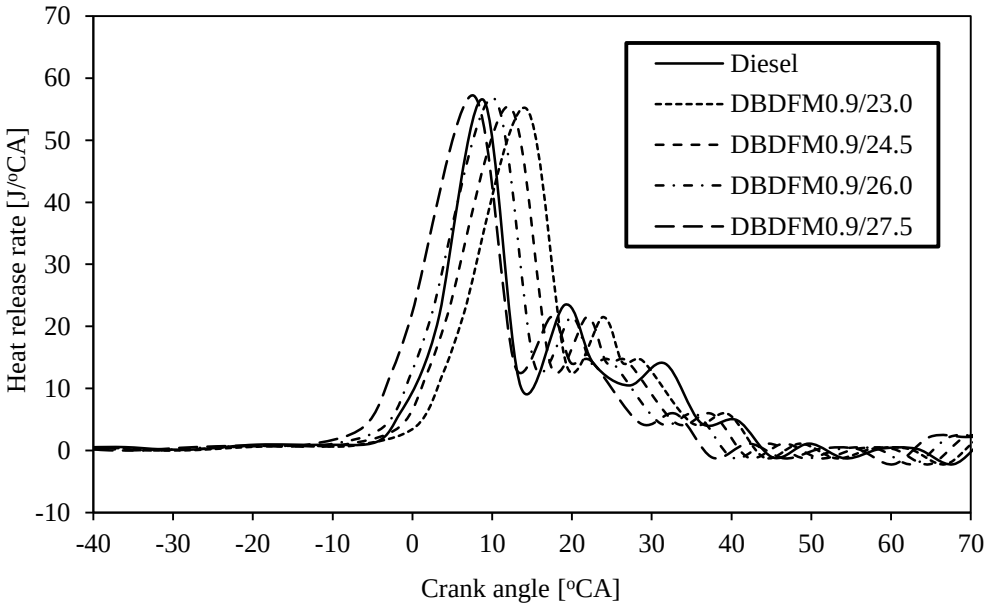

Figure 5.3.3 Variation of heat release rate with crank angle at full load.

It can be observed from the figure that, the maximum rate of heat release is noticed in the dual fuel operation and dual fuel operation with advanced injections than that of diesel operation at full load. This may be due to the increased accumulation of biogas during the relatively longer delay period, and the combined effect of the combustion of biogas and diesel in the immediate vicinity of the ignition and combustion centers of the pilot fuel, which extends the flammability zone around the pilot fuel. Similar reasons were given by Mustafi et al. [105], and Karim [220] in their investigations for the results they obtained from a biogas fueled DI diesel engine. The occurrence of heat release rate is found to be earlier in the dual fuel operation with advanced injections, than that of diesel. This is due to the advancement in the injection timing. Advanced injection timing gives a full spray penetration and higher injection quantity. The combustion starts earlier with respect to the top dead centre (TDC), and a maximum amount of fuel burns in the premixed combustion phase, releasing more energy. The maximum heat release rate for diesel occurs at about 8.9 ^{o}CA aTDC, whereas, for DBDFM0.9/23.0, DBDFM0.9/24.5, DBDFM0.9/26.0, and DBDFM0.9/27.5 the maximum heat release rate occurs at about 14.1 ^{o}CA aTDC, 12.1 ^{o}CA aTDC, 10.1 ^{o}CA aTDC and 7.6 ^{o}CA aTDC respectively, at full load.

5.3.2.4 Combustion duration

Figure 5.3.4 portrays the variation of the combustion duration for both the diesel and dual fuel operations at different injection timings. It can be observed from the figure that, the combustion duration increases with an increase in the load, owing to the increase in the fuel quantity. Lakshmanan and Nagarajan [208] have reported a similar reason for the results they have obtained from acetylene fueled DI diesel engine. In the diesel and DBDFM0.9/23, the combustion duration is found to be about 37.4 ^{o}CA and 40.4 ^{o}CA respectively, at full load. The combustion duration for DBDFM0.9/24.5 and DBDFM0.9/26.0 decreases, but for DBDFM0.9/27.5 the combustion duration increases drastically. The increase in the combustion duration is attributed to the suppression of the change due to the induction of biogas. The inducted biogas, alters the physical properties of the charge being compressed, and reduces the oxygen concentration in the charge mixture, and causes slower diffusion combustion, which results in a prolonged combustion duration. Similar reasons were also stated by Mustafi et al. [105]. In addition, the biogas causes a slower rate of burning of the pilot fuel, as it contains about 17% CO_2. In both the diesel and dual fuel operations, longer combustion duration is noticed, at higher loads than at lower loads; this is due to the consumption of more fuel at relatively higher loads.

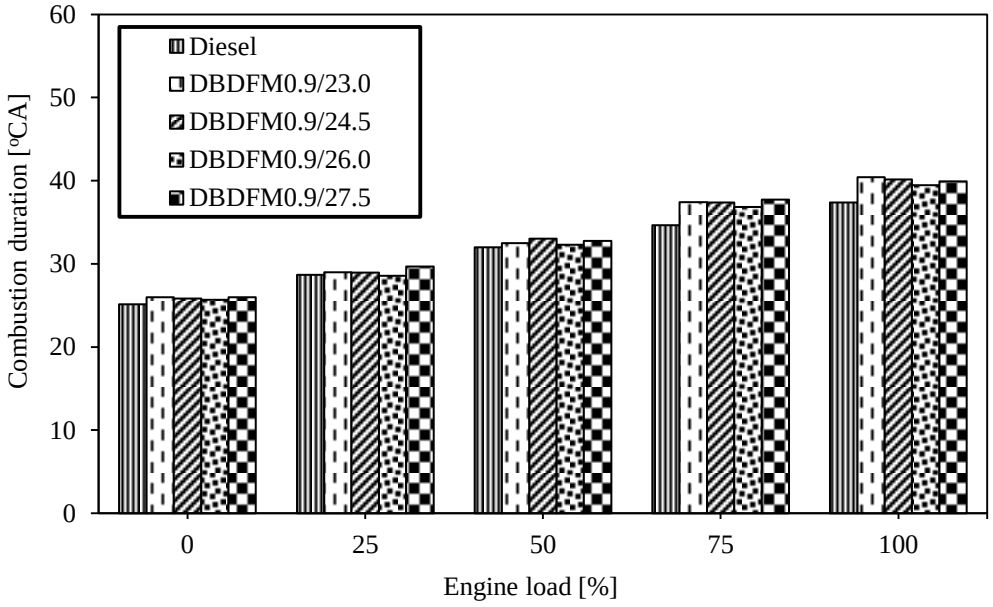

Figure 5.3.4 Variation of combustion duration with load.

5.3.2.5 Maximum cylinder pressure

Figure 5.3.5 portrays the variation of the maximum cylinder pressure with load, for both the diesel and dual fuel operations at different injection timings.

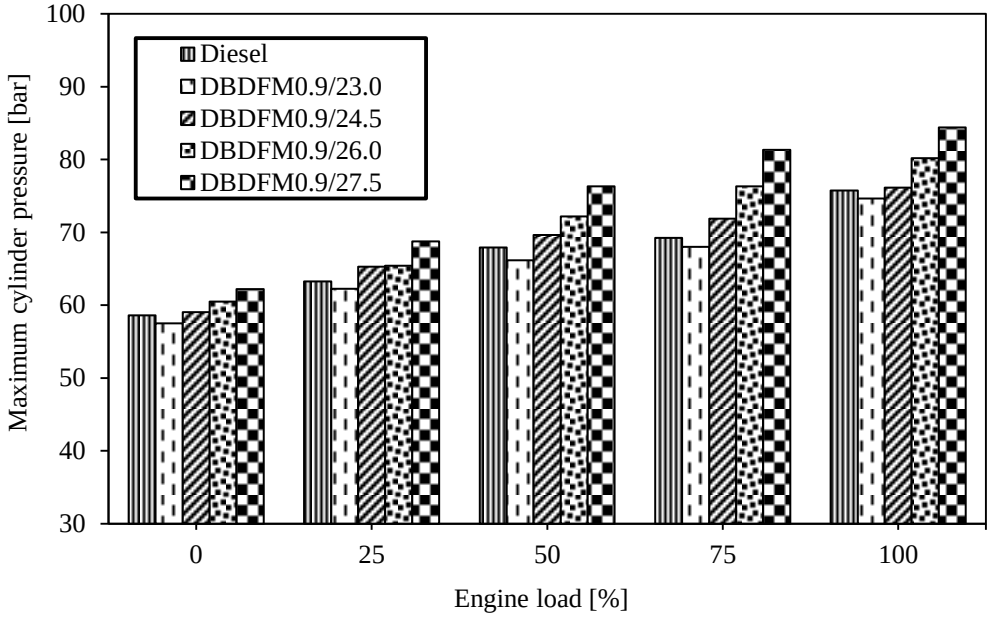

Figure 5.3.5 Variation of the maximum cylinder pressure with load.

It can be observed from the figure that, the cylinder pressure increases with the increase in the load, as expected. The maximum cylinder pressure for diesel is about 75.7 bar. But, the dual fuel operations of DBDFM0.9/23.0, DBDFM0.9/24.5, DBDFM0.9/26.0, and DBDFM0.9/27.5 give the maximum cylinder pressures of 74.6 bar, 76.1 bar, 80.2 bar and 84.4 bar respectively, at full load. This increase in the maximum cylinder pressure in the dual fuel operation than that of diesel is due to the induction of biogas through the intake manifold, and the intake biogas-air charge brings about a decrease and dilution of oxygen concentration, which may cause a longer ignition delay, leading to the increase in cylinder pressure in the premixed combustion phase. This reason is in good agreement with that of Carlucci et al. [83] for the results they obtained from a diesel-natural gas dual fuel diesel engine. Another reason for the increase in the maximum cylinder pressure in the dual fuel operation with advanced injection is due to the formation of a fuel rich mixture inside the combustion chamber. Karim [220] has reported similar reasons in his research work.

5.3.3 Performance analysis

5.3.3.1 BSFC

The variation of the BSFC with load at different injection timings is depicted in Figure 5.3.6. It can be observed from the figure that, the BSFC decreases in all the test conditions with the increase in the engine load, for both the diesel and dual fuel operations. This reduction in the BSFC can be explained by the fact that, as the engine load increases, the combustion quality and the efficiency improves. The in-cylinder pressure increases with the increase in the

engine load and increase in the injected fuel quantity, which burns more efficiently; therefore, the fuel consumption per unit brake power (i.e. BSFC) produced is decreased. Chandra et al. [100], and Agarwal et al. [232] have also documented similar reasons.

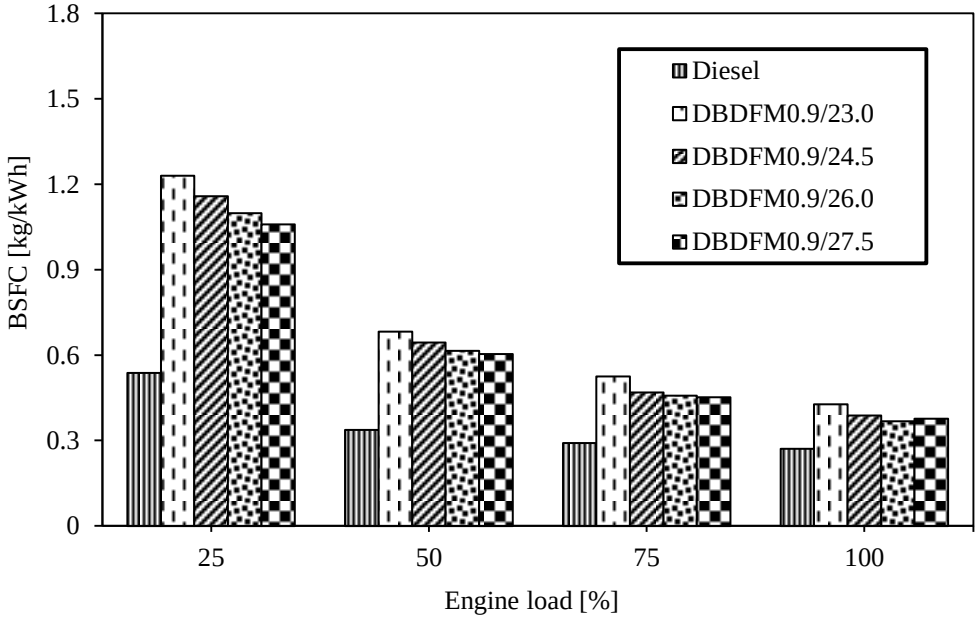

Figure 5.3.6 Variation of BSFC with load.

It is also revealed that the BSFC in the dual fuel operation, especially at low and intermediate engine load conditions, is considerably higher compared to that of diesel operation. This is due to the result of lower premixed controlled combustion during the initial stage of combustion at low load. In the dual fuel operation, with advanced injections, the use of a large quantity of pilot fuel leads to a total higher heat release during the premixed controlled combustion. This results in an increase in the cylinder charge temperature, which affects positively the rate of combustion of biogas during the second phase of combustion (diffusion combustion). This statement is in good agreement with Bari [106], and Papagiannakis et al. [237]. Moreover, for each pilot fuel amount, the advanced injection of DBDFM0.9/24.5, DBDFM0.9/26.0, and DBDFM0.9/27.5 leads to a gradual decrease in the BSFC, in comparison to DBDFM0.9/23.0. The increase in the ignition delay period in the dual fuel operation, leads to a rapid increase of the heat release curve during the premixed controlled combustion phase, and hence, improves the fuel conversion efficiency, and the combustion duration becomes shorter. This improvement is more worthwhile in high load operations. This reason matches with those given by Agarwal et al. [232], and Papagiannakis et al. [237]. The difference between the BSFC in the dual fuel operation with the original injection timing and advanced injection timings is not significantly different at full load, because at full load both the operations have similar fuel-energy conversion efficiency [91], as less energy from

the fuel is required at full load compared to low load, due to the increased cylinder temperature at full load. This reason is in good agreement with those given by Bedoya et al. [97], and Mustafi at al. [105] for the results they obtained from a biogas fueled dual fuel diesel engine. At full load, the BSFC for diesel and DBDFM0.9/23.0 is 0.27 kg/kWh and 0.42 kg/kWh. For DBDFM0.9/24.5, DBDFM0.9/26.0, and DBDFM0.9/27.5 the BSFC is found to be 0.38 kg/kWh, 0.36 kg/kWh, and 0.37 kg/kWh respectively, at full load.

5.3.3.2 BTE

The variation of the BTE with load for the diesel and diesel-biogas dual fuel operations at different injection timings is depicted in Figure 5.3.7.

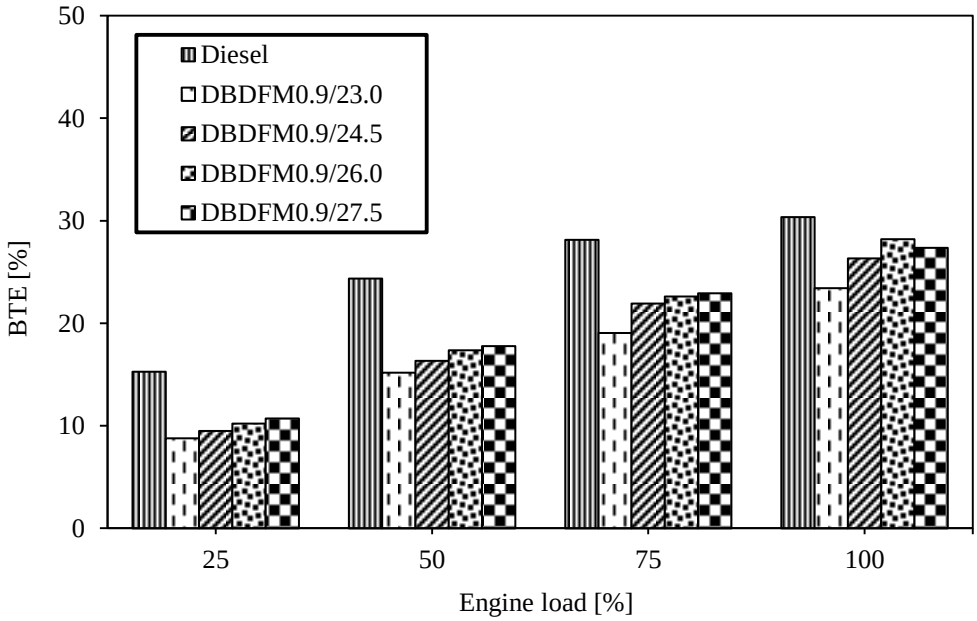

Figure 5.3.7 Variation of BTE with load.

It can be observed from the figure that, the BTE increases with the increase in the load. This is because of the increased cylinder temperature at relatively higher loads. The BTE of diesel is about 30.3%, and for DBDFM0.9/23.0 the BTE is about 26.1% at full load. A drop in the BTE of 4.2% is observed for DBDFM0.9/23.0 in comparison with diesel at full load. This drop in the BTE is due to the drop in the volumetric efficiency, caused by the induction of biogas through the intake manifold. A similar trend for the drop in the BTE was also reported by Paul et al. [88] and Ryu [92] when they carried out an investigation on a single cylinder, diesel engine fueled with natural gas, diesel and biodiesel. In the dual fuel operation, the variation of BTE with the injection timing is quite significant at medium and high loads. It can also be observed that, the dual fuel operation with the advanced injection timings causes an increase in the BTE throughout the load spectrum. DBDFM0.9/24.5, DBDFM0.9/26.0,

and DBDFM0.9/27.5 gives BTE of about 26.8%, 28.1% and 27.3% respectively, at full load. At 25% operating load, the BTE is improved from 8.4% to 10.7% for DBDFM0.9/27.5. At full load, DBDFM0.9/26.0 gives a higher BTE of 28.1%, which is the maximum compared to the other injection timings. In the dual fuel operation, advancing the injection timing to 3 ^{o}CA gives 4.7% increase in the BTE, at full load. This is due to the greater vaporization of the pilot fuel, and a better air fuel mixing at relatively advanced injections.

5.3.3.3 EGT

The variation of EGT at different injection timings, with the variation of load is depicted in Figure 5.3.8.

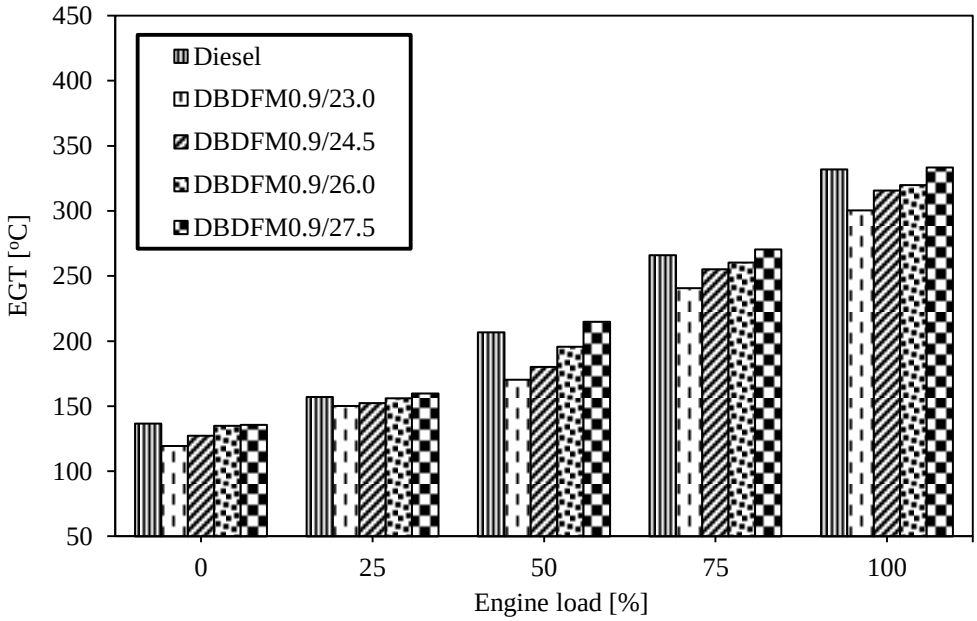

Figure 5.3.8 Variation of EGT with load.

It can be observed from the figure that, the EGT increases with the increase in the load. In diesel operation, the maximum EGT of 331.8 ^{o}C is noticed at full load. The EGT in the dual fuel operation with advanced injection timing increases steeply compared to that of diesel operation. This is due to the effect of advanced injection timing that enhances the combustion rate, results in a high cylinder temperature, and thus increases the EGT [82]. DBDFM0.9/27.5 exhibits the highest value of exhaust gas temperature of 333.3 ^{o}C at full load, whereas DBDFM0.9/23.0 exhibits a lower exhaust gas temperature in comparison with the other injection timings. This reduction in the exhaust gas temperature is due to the lower density of the inducted biogas, which decreases the local adiabatic flame temperature by absorbing the heat energy to auto ignite during combustion.

5.3.4 Emission analysis

5.3.4.1 CO emission

Figure 5.3.9 portrays the variation of the CO emission for the diesel and diesel-biogas dual fuel operations at different injection timings and different loads.

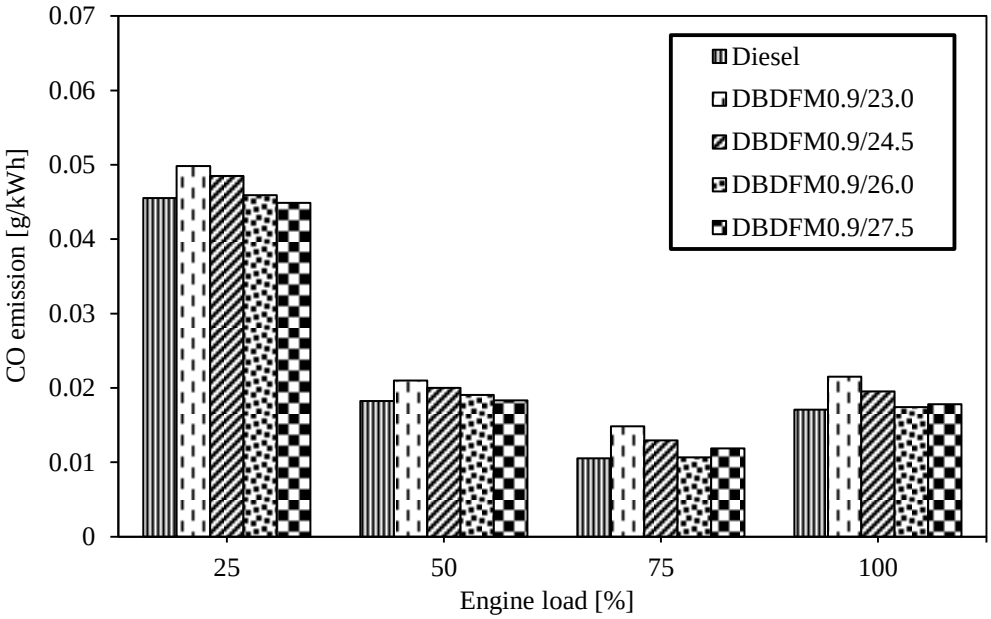

Figure 5.3.9 Variation of CO emission with load.

In general, the CO emission is due to incomplete combustion of fuel. The main reasons for the generation of higher CO emission are the low temperature of the reaction mixture, lack of oxidants, and suitable time duration for combustion. The CO emission is considerably higher in the dual fuel operation than that of diesel throughout the load spectrum. This is due to the existence of a flame extinction region, and most of the CO is due to the incomplete oxidation of premixed biogas. Liu et al. [84] reported a similar reason for CO emission in a CNG-diesel fueled dual fuel diesel engine. Another reason for the incomplete combustion in the dual fuel operation is the dilution of the charge with the CO_2 present in the biogas. The flame formed in the ignition region of the pilot fuel is normally suppressed, and does not proceed until the biogas fuel-air mixture reaches a minimum limiting value for auto ignition. At low load, the fuel air mixture in the peripheral zone of the injection spray becomes too lean to sustain the flame propagation and the local temperature falls, which reduces the oxidation of CO, and hence, the CO emission is high at low load. With the increase in the load, the CO emission decreases; this is attributed to the higher cylinder gas temperature at high load, that boosts the rate of combustion, and the subsequent higher energy release from the fuel. It can also be observed from the figure, that in the dual fuel operation, with the advanced injection timing,

the CO emission decreases in comparison with the original injection timing. This is because the advanced injection timing gives a higher cylinder temperature, and increases the oxidation between the carbon and oxygen molecules. Similar results were documented by Papagiannakis et al. [237] when they carried out an investigation on a dual fuel diesel engine. Lower CO emissions of about 9.2%, 19% and 17.3% are observed for DBDFM0.9/24.5, DBDFM0.9/26.0, and DBDFM0.9/27.5 respectively, than that of DBDFM0.9/23.0, at full load.

5.3.4.2 HC emission

The variation of the HC emission with load for different injection timings is depicted in Figure 5.3.10.

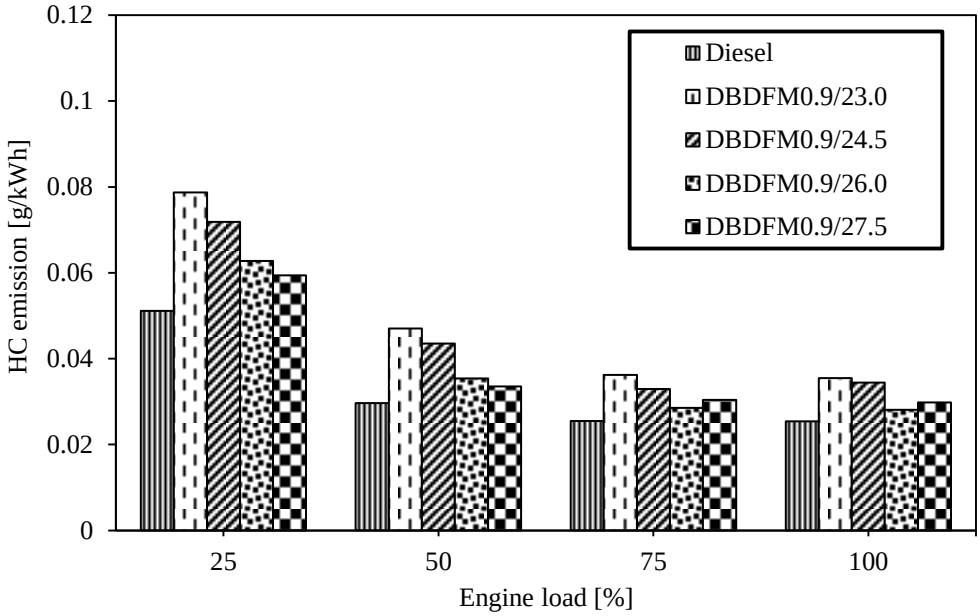

Figure 5.3.10 Variation of HC emission with load.

It can be observed from the figure that, the HC emission decreases with the increase in the load for both the diesel and dual fuel operations. This is due to the increase in the ignition energy, improved pilot fuel spray atomization characteristics, turbulence intensity, increase in the heat transfer to the air-fuel mixture, and increase in the number of ignition centers in the combustion chamber. This reason is in good agreement with that of Liu et al. [84], Duc and Wattanavichien [98], and Jingura and Matengaifa [238]. The concentration of HC emission in the dual fuel operation is considerably higher than that of diesel, under all the test conditions. For DBDFM0.9/23.0, the HC emission is found to be higher by about 43%, in comparison with diesel, at full load. This is due to the induction of biogas through the intake manifold, which reduces the volume of inducted air forming a richer mixture, and an increase in the

partial burning with less oxygen. A similar reason for higher HC emission in a dual fuel diesel engine was documented by Papagiannakis et al. [237]. The dual fuel operations of DBDFM0.9/24.5, DBDFM0.9/26.0, and DBDFM0.9/27.5 give lower HC emissions of about 5.7%, 23% and 18.4% respectively, than that of DBDFM0.9/23.0, at full load. This reduction in the HC emission with advanced injection timing is due to the earlier start of combustion relative to TDC; hence, the cylinder charge temperature becomes higher and a proper combustion of the compressed charge in the combustion chamber gives a lower unburned HC emission. Similar reasons are given by Yang et al. [239] based on their investigation on a turbocharged common rail dual fuel engine.

5.3.4.3 NO emission

The variation of NO emission with injection timing at different loads is depicted in Figure 5.3.11.

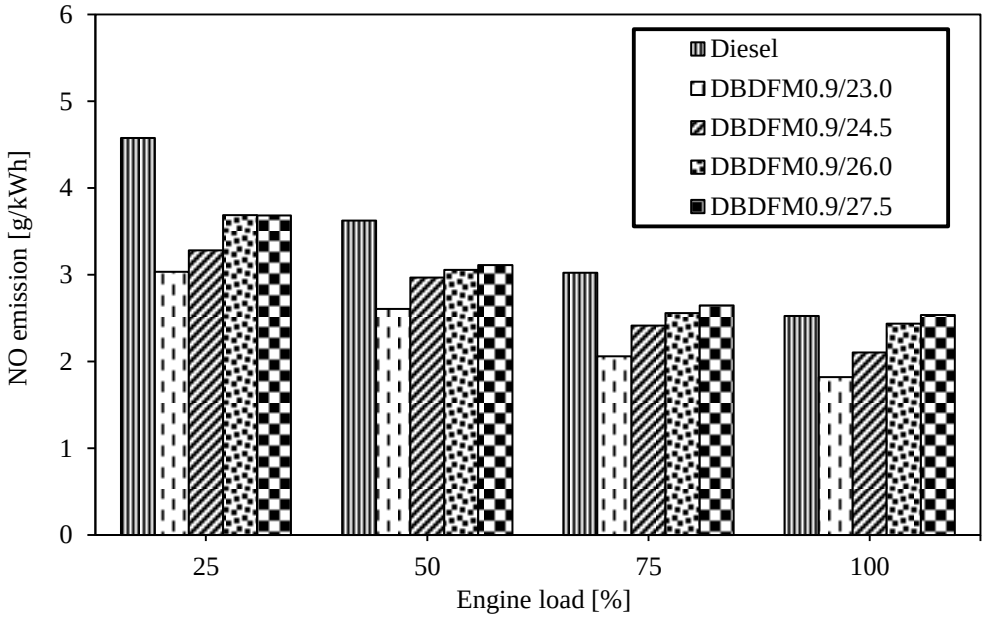

Figure 5.3.11 Variation of NO emission with load.

The concentration of the NO emission is found to decrease steeply for all the test conditions with an increase in the load. A lower NO emission of about 37.7% is observed for DBDFM0.9/23.0, in comparison with that of diesel, at full load. This is due to the presence of CO_2 in the biogas, which has a high molar specific heat that dilutes the charge and lowers the cycle temperature significantly, and thereby the NO formation is suppressed. This reason is in good agreement with those of Nathan et al. [197], Krishnan et al. [240], and Bedoya et al. [241], for the reason they correlated for NO emission in natural gas and biogas fueled HCCI engines [197,240]. The dual fuel operations of DBDFM0.9/24.5, DBDFM0.9/26.0, and

DBDFM0.9/27.5 give an increase in the NO emissions of about 15.7%, 33.8%, and 39.4% respectively, in comparison with DBDFM0.9/23.0, at full load. This is because the advanced injection timing increases the peak cylinder pressure and temperature, as more fuel burns close to the TDC. As a result, the NO emission increases. It is also observed that the NO emissions are about 28%, 16.7%, and 13.2% lower for DBDFM0.9/24.5, DBDFM0.9/26.0, and DBDFM0.9/27.5 respectively, than that of diesel, at full load.

5.3.4.4 Smoke emission

Figure 5.3.12 portrays the variation of the smoke emission with the injection timing at different loads.

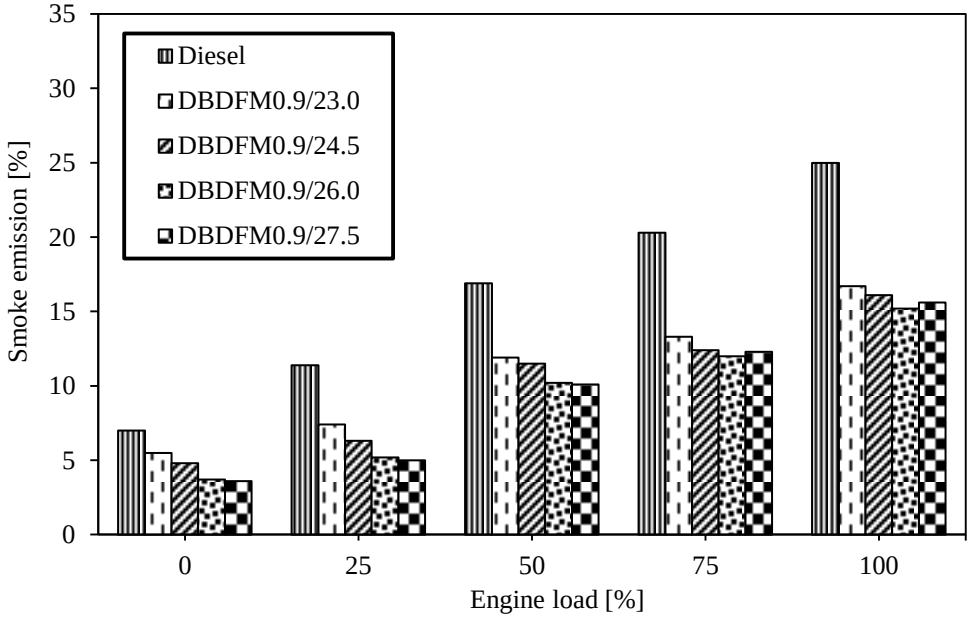

Figure 5.3.12 Variation of smoke emission with load.

It can be observed from the figure that, the smoke emission increases with the increase in load. This is due to the high stoichiometric air requirement at high load operations. Violeta et al. [99], and Alla et al. [242] have also reported a similar reason for the results they have obtained from a biogas fueled diesel engine. DBDFM0.9/23.0 gives a lower smoke emission of about 33% in comparison with diesel at full load. Using biogas in the dual fuel operation is a very effective method to reduce the smoke emission at almost all engine operating points. This is due to the presence of methane in biogas, as the main constituent, that is a lower member in the paraffin family, and possesses a very small tendency to produce soot. This reason matches well with that mentioned by Papagiannakis et al. [82]. In general, the reduction of smoke is attributed to the flame temperature reduction and increased oxidation of soot precursors in the soot forming region by the enhanced concentration of O and OH

around the flame (resulting in high oxidation) produced from the CO_2 in biogas. This reason is in good agreement with the one given by Mustafi et al. [105] in their research work carried out using a DI diesel engine fueled with natural gas and biogas. DBDFM0.9/24.5, DBDFM0.9/26.0, and DBDFM0.9/27.5 give lower smoke emissions of 35.6%, 39.2%, and 30.4% respectively, than diesel at full load. This reduction in the smoke opacity is due to the higher combustion rate, and longer time for the oxidation of the soot particles in the combustion chamber, due to the advanced injections.

5.3.5 Summary

The outcomes of this section are as follows:

- The dual fuel operation of DBDFM0.9/26.0 gives an optimum result in terms of the combustion, performance and emission than those of other injection timings.
- The BSFC for DBDFM0.9/26.0 is found to be higher by about 25% than that of diesel operation, at full load.
- At full load, DBDFM0.9/26.0 gives a maximum BTE of 28.1%, which is higher than that of other injection timings.
- In the dual fuel operation, on advancing the pilot fuel injection to 3 ^{o}CA over that of normal injection timing, the BTE increases by about 4.7%, at full load.
- DBDFM0.9/26.0 gives lower CO and HC emissions of about 19% and 23%, than that of DBDFM0.9/23.0 but, the CO and HC emissions are higher by about 2% and 10% respectively, than that of diesel, at full load.
- The NO emission for DBDFM0.9/26.0 is higher by about 26% than that of DBDFM0.9/23.0 but, it is lower by about 3.8% than that of diesel, at full load.
- DBDFM0.9/26.0 gives a lower smoke emission of about 39% than that of diesel, at full load.

Table 5.3 provides the values of the important parameters of the investigation carried out for diesel and diesel-biogas dual fuel operations with different advanced injection timings at full load.

Table 5.3 Summary of the values of the combustion, performance and emission parameters at full load, for diesel and diesel-biogas dual fuel with variation in injection timing.

Sl. No.	Parameters	Diesel	DBDFM0.9/23.0	DBDFM0.9/24.5	DBDFM0.9/26.0	DBDFM0.9/27.5
A. Combustion parameters						
1	Maximum cylinder pressure, bar	75.7	74.6	76.1	80.2	84.4
2	Maximum heat release rate, J/^{o}CA	56.5	55.2	55.4	56.8	57.2
3	Ignition delay, ^{o}CA	11.5	12.7	12.9	13.1	13.6
4	Combustion duration, ^{o}CA	37.4	40.4	40.1	39.4	39.9
B. Performance parameters						
1	BSFC, kg/kWh	0.27	0.42	0.38	0.36	0.37
2	BTE, %	30.3	26.1	26.8	28.1	27.3
3	EGT, ^{o}C	331	300	315	319	333
C. Emission parameters						
1	CO, g/kWh	0.017	0.021	0.019	0.017	0.017
2	HC, g/kWh	0.025	0.035	0.034	0.028	0.029
3	NO, g/kWh	2.52	1.81	2.10	2.43	2.53
4	Smoke emission, %	25	16.7	16.1	15.2	15.6

5.4 Biodiesel-biogas dual fuel mode with different flow rates of biogas

5.4.1 General

Biodiesel is a renewable fuel and considered as one of the potential liquid alternative fuel for diesel in developing countries. In recent years, many pilot and commercial biodiesel plants have been installed and are in operation. These plants use edible and nonedible seeds as raw materials. Biodiesel gives certain advantages over diesel when used in a diesel engine in the dual fuel mode. The diesel-biogas dual fuel mode gives a longer ignition delay and higher CO and HC emission, which is evident from the results of the previous section. The high cetane number and dissolved oxygen in biodiesel can shorten the ignition delay and reduce the CO and HC emission. Hence, in this section Karanja biodiesel, i.e. Karanja methyl ester (KME) extracted from the Karanja seed was used as a pilot fuel in place of diesel and the engine was set to operate in the dual mode with biogas. The biogas was generated from the Karanja de-oiled seed cakes. And the utilization of the whole part of the Karanja seed may also be possible. The combustion performance and emission characteristics of the engine are analyzed in the biodiesel-biogas dual fuel mode. For this purpose, biogas at four different flow rates was inducted in suction, while biodiesel was injected as the pilot fuel.

The biodiesel-biogas dual fuel mode is denoted by BBDFMX, where X indicates the flow rate of biogas in kg/h. The acronyms used in this investigation are as follows:

BBDFM0.3 - biodiesel + biogas 0.3 kg/h,

BBDFM0.6 - biodiesel + biogas 0.6 kg/h

BBDFM0.9 - biodiesel + biogas 0.9 kg/h

BBDFM1.2 - biodiesel + biogas 1.2 kg/h

The results of the investigation have already published in Energy Conversion and Management which is mentioned in the list of publication.

5.4.2 Combustion analysis

5.4.2.1 Pressure crank angle diagram

The variation of cylinder pressure with crank angle for diesel, KME and dual fuel operations are depicted in Figure 5.4.1. The peak cylinder pressure mainly depends mainly on the rate of combustion in the premixed combustion stage [234]. The peak cylinder pressure for KME is about 71.3 bar, which occurs at 6.8 ^{o}CA aTDC. In dual fuel operation the peak cylinder

pressures of 73.7 bar, 73.5 bar, 72.9 bar and 74.3 bar occur at 7.9 ^{o}CA aTDC, 10.2 ^{o}CA aTDC, 8.1 ^{o}CA aTDC and 12.7 ^{o}CA aTDC, for the biogas flow rates of 0.3 kg/h, 0.6 kg/h, 0.9 kg/h and 1.2 kg/h respectively, at full load. In the dual fuel operation, the increase in the biogas flow rate results in an increase in the cylinder pressure. The reason for the higher peak cylinder pressure in the dual fuel operation than that of KME operation is due to the induction of biogas with the intake-air charge that brings about a decrease and dilution of oxygen concentration, which may cause the ignition delay to extend, leading to a higher rate of increase in pressure in the premixed combustion phase. This reason matches with that given by Tonkunya and Wongwuttanasatian [243]. It is observed that the presence of CO_2 in biogas did not significantly affect the maximum cylinder pressure, but the ignition and peak cylinder pressure occurred a little later and shifted some degrees toward the expansion process. A similar reason is evidenced by Duc and Wattanavichien [98], and Mustafi et al. [105].

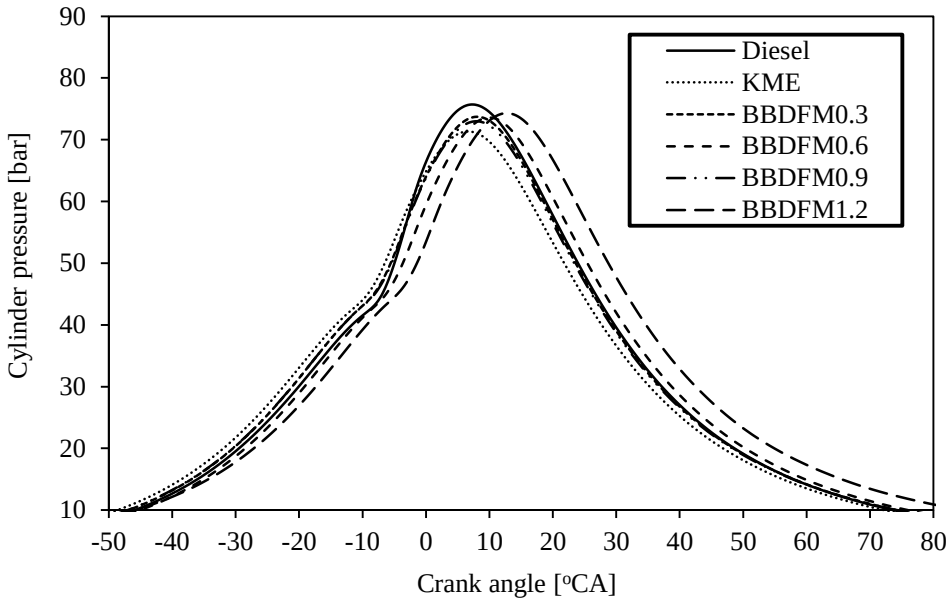

Figure 5.4.1 Variation of cylinder pressure with crank angle at full load.

5.4.2.2 Ignition delay

Figure 5.4.2 depicts the variation of ignition delay with load. Ignition delay is mainly influenced by parameters, such as the fuel type, fuel quality, air-fuel ratio, engine speed, fuel atomization quality, inducted air temperature, compression ratio, and pressure [234]. KME gives a shorter ignition delay than that of other fuels throughout the load spectrum. This is due to the presence of oxygen in the ester molecules. In dual fuel operation, with the increase in biogas quantity the ignition delay increases, throughout the load spectrum. The ignition delay in the dual fuel operation increases by about 1-2 ^{o}CA over that of KME. This is due to

the presence of biogas in the fuel-air mixture, which alters the pre-ignition property of the charge, and reduces the oxygen concentration. This reason is also evidenced by the research work documented by Yoon and Lee [103]. A shorter ignition delay is noticed for the fuels at full load, than that of no load, due to the higher cylinder temperature at full load. The ignition delay period usually increases with an increase in the amount of gaseous fuel in the charge, for most gaseous fuels under normal operating conditions. This reason matches with that given by Mustafi [105].

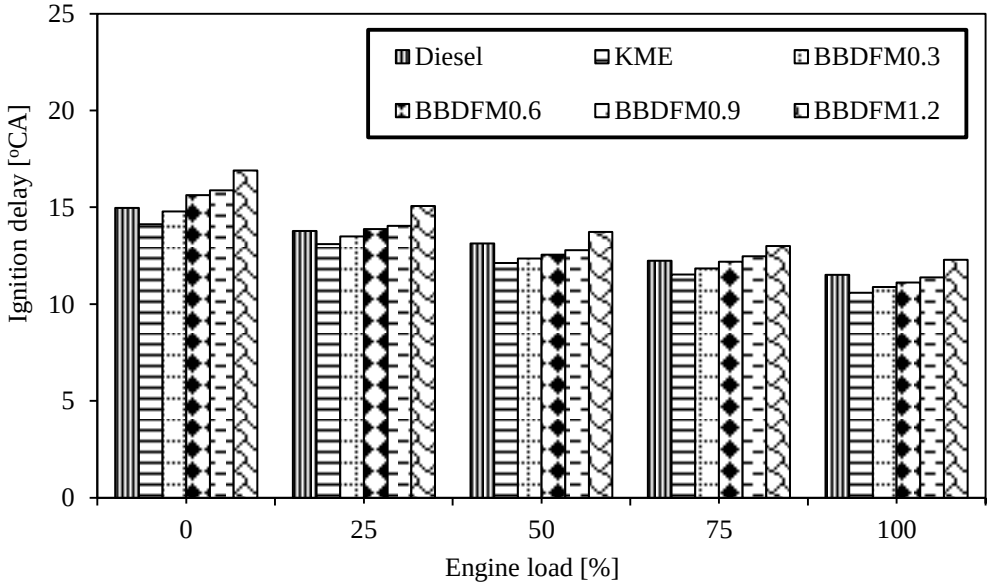

Figure 5.4.2 Variation of ignition delay with the variation in load.

5.4.2.3 Heat release rate

The variation of the heat release rate with crank angle for diesel, KME and dual fuel operations is depicted in Figure 5.4.3. The heat release rate in the premixed combustion phase depends on the ignition delay, mixture formation and the combustion rate in the initial stages [98]. The dual fuel operation gives a higher heat release rate than that of KME operation. This is due to the combined effect of the combustion of the pilot fuel and gaseous fuel in the immediate vicinity of the ignition and combustion centers of the pilot fuel. A similar reason is evidenced by Mustafi et al. [105] in their research. The heat release rate for diesel is higher irrespective of the fuels used. This is due to higher energy density of diesel than that of KME and biogas. The dual fuel operation of BBDFM0.6 gives a maximum heat release rate of 54.1 J/^{o}CA than that of BBDFM0.3, BBDFM0.9, and BBDFM1.2. This may be attributed to the maximum amount of energy released immediately following the commencement of auto-ignition of the pilot fuel. Because, with the increase in the concentration of biogas in the air

and with the corresponding excess air ratio, which modifies and extends significantly the flammability zone around the pilot fuel. A similar reason was given by Karim [220], and Patterson [244] when they carried out an investigation on a small diesel engine operating on the dual fuel mode. The occurrence of heat release rate is found to be earlier in KME operation, than that of dual fuel operation, due to its higher cetane number and the presence of oxygen molecules in the fuel itself. The maximum heat release rate for KME is observed at 6.8 ^{o}CA aTDC, whereas, for BBDFM0.3, BBDFM0.6, BBDFM0.9, and BBDFM1.2 the maximum heat release rate is observed at 9.95 ^{o}CA aTDC, 10.7 ^{o}CA aTDC, 8.1 ^{o}CA aTDC, and 11.7 ^{o}CA aTDC respectively, at full load.

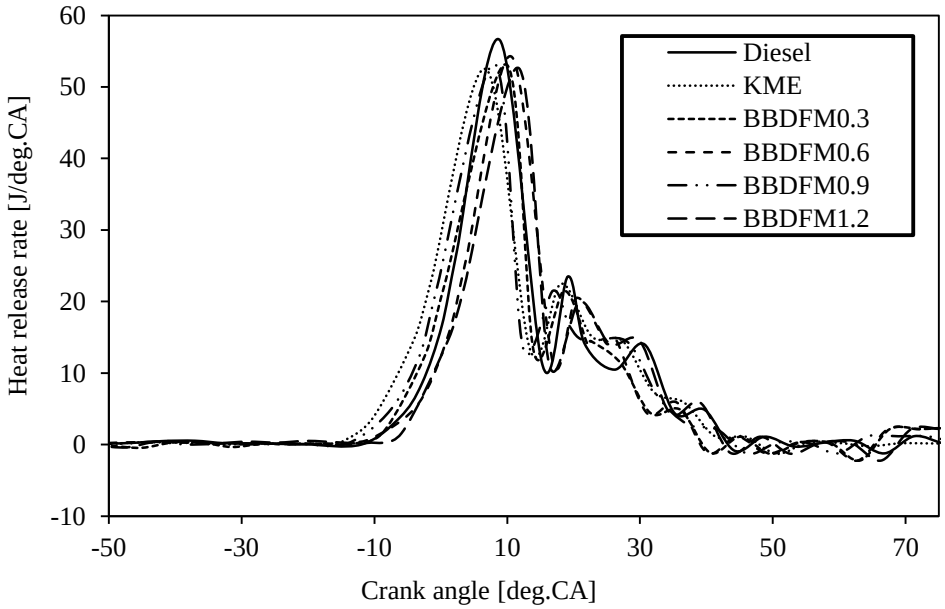

Figure 5.4.3 Variation of the heat release rate with crank angle at full load.

5.4.2.4 Combustion duration

The variation of combustion duration for diesel, KME and dual fuel operations with the variation in load is depicted in Figure 5.4.4. The combustion duration for KME is 39.3 ^{o}CA, at full load. The combustion duration for the dual fuel operation increases with an increase in the biogas quantity and vice versa. The biogas dual fuel operation of BBDFM0.3, BBDFM0.6, BBDFM0.9, and BBDFM1.2 gives a marginal increase in the combustion duration of 39.6 ^{o}CA, 39.8 ^{o}CA, 40.8 ^{o}CA and 41.8 ^{o}CA respectively, at full load. This is due to the induction of more quantity of biogas. The inducted biogas alters the physical properties of the charge being compressed, reduces the oxygen concentration in the charge mixture, causing slower diffusion combustion, which results in a prolonged combustion duration. A similar reason for the increase in combustion duration was given by Papagiannakis and

Hountalas [91], when they modified the diesel engine to operate on the dual fuel mode with diesel and biogas. In addition, biogas causes a slower rate of burning of the pilot fuel, as it contains about 17 % CO_2. In diesel, KME and dual fuel operations, longer combustion durations are noticed at full load than that of no load, due to the consumption of more fuel at relatively high load.

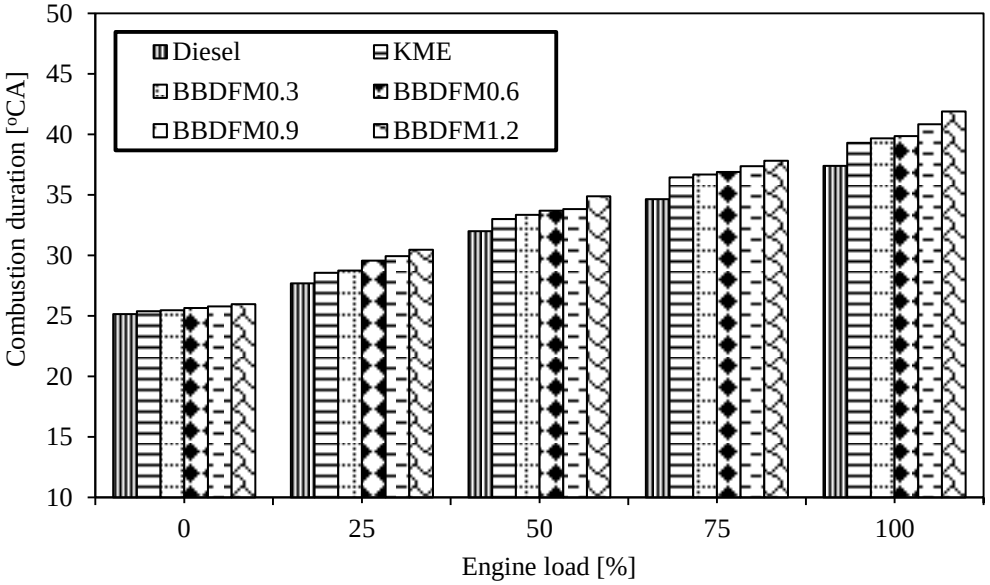

Figure 5.4.4 Variation of the combustion duration with load.

5.4.2.5 Maximum cylinder pressure

Figure 5.4.5 portrays the variation of the maximum cylinder pressure with load.

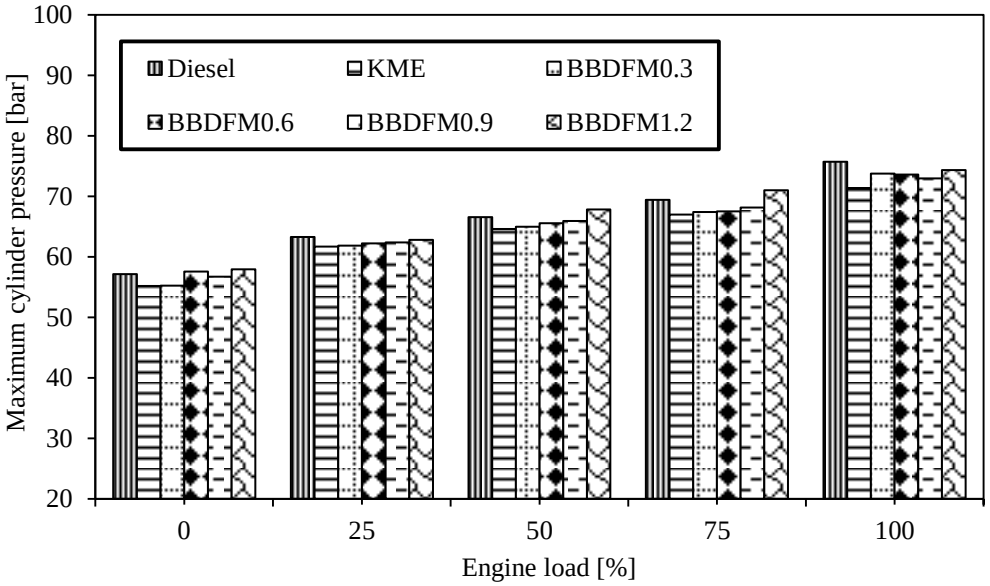

Figure 5.4.5 Variation of the maximum cylinder pressure with load.

In the dual fuel operation, the maximum cylinder pressure increases with the increase in the biogas quantity. The maximum cylinder pressure for diesel and KME are about 75.7 bar and 71.3 bar. BBDFM0.3, BBDFM0.6, BBDFM0.9, and BBDFM1.2 gives a higher cylinder pressure of 73.7 bar, 73.5 bar, 72.9 bar, and 74.29 bar respectively, at full load. The increase in the maximum cylinder pressure in the dual fuel operation is due to the induction of biogas with the intake-air charge brings about a decrease and dilution of oxygen concentration, which may cause the ignition delay to extend, leading to a higher rate of increase in pressure in the premixed combustion phase [243].

5.4.3 Performance analysis

5.4.3.1 BSFC

The variation of BSFC with the variation in load is depicted in Figure 5.4.6.

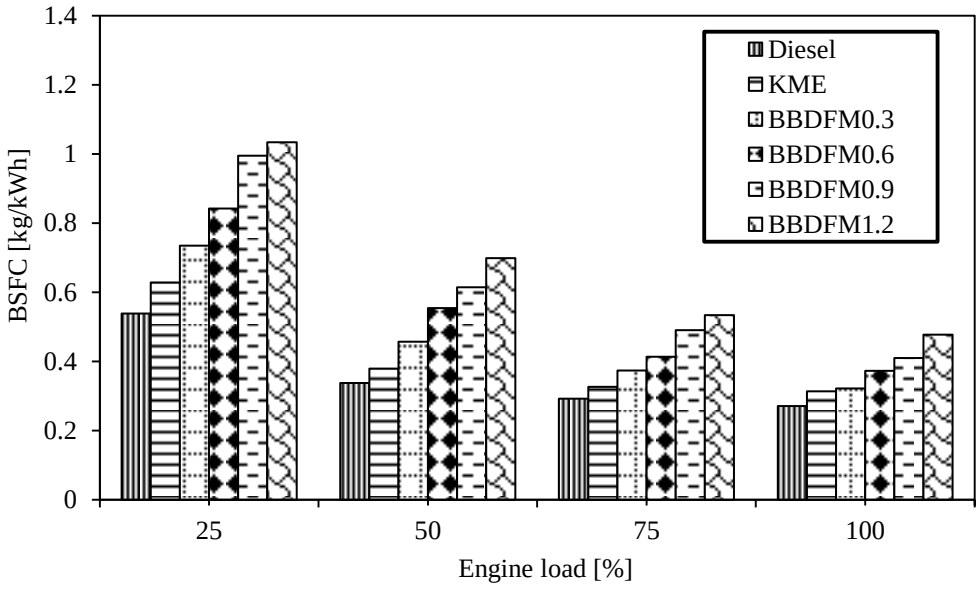

Figure 5.4.6 Variation of BSFC with load.

It can be observed from the figure that, a higher BSFC is noticed for the dual fuel operation than that of diesel and biogas at part load operation. This may be due to the lower energy density of biogas and the presence of CO_2 in biogas, which prevents faster burning [105]. The difference in BSFC for the diesel, KME and dual fuel operation is not significantly different at full load. At full load the dual fuel operation has similar fuel energy conversion efficiency to that of diesel and KME. Similar results have been reported by Papagiannakis and Hountalas [91], and Selim [245] during their investigation on a dual fuel diesel engine. This is because less energy from the fuel is required at full load, compared to that of no load, due to the increased cylinder temperature at full load [105]. The BSFC for diesel and KME are

0.27 kg/kWh and 0.31 kg/kWh. The BSFC for BBDFM0.3, BBDFM0.6, BBDFM0.9, and BBDFM1.2 is 0.32 kg/kWh, 0.37 kg/kWh, 0.40 kg/kWh and 0.49 kg/kWh respectively, at full load.

5.4.3.2 BTE

The variation of BTE with load for diesel, KME and KME-biogas dual fuel operation is illustrated in Figure 5.4.7. It can be observed from the figure that, the BTE for diesel is higher than that of KME and KME-biogas dual fuel operations. This is due to the higher calorific value of diesel. At full load, the BTE of diesel, and KME are 30.3% and 28% respectively, and in dual fuel operation of BBDFM0.3, BBDFM0.6, BBDFM0.9, and BBDFM1.2 the BTE is found to be 27.2%, 26.4%, 25.6%, and 24.1% respectively. A drop in BTE of 0.8%, 1.6%, 2.4%, and 3.9% is observed for BBDFM0.3, BBDFM0.6, BBDFM0.9, and BBDFM1.2 respectively in comparision to KME at full load. This reduction in the BTE is due to the deficiency of oxygen caused by the induction of biogas through the intake manifold. The deficiency of oxygen causes incomplete combustion and subsequent decrease in converting the input fuel energy, and results in a higher total fuel flow rate during the combustion process. Paul et al. [86] have also observed a similar trend for the drop in BTE. Also, another reason may be the decreased flame propagation speed and increased negative compression work, which in turn, are caused by the induction of a large quantity of air-biogas mixtures [103].

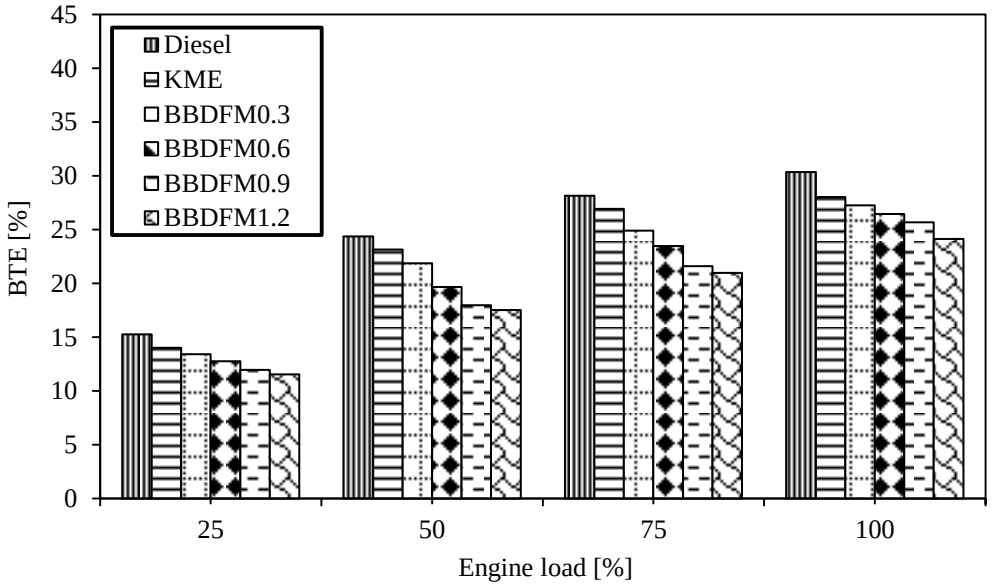

Figure 5.4.7 Variation of BTE with load.

5.4.3.3 Energy share

The variation of biogas induction quantity with biogas energy share is depicted in Figure 5.4.8. It can be observed from the figure that, the biogas energy share is low at full load, while the energy share is high at no load, for all the flow rates of biogas in dual fuel operation. This is due to more KME consumption at relatively high load than at no load. BBDFM1.2 gives the maximum energy share in comparison with the other flow rates throughout the load spectrum. At full load, BBDFM0.3, BBDFM0.6, BBDFM0.9, and BBDFM1.2 give energy shares of about 11.8%, 22%, 30.2% and 37.4% respectively.

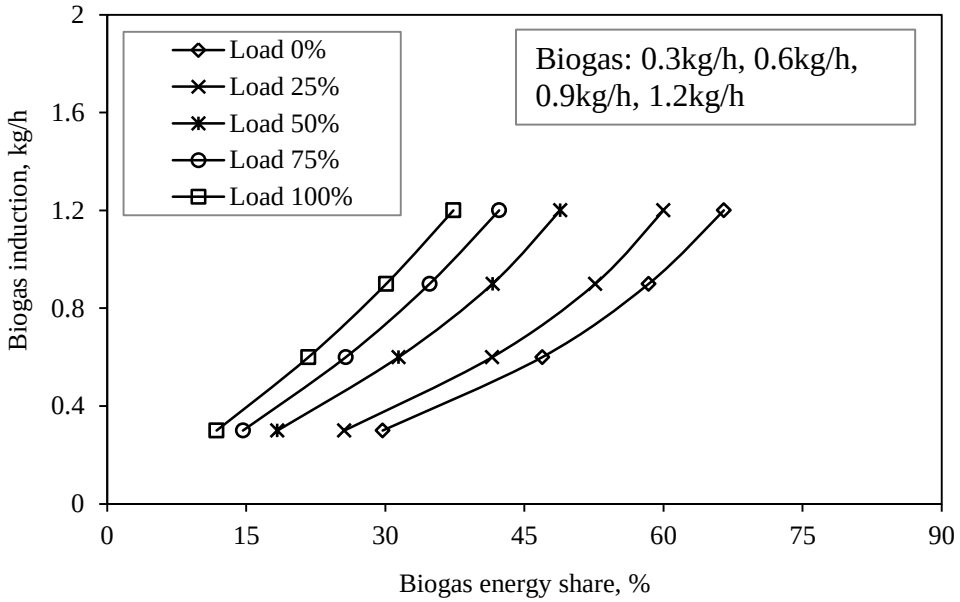

Figure 5.4.8 Variation of biogas induction quantity with energy share.

5.4.3.4 EGT

Figure 5.4.9 illustrates the variation of EGT with load. The KME operation gives the highest exhaust gas temperature throughout the load spectrum. The oxygen present in the ester molecule enhances the combustion process, and results in a higher EGT. In the dual fuel operation, the EGT drops with the increase in the biogas energy share. This is because, the biogas in the inducted air gets hotter to auto ignite during the combustion process, and absorbs the heat energy, which decreases the local adiabatic flame temperature, leading to a reduction in the EGT. On the other hand, the lower EGT is due to the increase in the diluent resulting from the 17% CO_2 in the biogas.

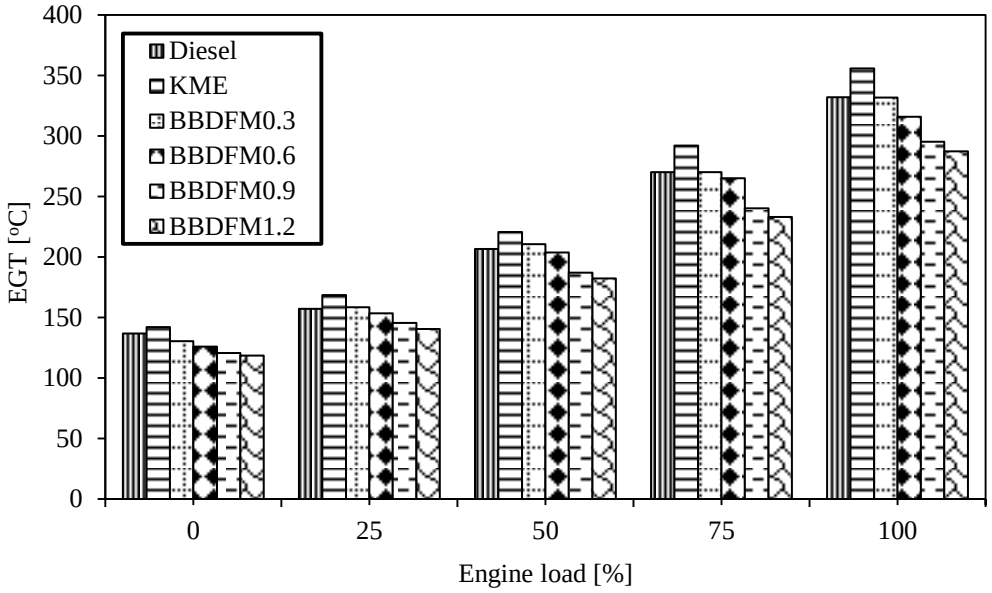

Figure 5.4.9 Variation of EGT with load.

5.4.3.5 Volumetric efficiency

Figure 5.4.10 depicts the variation of volumetric efficiency with the biogas energy share.

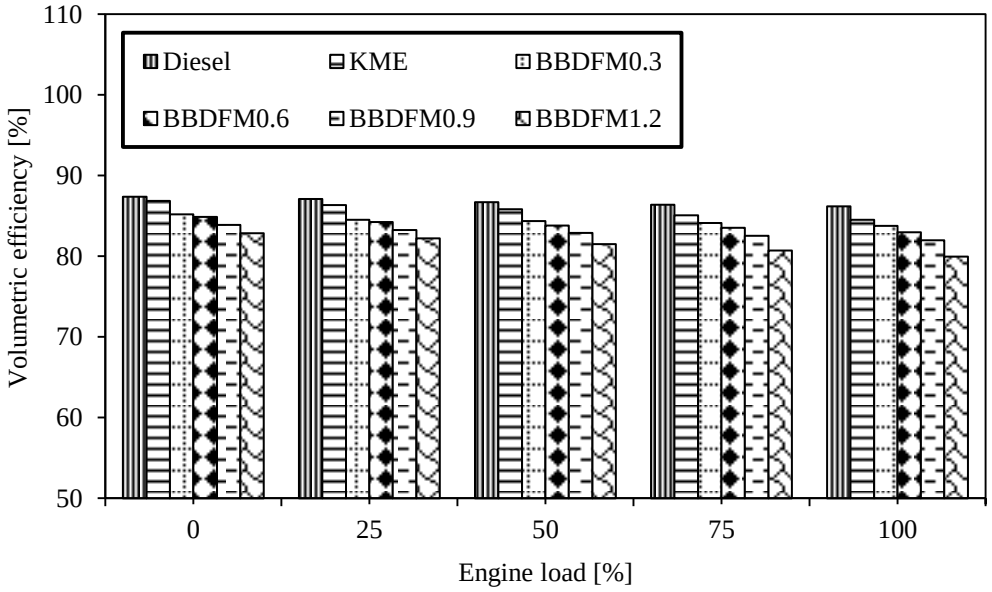

Figure 5.4.10 Variation of the volumetric efficiency with load.

The volumetric efficiency of diesel and KME are found to be higher than that of the dual fuel operation. The volumetric efficiency of diesel and KME are found to be about 86.2% and 84.5% at full load, whereas, the volumetric efficiencies of BBDFM0.3, BBDFM0.6, BBDFM0.9, and BBDFM1.2 are about 83.77%, 82.92%, 82% and 79.9% respectively, at full load. The reduction in the volumetric efficiency in the dual fuel operation is due to the induction of biogas with the air through the intake manifold, which replaces some of the fresh

air. The excess air ratio for the dual fuel operation decreases with the increase in the biogas energy share, which directly influences the volumetric efficiency. The drop in volumetric efficiency in full load in comparison to part load may be due to the increase in the inducted air temperature, because of the hot cylinder wall, which results in the reduction of air density, causing a reduction in the volumetric efficiency at full load. This reason is in good agreement with that of Lakshmanan and Nagarajan [208].

5.4.4 Emission analysis

5.4.4.1 CO emission

The concentration of the CO emission with respect to the variation of load is depicted in Figure 5.4.11. In general, the CO emission is formed as a result of incomplete combustion of the fuel. The dual fuel operation of BBDFM0.3, BBDFM0.6, BBDFM0.9, and BBDFM1.2 gives a higher CO emission of 7.1%, 14%, 28.5%, and 35.7% respectively, than that of KME at full load. This may be due to the dilution of the charge by the CO_2 present in the biogas which gives a higher CO emission. Muralidharan et al. [218] reported that, the lower CO emission from the KME operation is attributed to the additional oxygen present in the fuel. Also, the increased cetane number of KME lowers the probability of forming a fuel rich zone, and advanced ignition. It is also apparent from the figure that, the BSCO emissions are high at low loads due to poor mixture formation.

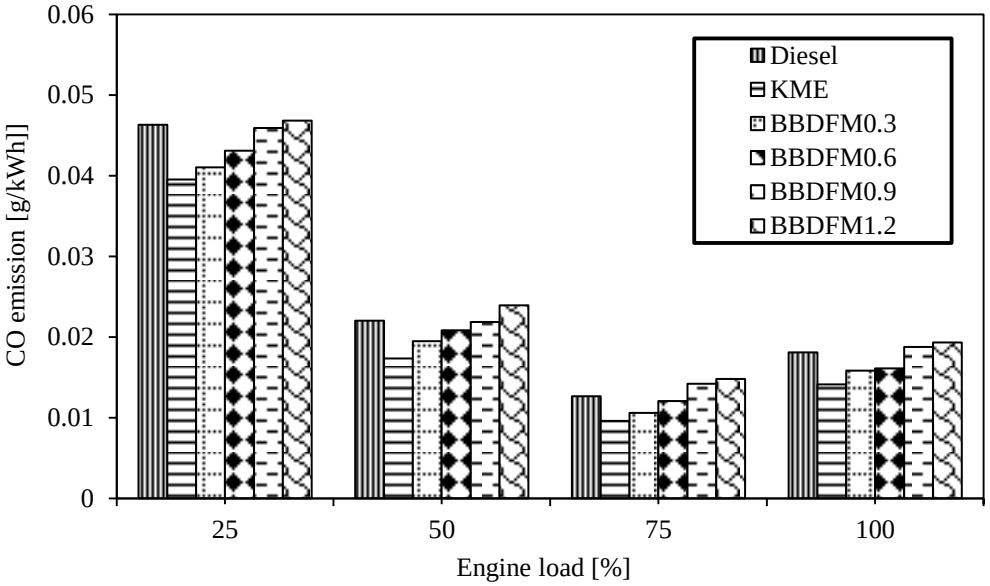

Figure 5.4.11 Variation of CO emission with load.

5.4.4.2 HC emission

The variation of the HC emission with load is depicted in Figure 5.4.12. The dual fuel operation shows a higher HC emission than that of diesel and KME operation. The higher HC emission in the dual fuel operation is due to the induction of excess amount of biogas through the intake manifold, which reduces the volume of inducted air forming a richer mixture, and an increase in the partial burning with less oxygen [93,237]. Thus, it is evident that the HC level goes up, whenever the biogas energy share increases and vice-versa. This reason is in good agreement with that of Ryu [93], when he carried out an investigation on a biogas run single cylinder DI diesel engine. The HC emission for KME is lower than that of dual fuel operation. Probably, the oxygen content in the KME causes complete combustion and reduces the level of HC emission. This reason is in good agreement with that of Yoon and Lee [103]. About 8.9%, 28.2%, 37%, and 46% increment in the HC emission is observed for BBDFM0.3, BBDFM0.6, BBDFM0.9, and BBDFM1.2 respectively, at full load.

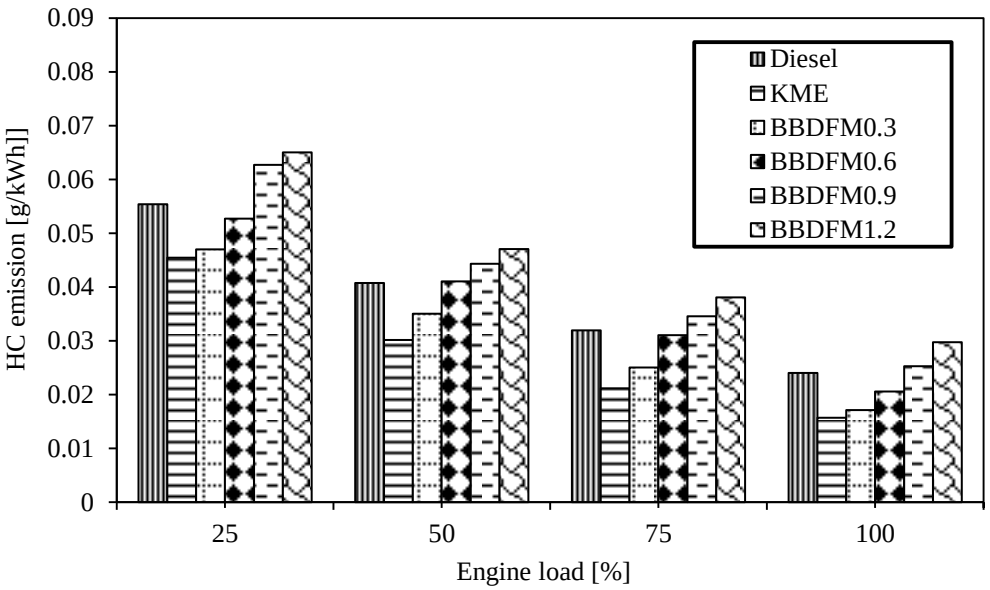

Figure 5.4.12 Variation of HC emission with load.

5.4.4.3 NO emission

The variation of the NO emission with load is shown in Figure 5.4.13. The concentration of NO for the dual fuel operation is considerably lower than that of diesel and KME operation. The NO formation is highly dependent on the combustion temperature, availability of oxygen, compression ratio and the retention time for the reaction. In the dual fuel operation, the presence of CO_2 having a high molar specific heat, dilutes the charge and lowers the cycle temperature significantly. In addition, the CO_2 in the biogas lowers the oxygen concentration

of the charge followed by an overall decrease in the cycle temperature. Hence, the NO formation is suppressed with the combined effect of these phenomena [197,228,241]. The higher NO emission for the KME operation is due to the higher oxygen concentration. A similar reason for a higher NO is reported by Ryu [92] in his investigation. A reduction of 13%, 23%, 26% and 38% in the NO emission is obtained for BBDFM0.3, BBDFM0.6, BBDFM0.9, and BBDFM1.2 respectively, in comparison with KME, at full load.

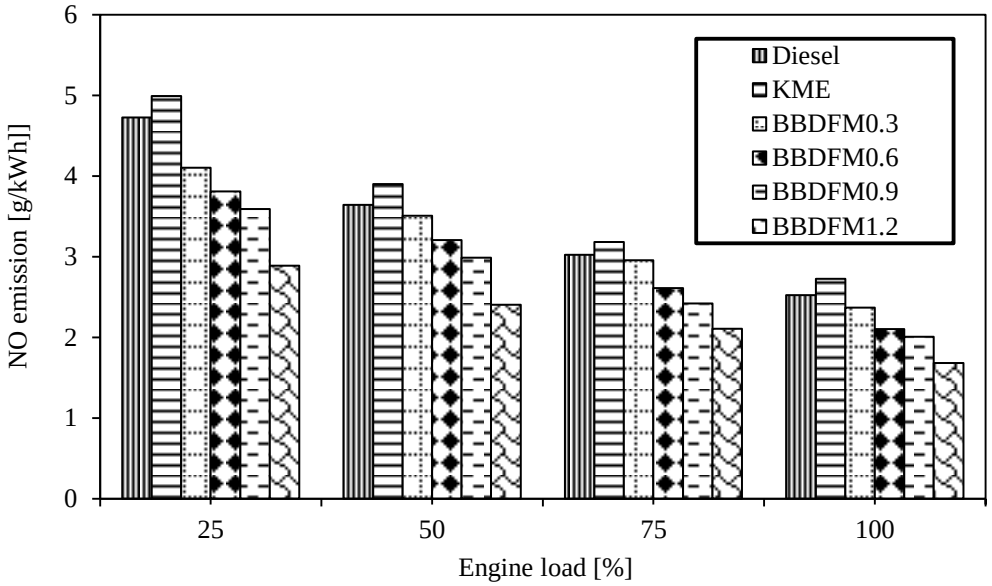

Figure 5.4.13 Variation of NO emission with load.

5.4.4.4 Smoke emission

Figure 5.4.14 depicts the variation of the concentration of smoke emission with engine load. It is observed that the dual fuel operation is a potential way of reducing smoke emission. Specifically, at low engine loads in dual fuel operation, the energy share of biogas is more and the percentage of KME substitution increases, and hence smoke opacity decreases. BBDFM0.3, BBDFM0.6, BBDFM0.9, and BBDFM1.2 give lower smoke emissions of 4%, 10.2%, 12.5% and 9.3% than that of KME, at full load, respectively. It is apparent that, in dual fuel operation, using biogas is a very effective method to reduce the smoke emission at almost all engine operating points. This is due to the presence of methane in biogas, as the main constituent; that is the lower member in the paraffin family, possesses a very low tendency to produce soot. This reason is in good agreement with that of Papagiannakis et al. [82]. In general the reduction of smoke is attributed to flame temperature reduction and increased oxidation of soot precursors in the soot forming region by the enhanced concentration of O and OH around the flame (resulting a high oxidation) produced from the

CO_2 in the biogas. A similar reason is given by Mustafi [105] when he investigated the application of biogas in a diesel engine in the dual fuel mode. The CO_2 concentration in the fuel causes a decrease in the overall cycle temperature, which has a positive (i.e. reduction) impact on smoke formation and, at the same time, does not seem to have an adverse (i.e. increase) effect on the NO emissions as generally happens in normal diesel engines.

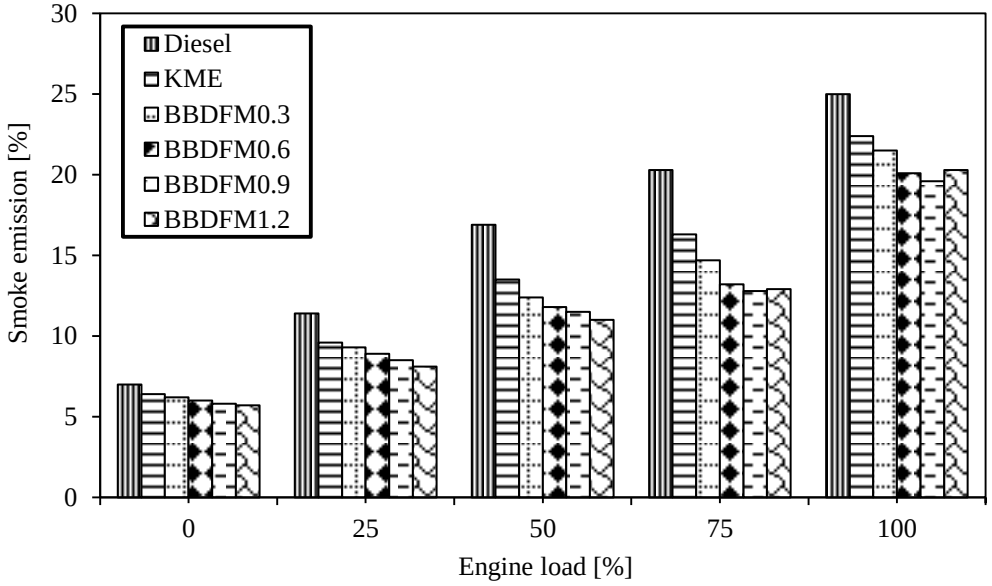

Figure 5.4.14 Variation of smoke emission with load.

5.4.5 Summary

The conclusions drawn from the results of the investigation are as follows;

- In dual fuel operation BBDFM0.9 gives the optimum results, in terms of the performance, combustion and emission, than that of other flow rates, tested in this study.
- The BSFC for BBDFM0.9 is found to be higher by about 29% than that of KME at full load.
- BBDFM0.9 gives a drop in BTE of about 2.4% than that of KME at full load.
- The CO and HC emissions are found to be higher by about 28.5% and 37% for BBDFM0.9 in comparison with KME at full load.
- The NO and smoke emissions at full load are found to be lower by about 26% and 12.5% respectively, for BBDFM0.9, in comparison with KME.

Table 5.4 provides the values of the important parameters of the investigation obtained from the biodiesel and biodiesel-biogas dual fuel operation at full load.

Table 5.4 Summary of the values of the combustion, performance and emission parameters at full load for biodiesel and biodiesel-biogas dual fuel.

Sl. No.	Parameters	Diesel	KME	BBDFM0.3	BBDFM0.6	BBDFM0.9	BBDFM1.2
A. Combustion parameters							
1	Maximum cylinder pressure, bar	75.4	71.3	73.7	73.5	72.9	74.2
2	Ignition delay, ^{o}CA	11.5	10.5	10.88	11.12	11.38	12.29
3	Maximum heat release rate, J/^{o}CA	56.5	52.4	53.1	54.1	53.2	52.6
4	Combustion duration, ^{o}CA	37.4	39.3	39.6	39.8	40.8	41.8
B. Performance parameters							
1	BSFC, kg/kWh	0.27	0.31	0.32	0.37	0.40	0.47
2	BTE, %	30.3	28	27.2	26.4	25.6	24.1
3	Biogas energy share, %	-	-	11.8	22	30.2	37.4
4	EGT, ^{o}C	331.8	355.8	331.7	315.8	295.1	287.3
5	Volumetric efficiency, %	86.2	84.5	83.7	82.9	82	79.9
C. Emission parameters							
1	CO, g/kWh	0.017	0.014	0.015	0.016	0.018	0.019
2	HC, g/kWh	0.024	0.0156	0.017	0.020	0.025	0.029
3	NO, g/kWh	2.523	2.726	2.367	2.101	2.007	1.682
4	Smoke opacity, %	25	22.4	21.5	20.1	19.6	20.3

5.5 Biodiesel-biogas dual fuel mode with optimum flow of biogas at different injection timings

5.5.1 General

From the results of the previous section, it was understood that the biogas flow rate of 0.9 kg/h can be chosen as the optimum flow rate. Further, the investigation was carried out to determine the injection timing of the pilot fuel, used in the dual fuel mode. The combustion, performance and emission characteristics of the engine run on the biodiesel-biogas dual fuel mode, with the optimum biogas flow rate, at different injection timings, are presented in this section. The acronyms used for the investigation are as follows:

BBDFM0.9/21.5 – biodiesel + biogas 0.9 kg/h with biodiesel injection timing of 21.5 ^{o}CA bTDC

BBDFM0.9/23.0 - biodiesel + biogas 0.9 kg/h with biodiesel injection timing of 23 ^{o}CA bTDC

BBDFM0.9/24.5 – biodiesel + biogas 0.9 kg/h with biodiesel injection timing of 24.5 ^{o}CA bTDC

BBDFM0.9/26.0 – biodiesel + biogas 0.9 kg/h with biodiesel injection timing of 26 ^{o}CA bTDC

BBDFM0.9/27.5 – biodiesel + biogas 0.9 kg/h with biodiesel injection timing of 27.5 ^{o}CA bTDC

5.5.2 Combustion analysis

5.5.2.1 Pressure crank angle diagram

Figure 5.5.1 portrays the variation of cylinder pressure with the crank angle at full load, for diesel, KME, and biodiesel-biogas dual fuel operations with advanced and retarded injection timings. It can be observed that, the peak cylinder pressures for diesel and KME operations are about 75.7 bar and 71.3 bar, which occur at 7.4 and 6.8 ^{o}CA aTDC respectively. For BBDFM0.9/21.5, BBDFM0.9/23.0, BBDFM0.9/24.5, BBDFM0.9/26 and BBDFM0.9/27.5, the peak cylinder pressure was about 67.8 bar, 73 bar, 78 bar, 82.6 bar and 87.6 bar, and occured at about 9.2 ^{o}CA aTDC, 8.1 ^{o}CA aTDC, 6.3 ^{o}CA aTDC, 4.8 ^{o}CA aTDC and 3.8 ^{o}CA aTDC respectively. The BBDFM0.9/23.0 gives a higher cylinder pressure than that of KME at full load. This is due to the supply of biogas with the intake air charge that brings about a decrease in the oxygen concentration, which may cause the ignition delay to extend, leading to a higher rate of increase in pressure in the premixed combustion stage. Similar reasons are given by Duc and Wattanavichien [98] for the results they obtained from a DI diesel engine operated on the biogas-

diesel dual fuel mode. It can also be observed that, the peak cylinder pressure increases with the advanced injection of KME in the dual fuel operation. This is due to the formation of a fuel rich zone inside the combustion chamber. With advanced injections, the combustion takes place in the earlier crank angles in the cycle, and more rapid burning takes place in the premixed phase of combustion. Hence, the maximum amount of fuel burns before the top dead centre (TDC) and the peak cylinder pressure moves closer to the TDC. The same reason was reported by many researchers, for instance Sahoo et al. [61] and Agarwal et al. [232] in their studies.

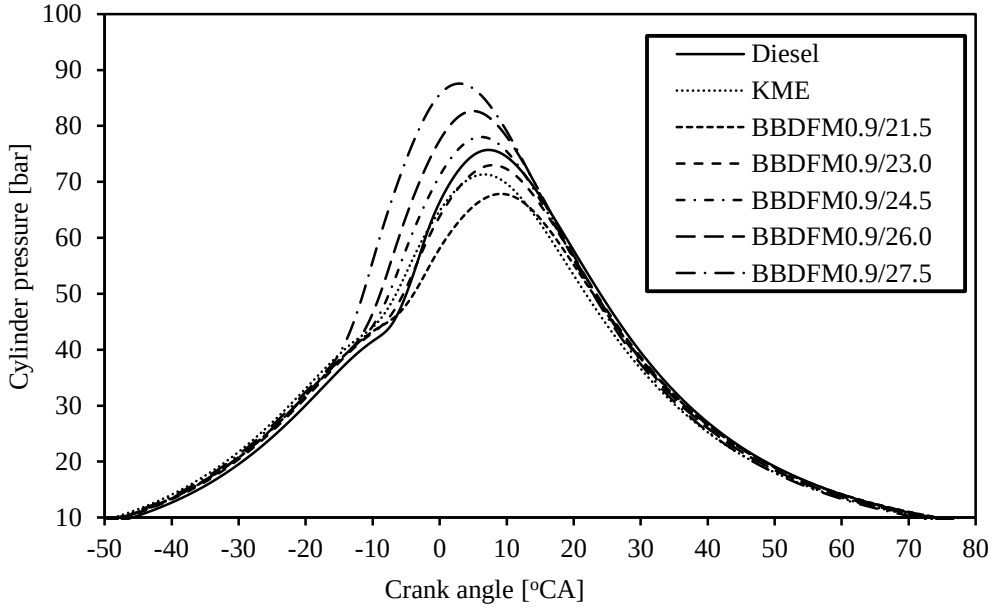

Figure 5.5.1 Variation of cylinder pressure with the crank angle at full load.

5.5.2.2 Ignition delay

The variation of ignition delay with load for diesel, KME and biodiesel-biogas dual fuel operations with advanced and retarded injection timings is depicted in Figure 5.5.2. It is seen that KME exhibits a shorter ignition delay than that of diesel and dual fuel operations throughout the load spectrum. This is due to the higher cetane number of KME and the existence of oxygen in the fuel. The ignition delay in the dual fuel operation of BBDFM0.9/23.0 is longer than that of KME throughout the load spectrum. This is due to the induction of biogas through the intake manifold which replaces the fresh air supply, which in turn reduces the oxygen concentration in the charge, and effects the pre-ignition of the KME-biogas mixture, leading to a delay in the ignition. Similar reasons were described by Paul et al. [88], and Ryu [92] in their investigation for the results they obtained from a CNG-biodiesel fueled DI diesel engine. It can also be

observed that, the ignition delay in the dual fuel operation decreases with the retarded injection timing due to the high in-cylinder pressure and temperature. In the dual fuel operation, with advanced injection timing, the ignition delay was found to be longer. This may be due to the low in-cylinder temperature at early injections that delayed the pilot ignition. This reason is also endorsed by Ryu [92] for the work he carried out on a single cylinder, DI diesel engine run on the CNG-biodiesel dual fuel mode. At full load, a shorter ignition delay is noticed than that of no load, for all the test fuels, due to the higher cylinder temperature at full load. The ignition delay for diesel and KME are found to be 11.5 ^{o}CA and 10.5 ^{o}CA, whereas BBDFM0.9/21.5, BBDFM0.9/23.0, BBDFM0.9/24.5, BBDFM0.9/26, and BBDFM0.9/27.5 exhibit longer ignition delay of 10.9 ^{o}CA, 11.3 ^{o}CA, 11.9 ^{o}CA, 12.5 ^{o}CA, and 12.8 ^{o}CA at full load respectively.

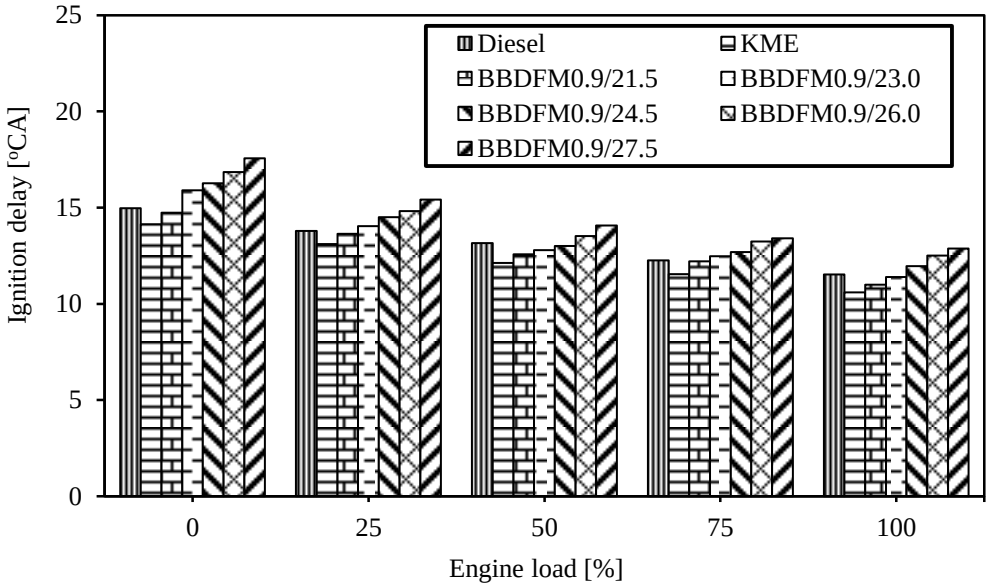

Figure 5.5.2 Variation of ignition delay with load.

5.5.2.3 Heat release rate

Figure 5.5.3 portrays the variation of the heat release rate with the crank angle at full load for diesel, KME, and biodiesel-biogas dual fuel operations with advanced and retarded injection timings. It can be observed from the figure that, the maximum heat release rate of 56.5 J/^{o}CA is noticed in the diesel operation at about 8.9 ^{o}CA aTDC. This is due to the higher energy density of diesel. Sayin and Canakci [246] reported a similar reason for the results they obtained in their research on a diesel engine operated on the diesel-biogas dual fuel mode. The dual fuel operation with the advanced injection timing gives a gradual increase in the heat release rate than that of

BBDFM0.9/23.0. This is due to the increased accumulation of biogas during the relatively longer delay period, and the combined effect of KME and biogas in the vicinity of the combustion and ignition centers of the pilot fuel, which extends the flammability zone. Mustafi et al. [105], and Karim [220] have reported a similar reason for the results they have obtained in a biogas run DI diesel engine. Also, the occurrence of the heat release for BBDFM0.9/24.5, BBDFM0.9/26.0 and BBDFM0.9/27.5 is earlier than that of BBDFM0.9/21.5 and BBDFM0.9/23.0. This may be due to the advanced injection of KME, which gives a full spray and higher injection quantity. Hence, the combustion starts earlier with respect to the TDC, and the maximum percentage of fuel burns in the premixed phase giving more energy. This is in good agreement with the observations of Bora and Saha [247], and Sahoo et al. [61] who conducted their investigation on a DI diesel engine operated in the biogas-biodiesel dual fuel mode. The heat release rate for KME is 52.47 J/^{o}CA, which occurs at 6.83 ^{o}CA aTDC, whereas for BBDFM0.9/21.5, BBDFM0.9/23.0, BBDFM0.9/24.5, BBDFM0.9/26, and BBDFM0.9/27.5 the values were about 50.4 J/^{o}CA, 53.2 J/^{o}CA, 54.3 J/^{o}CA, 54.8 J/^{o}CA, and 55.4 J/^{o}CA, which occur at about 9.2 ^{o}CA aTDC, 8.2 ^{o}CA aTDC, 5 ^{o}CA aTDC, 3.6 ^{o}CA aTDC, and 2.6 ^{o}CA aTDC respectively.

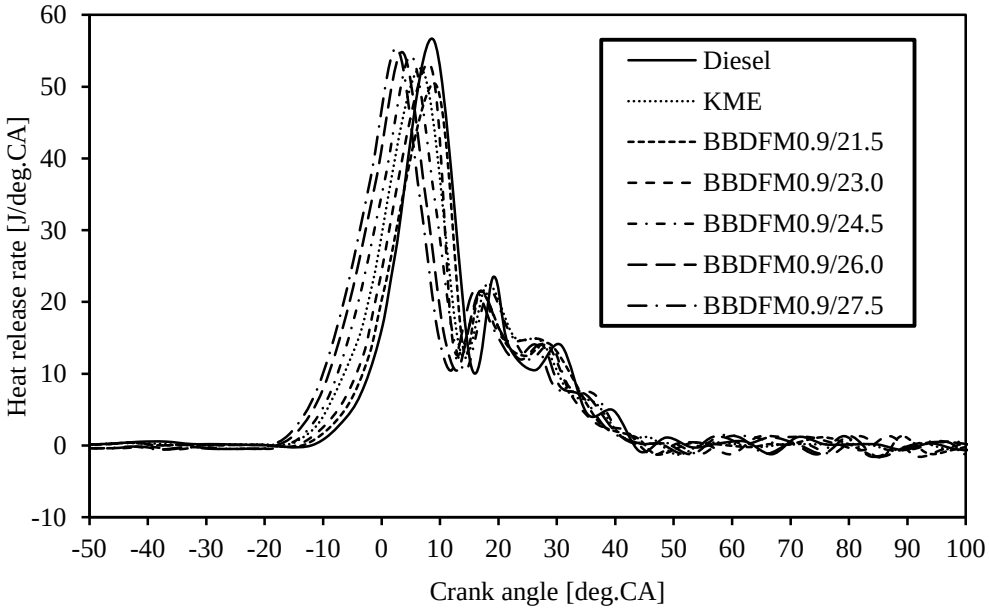

Figure 5.5.3 Variation of the heat release rate with the crank angle at full load.

5.5.2.4 Combustion duration

The variation of the combustion duration with load for diesel, KME and biodiesel-biogas dual fuel operations with advanced and retarded injection timings is shown in Figure 5.5.4.

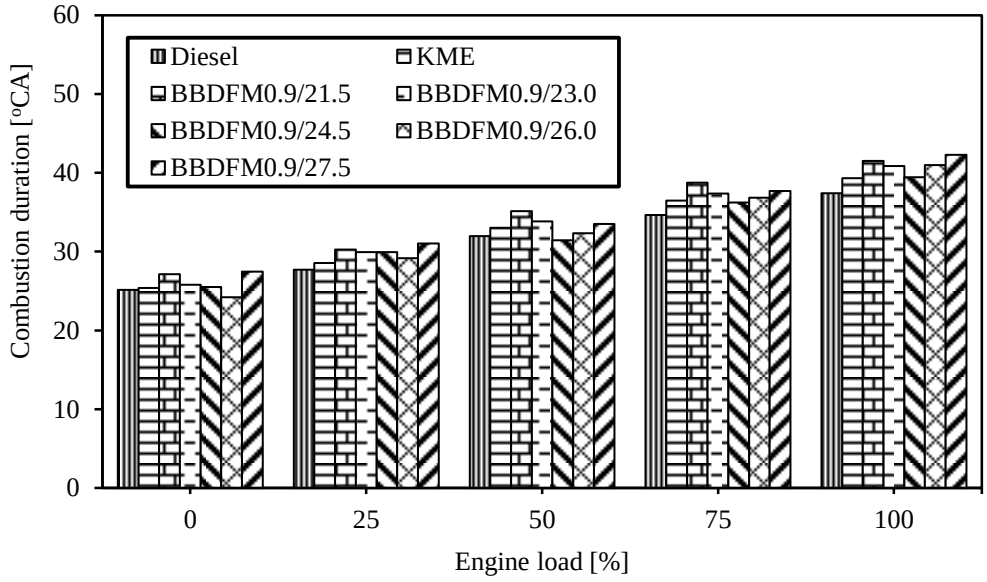

Figure 5.5.4 Variation of the combustion duration with load.

It can be observed that, the combustion duration increases with the increase in load for all the test fuels. This is due to the consumption of more quantity of fuel at relatively higher loads. In the diesel and KME operations, the combustion duration was found to be 37.4 ^{o}CA and 39.3 ^{o}CA respectively, at full load. For BBDFM0.9/23.0, the combustion duration is found to be 40.8 ^{o}CA, at full load. The reason for the increase in combustion duration for BBDFM0.9/23.0 than that of KME is due to the slower rate of burning of the biogas-KME mixture. For BBDFM0.9/24.5 the combustion duration decreases, but while advancing to 26 ^{o}CA and 27.5 ^{o}CA, the combustion duration increased, which may be attributed to the suppression of the charge due to the induction of biogas and lower temperature of the compressed air at far too advanced injections. Bora and Saha [247] have reported a similar reason for the results they have obtained in a biogas-biodiesel fueled DI diesel engine. Another reason for this may be the inducted biogas, which contains CO_2 in it, and alters the properties of the compressed charge, reduces the oxygen concentration, and causes slower diffusion combustion, and prolongs the duration of combustion.

5.5.2.5 Maximum cylinder pressure

Figure 5.5.5 portrays the variation of maximum cylinder with load, for diesel, KME, and KME-biogas dual fuel operations at different injection timings. It can be observed from the figure that, the cylinder pressure increases with the increase in the load, as expected. The maximum cylinder pressure for diesel is about 75.7 bar at full load. But, the dual fuel operations of

BBDFM0.9/21.5, BBDFM0.9/23.0, DBDFM0.9/24.5, DBDFM0.9/26.0, and DBDFM0.9/27.5 give the maximum cylinder pressures of 67.8 bar, 73bar, 78 bar, 82.6 bar, and 87.5 bar respectively, at full load. The reason for the higher maximum cylinder pressure in the dual fuel operation is due to the induction of biogas through the intake manifold, and the intake biogas-air charge that brings about a decrease and dilution of the oxygen concentration, which may cause a longer ignition delay. This may lead to an increase in the cylinder pressure in the premixed combustion phase. This reason is in good agreement with that of Ryu [92] reported for the results obtained in a diesel-natural gas dual fuel diesel engine. Another reason for the increase in the maximum cylinder pressure in the dual fuel operation with advanced injection is due to the formation of a fuel rich mixture inside the combustion chamber. Karim [220] has reported similar reasons in his research work.

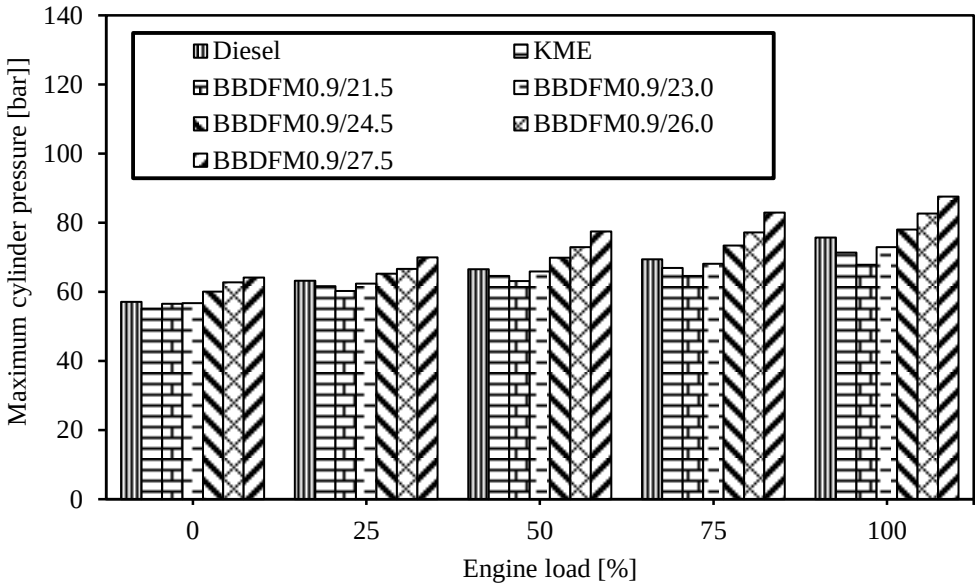

Figure 5.5.5 Variation of the maximum cylinder pressure with load.

5.5.3 Performance analysis

5.5.3.1 BSFC

Figure 5.5.6 portrays the variation of BSFC with load for diesel, KME and biodiesel-biogas dual fuel operations with advanced and retarded injection timings.

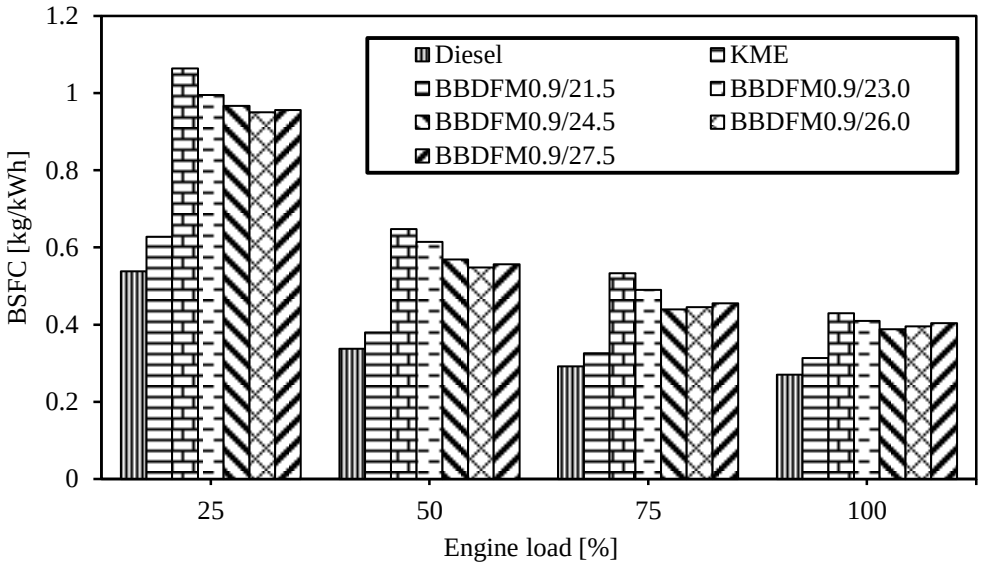

Figure 5.5.6 Variation of BSFC with load.

The BSFC decreases with the increase in load for all the test fuels because, as the load increased, the combustion quality and efficiency increases. The BSFC in the dual fuel operation, at low and intermediate load conditions, is considerably higher in comparison to those of diesel and KME operations. This may be due to the slower premixed controlled combustion during the initial stages of combustion at low load. This reason is in good agreement with that of Papagiannakis et al. [237] reported for the results obtained in a dual fuel diesel engine. In the dual fuel operation, with advanced injections, the use of a large quantity of pilot fuel leads to a total higher heat release during the controlled premixed combustion. This increases the cylinder charge temperature, and the biogas achieves its ignition temperature and affects positively on the rate of combustion of biogas in the second phase of combustion (diffusion combustion). This reason is also evidenced from the research work documented by Bari [106], and Nwafor [233] for the work they have carried out on a diesel engine run on biogas or natural gas on the dual fuel mode. Moreover, for each pilot fuel amount, BBDFM0.9/24.5 leads to a gradual decrease in BSFC, in comparison to that of BBDFM0.9/23.0. The difference between the BSFC for BBDFM0.9/23.0 and BBDFM0.9/24.5, BBDFM0.9/26.0 and BBDFM0.9/27.5 is not significantly different at full load, because at full load the fuel energy conversion efficiency is relatively similar, and less energy from fuel is required at full load compared to low load, due to the increased cylinder temperature at full load. Nwafor [233] has reported a similar reason for the results he has obtained in a biogas-fueled DI diesel engine. The BSFC for diesel and KME are about 0.27

kg/kWh and 0.31 kg/kWh respectively at full load. The BSFC for BBDFM0.9/21.5, BBDFM0.9/23.0, BBDFM0.9/24.5, BBDFM0.9/26.0 and BBDFM0.9/27.5 are found to be higher by about 35.4%, 29%, 22.5%, 25.8%, and 29% respectively, than that of KME at full load.

5.5.3.2 BTE

The variation of the BTE for diesel, KME and the KME-biogas dual fuel mode for different injection timings is depicted in Figure 5.5.7.

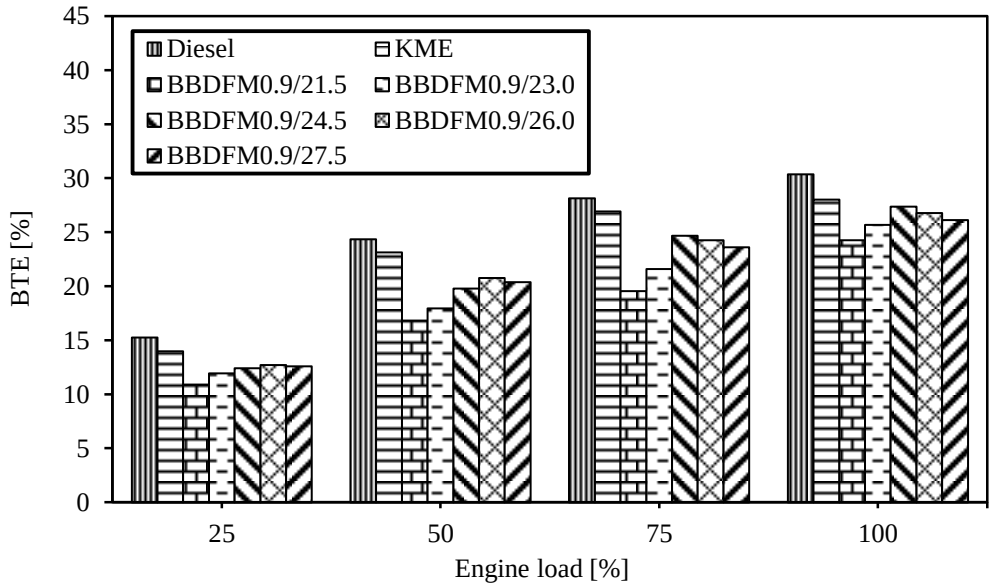

Figure 5.5.7 Variation of BTE with load.

Diesel gives the highest BTE throughout the load spectrum over that of KME and KME-biogas dual fuel operation with different injection timings. This is due to the higher calorific value of diesel. The BTE for the test fuels increases with the increase in load. This is obvious due to the increased cylinder temperature at relatively higher loads. The BTE for diesel and KME operations is about 30.3% and 28% at full load. The BTE of BBDFM0.9/23.0 is 25.6%. A drop in BTE of 2.4 is observed for BBDFM0.9/23.0 in comparison with the KME operation. This drop in BTE may be attributed to the incomplete combustion of KME, due to drop in the volumetric efficiency, caused by the induction of biogas through the intake manifold. Similar reasons were given by Ryu [92], and Paul et al. [88] for the results they obtained from their investigation of a CNG-biodiesel fueled DI diesel engine. BBDFM0.9/24.5 gives a BTE of 27.3%, which is 3.1%, 1.7%, 0.6% and 1.2% higher than that of BBDFM0.9/21.5,

BBDFM0.9/23.0, BBDFM0.9/26.0, and BBDFM0.9/27.0 respectively at full load. BBDFM0.9/24.5 gives a higher BTE of 1.7% than that of BBDFM0.9/23.0 at full load.

5.5.3.3 EGT

The variation of the EGT with load for diesel, KME and biodiesel-biogas dual fuel operations with advanced and retarded injection timings is illustrated in Figure 5.5.8.

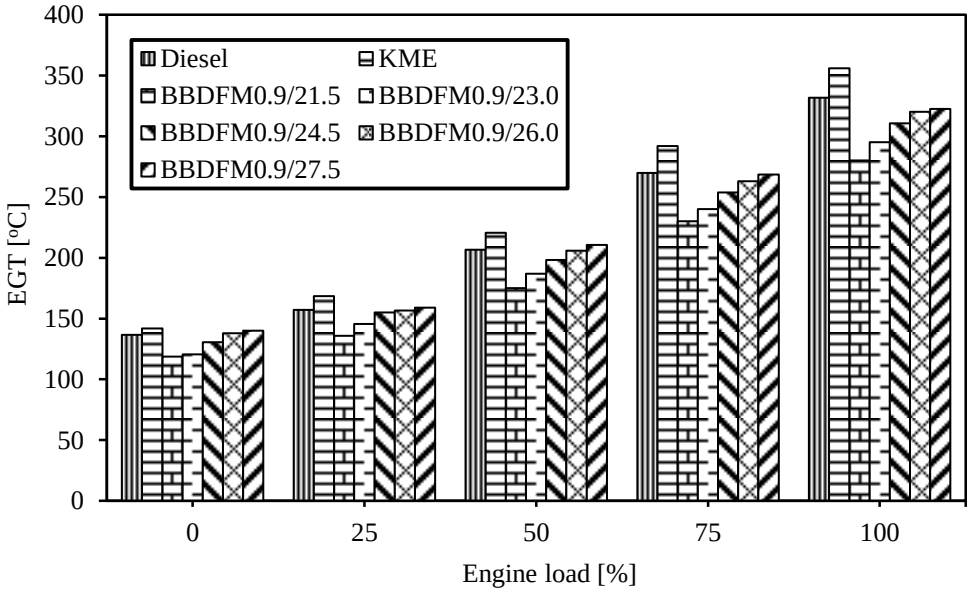

Figure 5.5.8 Variation of the EGT with load.

The KME operation gives the highest exhaust gas temperature than that of diesel and dual fuel operations throughout the load spectrum. The presence of oxygen in the ester molecules enhances the combustion process and results in a higher EGT. The dual fuel operation gives a lower EGT than that of diesel and KME operation. This may be due to the presence of biogas in the fuel-air mixture, which absorbs the heat from the compressed charge to auto ignite during the combustion process, and decreases the local adiabatic flame temperature. This reason is in good agreement with that given by Nwafor [233] for the results obtained from a biogas-fueled dual fuel diesel engine. Another reason for the drop in the EGT may be the dilution of CO_2 (about 17%) in the biogas. With advanced injection timing, the EGT increases. This may be due to the effect of advanced injection, which gives a longer spray of KME, which enhances the rate of combustion, and gives a higher cylinder temperature. A similar reason for the increase in EGT is described by Papagiannakis et al. [82]. The EGT for diesel and KME are found to be 331.8 ^{o}C and 355.8 ^{o}C, whereas the EGT for BBDFM0.9/21.5, BBDFM0.9/23.0, BBDFM0.9/24.5,

BBDFM0.9/26, and BBDFM0.9/27.5 are found to be lower by about 21.2%, 17%, 12.7%, 10%, and 9.3% respectively, than that of KME at full load.

5.5.4 Emission analysis

5.5.4.1 CO emission

The variation of CO emission with load is illustrated in Figure 5.5.9. The CO emission for KME is considerably lower than that of diesel throughout the load spectrum. This is due to the presence of oxygen in KME, which gives a complete oxidation of CO, and hence, the CO reduces. In dual fuel operation, by varying the injection timing, the CO emission is marginally higher than that of KME, throughout the load spectrum. This is due to the existence of a flame extinction region, and the incomplete oxidation of premixed biogas in the dual fuel mode. The reason for the incomplete oxidation is due to the dilution of the charge with CO_2 in the biogas. Hence, the flame is suppressed in the ignition region of the pilot fuel, and does not proceed until the biogas-air mixture reaches a minimum limiting value for auto ignition. This statement is in good agreement with that of Liu et al. [84] reported for the results obtained from a CNG-diesel dual fuel diesel engine.

It is also observed that, the CO emission is higher at part load operations. This is due to the formation of a lean fuel-air mixture in the adjacent zone of the injection spray, in which the flame struggles to propagate, and the local temperature falls, which reduces the oxidation reaction, and results in a higher CO emission at part load operation. The CO emission decreases with the increase in load. This is attributed to the higher cylinder gas temperature which boosts the rate of combustion. A similar reason for the decrease in CO emission is given by Prakash et al. [206]. BBDFM0.9/24.5 gives a lower CO emission than that of other injection timing cases. This is because, advancing the injection timing gives a higher cylinder temperature, and enhances the oxidation of carbon with oxygen. However, on advancing the injection timing to 26.0 ^{o}CA and 27.5 ^{o}CA, the ignition is delayed, allowing less time to the fuel for oxidation, thus giving a higher CO emission. Similar reasons were given by Ryu [92] for the results he obtained from a CNG-biodiesel fueled DI diesel engine. The BBDFM0.9/24.5 operation gives a lower CO emission of 17.1% than that of BBDFM0.9/23.0 at full load.

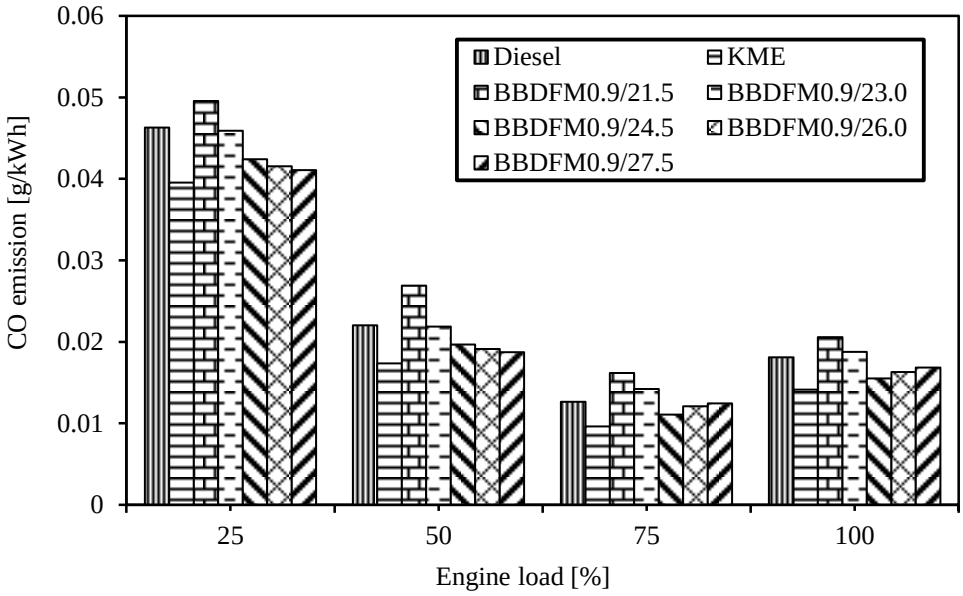

Figure 5.5.9 Variation of CO emission with load.

5.5.4.2 HC emission

The variation of HC emission with load for diesel, KME and biodiesel-biogas dual fuel operations with advanced and retarded injection timings is depicted in Figure 5.5.10.

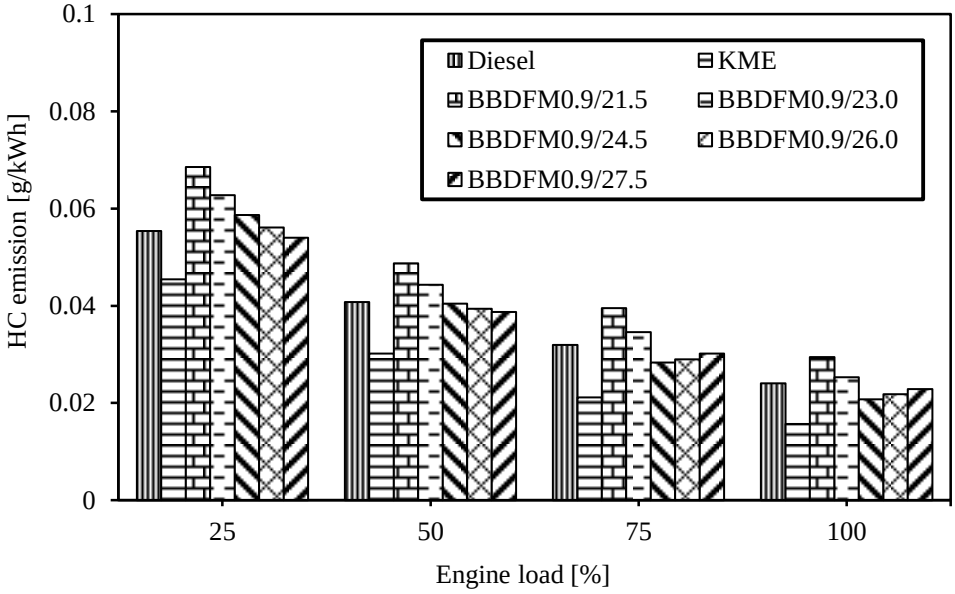

Figure 5.5.10 Variation of HC emission with load.

It can be observed that, KME gives a lower HC emission than diesel, and dual fuel operations with injection timings. This is due to the existence of oxygen in the KME which gives complete

combustion. This statement is in good agreement with that of Yoon and Lee [103]. The HC emission decreases with the increase in load for all the test fuel cases. This may be due to the increase in ignition energy, improved pilot fuel spray atomization, increase in turbulence intensity, increased heat transfer to the air-fuel mixture, and increase in the number of ignition centers in the combustion chamber of the cylinder. These reasons are well suited with the reasons mentioned by Liu et al. [84], and Duc and Wattanavichien [98] for the results they have obtained from a DI diesel engine operated on premixed biogas-diesel, and CNG-diesel dual fuel. The KME-biogas dual fuel operation with different injection timings gives a higher HC emission than that of KME throughout the load spectrum. This may be due to the induction of biogas through the intake manifold, which reduces the volume of the inducted air, and forms a fuel rich mixture zone, increasing the partial burning with less oxygen. Similar reasons were given by Ryu [93], and Papagiannakis et al. [237] for the results they obtained from a DI diesel engine operated on the dual fuel mode. BBDFM0.9/23.0 operation gives 62% higher HC emission than that of KME at full load. But, with advanced injection timing in the dual fuel operation, the HC emission decreased. BBDFM0.9/24.5 gives 18.2% lower HC emission than that of BBDFM0.9/23.0, at full load. This reduction in the HC emission with advanced injection timing is due to the earlier start of combustion relative to the TDC, hence, the cylinder charge temperature becomes higher, and a smoother combustion of the KME-biogas mixture gives lower HC emission. This statement is in good agreement with that of Yang et al. [239] given in their investigation on a turbocharged common rail dual fuel engine operated with diesel-natural gas dual fuel.

5.5.4.3 NO emission

The variation of NO emission with load for diesel, KME and biodiesel-biogas dual fuel operations with advanced and retarded injection timings is illustrated in Figure 5.5.11. It can be observed that, the NO emission for KME is higher than that of diesel through the load spectrum. This is due to the higher oxygen concentration in KME. The concentration of NO emission in dual fuel operation is considerably lower than that of KME. This may be due to the presence of CO_2 in the biogas, which dilutes the charge and lowers the cycle temperature significantly, and thereby the NO emission is suppressed. Similar reasons were reported by Violeta et al. [99], and Krishnan et al. [240] for the results they have obtained in a pilot-ignited natural gas -diesel dual fuel engine, and biogas-diesel dual fuel DI diesel engine respectively. Another possible reason that can aid this is the drop in volumetric efficiency in dual fuel operation. BBDFM0.9/23.0

gives a lower NO emission of 26.3% than that of KME at full load. With advanced injections in the dual fuel operation, the NO emission increases steeply. BBDFM0.9/24.5, BBDFM0.9/26.0 and BBDFM0.9/27.5 exhibit a higher NO emission of 5.5%, 9.9% and 14.3% than that of BBDFM0.9/23.0 at full load, but BBDFM0.9/24.5, BBDFM0.9/26.0 and BBDFM0.9/27.5 give 22.2%, 19% and 15.7% lower NO emissions than that of KME, at full load. This increase in NO emission in dual fuel operation with advanced injection timing is due to the advanced fuel injection, which increases the peak cylinder pressure and temperature, because more fuel burns close to the TDC. This reason is in good agreement with that Sahoo et al. [61], and Krishnan et al. [240] for the results they have obtained from a dual fuel DI diesel engine.

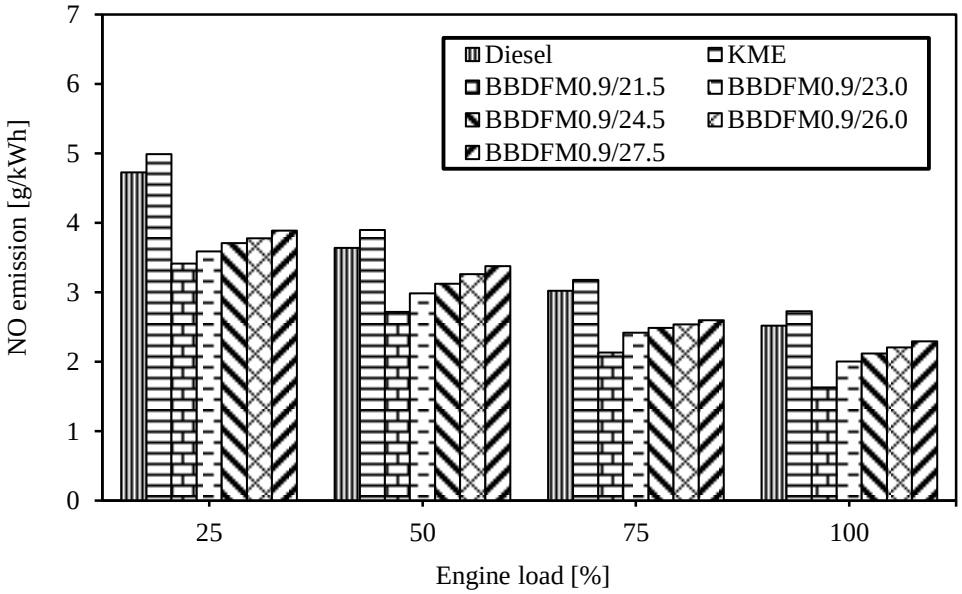

Figure 5.5.11 Variation of NO emission with load.

5.5.4.4 Smoke emission

Figure 5.5.12 portrays the variation of smoke emission with load for diesel, KME and biodiesel-biogas dual fuel operations with advanced and retarded injection timings. It can be observed from the figure that, KME gives a lower smoke emission than diesel throughout the load spectrum. This is due to the lower stoichiometric air requirement for KME, because of the available oxygen in it. BBDFM0.9/23.0 exhibits a lower smoke emission of 12.5% than that of KME at full load. This may be attributed to the reduction in flame temperature as a result of the presence of CO_2 in the biogas. Another reason may be the presence of methane in biogas, as the main constituent, that is the lower member of the paraffin family and has a very low tendency to

produce soot. A similar reason for the lower smoke emission in the methane-enriched dual fuel engine is given by Papagiannakis et al. [82]. It is also observed that, with the advanced injection timing in the dual fuel operation, the smoke emission decreases. It is apparent that the BBDFM0.9/24.5 operation gives a lower smoke emission of 2.1% than that of BBDFM0.9/23.0 at full load.

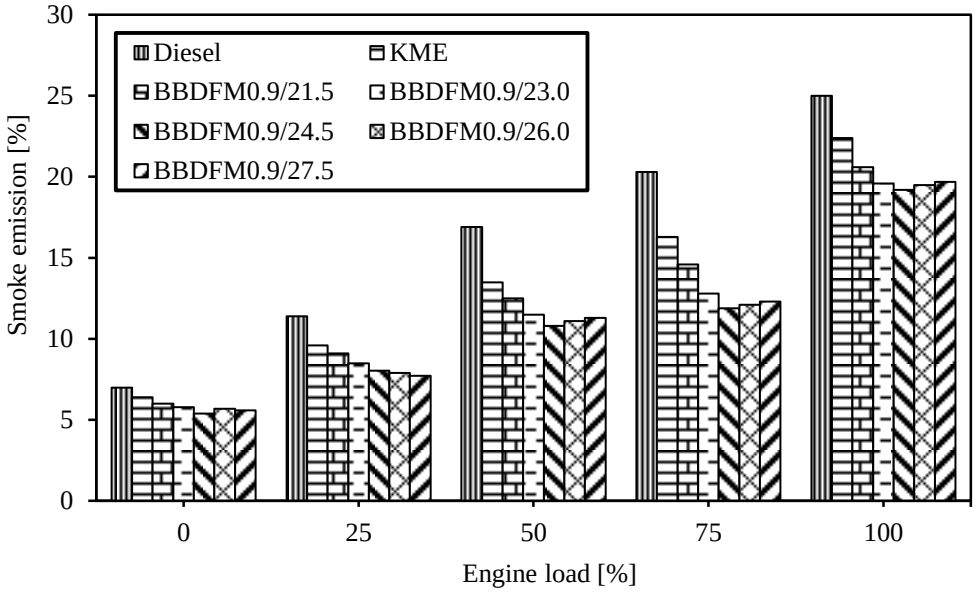

Figure 5.5.12 Variation of smoke emission with load.

5.5.5 Summary

The injection timing of KME in the KME-biogas dual fuel operation is varied to get the optimum results in terms of the combustion, performance, and emissions. BBDFM0.9/24.5 gives an optimum result for the combustion, performance and emission characteristics, than those of other injection timing cases. The BSFC for BBDFM0.9/24.5 is found to be higher by about 23.9% than that of KME, but it is 5.1% lower than that of BBDFM0.9/23.0, at full load. About 6.6% increase in BTE is observed for BBDFM0.9/24.5 in comparison with the BBDFM0.9/23.0, at full load. BBDFM0.9/24.5 gives a reduction in CO, HC and smoke emissions of 17.1%, 18.2%, and 2.1%, in comparison with BBDFM0.9/23.0, at full load, respectively. But, the NO emission for BBDFM0.9/24.5 is marginally higher by about 5.5% than that of BBDFM0.9/23.0, at full load.

The ignition delay in the dual fuel mode is found to be longer than that of diesel and KME operations. This may overcome by injecting DEE (an ignition improver) to the air-biogas flow line, and the results are discussed in the next section.

Table 5.5 provides the values of the important parameters of the investigation obtained for the diesel, KME, and KME-biogas dual fuel operations at different injection timings, at full load.

Table 5.5 Summary of the values of the combustion, performance and emission parameters, for diesel, KME, and KME-biogas dual fuel operations with variation in injection timing, at full load.

Sl. No.	Parameters	Diesel	KME	BBDFM0.9/21.5	BBDFM0.9/23	BBDFM0.9/24.5	BBDFM0.9/26	BBDFM0.9/27.5
A. Combustion parameters								
1	Maximum cylinder pressure, bar	75.7	71.3	67.8	72.9	78	82.6	87.6
2	Maximum heat release rate, J/^{o}CA	56.5	52.47	50.4	53.2	54.3	54.8	55.4
3	Ignition delay, ^{o}CA	11.5	10.5	10.9	11.3	11.9	12.5	12.8
4	Combustion duration, ^{o}CA	37.4	39.3	41.5	40.8	39.4	40.9	42.2
B. Performance parameters								
1	BSFC, kg/kWh	0.27	0.31	0.42	0.40	0.38	0.39	0.40
2	BTE, %	30.3	28	24.2	25.6	27.3	26.7	26.1
3	EGT, ^{o}C	331.8	355.8	280.2	295.1	310.6	320.1	322.6
C. Emission parameters								
1	CO, g/kWh	0.017	0.014	0.020	0.018	0.015	0.016	0.016
2	HC, g/kWh	0.025	0.015	0.029	0.025	0.020	0.021	0.022
3	NO, g/kWh	2.923	2.523	1.631	2.007	2.119	2.207	2.296
4	Smoke emission, %	25	22.4	20.6	19.6	19.2	19.5	19.7

5.6 Biodiesel-biogas optimum flow rate + optimum injection timing + DEE injection

5.6.1 General

This section presents the experimental results of the combustion, performance and emission characteristics of the same engine run on the dual fuel mode with an optimum biogas flow of 0.9 kg/h, optimum injection timing of 24.5 ^{o}CA bTDC and three different percentages of DEE injections. DEE was injected to still reduce the ignition delay and to increase the performance. For the investigation, 2%, 4%, and 6% of DEE were injected near the intake port with the help of an electronic injector. The acronyms used for the investigation are as follows:

BBDFM0.9/23.0 - biodiesel + biogas 0.9 kg/h with biodiesel injection timing of 23 ^{o}CA bTDC

BBDFM0.9/24.5 - biodiesel + biogas 0.9 kg/h with biodiesel injection timing of 24.5 ^{o}CA bTDC

BBDFM0.9/24.5/DEE2 - biodiesel + biogas 0.9 kg/h with biodiesel injection timing of 24.5 ^{o}CA bTDC and DEE injection of 2%.

BBDFM0.9/24.5/DEE4 - biodiesel + biogas 0.9 kg/h with biodiesel injection timing of 24.5 ^{o}CA bTDC and DEE injection of 4%.

BBDFM0.9/24.5/DEE6 - biodiesel + biogas 0.9 kg/h with biodiesel injection timing of 24.5 ^{o}CA bTDC and DEE injection of 6%.

The results of this investigation have been already published in Fuel journal which is given in the list of publication.

5.6.2 Combustion analysis

5.6.2.1 Pressure crank angle diagram

Figure 5.6.1 portrays the variation of cylinder pressure with the crank angle at full load. It can be observed that, the peak cylinder pressures for diesel, KME and BBDFM0.9/23.0 are about 75.7 bar, 71.3 bar, and 72.9 bar, which occur at 7.4 ^{o}CA aTDC, 6.8 ^{o}CA aTDC, and 8.1 ^{o}CA aTDC respectively. BBDFM0.9/24.5 gives a higher cylinder pressure of 78 bar than that of BBDFM0.9/23.0, which occurs at 6.2 ^{o}CA aTDC. This may be due to the formation of a fuel rich zone inside the combustion chamber with advanced injections. The combustion takes place in the earlier crank angles in the cycle, and more rapid burning takes place in the

premixed combustion phase. And a maximum amount of fuel burns before the TDC and the peak cylinder pressure moves closer to the TDC. Similar reasons are described by Sahoo et al. [61], and Agarwal et al. [232]. BBDFM0.9/24.5/DEE2, BBDFM0.9/24.5/DEE4 and BBDFM0.9/24.5/DEE6 exhibit a gradual increase in the cylinder pressures of 78.6 bar, 79.7 bar, and 82.5 bar, which occur at 2.7 ^{o}CA aTDC, 1.4 ^{o}CA aTDC and 1.2 ^{o}CA aTDC respectively, at full load. This may be due to the early ignition of DEE in the combustion chamber that helps to modulate the ignition of biogas rapidly at an earlier stage of the crank angle. This reason is in good agreement with that of Geo et al. [248] for the results they have obtained from a DI diesel engine fueled with rubber seed oil and DEE port injection.

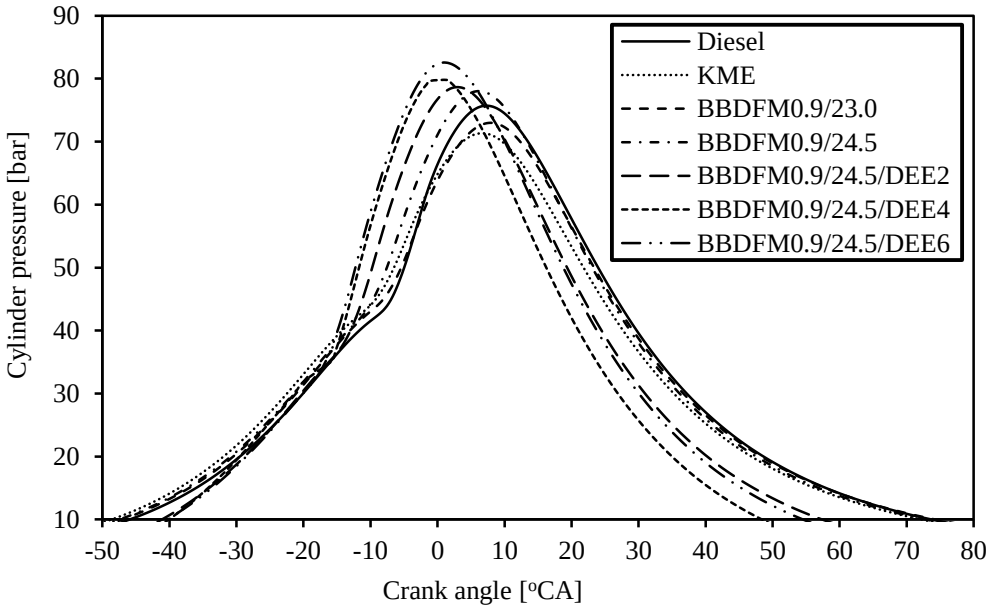

Figure 5.6.1 Variation of cylinder pressure with the crank angle at full load.

5.6.2.2 Ignition delay

The variation of ignition delay with load for diesel, KME, and KME-biogas dual fuel operations with DEE injections is depicted in Figure 5.6.2. It can be observed that, the KME exhibits a shorter ignition delay than that of diesel and the dual fuel operations throughout the load spectrum. This is due to the higher cetane number of KME, and the existence of oxygen in the fuel. The ignition delay of BBDFM0.9/23.0 is longer than that of KME at full load. This is due to the induction of biogas through the intake manifold that replaces the fresh air supply, which reduces the oxygen concentration in the charge and effects the pre-ignition of KME-biogas mixture, leading to a delay in ignition. Similar reasons were described by Paul et al. [88], and Ryu [92] in their investigations for the results they obtained from a CNG-biodiesel fueled DI diesel engine. For BBDFM0.9/24.5, the ignition delay increases due to

the low in-cylinder temperature at an early injection of the pilot fuel. The DEE injection in the dual fuel operation offers a reduction in the ignition delay by about 2 ^{o}CA, at full load. This shorter ignition delay may be due to the higher cetane number of DEE (about 125). This reason is also evidenced from the research work documented by Geo et al. [248] for the work they carried out on a single cylinder DI diesel engine run on rubber seed oil and DEE. The auto-ignition temperature of DEE is lower than that of KME and biogas. During compression of the charge, early burning starts for DEE and the biogas, and the KME absorb the surrounding heat to auto ignite. Hence, with the increase in the DEE percentage, the ignition delay in the dual fuel operation decreases. The ignition delays for diesel, KME, BBDFM0.9/23.0, and BBDFM0.9/24.5 are found to be about 11.5 ^{o}CA, 10.5 ^{o}CA, 11.3 ^{o}CA, and 11.9 ^{o}CA respectively, at full load.

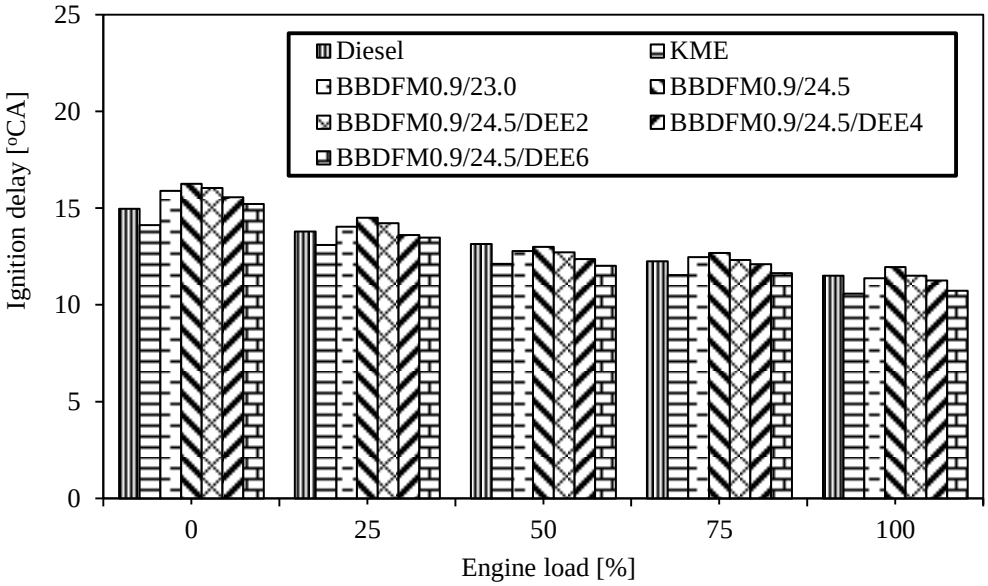

Figure 5.6.2 Variation of ignition delay with load.

5.6.2.3 Heat release rate

Figure 5.6.3 illustrates the variation of the heat release rate with the crank angle at full load. It can be observed from the figure that, a maximum heat release rate of 56.5 J/^{o}CA is noticed in the diesel operation, which occurs at 8.9 ^{o}CA aTDC. This is due to the higher energy density of diesel. A similar reason for a higher heat release for diesel is described by Sayin and Canakci [246] for the results they obtained in their research. BBDFM0.9/24.5 shows a higher heat release rate of 54.3 J/^{o}CA, than that of BBDFM0.9/23.0, which occurs at 5 ^{o}CA aTDC. This may be due to the increased accumulation of biogas during the relatively longer delay period, and the combined effect of KME and biogas in the vicinity of the combustion and

ignition centers of the pilot fuel which extends the flammability zone. Mustafi et al. [105], and Karim [220] have reported similar type of results they have obtained from a biogas run DI diesel engine. Also, another reason may be due to the advanced injection of KME, which might form a better fuel spray and higher injection quantity. Hence, the combustion starts earlier with respect to the TDC and a maximum percentage of fuel burns in the premixed phase giving more energy. This is in good agreement with the observations of Sahoo et al. [61] who conducted an their investigation on a DI diesel engine operated in the biogas-biodiesel dual fuel mode. BBDFM0.9/24.5/DEE2, BBDFM0.9/24.5/DEE4, and BBDFM0.9/24.5/DEE6 gave a higher heat release rate of about 55.2 J/^{o}CA, 56.4 J/^{o}CA, and 53.7 J/^{o}CA, than that of BDFM24.5, which occurs at about 4.7 ^{o}CA aTDC, 2.3 ^{o}CA aTDC, and 1.5 ^{o}CA aTDC respectively, at full load. This increase in the heat release rate may be due to the injection of DEE, which advances the early burning and increases the premixed combustion. Also, the availability of oxygen and high cetane number of DEE forms many ignition centers at different locations inside the combustion chamber, and increases the rate of combustion of premixed biogas. Geo et al. [248] have also documented similar reasons for the results they have obtained from a DI diesel engine fueled with rubber seed oil and DEE port injection.

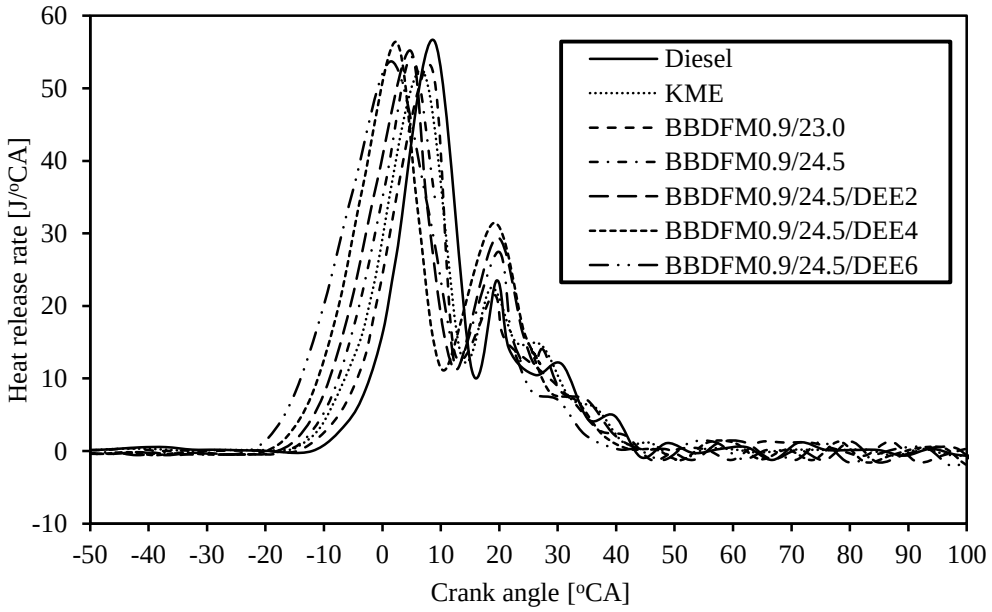

Figure 5.6.3 Variation of heat release rate with the crank angle at full load.

5.6.2.4 Combustion duration

The variation of combustion duration with load is depicted in Figure 5.6.4. It can be observed that the combustion duration increases with the increase in load irrespective of the fuels used.

This is due to the consumption of more quantity of fuel at relatively higher loads. In diesel and KME operations, the combustion duration is found to be about 37.4 ^{o}CA and 39.3 ^{o}CA, at full load respectively. For BBDFM0.9/23.0, the combustion duration is found to be about 40.8 ^{o}CA, at full load. The reason for the increase in the combustion duration for the BBDFM0.9/23.0 than that of KME is the slower rate of the burning of biogas. The reason was commonly reported by many researchers, for instance Sahoo et al. [61]. The dual fuel operation with DEE gives a gradual decrease in the combustion duration. This may be attributed to the faster ignition and increased ignition centers in the charge (biogas-KME-DEE-air mixture), due to the high cetane number of DEE. Also, the burning velocity of DEE is very high, and it improves the flame speed of KME and biogas, and reduces the combustion duration. This reason is also evidenced from the research work documented by Geo et al. [248] for the work they carried out on a single cylinder DI diesel engine run on rubber seed oil and DEE. BBDFM0.9/24.5/DEE2, BBDFM0.9/24.5/DEE4, and BBDFM0.9/24.5/DEE6 exhibit a shorter combustion duration which is about 38.6 ^{o}CA, 37.2 ^{o}CA, and 36.5 ^{o}CA at full load respectively.

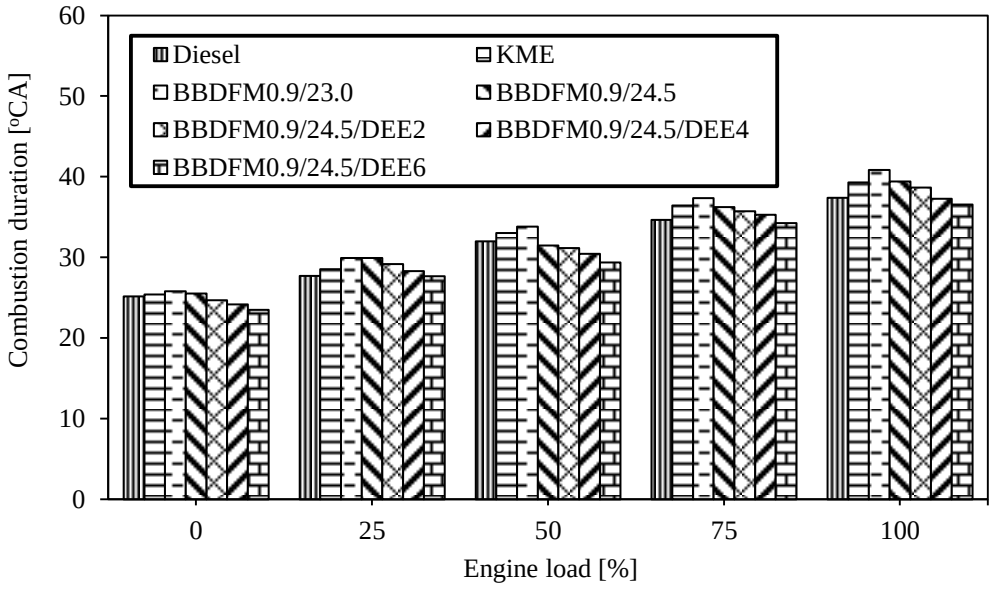

Figure 5.6.4 Variation of combustion duration with load.

5.6.2.5 Maximum cylinder pressure

Figure 5.6.5 illustrates the variation of the maximum cylinder pressure with load for diesel, KME, and dual fuel operation with DEE injection. It can be observed from the figure that, the cylinder pressure increases with the increase in the load, as expected. The maximum cylinder pressure for diesel and KME is about 75.7 bar and 71.3 bar, at full load. However, the dual

fuel operation of BBDFM0.9/23.0 and BBDFM0.9/24.5 gives a maximum cylinder pressure of 72.9 bar, and 78 bar respectively, at full load. This increase in the maximum cylinder pressure in the dual fuel operation than that of diesel is due to the induction of biogas through the intake manifold, and the intake biogas-air charge brings about a decrease, and dilution of oxygen concentration, which may cause a longer ignition delay, leading to the increase in cylinder pressure in the premixed combustion phase. Mustafi et al. [105], and Karim [220] have reported the similar type of results for their experiment on a biogas run DI diesel engine. Another reason for the increase in the maximum cylinder pressure in the dual fuel operation with advanced injection is due to the formation of a fuel rich mixture inside the combustion chamber. Ryu [92] has reported similar reasons in his research work. With DEE injection in the dual fuel operation of BBDFM0.9/24.5/DEE2, BBDFM0.9/24.5/DEE4, and BBDFM0.9/24.5/DEE6 the cylinder pressure increases. This is attributed to the early ignition of DEE in the combustion chamber that helps to modulate the ignition of biogas rapidly at an earlier stage of crank angle. Geo et al. [248] and Hansdah and Murugan [249] reported similar reason for their investigation in a DI diesel engine fueled with biodiesel-DEE and ethanol-DEE dual fuel. BBDFM0.9/24.5/DEE2, BBDFM0.9/24.5/DEE4, and BBDFM0.9/24.5/DEE6 give the maximum cylinder pressures of 78.6 bar, 79.7, and 82.5 bar respectively, at full load.

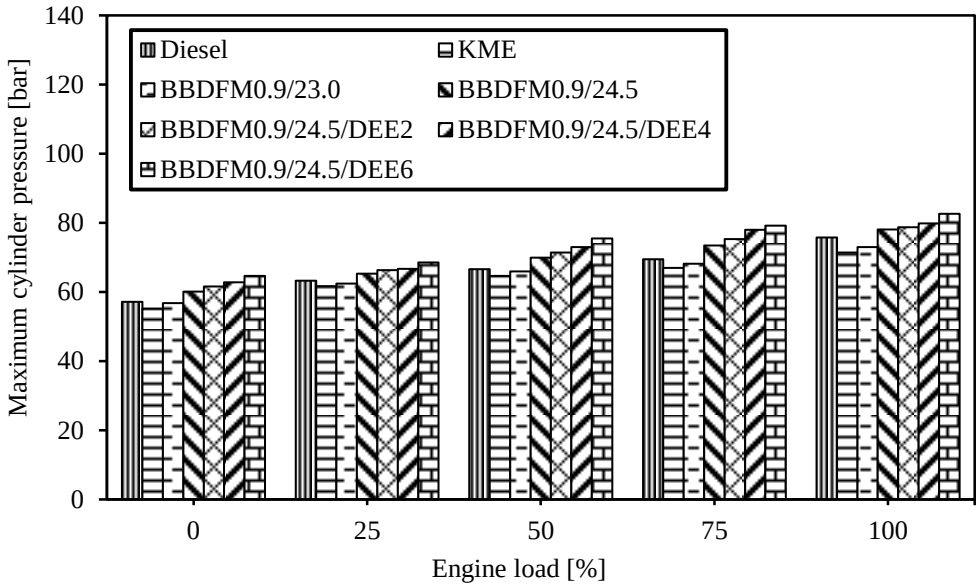

Figure 5.6.5 Variation of maximum cylinder pressure with load.

5.6.3 Performance analysis

5.6.3.1 BSFC

Figure 5.6.6 portrays the variation of BSFC with load for diesel, KME, and dual fuel operation with DEE injection.

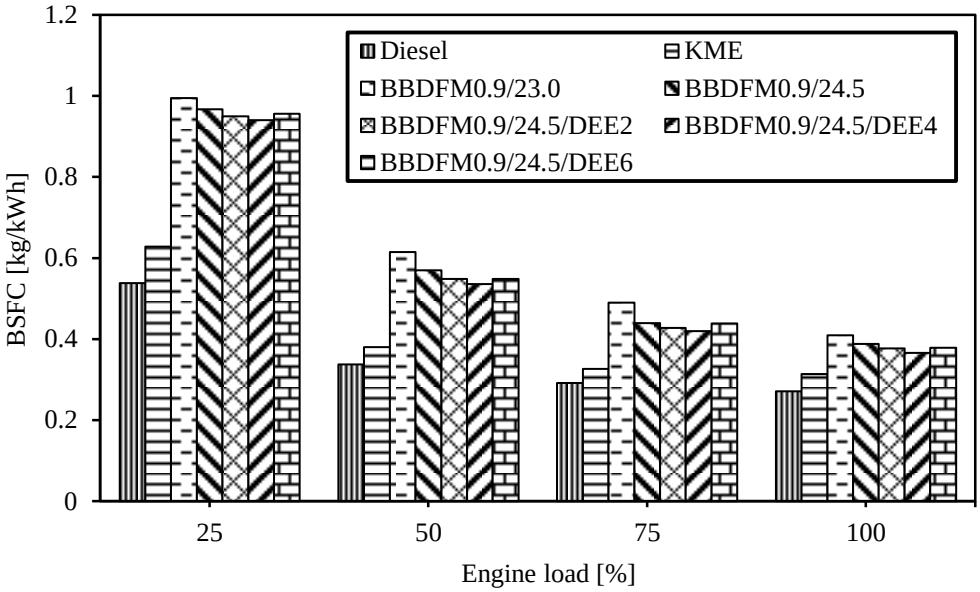

Figure 5.6.6 Variation of BSFC with load.

It can be observed from the figure that, the BSFC decreases with an increase in the load for all the test fuels because, as the load of the engine increases, the fuel atomization, and combustion quality increases. The BSFC for diesel, KME, BBDFM0.9/23.0 and BBDFM0.9/24.5 are found to be about 0.27 kg/kWh, 0.31 kg/kWh, 0.4 kg/kWh, and 0.38 kg/kWh respectively, at full load. The BSFC in the dual fuel operation, at low and intermediate load conditions, is considerably higher in comparison with those of diesel and KME operations. This may be due to the slower premixed controlled combustion during the initial stages of combustion at low load. This reason is in good agreement with that of Papagiannakis et al. [237] for the results obtained from a dual fuel diesel engine. BBDFM0.9/24.5 gives a lower BSFC than BBDFM0.9/23.0 at full load. This is due to the higher maximum heat release during the premixed combustion at the advanced injection timing. This increases the cylinder charge temperature, and the biogas achieves its ignition temperature, and increases the rate of combustion in the second phase of combustion (diffusion combustion), and decreases the BSFC. This reason is also evidenced from the research work documented by Bari [106] for the work they carried out on a diesel engine run on biogas or natural gas in the dual fuel mode. For the BBDFM0.9/24.5/DEE2 and

BBDFM0.9/24.5/DEE4 operations, the BSFC values are about of 0.37 kg/kWh and 0.36 kg/kWh respectively at full load, which are lower than those of BBDFM0.9/23.0 and BBDFM0.9/24.5. The reason for the reduction in the BSFC for the DEE operation is due to the improved combustion and additional energy supply from the DEE. This reason is also evidenced from the research work documented by Geo et al. [248] for the work they carried out on a single cylinder DI diesel engine run on rubber seed oil and DEE.

5.6.3.2 BTE

The variation of BTE with load for diesel, KME and dual fuel operation with DEE injection is illustrated in Figure 5.6.7.

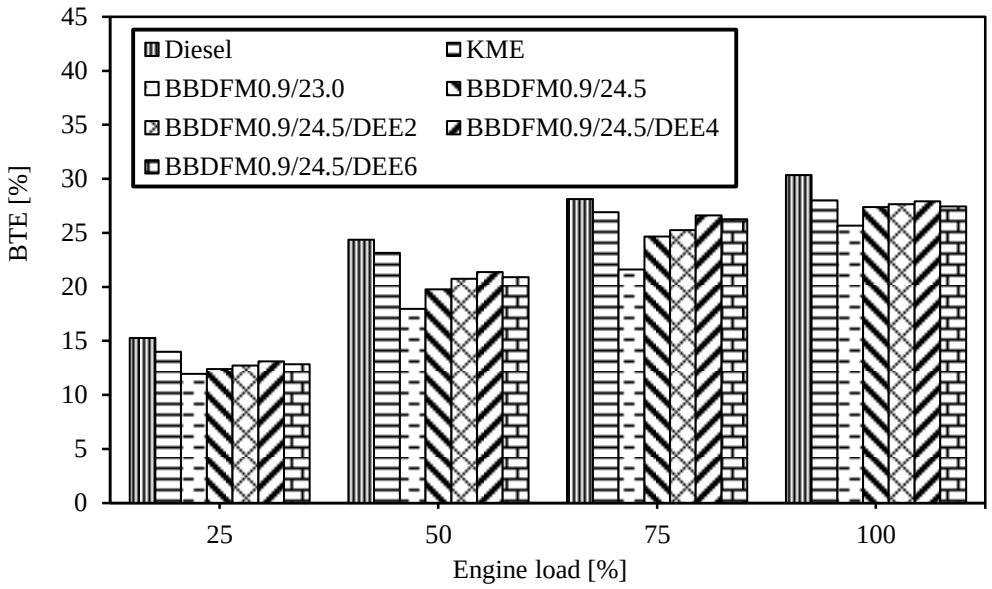

Figure 5.6.7 Variation of BTE with load.

Diesel operation offers the highest BTE throughout the load spectrum irrespective of the fuels used in the experiment. This is due to the higher heating value of diesel. The BTE of KME is found to be about 28%, which is 2.3% lower than that of diesel, at full load. The BTE for the test fuels increases with the increase in the load. This is due to the increased cylinder temperature at relatively higher loads. BBDFM0.9/23.0 gives a 2.4% drop in BTE than that of KME. This drop in BTE may be attributed to the incomplete combustion of the fuel, due to the drop in the volumetric efficiency, caused by the induction of biogas through the intake manifold. Similar reasons were described by Paul et al. [88] in their investigations for the results they obtained from a CNG-biodiesel fueled DI diesel engine. BBDFM0.9/24.5 shows an increase in BTE of 1.7% than that of BBDFM0.9/23.0, at full load. This is due to a greater vaporization of the pilot fuel, and a better air-fuel mixture formation at relatively advanced

injections. BBDFM0.9/24.5/DEE2 and BBDFM0.9/24.5/DEE4 show a gradual increase in the BTE of 7.2% and 8% than that of BBDFM0.9/23.0 at full load respectively. This increase in the BTE with the DEE injection is due to the quicker evaporation, and easy mixing of DEE with the air-biogas that forms a homogeneous mixture and causes a complete combustion releasing more energy. Also, the early start of ignition of DEE gives a better combustion phasing to biogas and boosts the rate of combustion of KME and the BTE increases. This reason is in good agreement with those given by Geo et al. [248], and Imtenan et al. [250] for the results they have obtained in a single cylinder, DI diesel engine, and a multi-cylinder diesel engine fueled with biodiesel, and DEE as ignition improver, and oxygenated additive respectively.

5.6.3.3 Volumetric efficiency

The variation of volumetric efficiency with load for diesel, KME, and dual fuel operation with DEE injection is depicted in Figure 5.6.8.

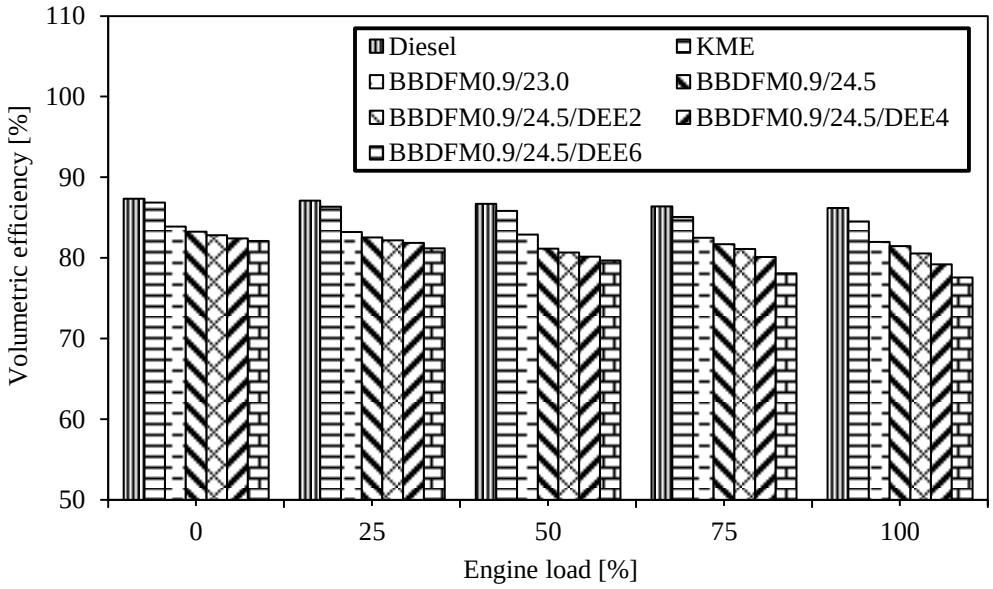

Figure 5.6.8 Variation of volumetric efficiency with load.

The volumetric efficiency of diesel and KME is found to be higher than that of the dual fuel operations throughout the load spectrum. The volumetric efficiency of diesel and KME is found to be about 86.2% and 84.5% at full load, whereas, in the dual fuel operation of BBDFM0.9/23.0, BBDFM0.9/24.5, the volumetric efficiency is found to be about 82% and 81.4%. This reduction in volumetric efficiency is due to the induction of biogas through the intake manifold which reduces the supply of fresh air. Similar reasons were described by Chandra et al. [100] in their investigations for the results they obtained in a CNG, and

methane-enriched biogas fueled dual fuel diesel engine. The dual fuel operation with increasing DEE injection gives a gradual drop in volumetric efficiency. This is obvious due to the simultaneous induction of biogas and DEE through the manifold. It is also observed that, with an increase in load the volumetric efficiency drops irrespective of the fuels used. This may be due to the hot cylinder wall, which reduces the induced air density, and results in a drop in the volumetric efficiency. This reason is in good agreement with those given by Yoon and Lee [103] for the results obtained in a biogas-fueled dual fuel diesel engine.

5.6.3.4 EGT

The variation of EGT with load is depicted in Figure 5.6.9.

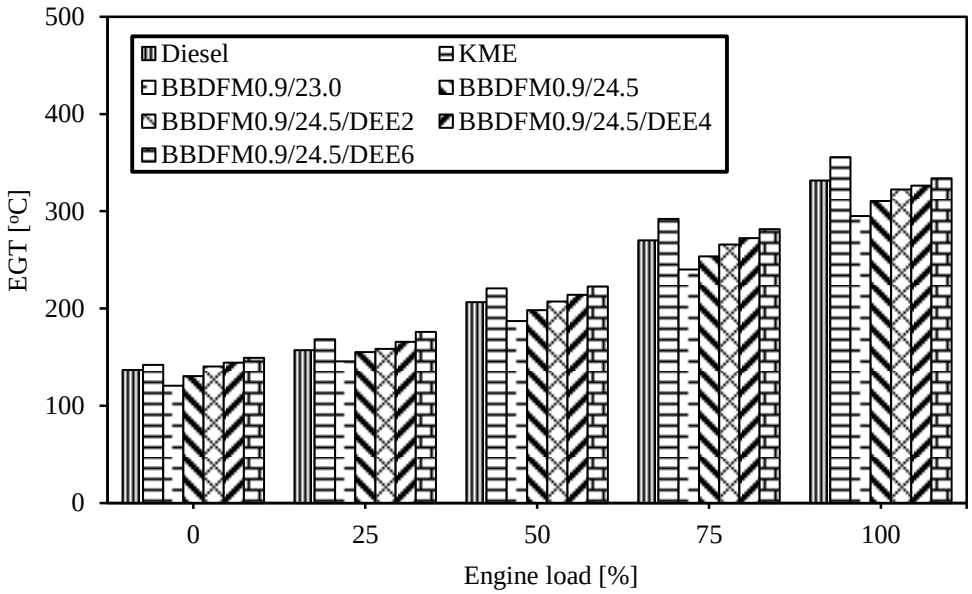

Figure 5.6.9 Variation of EGT with load.

The KME operation exhibits the highest EGT than that of the diesel and dual fuel operations with and without DEE injection throughout the load spectrum. The presence of oxygen in the ester molecules enhances the combustion process and results in a higher EGT. The BBDEF0.9/23.0 operation gives the lowest EGT, irrespective of fuels used in diesel, KME, and dual fuel operations with and without DEE injection. This may be due to the absorption of heat by the biogas from the compressed charge to auto-ignite during the combustion process, which decreases the local adiabatic flame temperature, and EGT drops. This reason is in good agreement with that given by Nwafor [233] for the results obtained in a biogas-fueled dual fuel diesel engine. Also, the presence of CO_2 (about 17%) in the biogas increases the dilution and results in a reduction of EGT. The BBDFM0.9/24.5 operation shows an increase in the EGT than that of BBDFM0.9/23.0. This is due to the longer spray of the pilot

fuel during the advanced injection timing, which enhances the rate of combustion, and increases the EGT. BBDFM0.9/24.5/DEE2, BBDFM0.9/24.5/DEE4, and BBDFM0.9/24.5/DEE6 exhibit a gradual increase in the EGT. This may be due to the increase in combustion temperature, and flame speed of DEE. A similar reason for the increase in the exhaust gas temperature is described by Hariharan et al. [251] in their research work to study the effect of DEE on a tyre pyrolysis oil fueled DI diesel engine. The EGT for diesel and KME are found to be 331.8 ^{o}C and 355.8 ^{o}C, whereas the EGT for BBDFM0.9/23.0, BBDFM0.9/24.5, BBDFM0.9/24.5/DEE2, BBDFM0.9/24.5/DEE4, and BBDFM0.9/24.5/DEE6 are found to be lower by about 17%, 12.7%, 9.3%, 8.2%, and 6.1% respectively, than that of KME at full load.

5.6.4 Emission analysis

5.6.4.1 CO emission

The variation of CO emission with load for diesel, KME and dual fuel operations with DEE injection is depicted in Figure 5.6.10. The main reasons for the generation of higher CO emission are improper mixing of fuel and air, the low temperature of the reaction mixture, lack of oxidants, and unsuitable time duration for combustion. The CO emission for the KME operation is considerably lower than that of diesel and dual fuel operations, with and without DEE injection, throughout the load spectrum. This is due to the presence of oxygen in KME, that causes a complete oxidation of CO, and hence, the CO reduces. For BBDFM0.9/23.0, the CO emission is considerably higher than that of KME. This is due to the existence of a flame extinction region, and the incomplete oxidation of the premixed biogas in the dual fuel mode. The reason for the incomplete oxidation is due to the dilution of the charge with the CO_2 in the biogas. Hence, the flame is suppressed in the ignition region of the pilot fuel, and does not proceed until the biogas-air mixture reaches a minimum limiting value for auto ignition. This statement is in good agreement with that of Liu et al. [84] for the results obtained from a CNG-diesel dual fuel diesel engine. It can also be observed that, the CO emission is higher at part load operations. This is due to the formation of the lean fuel-air mixture in the adjacent zone of the injection spray, in which the flame struggles to propagate, and the local temperature falls, which reduces the oxidation reaction, and results in a higher CO emission at part load operations. The CO emission decreases with the increase in the load. This is attributed to the higher cylinder gas temperature that boosts the rate of combustion. A similar reason for the decrease in CO emission is described by Prakash et al. [206]. BBDFM0.9/24.5 offers a reduction of 17.1% in CO emission than that of BBDFM0.9/23.0, at full load. This is

because the advanced injection of KME gives a higher cylinder temperature, and increases the oxidation of CO. Similar reasons were given by Ryu [92] in his investigations for the results he obtained from a CNG-biodiesel fueled DI diesel engine. BBDFM0.9/24.5/DEE2, BBDFM0.9/24.5/DEE4 and BBDFM0.9/24.5/DEE6 also offer a reduction of 22.9%, 27.2%, and 23.5% in CO emissions respectively, with respect to BBDFM0.9/23.0, at full load. This may be due to the injection of DEE, which improves the start of ignition, and decreases the ignition delay, and allows more time for oxidation of the fuel. Also, the port injection of DEE helps it to mix properly with the air-biogas mixture, and forms many ignition centers in the combustion chamber, and gives a lower CO emission. Geo et al [248], Sudheesh and Mallikarjuna [252], and Swaminathan and Sarangan [253] have also claimed similar reasons for the results obtained from their research on a DI diesel engine fueled with rubber seed oil, biogas, and fish oil methyl ester respectively, with DEE as an ignition improver.

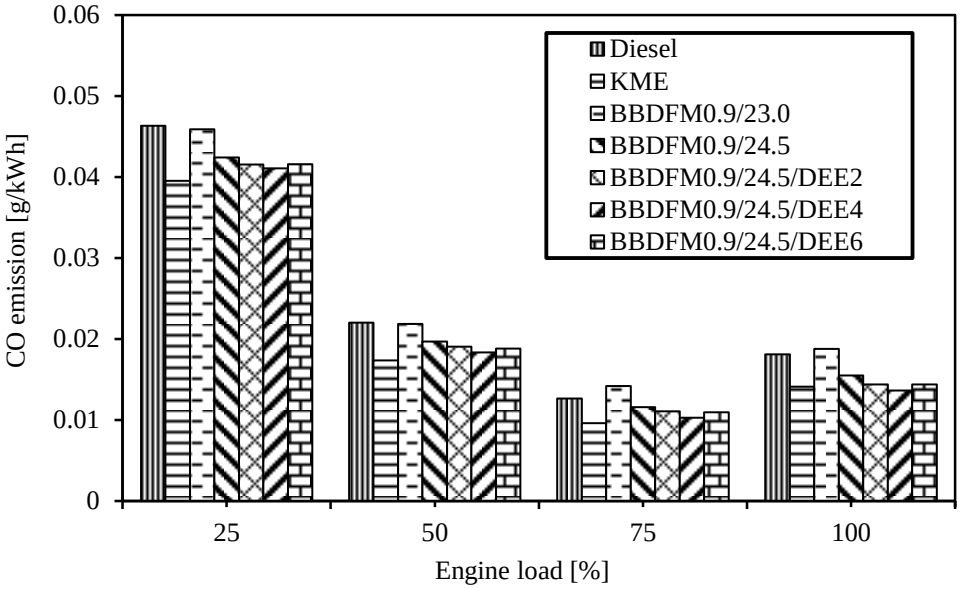

Figure 5.6.10 Variation of CO emission with load.

5.6.4.2 HC emission

Figure 5.6.11 illustrates the variation of HC emission with the load for diesel, KME, and dual fuel operation, with DEE injections. KME gives a lower HC emission than that of diesel and dual fuel operations, with and without DEE injection. This is due to the existence of oxygen in the KME which gives a complete combustion. The BBDFM0.9/23.0 operation suffers from a higher HC emission than that of KME throughout the load spectrum. This may be due to the induction of biogas through the intake manifold, which reduces the volume of the inducted air, and forms a fuel rich mixture zone, and increases the partial burning with less oxygen.

This statement is in good agreement with the reasons given by Ryu [93], and Papagiannakis et al. [237] and for the results obtained from a direct injection diesel engine fueled with biodiesel-CNG dual fuel. The HC emission for BBDFM0.9/24.5 is reduced by about 18.2%, when the injection timing is advanced by 1.5 ^{o}CA from the original injection timing of BBDFM0.9/23.0, at full load. This is due to the earlier start of combustion relative to the TDC, as the cylinder charge temperature becomes higher and complete combustion gives lower HC emission. The DEE injection in the dual fuel operation offers a reduction of HC emission in the range of 3.8%-10.6 % in comparison with that of BBDFM0.9/24.5, at full load. This is due to the earlier start of combustion, that advances and leads to a comparatively higher cylinder gas temperature, which improves the oxidization of biogas with the help of increased oxygen concentration in charge, due to the simultaneous effort of DEE and KME. Similar reasons were described by Geo et al. [248], Sudheesh and Mallikarjuna [252], and Qi et al. [254] for the results they obtained from a DI diesel engine operated with biodiesel and diesel, with DEE as an ignition improver.

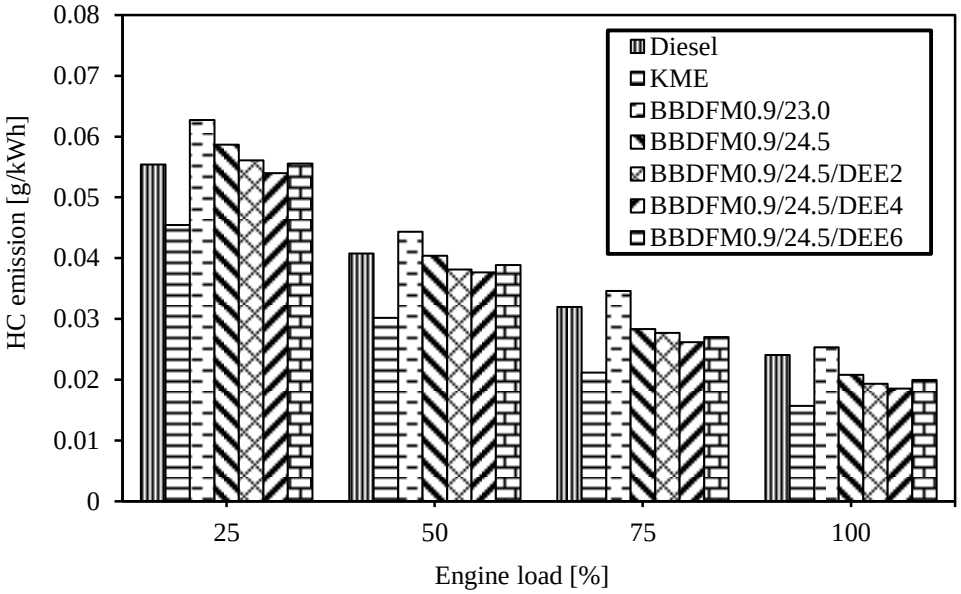

Figure 5.6.11 Variation of HC emission with load.

5.6.4.3 NO emission

Figure 5.6.12 portrays the variation of NO emission with load. KME gives a higher NO emission than that of diesel and dual fuel operations, with and without DEE injection. This is due to the higher oxygen concentration in KME. The concentration of NO emission in the dual fuel operation is considerably lower than that of KME at full load. This may be due to the drop in volumetric efficiency in the dual fuel operation, by the induction of fuel through

the intake manifold. Similar reasons were reported by Violeta et al. [99], and Krishnan et al. [240] for the results they obtained from a pilot-ignited natural gas -diesel dual fuel engine and biogas-diesel dual fuel DI diesel engine respectively. BBDFM0.9/23.0 operation gives a lower NO emission of 26.3% than that of KME at full load. The BBDFM0.9/24.5 shows a higher NO emission of 5.5% than that of BBDFM0.9/23.0, at full load. For BBDFM0.9/24.5, the NO emission is lower by about 22.2% than that of KME at full load. This increase in NO emission is due to the advanced injection, which increases the peak cylinder pressure and temperature, because more fuel burns close to the TDC. This statement is in good agreement with that of Sahoo et al. [61], and Krishnan et al. [240]. BBDFM0.9/24.5/DEE2, BBDFM0.9/24.5/DEE4, and BBDFM0.9/24.5/DEE6 give a gradual increase in NO emission of 10%, 12.7% and 17.5% in comparison with BBDFM0.9/24.5 at full load respectively. This increase in NO emission with the DEE injection is attributed to the higher oxygen enrichment (from both DEE and KME), and a more complete combustion may give a higher thermal NO due to the high combustion temperature. This reason matches well with the results mentioned by Qi et al. [254], and Sivalakshmi et al. [255] for the results they obtained from a DI diesel engine fueled with biodiesel, diesel, and DEE. The NO emissions for BBDFM0.9/24.5/DEE2, BBDFM0.9/24.5/DEE4, and BBDFM0.9/24.5/DEE6 are about 13.5%, 10.9%, and 5.7% lower than that of KME, at full load operation respectively.

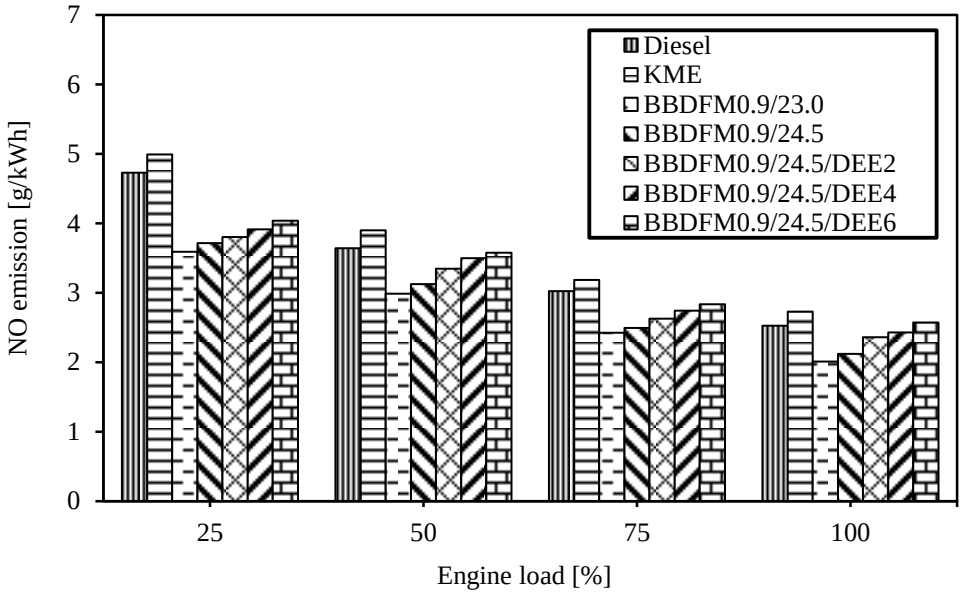

Figure 5.6.12 Variation of NO emission with load.

5.6.4.4 Smoke emission

The variation of smoke emission with load for diesel, KME, and dual fuel operations with DEE injection is depicted in Figure 5.6.13.

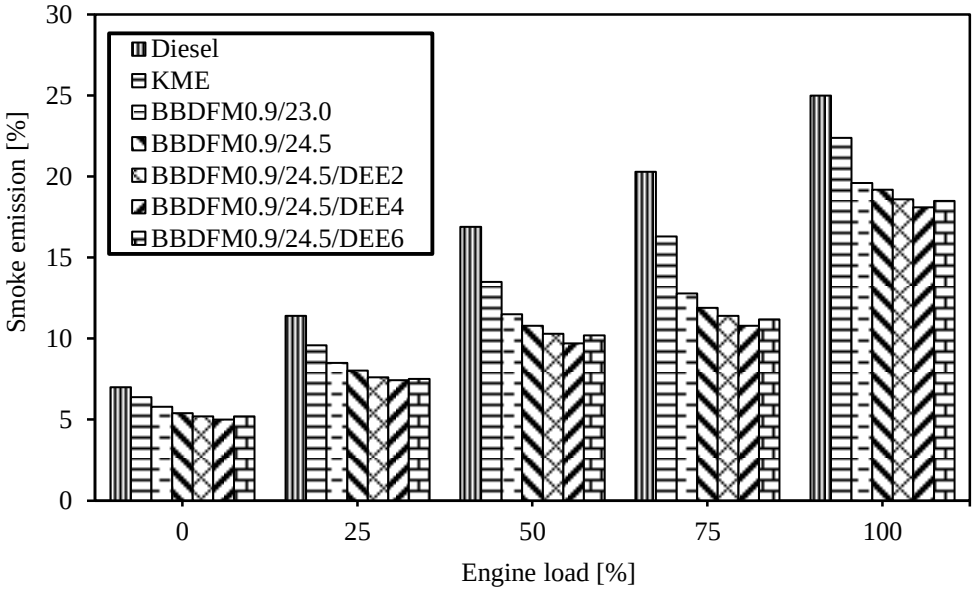

Figure 5.6.13 Variation of smoke emission with load.

It can be observed from the figure that, KME gives a lower smoke emission than that of diesel throughout the load spectrum. This is due to the lower stoichiometric air requirement for KME, because of the available oxygen in it. BBDFM0.9/23.0 exhibits a lower smoke emission of 12.5% than that of KME at full load. This may be attributed to the flame temperature reduction, due to the existence of CO_2 in the biogas. Another reason may be the presence of methane in biogas, as the main constituent, that is the lower member of the paraffin family, which has a very low tendency to produce soot. This statement is in good agreement with that of Papagiannakis et al. [82], for the results they obtained from a natural gas-diesel fueled dual fuel diesel engine. BBDFM0.9/24.5 gives a lower smoke emission of 2.1% than that of BBDFM0.9/23.0 at full load. This reduction in the smoke is due to the higher rate of combustion, and longer time for the oxidation of the soot particles in the combustion chamber, due to the advanced injections. Similar reasons were reported by Liu et al. [84] for the results they obtained in their research on a CNG-diesel dual fuel engine. The DEE injection in the dual fuel operation gives a reduction in smoke emission than that of BBDFM0.9/24.5. This may be attributed to the early start of combustion due to the high cetane number of DEE, which allows more time for the oxidation of soot with the available oxygen. Also, the reduced ignition delay due to the DEE injection reduces the accumulation

of fuel in the combustion chamber and suppresses the probability of a fuel rich zone in the premixed combustion phase, and decreases the smoke emission. This is in good agreement with the observations of Imtenan et al. [250], and Sudheesh and Mallikarjuna [252] for the results they obtained from a diesel engine fueled with biodiesel, diesel, and DEE.

5.6.5 Summary

The experimental results of the dual fuel operation with DEE injection are compared with those of diesel, KME and dual fuel operations, without and with DEE injection, and presented in this section. The summary of the results are as follows:

BBDFM0.9/24.5/DEE4 gives the optimum results for the combustion, performance and emission characteristics of the engine, than those of other DEE injection quantities. BBDFM0.9/24.5/DEE4 gives an increase in BTE of 2.3% than that of BBDFM0.9/24.5 at full load. The BSFC for BBDFM0.924.5/DEE4 is found to be lower by about 5.8% than that of BBDFM0.9/24.5 at full load. BBDFM0.9/24.5/DEE4 gives a reduction in CO, HC and smoke emissions of 12.2%, 10.6% and 5.7% than that of BBDFM0.9/24.5, respectively at full load. The NO emission for the BBDFM0.9/24.5/DEE4 operation is 12.7% higher than that of BBDFM0.9/24.5, at full load. But it is found to be 10.9% lower than that of KME at full load.

Table 5.6 provides the values of the important parameters of the investigation conducted for diesel, KME and KME-biogas dual fuel operations with different percentages of DEE injection, at full load.

Table 5.6 Summary of the values of the combustion, performance and emission parameters, for diesel, KME and KME-biogas dual fuel operations with different percentages of DEE injection, at full load.

Sl. No.	Parameters	Diesel	KME	BBDFM0.9/23.0	BBDFM0.9/24.5	BBDFM0.9/24.5/ DEE2	BBDFM0.9/24.5/ DEE4	BBDFM0.9/24.5/ DEE6
A. Combustion parameters								
1	Maximum cylinder pressure, bar	75.7	71.3	73	78	78.6	79.7	82.5
2	Maximum heat release rate, J/^{o}CA	56.5	52.47	53.2	54.3	55.2	56.4	53.7
3	Ignition delay, ^{o}CA	11.5	10.5	11.3	11.9	11.5	11.2	10.7
4	Combustion duration, ^{o}CA	37.4	39.3	40.8	39.4	38.6	37.2	36.5
B. Performance parameters								
1	BSFC, kg/kWh	0.27	0.31	0.40	0.38	0.376	0.365	0.378
2	BTE, %	30.3	28	25.6	27.3	27.6	27.9	27.4
3	EGT, ^{o}C	331.8	355.8	295.1	310.6	322.5	326.4	334.1
4	Volumetric efficiency, %	86.2	84.5	82	81.4	80.5	79.2	77.5
C. Emission parameters								
1	CO, g/kWh	0.017	0.014	0.018	0.015	0.014	0.013	0.014
2	HC, g/kWh	0.025	0.015	0.025	0.020	0.019	0.018	0.019
3	NO, g/kWh	2.923	2.726	2.007	2.119	2.356	2.428	2.569
4	Smoke emission, %	25	22.4	19.6	19.2	18.6	18.1	18.5

5.7 Biodiesel-upgraded biogas optimum flow rate + optimum injection timing + DEE injection

5.7.1 General

Although, the biodiesel-biogas dual fuel mode with DEE injection operated well, the engine would produce the oxides of sulfur and more CO_2 as the biogas containd CO_2 and H_2S. Hence, a comparative analysis made between the combustion, performance and emission characteristics of the engine run on biodiesel-biogas dual fuel mode with different DEE injection quantity before and after purification of biogas.

This section presents the experimental results of the combustion, performance and emission characteristics of the engine run on a dual fuel mode, with upgraded biogas at a flow of 0.9 kg/h, with optimum injection timing of 24.5 ^{o}CA bTDC and three different percentages of DEE injections. For this investigation, 2%, 4%, and 6% of DEE was injected near the intake port with the help of an electronic injector. The important results of comparison between the raw biogas and the upgraded biogas utilization in diesel engine on the dual fuel mode are presented. The acronyms used for the investigation are as follows:

BUBDFM0.9/24.5/DEE2 - biodiesel injected at 24.5 ^{o}CA bTDC + upgraded biogas 0.9 kg/h and DEE injection of 2%.

BUBDFM0.9/24.5/DEE4 - biodiesel injected at 24.5 ^{o}CA bTDC + upgraded biogas 0.9 kg/h and DEE injection of 4%.

BUBDFM0.9/24.5/DEE6 - biodiesel injected at 24.5 ^{o}CA bTDC + upgraded biogas 0.9 kg/h and DEE injection of 6%.

5.7.2 Combustion analysis

5.7.2.1 Pressure crank angle diagram

Figure 5.7.1 portrays the variation of cylinder pressure with the crank angle at full load. It can be observed that, the peak cylinder pressure for diesel, and BBDFM0.9/24.5/DEE4 are about 75.7 bar, and 79.4 bar, which occur at 7.4 ^{o}CA aTDC, and 1.4 ^{o}CA aTDC respectively. In the dual fuel operation with an increase in DEE injection the peak cylinder pressure gradually increases. This may be attributed to the early ignition of DEE in the combustion chamber that helps to modulate the ignition of biogas rapidly at an earlier stage of crank angle. This reason is in good agreement with Geo et al. [248] for the results they have obtained in a DI diesel engine fueled with rubber seed oil and DEE port injection. It is also observed that, the dual

fuel operation with upgraded biogas gives a lower peak cylinder pressure, than that of dual fuel operation with raw biogas, at full load. This is due to the accumulation of a little amount of fuel during the delay period for the upgraded biogas dual fuel operation, than that of raw biogas operation.

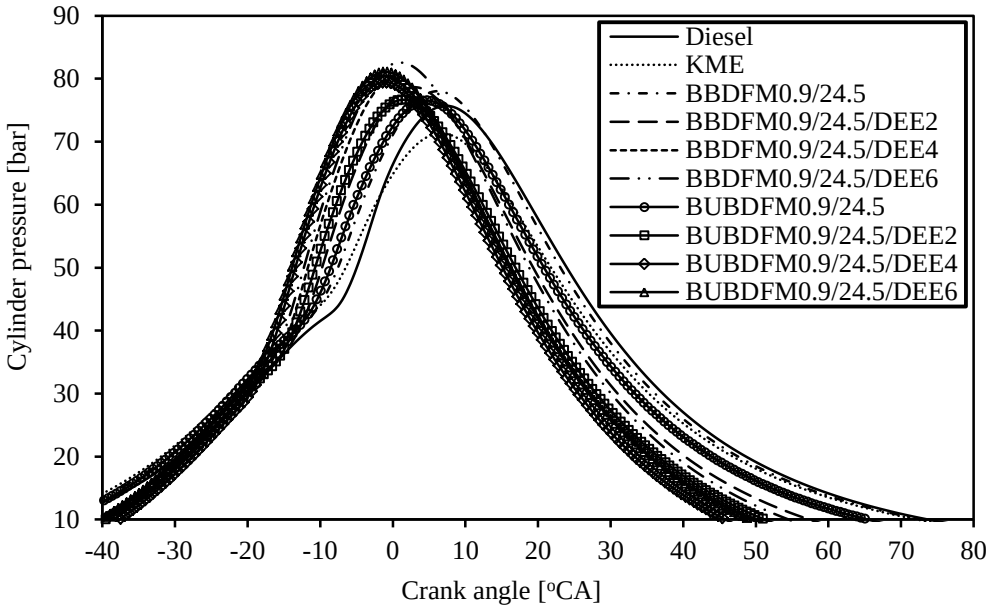

Figure 5.7.1 Variation of cylinder pressure with the crank angle at full load.

5.7.2.2 Ignition delay

The variation of ignition delay with load for diesel, KME, KME-biogas, and KME-upgraded biogas dual fuel modes with DEE injections is depicted in Figure 5.7.2. It can be observed from the figure that, BBDFM0.9/24.5 gives a longer ignition delay than that of other fuels throughout the load spectrum. This is due to the low in-cylinder temperature at an early injection of the pilot fuel, which delays the ignition. The dual fuel operations with the increase in DEE injection give a gradual decrease in the ignition delay. This may be due to the effect of higher cetane number of DEE (about 125), which enhances the start of ignition. The autoignition temperature of DEE is lower, hence during compression of the charge, early burning starts for DEE and the biogas-KME absorb the surrounding heat to auto ignite. Hence, with the increase in the DEE percentage, the ignition delay in the dual fuel operation decreases. This reason is also evidenced from the research work documented by Geo et al. [248] for the work they have carried out on a single cylinder DI diesel engine run on rubber seed oil and DEE. The dual fuel operation with upgraded biogas gives a shorter ignition delay than that of dual fuel with the raw biogas operation, throughout the load spectrum. This is due to the lower percentage of CO_2 in the upgraded biogas (about 4.2%) in comparison to raw

biogas (about 17%), which auto ignites little earlier. The dual fuel operations of BUBDFM0.9/24.5/DEE2, BUBDFM0.9/24.5/DEE4, and BUBDFM0.9/24.5/DEE6 give a shorter ignition delay of 10.8 ^{o}CA, 10.1 ^{o}CA and 9 ^{o}CA, at full load.

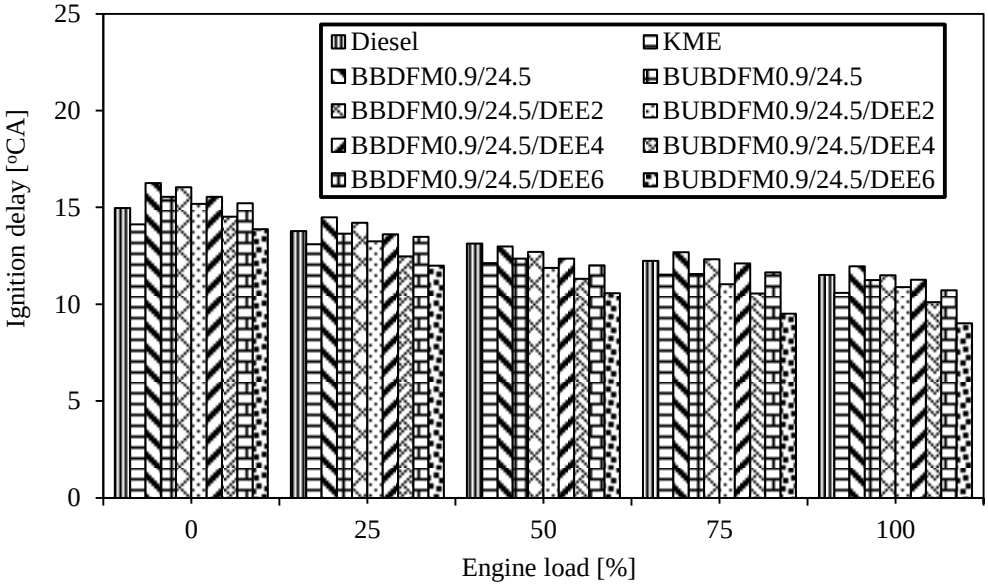

Figure 5.7.2 Variation of ignition delay with load.

5.7.2.3 Heat release rate

The heat release rate for diesel, KME, KME-biogas, and KME-upgraded biogas dual fuel mode with different DEE injections is illustrated in Figure 5.7.3. It can be observed from the figure that, the dual fuel operation with the upgraded biogas-DEE injection gives a higher heat release rate than that of dual fuel operation with raw biogas-DEE injection. This is due to the higher energy density of the upgraded biogas. The dual fuel operations with the upgraded biogas of BUBDFM0.9/24.5/DEE2, BUBDFM0.9/24.5/DEE4, and BUBDFM0.9/24.5/DEE6 give a gradual increase in the heat release rate 56.2 J/^{o}CA, 57.4 J/^{o}CA, and 58.4 J/^{o}CA, which occurred at 3.2 ^{o}CA aTDC, 1.1 ^{o}CA aTDC, and 0.5 ^{o}CA bTDC respectively, at full load. This increase in the heat release rate may be attributed to the injection of DEE, which advances the early burning, and increases the premixed combustion [248]. Also, the availability of oxygen and high cetane number of DEE forms many ignition centers at different locations inside the combustion chamber, and increases the rate of combustion of premixed biogas. This is in good agreement with Sahoo et al. [61] demonstrated in their investigation on a DI diesel engine operated with the biogas-biodiesel dual fuel mode.

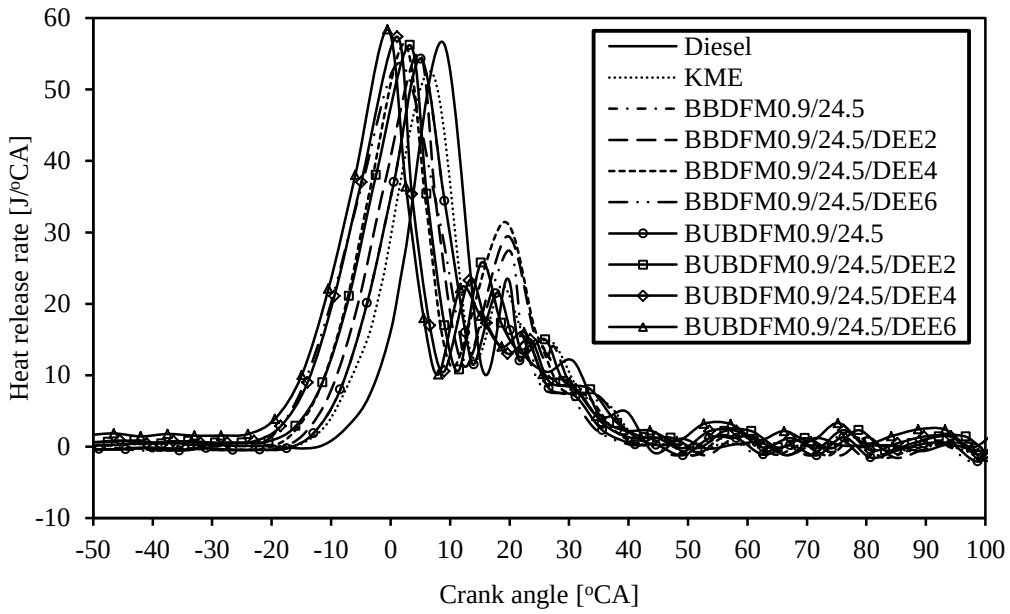

Figure 5.7.3 Variation of heat release rate with the crank angle at full load.

5.7.2.4 Combustion duration

The variation of combustion duration with load is depicted in Figure 5.7.4. It can be observed that, the combustion duration increases with the increase in load irrespective of the fuels used. This is due to the consumption of more quantity of fuel at relatively higher loads. The BBDFM0.9/24.5 gives a longer combustion duration throughout the load spectrum. This is due to the slower burning rate of raw biogas. With the use of upgraded biogas the combustion duration decreases. BUBDFM0.9/24.5 gives a shorter combustion duration of 37.1 ^{o}CA at full load. In the dual fuel mode with the DEE injection, for raw biogas and upgraded biogas, shorter combustion durations were observed. This is due to the effect of DEE which attributes to the faster ignition and increase in the ignition centers inside the combustion chamber. This reason is well matched with the research results documented by Geo et al. [248] for the work they have carried out on a single cylinder DI diesel engine run on rubber seed oil and DEE. The dual fuel operations with the upgraded biogas give shorter combustion duration than that of the dual fuel oparation with raw biogas. This is due to the effect of increased percentage of CH_4 in the fuel, which has a higher burning velocity, that increases the flame speed and reduceses the combustion duration. BUBDFM0.9/24.5/DEE2, BUBDFM0.9/24.5/DEE4, and BUBDFM0.9/24.5/DEE6 give a shorter combustion duration of 36.1 ^{o}CA, 35.2 ^{o}CA, and 34.6 ^{o}CA, at full load respectively.

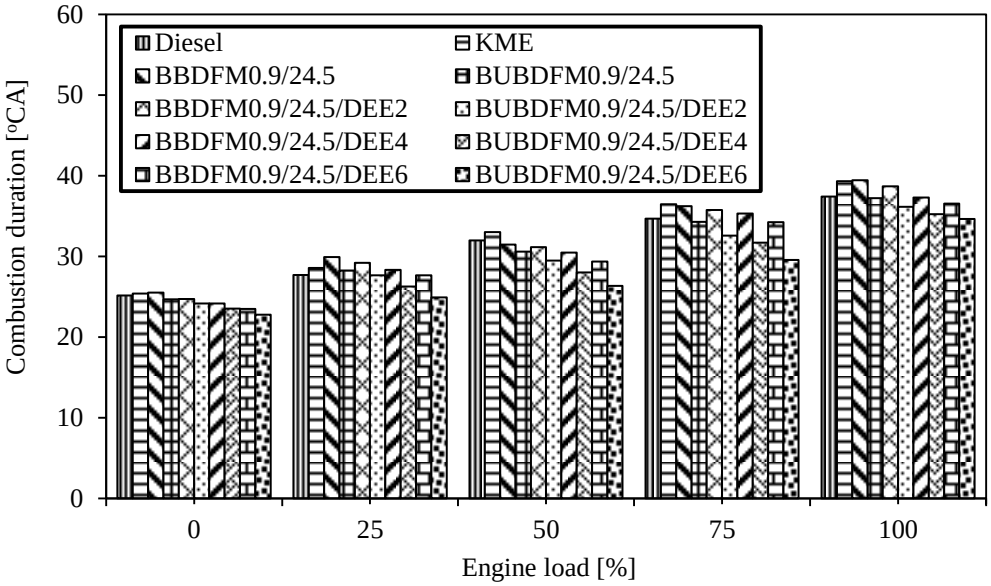

Figure 5.7.4 Variation of combustion duration with load.

5.7.2.5 Maximum cylinder pressure

Figure 5.7.5 illustrates the variation of maximum cylinder pressure with the load for diesel, KME, and dual fuel operations with raw and upgraded biogas and DEE injection. It can be observed from the figure that, the cylinder pressure increases with the increase in the load, as expected. The maximum cylinder pressure for diesel and KME is about 75.7 bar and 71.3 bar at full load, respectively. The dual fuel operation with the advanced injection timing of BBDFM0.9/24.5 and BUBDFM0.9/24.5 give higher cylinder pressures of about 78 bar and 78.6 bar than that of diesel, at full load. The reason for the increase in the maximum cylinder pressure in the dual fuel operation, with the advanced injection timing is due to the formation of fuel rich mixture inside the combustion chamber. Ryu [92], Mustafi et al. [105], and Karim [220] have reported the similar type of results for their experiment in a biogas run DI diesel engine. The dual fuel operations with raw and upgraded biogas with the DEE injection give a gradual increase in the cylinder pressure throughout the load spectrum. This is because of the early ignition of DEE in the combustion chamber that helps to modulate the ignition of biogas rapidly at an earlier stage of crank angle. Geo et al. [248] and Hansdah and Murugan [249] reported the similar reason for their investigation in a DI diesel engine fueled with the biodiesel-DEE and ethanol-DEE dual fuel operations. The dual fuel operation with the raw biogas gives a marginal increase in pressure than that of upgraded biogas operation. This increase in pressure in the raw biogas dual fuel operation is attributed to the longer delay period, caused by the presence of CO_2 in raw biogas. This brings about a decrease and

dilution of charge, and may cause ignition delay to extend, leading to a higher rate of increase in pressure in the premixed combustion phase. Similar reasons were described by Ryu [92], and Paul et al. [88] in their investigations for the results they obtained in a CNG-biodiesel fueled DI diesel engine. The dual fuel operations of BUBDFM0.9/24.5/DEE2, BUBDFM0.9/24.5/DEE4, and BUBDFM0.9/24.5/DEE6 give maximum cylinder pressure of 76.6 bar, 79.4 bar, and 81 bar respectively, at full load.

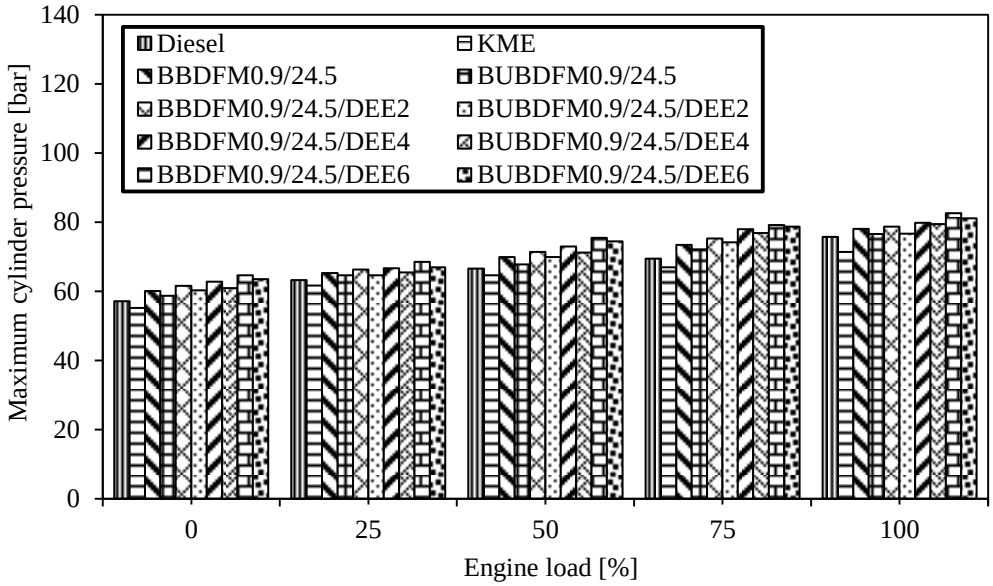

Figure 5.7.5 Variation of maximum cylinder pressure with load.

5.7.3 Performance analysis

5.7.3.1 BSFC

Figure 5.7.6 portrays the variation of BSFC with load for diesel, KME, and dual fuel operations with raw and upgraded biogas and different quantities of DEE injection. It can be observed from the figure that, the BSFC decreases with the increase in the load for the entire test fuels because; as the load of the engine increases, the fuel atomization, and combustion quality increases. The BSFC in the dual fuel operation, at low and intermediate load conditions, is considerably higher in comparison with those of the diesel and KME operations. This may be due to the slower premixed controlled combustion during the initial stages of combustion at low load. This reason is in good agreement with Papagiannakis et al. [237] for the reason they have reported for the results obtained in a dual fuel diesel engine. In dual fuel operations with the DEE injection, the BSFC decreases. This decrease in BSFC with the DEE injection is due to the increase in combustion quality of biogas, and additional energy supply from the DEE. This reason is also evidenced from the research work

documented by Geo et al. [248] for the work they have carried out on a single cylinder DI diesel engine run on rubber seed oil and DEE. The dual fuel operations with the upgraded biogas gives a lower BSFC than that of dual fuel operation with raw biogas. This may be due to the increased combustion quality of higher percentage of methae in upgraded biogas than that of raw biogas. This reason is also matched with the reason reported by Bari [106] for the work he has carried out on a diesel engine run on a dual fuel mode, with different percentages of CO_2 in biogas and natural gas. BUBDFM0.9/24.5/DEE2, BUBDFM0.9/24.5/DEE4, and BUBDFM0.9/24.5/DEE6 give the BSFC values of 0.34 kg/kWh, 0.33 kg/kWh, and 0.31 kg/kWh respectively, which is 22%, 19.7% and 13.3% higher than that of diesel at full load.

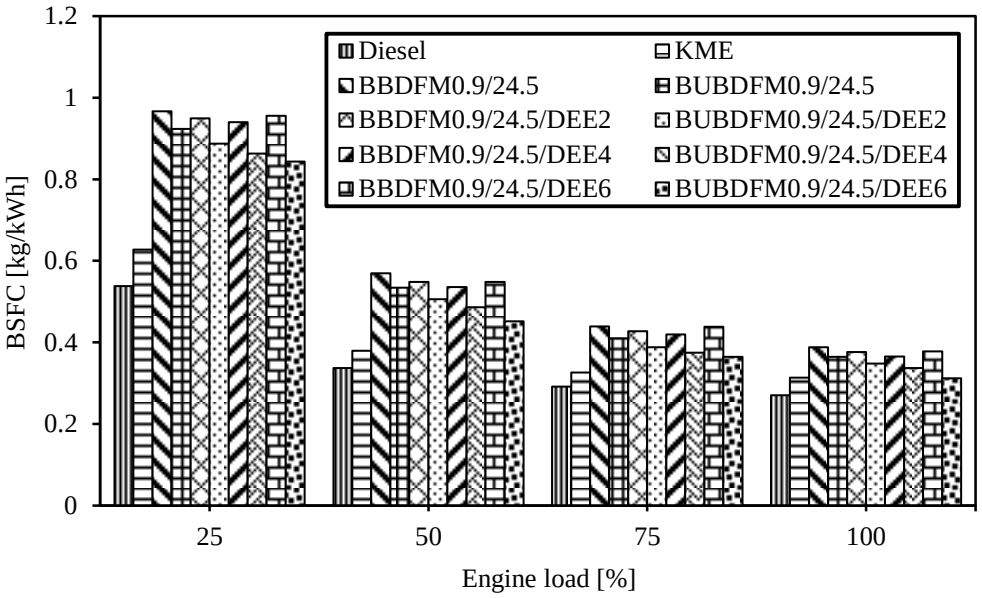

Figure 5.7.6 Variation of BSFC with load.

5.7.3.2 BTE

The variation of BTE with load for diesel, KME and dual fuel operation with raw and upgraded biogas with different DEE injection quantities is illustrated in Figure 5.7.7. Diesel operation offers the highest BTE throughout the load spectrum irrespective of the fuels used in the experiment. This is due to the higher heating value of diesel. The BTE of KME is found to be about 28%, which is 2.3% lower than that of diesel, at full load. The BTE for the test fuels increases with the increase in the load. This is due to the increased cylinder temperature at relatively higher loads. In dual fuel operations, with the increase in the DEE injection quantity the BTE increases gradually. This is attributed to the the quicker evaporation, and easy mixing of DEE with biogas-air mixture, that forms a homogeneous charge and gives a complete combustion releasing more energy. Also, the early start of

ignition of DEE gives a better combustion phasing to biogas and boosts the rate of combustion of KME and the BTE increases. This reason is in good agreement with the reasons described by Geo et al. [256], and Imtenan et al. [250] for the results they have obtained in a single cylinder, DI diesel engine, and a multi-cylinder diesel engine fueled with biodiesel, and DEE as an ignition improver, and oxygenated additive respectively. BUBDFM0.9/24.5/DEE2, BUBDFM0.9/24.5/DEE4, and BUBDFM0.9/24.5/DEE6 operations give the BTE values of about 28.5%, 28.8%, and 29.1% than that of dual fuel with raw biogas operation, at full load. The BTE of BUBDFM0.9/24.5/DEE2, BUBDFM0.9/24.5/DEE4, and BUBDFM0.9/24.5/DEE6 is found to be lower by about 6%, 5.1%, and 4.1% than diesel, at full load.

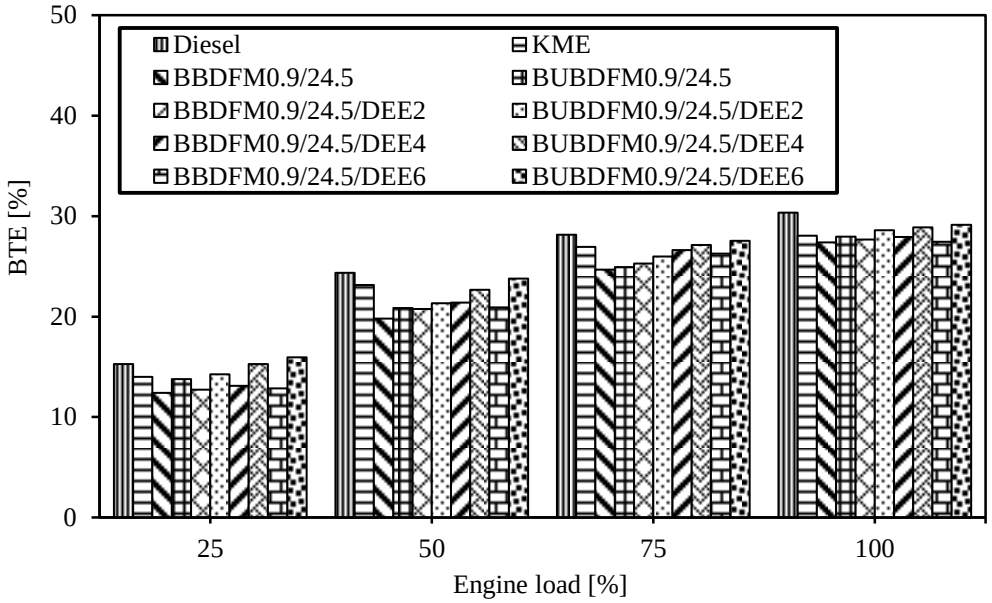

Figure 5.7.7 Variation of BTE with load.

5.7.3.3 EGT

The variation of EGT with the load is depicted in Figure 5.7.8. It can be observed from the figure that, KME exhibit the highest EGT than that of the other fuels tested in the investigation. The presence of oxygen in the ester molecules enhances the combustion process and results in a higher EGT. The dual fuel operation with the biogas induction gives lower EGT. This may be due to the absorption of heat by the biogas to occur auto ignition, and decreases the adiabatic flame temperature. This reason is in good agreement with the reason described by Nwafor [233] for the results obtained in a biogas-fueled dual fuel diesel engine. The DEE injection in the dual fuel operation gives an increase in the EGT for both raw and upgraded biogas. This may be due to the increase in the flame speed of DEE, which

boosts the combustion of biogas. A similar reason for the increase in the EGT is described by Hariharan et al. [251] in their research work to study the effect of DEE on tyre pyrolysis oil fueled DI diesel engine. The EGT for the upgrade biogas operation BUBDFM0.9/24.5/DEE2, BUBDFM0.9/24.5/DEE4, and BUBDFM0.9/24.5/DEE6 is marginally lower than that of raw biogas operation. This is due to the shorter delay period and shorter combustion duration, which allows improved diffusion combustion due to higher percentage of methane in upgraded biogas, and this, is evidenced in the heat release diagram.

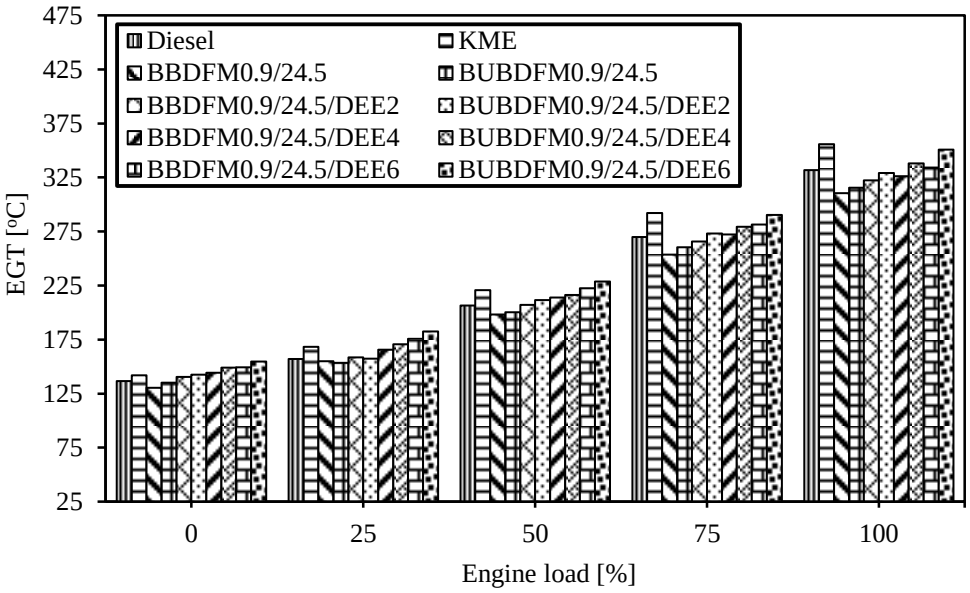

Figure 5.7.8 Variation of EGT with load.

5.7.4 Emission analysis

5.7.4.1 CO emission

The variation of CO emission with load is depicted in Figure 5.7.9. It can be observed from the figure that, KME gives a lower CO mission than that of diesel, and dual fuel operations throughout the load spectrum. This is due to the presence of oxygen in KME, that gives a complete oxidation, and hence CO reduces. The dual fuel operations with DEE injection give a gradual decrease in CO emission throughout the load spectrum. This may be due to the port injection of DEE helps it to mix properly with the air-biogas mixture, and forms many ignition centers in the combustion chamber, results complete combustion of the fuel, and hence the CO lowers. This reason is also evidenced from the research work documented by Geo et al. [248] for the work they have carried out on a single cylinder DI diesel engine run on rubber seed oil and DEE. The dual fuel operations with upgraded biogas and the DEE injection give a lower CO emission than that of diesel, KME and other dual fuel operations at

full load. This may be due to the combined effect of injection of DEE and KME, both of which contains dissolved oxygen, which improves the start of ignition of biogas, and decreases the ignition delay, and allows more time for oxidation of the charge, and CO reduces. This statement is in good agreement with Liu et al. [84] for the reason they have reported for the results obtained in a CNG-diesel dual fuel diesel engine. An overall reduction of about 27% to 33% in the CO emission is noticed for the biodiesel-upgraded biogas and DEE injection than that of diesel at full load respectively.

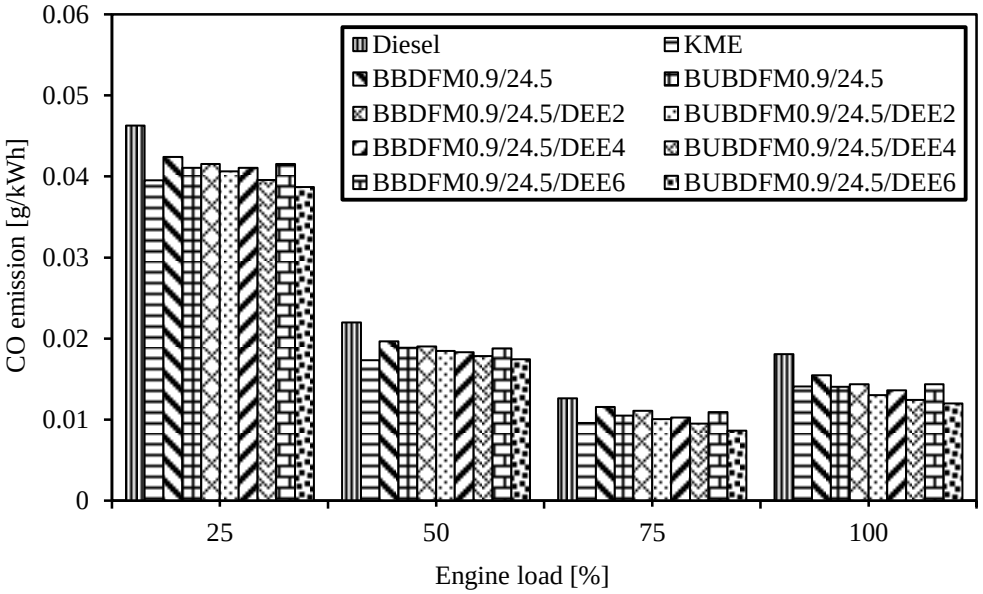

Figure 5.7.9 Variation of CO emission with load.

5.7.4.2 HC emission

The variation of HC emission with load is depicted in Figure 5.7.10. KME gives a lower HC emission throughout the load spectrum, than that of diesel and dual fuel operations with DEE injection quantities. This is due to the existence of oxygen in the KME gives a complete combustion. The DEE injection in the dual fuel operation offers a reduction of HC emission for both the raw biogas and upgraded biogas operations throughout the load spectrum. This is due to the earlier start of combustion advances and leads to comparatively higher cylinder gas temperature, which improves oxidization of biogas with the help of increased oxygen concentration in charge, due to simultaneous effort of DEE and KME. Similar reasons were described by Sudheesh and Mallikarjuna [252], and Qi et al. [254] in their investigations for the results they have obtained in a DI diesel engine operated with biodiesel and diesel with DEE as an ignition improver. The dual fuel operation with the upgraded biogas and different DEE injection quantities gives a lower HC emission than that of dual fuel operation with the

raw biogas. This may be due to the induction of methane enriched biogas which effects to reduce the partial buring. This statement is in good agreement with Papagiannakis et al. [237], and Ryu [93] for the reasons they have mentioned for the results obtained in a direct injection diesel engine fueled with biodiesel-CNG dual fuel. A reduction in HC emission of 25%, 29.1% and 33.3% is observed for BUBDFM0.9/24.5/DEE2, BUBDFM0.9/24.5/DEE4, and BUBDFM0.9/24.5/DEE6 in comparison with diesel at full load. But, the HC emission for BUBDFM0.9/24.5/DEE2, BUBDFM0.9/24.5/DEE4, and BUBDFM0.9/24.5/DEE6 is found to be higher by about 20%, 13.3%, and 6.7% than that of KME, at full load respectively.

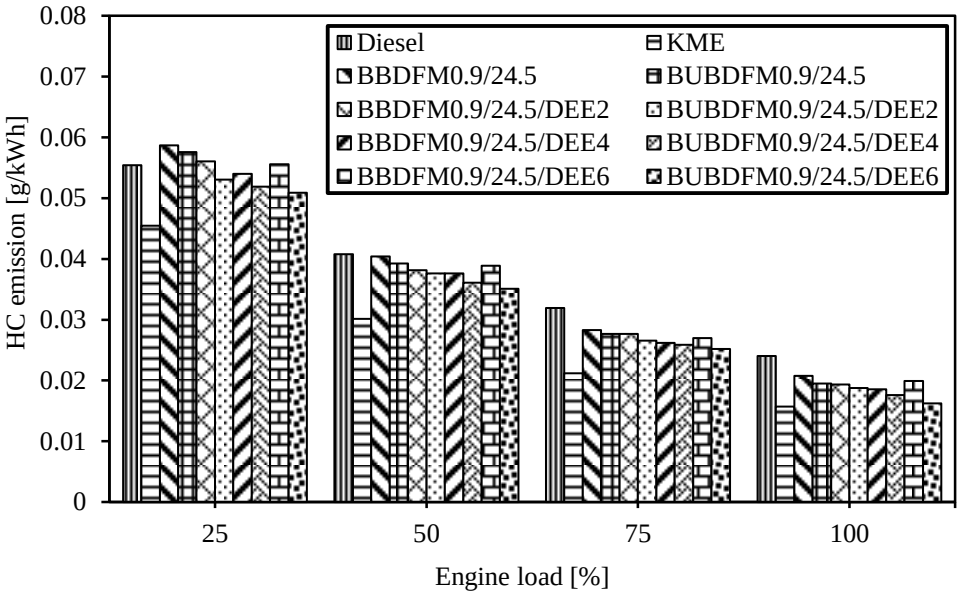

Figure 5.7.10 Variation of HC emission with load.

5.7.4.3 NO emission

Figure 5.7.11 portrays the variation of NO emission with the load. KME gives a higher NO emission than that of diesel and the dual fuel operations. This is due to the higher oxygen concentration in KME. The concentration of NO emission in the dual fuel operation is considerably lower than that of KME throughout the load spectrum. This may be due to the drop in volumetric efficiency in the dual fuel operation, by the induction of biogas through the intake manifold. The dual fuel operations with the raw and upgraded biogas give a gradual increase in NO emission with the increase in DEE injection irrespective of the load. This increase in NO emission with the DEE injection is attributed to the higher oxygen enrichment (from both DEE and KME), and a more complete combustion may give higher thermal NO. This reason is well matched with the results mentioned by Qi et al. [254], and Sivalakshmi et al. [255] for the results they have obtained in a DI diesel engine fueled with

biodiesel, diesel, and DEE. The upgraded biogas dual fuel operation of BUBDFM0.9/24.5/DEE6 gives a higher NO emission of 11.3%, 8.6% and 3.3%, than that of BBDFM0.9/24.5/DEE2, BBDFM0.9/24.5/DEE4, and BBDFM0.9/24.5/DEE6, at full load respectively. This increase in NO emission for the upgraded biogas dual fuel operation is due to the increase in the combustion temperature due to the higher percentage of methane, which has a fast burning speed and a higher heating value.

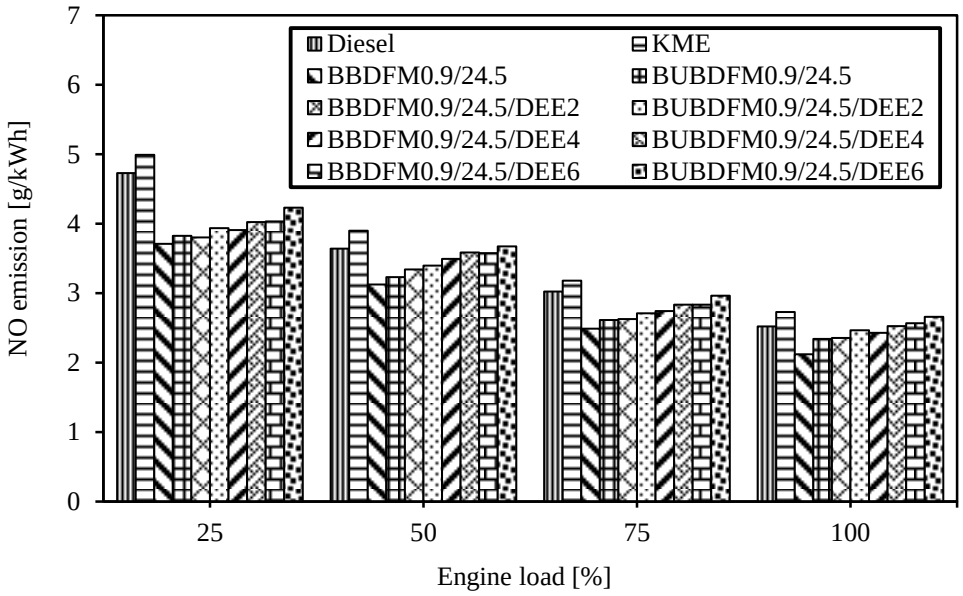

Figure 5.7.11 Variation of NO emission with load.

5.7.4.4 Smoke emission

Figure 5.7.12 portrays the variation of smoke emission with the load. It can be observed from the figure that, the smoke emission increases with the increase in load irrespective of the fuels used. This is due to the decrease in excess air ratio and increase in diesel consumption at relatively high loads, which gives a lower oxidation of soot particles. KME gives a lower smoke emission than that of diesel throughout the load spectrum. This is due to the lower stoichiometric air requirement for KME, because of available oxygen in it. The dual fuel operations with raw and upgraded biogas with DEE injection give a gradual decrease in smoke emission throughout the load spectrum. This may be attributed to the early start of combustion of biogas due to the effect of high cetane number of DEE, and allows more time for the oxidation of soot. Also, reduced ignition delay due to the DEE injection reduces the accumulation of fuel in the combustion chamber and suppresses the probability of fuel rich zone in the premixed combustion phase, and decreases the smoke emission. Similar reasons were reported by Liu et al. [84] for the results they have obtained in their research on a CNG-

diesel dual fuel engine. The dual fuel operations with the upgraded biogas give a lower smoke emission than that of dual fuel operations with the raw biogas, throughout the load spectrum. This may be due to the enriched methane percentage in upgraded biogas, which is the lower member of the paraffin family, and have a very small tendency to produce soot, and lowers the smoke emission. This statement is in good agreement with Papagiannakis et al. [82] for the results they obtained in a natural gas-diesel fueled dual fuel diesel engine. BUBDFM0.9/24.5/DEE2, BUBDFM0.9/24.5/DEE4, and BUBDFM0.9/24.5/DEE6 give a lower smoke emission of 30.4%, 32.4%, and 38% than that of diesel at full load.

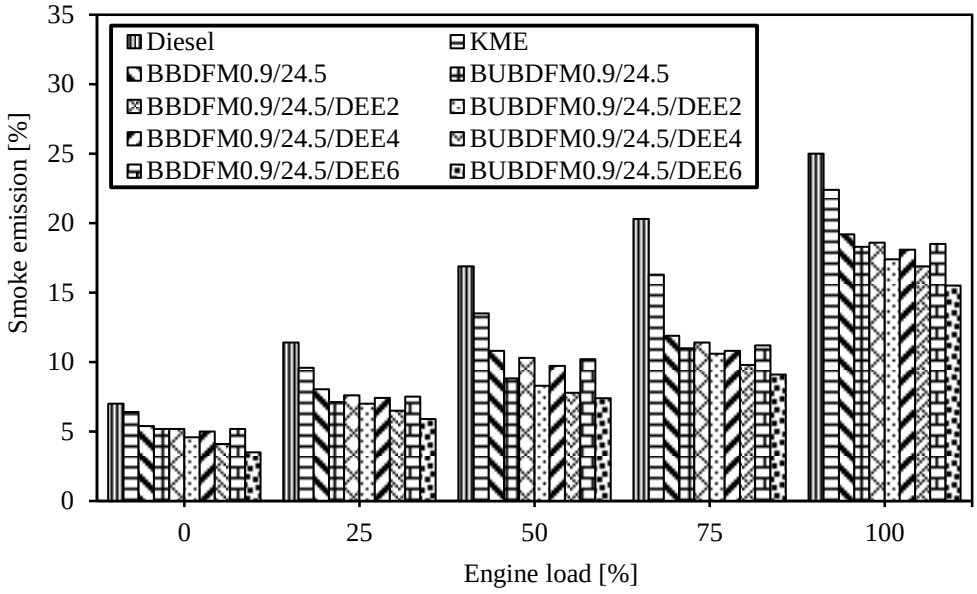

Figure 5.7.12 Variation of smoke emission with load.

5.7.5 Summary

The experimental results of the dual fuel operation with the raw and upgraded biogas with different percentages of DEE injection are compared with those of the diesel and KME and presented in this section. The summary of the results are as follows:

BUBDFM0.9/24.5/DEE6 gives optimum results for the combustion, performance and emission characteristics of the engine, than those of other dual fuel operations. BUBDFM0.9/24.5/DEE6 gives an increase in BTE of about 4.1%, and 5.8% than that of BBDFM0.9/24.5/DEE4, and BBDFM0.9/24.5/DEE6 at full load respectively. The BSFC for BUBDFM0.9/24.5/DEE6 is found to be lower by about 16.9%, and 21.1% than that of BBDFM0.9/24.5/DEE4, and BBDFM0.9/24.5/DEE6 at full load respectively. BUBDFM0.9/24.5/DEE6 gives a reduction in CO, HC and smoke emissions of 8.3%, 12.5%

and 16.7% than that of BBDFM0.9/24.5/DEE4, at full load respectively. The NO emission for the BUBDFM0.9/24.5/DEE6 is 4.9% higher than that of diesel at full load.

Table 5.7 provides the values of important parameters of the investigation obtained for the diesel, KME, KME-raw biogas, and KME-upgraded biogas dual fuel operations, with different percentages of DEE injection, at full load.

Table 5.7 Summary of the values of the combustion, performance and emission parameters, for diesel, KME, KME-raw biogas, and KME-upgraded biogas dual fuel operations, with different percentages of DEE injection, at full load.

Sl. No.	Parameters	Diesel	BBDFM0.9/ 24.5/DEE4	BUBDFM0.9/ 24.5	BUBDFM0.9/ 24.5/DEE2	BUBDFM0.9/ 24.5/DEE4	BUBDFM0.9/ 24.5/DEE6
A. Combustion parameters							
1	Maximum cylinder pressure, bar	75.7	79.7	76.5	76.6	79.4	81.0
2	Maximum heat release rate, J/^{o}CA	56.5	56.4	54.3	56.2	57.4	58.4
3	Ignition delay, ^{o}CA	11.5	11.2	11.2	10.8	10.1	9.0
4	Combustion duration, ^{o}CA	37.4	37.2	37.1	36.1	35.2	34.6
B. Performance parameters							
1	BSFC, kg/kWh	0.27	0.365	0.36	0.34	0.33	0.31
2	BTE, %	30.3	27.9	27.9	28.5	28.8	29.1
3	EGT, ^{o}C	331.8	326.4	315.6	329.2	338.1	350.8
C. Emission parameters							
1	CO, g/kWh	0.017	0.0136	0.014	0.013	0.0124	0.0120
2	HC, g/kWh	0.025	0.0185	0.0194	0.0187	0.0175	0.0162
3	NO, g/kWh	2.923	2.428	2.34	2.46	2.52	2.65
4	Smoke opacity, %	25	18.1	18.3	17.4	16.9	15.5

5.8 Biodiesel-upgraded biogas optimum flow rate + optimum injection timing + optimum DEE injection + compression ratio

5.8.1 General

Although, the biodiesel-upgraded biogas dual fuel mode with DEE injection operated well and gave better performance and lower emissions than that of the biodiesel-raw biogas dual fuel mode, the engine produced lower brake thermal efficiency compared to diesel operation. In order to increase the efficiency and getting an optimum compression ratio for biodiesel-upgraded biogas dual fuel operation, the compression ratio of the engine is varied from 16.5, 17.5, and 18.5.

This section presents the experimental results of the combustion, performance and emission characteristics of the engine run on a dual fuel mode, with upgraded biogas at a flow of 0.9 kg/h, with optimum injection timing of 24.5 ^{o}CA bTDC and optimum DEE injection of 6%, and three different compression ratios. The important results of comparison between the upgraded biogas utilization in diesel engine operated with different compression ratios on the dual fuel mode are presented. The acronyms used for the investigation are as follows:

BUBDFM0.9/24.5/DEE6/CR16.5 - biodiesel injected at 24.5 ^{o}CA bTDC + upgraded biogas 0.9 kg/h and DEE injection of 6% at compression ratio 16.5.

BUBDFM0.9/24.5/DEE6/CR17.5 - biodiesel injected at 24.5 ^{o}CA bTDC + upgraded biogas 0.9 kg/h and DEE injection of 6% at compression ratio 17.5.

BUBDFM0.9/24.5/DEE6/CR18.5 - biodiesel injected at 24.5 ^{o}CA bTDC + upgraded biogas 0.9 kg/h and DEE injection of 6% at compression ratio 18.5.

5.8.2 Combustion analysis

5.8.2.1 Pressure crank angle diagram

Figure 5.8.1 depicts the variation of cylinder pressure with crank angle at full load for diesel, KME and dual fuel operations. It can be observed from the figure that the peak cylinder pressure for diesel and KME are found to be 75.7 bar and 71.3 bar which occur at 7.4 ^{o}CA aTDC and 6.8 ^{o}CA aTDC respectively, at full load. In the dual fuel operation, with the increase in the compression ratio the peak cylinder pressure increases gradually. This may be attributed to the increase in the cylinder charge temperature at the end of the compression stroke, due to effect of

higher copmression ratio. And hence, the flames propagate more rapidly, and the peak cylinder pressure increases. This reason is in good agreement with Bora and Saha [102] for the results they have obtained in a single cylinder DI diesel engine, modefied to operate on diesel-biogas dual fuel mode. In dual fuel operation with compression ratios of 16.5, 17.5, and 18.5 the peak cylinder pressure is found to be higher by about 76.3 bar, 81 bar, and 84 bar respectively, than that of diesel at full load.

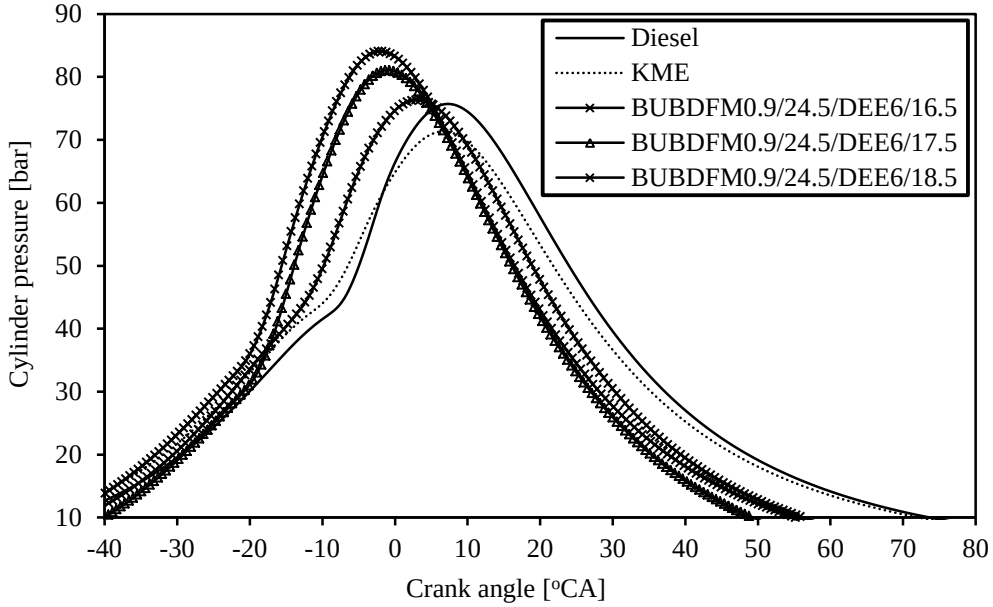

Figure 5.8.1 Variation of cylinder pressure with the crank angle at full load.

5.8.2.2 Ignition delay

Figure 5.8.2 illustrates the variation of ignition delay with the variation in load. It can be observed from the figure that the ignition delay for diesel is found to be longer than that of dual fuel operations, throughout the load spectrum. The shorter ignition delay for the dual fuel operation than that of diesel may be due to the injection of DEE, which improves the ignition. In the dual fuel operation with the increase in compression ratio, the ignition delay decreases throughout the load spectrum. This is due to the increased pre-ignition reaction of the pilot fuel, and that is believed to affect the ignition of the biogas. This reason is also evidenced from the research work documented by Tangoz et al. [256] for the work they have carried out on a single cylinder DI diesel engine run CNG-diesel, and HCNG-diesel dual fuel mode with variation in compression ratio. The ignition delay for diesel and KME are about 11.5 ^{o}CA and 10.5 ^{o}CA, at

full load. In dual fuel operation with the compression ratio of 16.5, 17.5, and 18.5 the ignition delay is shorter by about 10.4 ^{o}CA, 9 ^{o}CA, and 7.8 ^{o}CA respectively, at full load.

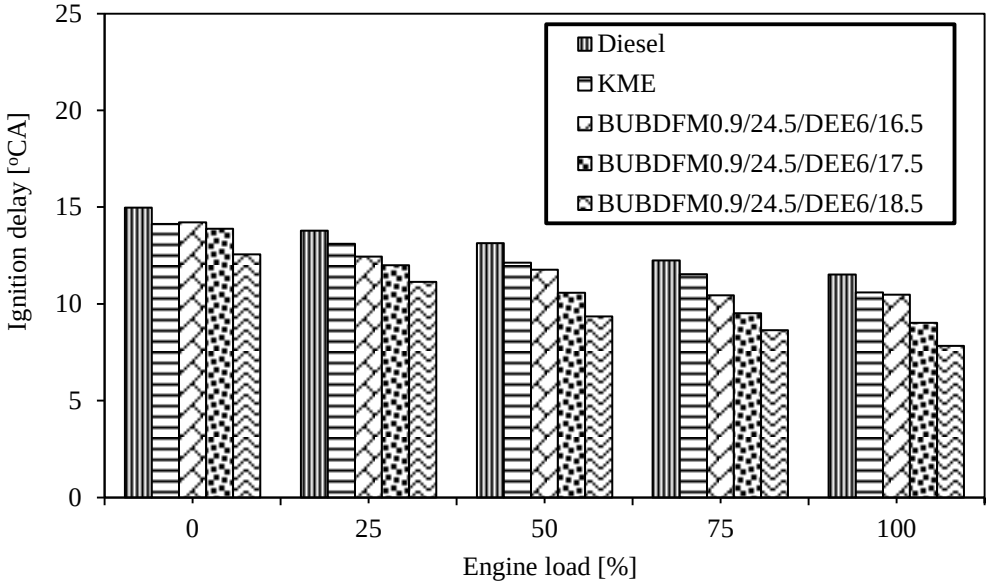

Figure 5.8.2 Variation of ignition delay with load.

5.8.2.3 Heat release rate

The variation of heat release rate with the variation in crank angle for diesel, KME and dual fuel operations with compression ratio is depicted in Figure 5.8.3.

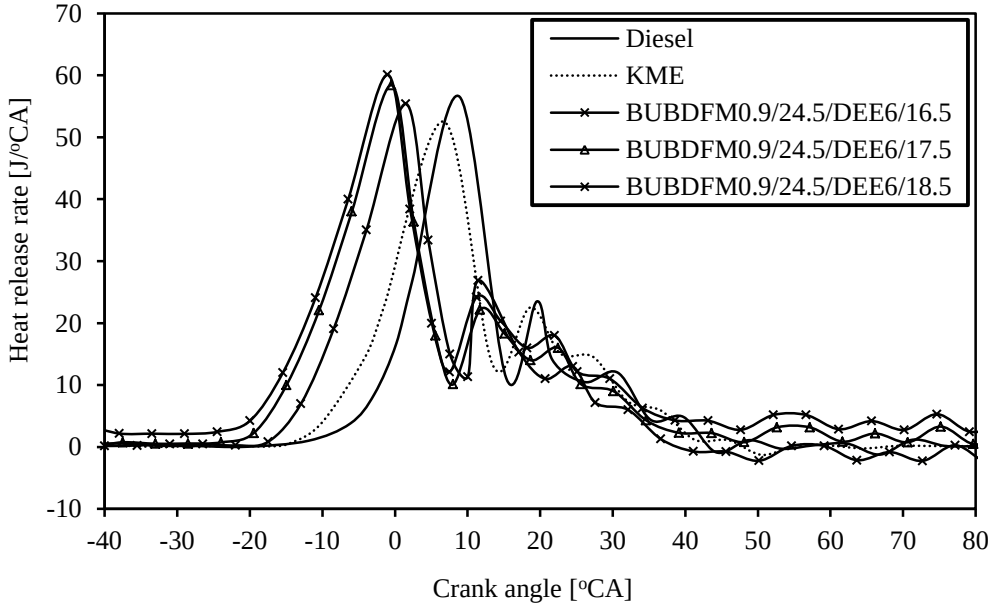

Figure 5.8.3 Variation of heat release rate with crank angle at full load.

Diesel and KME gives heat release rate of 56.5 J/^{o}CA, and 52.4 J/^{o}CA. In dual fuel operation with increase in compression ratio the heat release rate increases. The dual fuel operation with compression ratio of 16.5, 17.5, and 17.5 gives heat release rate of 55.4 J/^{o}CA, 58.4 J/^{o}CA, and 60 J/^{o}CA. This increase in heat release rate in the dual fuel operation, with the increase in compression ratio is due to the increase in the combustion efficiency of the biogas. This is because, as the compression ratio increases, the clearance volume decreases, which in turn increases the temperature and pressure of the charge during the end of the compression stroke. The increased combustion temperature results in better combustion of the fuel and increases the heat release rate. This reason is well matched with the research results documented by Ibrahim et al. [257] for the work they have carried out on a twin cylinder, water cooled, DI diesel engine run on premixed biogas-diesel dual fuel mode.

5.8.2.4 Combustion duration

The variation of combustion duration with the variation in load is depicted in Figure 5.8.4.

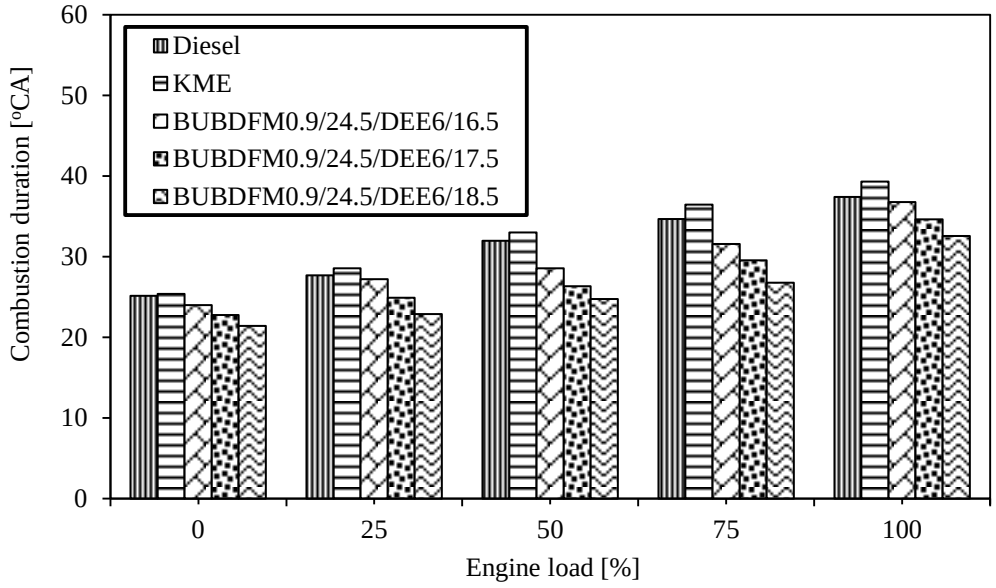

Figure 5.8.4 Variation of combustion duration with load.

It can be observed from the figure that KME gives a higher combustion duration than that of diesel. This is due to the poor spray formation by KME due to its higher viscosity. With the increase in load the combustion duration increases irrespective of the fuels used. This is due to the consumption of more quantity of fuel at relatively higher loads. In dual fuel operation with the increase in compression ratio the combustion duration increases. This may be due to the

shorter ignition delay and early start of burning of the pilot fuel at high compression ratio, which enhances the combustion of biogas rapidly in the premixed phase of combustion. This is in good agreement with Bora and Saha [258] demonstrated in their investigation on a DI diesel engine operated with the biogas-biodiesel dual fuel mode. The dual fuel operation with compression ratio of 16.5, 17.5, and 18.5 gives a gradual decrease in combustion duration of 36.7^{o}CA, 34.6 ^{o}CA and 32.5 ^{o}CA respectively, than that of diesel at full load.

5.8.2.5 Maximum cylinder pressure

The variation of maximum cylinder pressure with the variation in load is depicted in Figure 5.8.5. It can be observed from the figure that, the cylinder pressure increases with the increase in the load, as expected. The maximum cylinder pressure for diesel and KME is about 75.7 bar and 71.3 bar at full load, respectively. In dual fuel operation, with the increase in compression ratio the maximum cylinder pressure increases. This is due to the increased pre-ignition reaction of the pilot fuel, and that is believed to affect the ignition of the biogas rapidly, and increases the cylinder pressure. Guerry et al. [259] reported the similar reason for their investigation in a DI diesel engine fueled with the premixed diesel-methane dual fuel mode. Dual fuel operation of BUBDFM0.9/24.5/DEE6/18.5 gives a maximum cylinder pressure of 84 bar, than that of other dual fuel operations at full load.

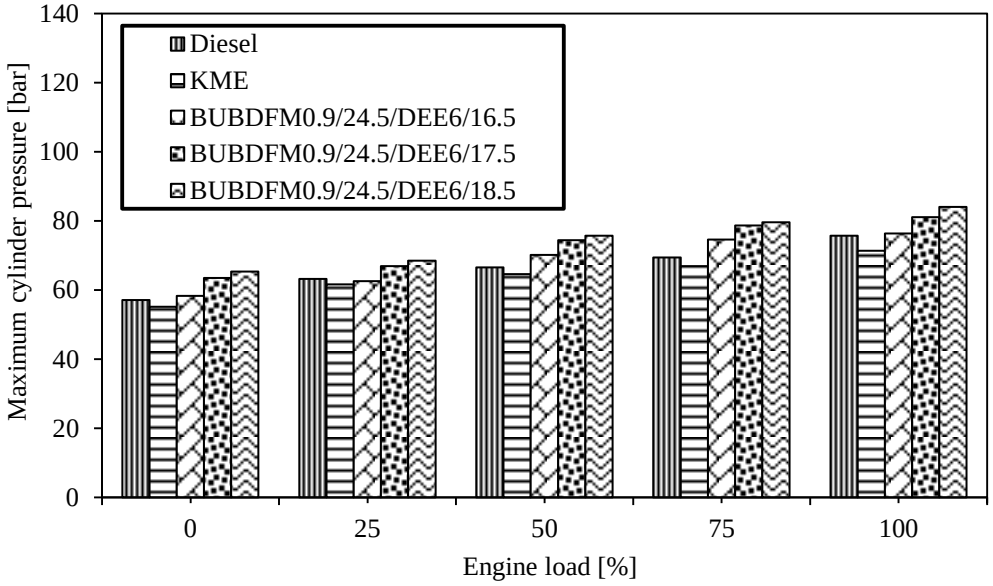

Figure 5.8.5 Variation of maximum cylinder pressure with load.

5.8.3 Performance analysis

5.8.3.1 BSFC

The variation of BSFC with the variation in load is illustrated in Figure 5.8.6. It can be observed from the figure that, the BSFC decreases with the increase in the load for the entire test fuels because; as the load of the engine increases, the fuel atomization, and combustion quality increases. The BSFC in the dual fuel operation with the variation in compression ratio, at low and intermediate load conditions, is considerably higher in comparison with those of the diesel and KME operations. This may be due to the slower premixed controlled combustion during the initial stages of combustion at low load. This reason is in good agreement with Papagiannakis et al. [237] for the reason they have reported for the results obtained in a dual fuel diesel engine. In dual fuel operation, with the increase in compression ratio the BSFC decreases. This is due to the improved combustion and reduced combustion duration of the fuel at high compression ratio.

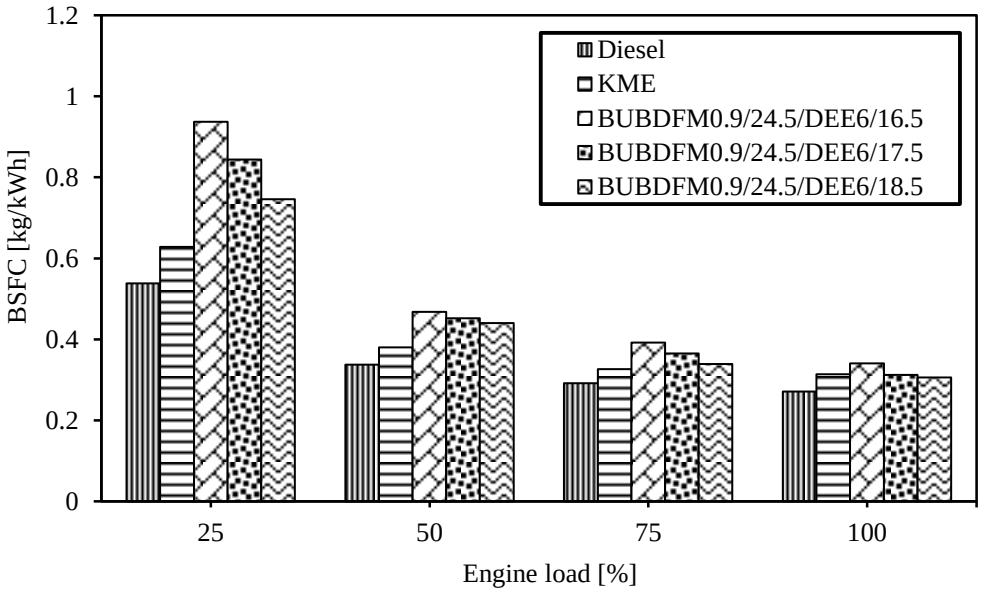

Figure 5.8.6 Variation of BSFC with load.

5.8.3.2 BTE

The variation of BTE with the variation in load is depicted in Figure 5.8.7. Diesel operation offers the highest BTE throughout the load spectrum irrespective of the fuels used in the experiment. This is due to the higher heating value of diesel. The BTE of KME is found to be about 28%, which is 2.3% lower than that of diesel, at full load. The BTE for the test fuels

increases with the increase in the load. This is due to the increased cylinder temperature at relatively higher loads. In dual fuel operation, with the increase in compression ratio the BTE increases. This is due to the increase in the combustion efficiency of the biogas. Also the early start of ignition of pilot fuel due to high compression ratio, gives a better combustion phasing to biogas and boosts the rate of combustion and the BTE increases. This reason is in good agreement with Bora and Saha [102] for the results they have obtained in a single cylinder DI diesel engine, modefied to operate on diesel-biogas dual fuel mode.

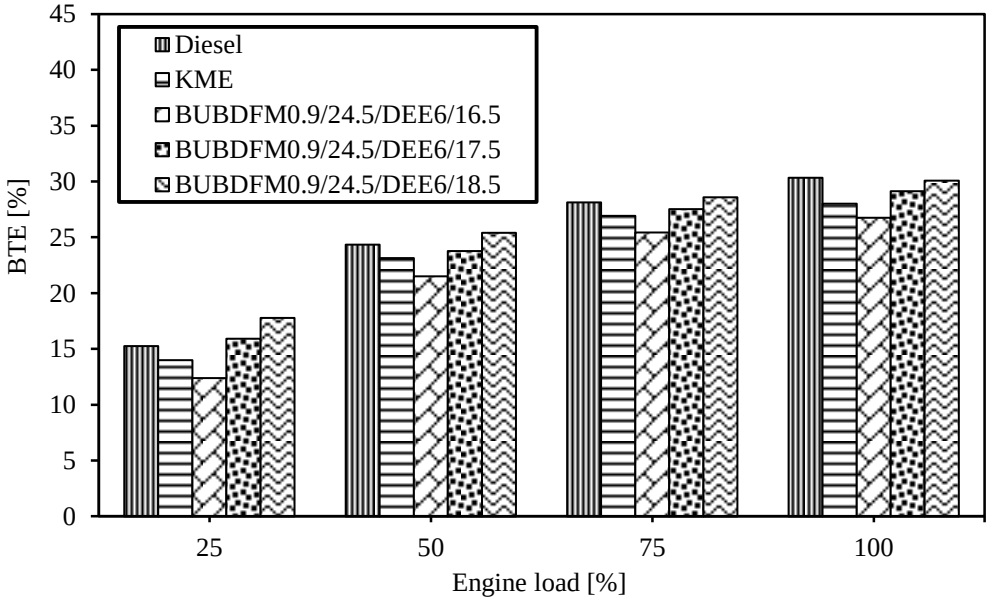

Figure 5.8.7 Variation of BTE with load.

5.8.3.3. EGT

The variation of EGT with the load is depicted in Figure 5.8.8. It can be observed from the figure that, at full load KME exhibit the highest EGT than that of the other fuels tested in the investigation. The presence of oxygen in the ester molecules enhances the combustion process and results in a higher EGT. The dual fuel operation with compression ratio of 16.5 the EGT decreases. This may be due to the absorption of heat by the biogas to occur auto ignition at lower compression ratio, and decreases the adiabatic flame temperature. But, with the increase in compression ratio the EGT increases slightly. This is due to the high temperature combustion of the air-biogas mixture at higher compression ratio of the engine. This reason is in good agreement with the reason described by Chintala and Subramanian [260] for the results obtained in a hydrogen-dual fueled dual fuel engine operated with variation in compression ratio.

BUBDFM0.9/24.5/DEE6/18.5 gives exhaust gas temperature of 354.7 ^{o}C at full load, which is about 2% lower than that of the KME.

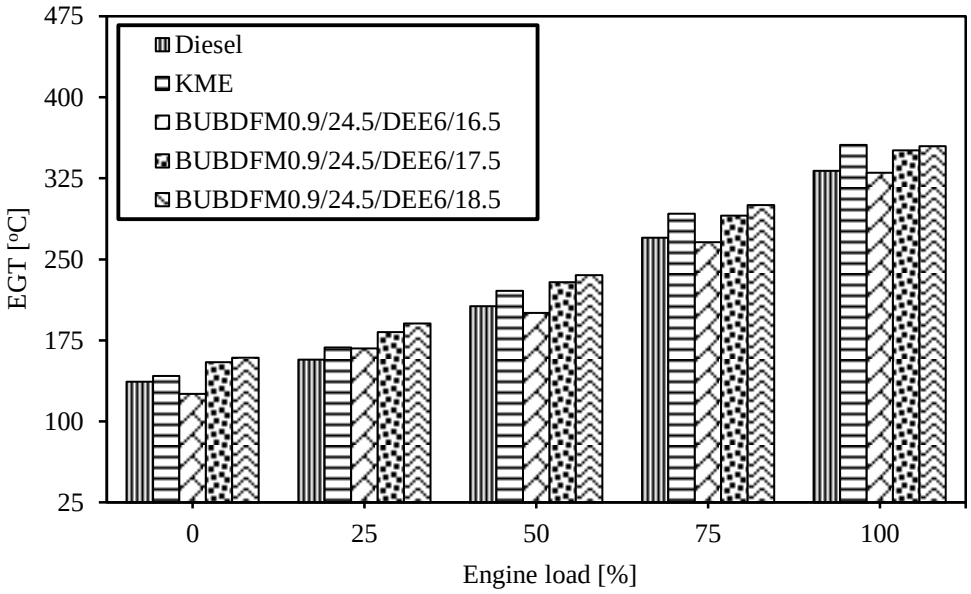

Figure 5.8.8 Variation of EGT with load.

5.8.4 Emission analysis

5.8.4.1 CO emission

The variation of CO emission with load is depicted in Figure 5.8.9. It can be observed from the figure that, KME gives a lower CO emission than that of diesel, and dual fuel operations throughout the load spectrum. This is due to the presence of oxygen in KME, that gives a complete oxidation, and hence CO reduces. In dual fuel operation with the increase in compression ratio the CO emission decreases. This is due to the high temperature combustion of the fuel because of the increase in compression ratio. High compression ratio gives high temperature and at high temperature operation, the start of ignition of biogas improves, and decreases the ignition delay, and allows more time for oxidation of the charge, and the CO emission reduces. This reason is also evidenced from the research work documented by Bora and Saha [102] for the results they have obtained in a single cylinder DI diesel engine, modefied to operate on diesel-biogas dual fuel mode. A reduction in CO emission of 44% and 22% is observed for BUBDFM0.9/24.5/DEE6/18.5 in comparison with diesel and KME, at full load respectively.

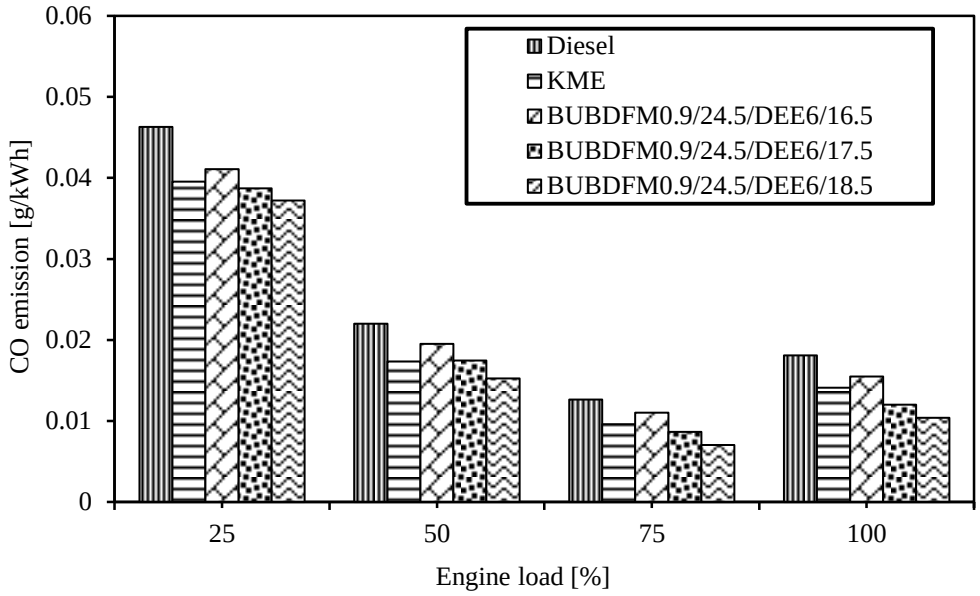

Figure 5.8.9 Variation of CO emission with load.

5.8.4.2 HC emission

The variation of HC emission with load is depicted in Figure 5.8.10.

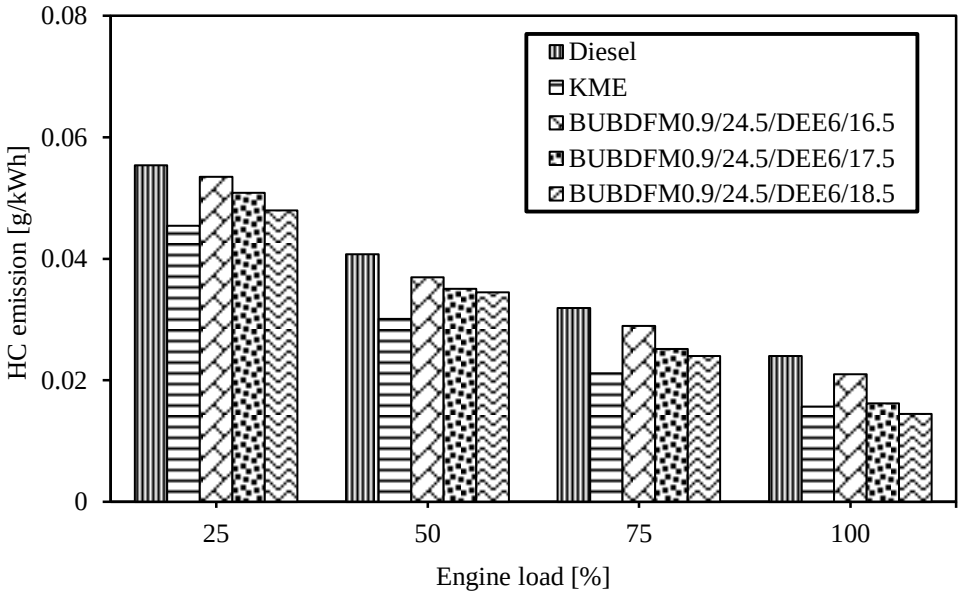

Figure 5.8.10 Variation of HC emission with load.

KME gives a lower HC emission than that of diesel and dual fuel operations, throughout the load spectrum. This is due to the existence of oxygen in the KME gives a complete combustion and HC emission reduces. In dual fuel operation, with the increase in compression ratio the HC

emission reduces. Because, high compression ratio results more growth of temperature during the compression stroke, which results in better combustion. This leads to a low emission of HC emission. This statement is in good agreement with Sayin and Gumus [261] for the reason they have reported for the results obtained in a biodiesel-diesel blended diesel engine operated with higher compression ratio. A reduction in HC emission of 42% is observed for BUBDFM0.9/24.5/DEE6/18.5, than that of diesel at full load.

5.8.4.3 NO emission

Figure 5.8.11 portrays the variation of NO emission with load. KME gives a higher NO emission than that of diesel and the dual fuel operations. This is due to the higher oxygen concentration in KME.

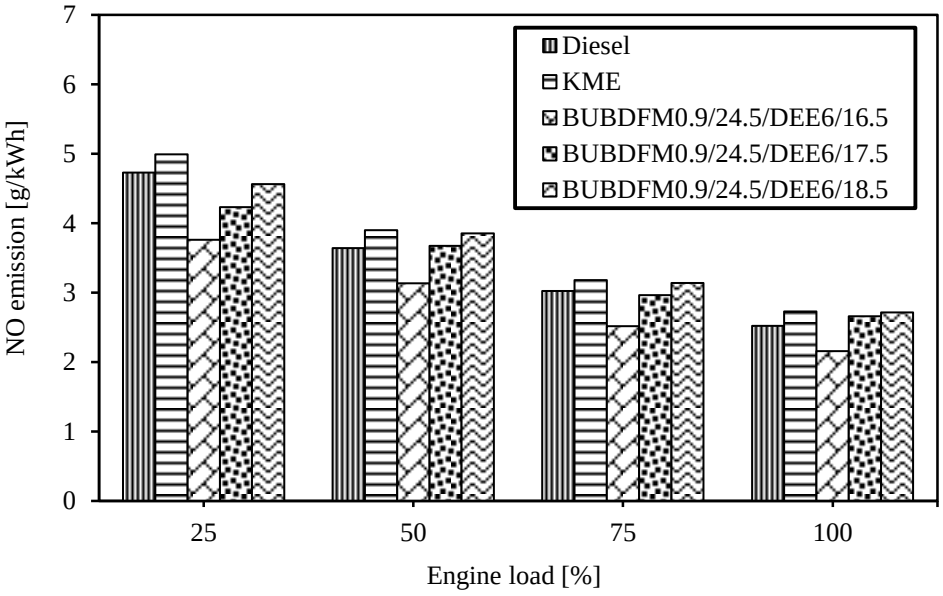

Figure 5.8.11 Variation of NO emission with load.

The concentration of NO emission in the dual fuel operation is considerably lower than that of KME throughout the load spectrum. This may be due to the drop in volumetric efficiency in the dual fuel operation, by the induction of biogas through the intake manifold. The dual fuel operation with the increase in compression ratio gives an increase in NO emission throughout the load spectrum. This is due to the increase in the combustion temperature due to the higher compression ratio, which gives a faster burning speed and a higher thermal NO. This is in good agreement with Bora and Saha [258] demonstrated in their investigation on a DI diesel engine operated with the biogas-biodiesel dual fuel mode. The NO emission for

BUBDFM0.9/24.5/DEE6/18.5 is about 7.6% higher than that diesel. But it is 1.2% lower than KME, at full load.

5.8.4.4 Smoke emission

The variation of smoke emission with the variation in load is depicted in Figure 5.8.12. It can be observed from the figure that, the smoke emission increases with the increase in load irrespective of the fuels used. This is due to the decrease in excess air ratio and increase in diesel consumption at relatively high loads, which gives a lower oxidation of soot particles. KME gives a lower smoke emission than that of diesel throughout the load spectrum. This is due to the lower stoichiometric air requirement for KME, because of available oxygen in it. The dual fuel operation with increase in compression ratio gives a gradual decrease in smoke emission throughout the load spectrum. This is because, as the compression ratio increases, the clearance volume decreases, which in turn increases the temperature and pressure of the charge during the end of the compression stroke. The increased combustion temperature results in better combustion of the fuel and the smoke emission decreases. This reason is also evidenced from the research work documented by Tangoz et al. [256] for the work they have carried out on a single cylinder DI diesel engine run CNG-diesel, and HCNG-diesel dual fuel mode with variation in compression ratio. BUBDFM0.9/24.5/DEE6/18.5 gives a reduction in smoke emission of 42.8% than that of diesel, at full load.

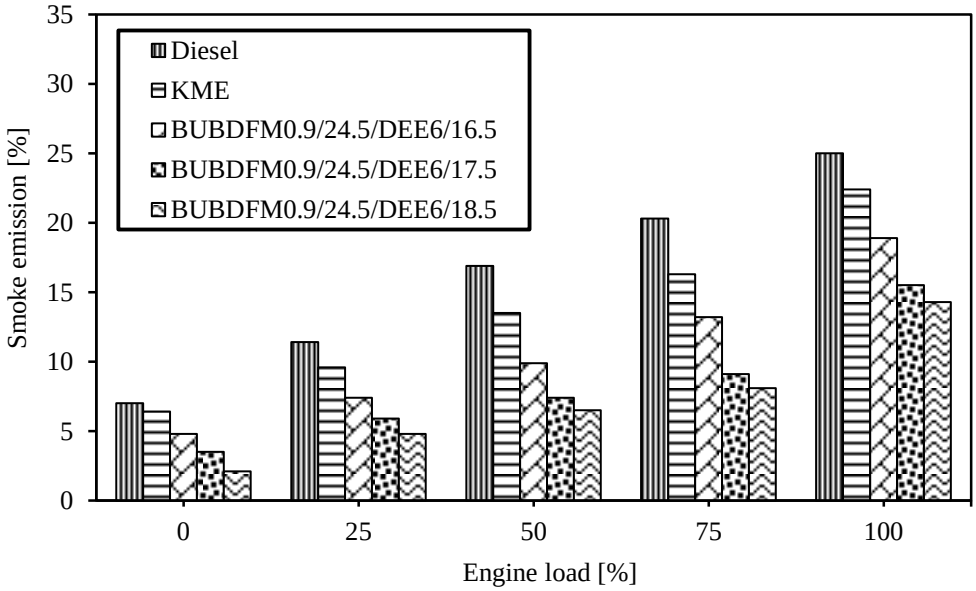

Figure 5.8.12 Variation of smoke emission with load.

5.8.5 Summary

The experimental results of the biodiesel dual fuel operation with the upgraded biogas, and 6% of DEE injection, with the variation in compression ratio were compared with those of the diesel and KME, and presented in this section. The summary of the results are as follows:

- BUBDFM0.9/24.5/DEE6/18.5 gives optimum results for the combustion, performance and emission characteristics of the engine, than those of other compression ratios.
- BUBDFM0.9/24.5/DEE6/18.5 gives an increase in BTE of about 7.1% than that of KME at full load. But the BTE is found to be 0.6% lower than that of diesel, at full load.
- The BSFC for BUBDFM0.9/24.5/DEE6/18 is found to be lower by about 2.2% than that of KME at full load, but it is 13.3% higher than that of diesel at full load.
- BUBDFM0.9/24.5/DEE6/18 gives a reduction in CO, HC and smoke emissions of 44%, 42% and 42.8% than that of diesel, at full load respectively.
- The NO emission for the BUBDFM0.9/24.5/DEE6/18.5 is 7.6% higher than that of diesel, but 1.2% lower than that of KME, at full load.

Table 5.8 provides the values of important parameters of the investigation obtained for the diesel, KME, and KME-upgraded biogas dual fuel operations, with different percentages of DEE injection, and different compression ratios, at full load.

Table 5.8 Summary of the values of the combustion, performance and emission parameters, for diesel, KME, and KME-upgraded biogas dual fuel operations, with different percentages of DEE injection, and different compression ratios, at full load.

Sl. No.	Parameters	Diesel	KME	BUBDFM0.9/24.5/ DEE6/16.5	BUBDFM0.9/24.5/ DEE6/17.5	BUBDFM0.9/24.5/ DEE6/18.5
A. Combustion parameters						
1	Maximum cylinder pressure, bar	75.7	71.3	76.34	81.0	84.05
2	Maximum heat release rate, J/^{o}CA	56.5	52.47	55.4	58.4	60.1
3	Ignition delay, ^{o}CA	11.5	10.5	10.48	9.0	7.82
4	Combustion duration, ^{o}CA	37.4	39.3	36.7	34.6	32.5
B. Performance parameters						
1	BSFC, kg/kWh	0.27	0.31	0.340	0.312	0.306
2	BTE, %	30.3	28	26.75	29.13	30.1
3	EGT, ^{o}C	331.8	355.8	330.2	350.8	380.75
C. Emission parameters						
1	CO, g/kWh	0.017	0.014	0.015	0.0120	0.010
2	HC, g/kWh	0.025	0.015	0.021	0.0162	0.014
3	NO, g/kWh	2.923	2.726	2.156	2.658	2.825
4	Smoke emission, %	25	22.4	18.9	15.5	14.3

5.9 Endurance test and lubrication oil analysis of the diesel engine fueled with BUBDFM0.9/24.5/DEE6/18.5

5.9.1 General

After carrying out necessary investigation and satisfactory results on the utilization of two different renewable fuels (biodiesel and biogas) in a CI engine, the engine was subjected to a short term endurance test.

This chapter discusses the endurance test analysis of a single cylinder, four stroke, DI diesel engine modified to operate on a dual fuel mode with simultaneous injection of Karanja biodiesel and DEE and upgraded biogas as an inducted fuel at a compression ratio of 18.5. The main objective of this endurance test was to evaluate the wear characteristics of the engine components, and changes in the lubrication oil properties, when the engine fueled with BUBDFM0.9/24.5/DEE6/18.5. The photographic views taken before and after the completion of 100 hrs of endurance test, and visual inspection of the engine components, wear and carbon deposits are discussed in this chapter. The lubrication oil samples were collected from the engine and subjected to atomic absorption spectroscopy (AAS) for the measurement of the various wear metal traces present in the engine oil due to the effect of friction and corrosion.

5.9.2 Carbon deposit on engine components

5.9.2.1 Cylinder head and piston crown

As described in Chapter 4, the engine was allowed to run for 100 h to observe the wear characteristics of the components, such as the cylinder head, piston crown and fuel injector tip. After running the engine with BUBDFM0.9/24.5/DEE6/18.5 very little black carbon deposits were clearly noticed in the combustion chamber, particularly on the cylinder head, the piston crown, and the injector tip. A comparison of the carbon deposits on the cylinder head and piston crown before and after the endurance test is depicted in Figure 5.9.1. A maximum of about 6 mg of carbon deposits were noticed in the cylinder head and combustion chamber. Carbon deposits are related to soot formation during combustion of fuel in the engine and fuel oxidation. Karanja biodiesel has a tendency to produce very low soot, which is consistent to the reduced PM emissions. Because the ester molecules contains dissolved oxygen. Also, methane is the main

constituent in upgraded biogas, which is the lower member in the paraffin family, and has a very low tendency to produce shoot.

(a) Piston crown (before)

(b) Piston crown (after)

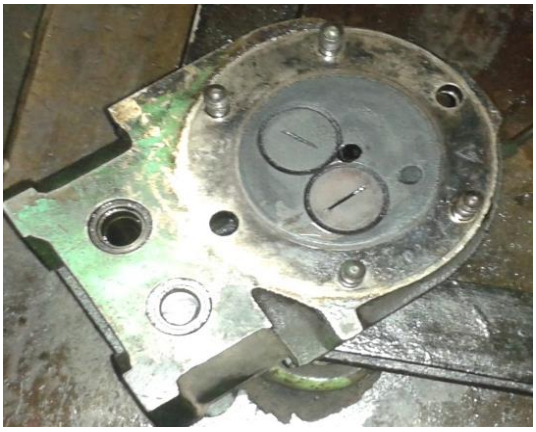

(c) Cylinder head (before)

(d) Cylinder head (after)

Figure 5.9.1 Comparison of carbon deposits before and after the endurance test on piston crown and cylinder head.

5.9.2.2 Fuel injector

The fuel injector components were dismantled after running the engine with the biodiesel-upgraded biogas dual fuel mode. Important parts like the needle and nozzle tip were visually inspected and analyzed. The photographic views of the fuel injector before and after the endurance test are shown in Figure 5.9.2. The carbon deposits were found in the injector nozzle and in between the holes. It was observed that the fuel spray of the nozzle observed to be

distorted. This was due to the blockage of the holes by small carbon deposits in the injector holes. The deposited carbon content was measured with the help of the weight balance and given in Table 5.9.

(a) Injector nozzle tip (before)

(b) Injector nozzle tip (after)

Figure 5.9.2 Comparison of carbon deposits before and after the endurance test on injector nozzle.

Table 5.9 Carbon deposit on cylinder head, piston crown and nozzle tip.

Component name	Weight
Deposit on cylinder head, mg	2.7
Deposit on piston crown, mg	3.3
Deposit on injector nozzle tip, mg	1.2

5.9.2.3 Fuel injection pump

Figure 5.9.3 show the photographic views of the dismantled fuel injection pump components, which were considered for the wear analysis. It can be observed from the figure that, with the biodiesel injection, a little wear is found in the fuel injection pump and its components after the endurance test. This lower percentage of wear in the pump may be due to the higher lubricity property of biodiesel. The wear in the fuel injection pump is considered as an important factor, because it may affect the ceiling between the plunger and the barrel, which may cause a pressure loss in the system and subsequently affect the fuel injection. The accessories of the fuel injection

pump were measured, before and after the endurance test. An electronic balance was used to measure the weigh the components. The weight differences are given in Table 5.9.

(a) Pump barrel

(b) Spring

(c) Plunger

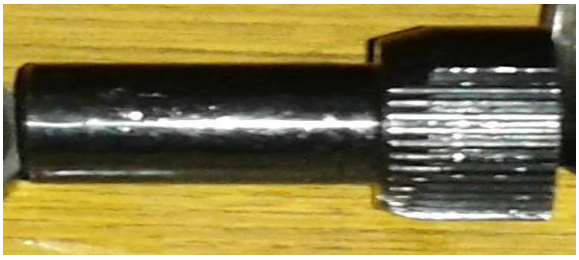

(d) Pinion

Figure 5.9.3 Photographic view of the dismantled fuel injection pump components.

Table 5.10 Amount of wear on different components of the fuel injection pump.

Component name	Component weight, g		Decrease in weight, %
	Before endurance test	After endurance test	
Pump barrel	304	302.5	0.49
Spring	210	208	0.95
Plunger	252	249	1.19
Pinion	180	175	2.77

5.9.3 Lubrication oil analysis

The use of a new alternative fuel in the diesel engine may affect the tribological properties of the lubricating oil, and is very important for assessing the suitability of new fuel for the existing engine. Hence, the various lubricating oil property analyses of the engine run with

BUBDFM0.9/24.5/DEE6/18.5 was carried out and the properties were compared with the diesel operation and presented.

5.9.3.1 Kinematic viscosity

Figure 5.9.4 portrays the variation of kinematic viscosity of lubricating oil with engine run time. Viscosity can be defined as the measurement of fluid internal resistance to flow at a particular temperature. Viscosity plays a major role in developing and maintaining a film thickness between the two moving surfaces (piston and cylinder). It can be observed from the figure that, BUBDFM0.9/24.5/DEE6/18.5 gives a higher reduction in kinematic viscosity than that of diesel, throughout the engine run time. This may be due to more fuel dilution and moisture content of Karanja biodiesel results in deterioration of kinematic viscosity of the lubricating oil [262]. Another possible reason for the decrease in kinematic viscosity of the lubricating oil may be due to the higher viscosity of the Karanja biodiesel, which increases the spray length of fuel spray in the engine combustion chamber, and leads to higher probability of fuel droplets hitting the liner walls, which in-turn increases the chances of mixing of fuel with the lubricating oil, resulting in increased fuel dilution [263].

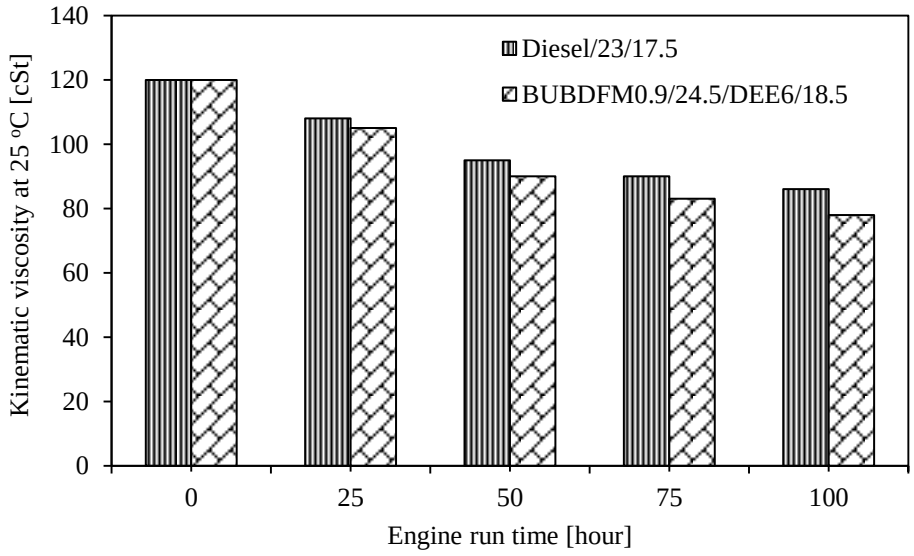

Figure 5.9.4 Variation of kinematic viscosity of lubricating oil with engine run time.

5.9.3.2 Flash point

Flash point is the lowest temperature at which a lubricant can vaporize to form an ignitable mixture with air. The flash point for a good lubricating oil should be always higher to reduce the

volatility [264]. The variation of flash point temperature of the lubricating oil with engine run time is depicted in Figure 5.9.5. It can be observed from the figure that, the flash point of the lubricating oil decreases with the increase in engine run time. After 100 h run the flash point of diesel was 207 ^{o}C, which was 2% higher than that of BUBDFM0.9/24.5/DEE6/18.5. The reduction in flash point for the BUBDFM0.9/24.5/DEE6/18.5 may be due to the presence of more moisture and free fatty acids content in Karanja biodiesel, which gives a higher percentage of dilution and increases the sump oil temperature and depress the flash point temperature.

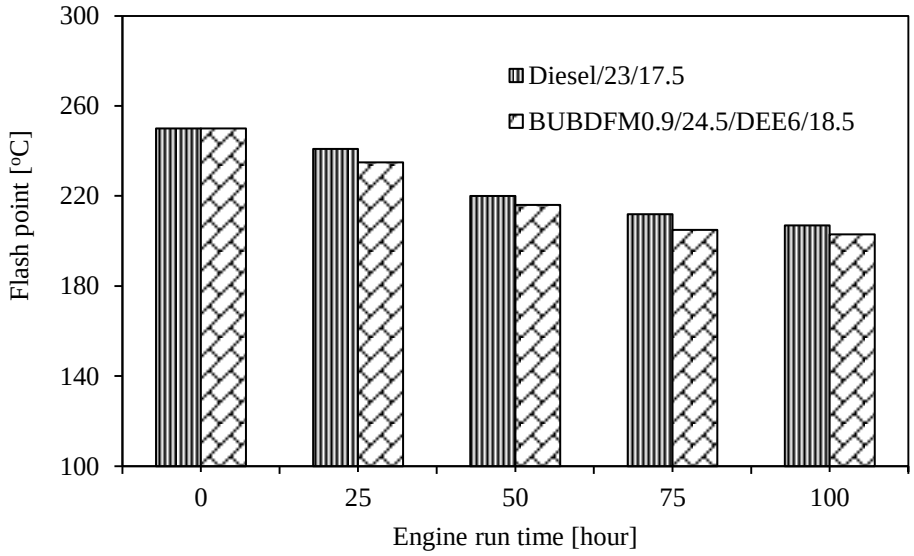

Figure 5.9.5 Variation of flash point temperature of the lubricating oil with engine run time.

5.9.3.3 Density

Figure 5.9.6 portrays the variation of lubricating oil density with the variation in engine run time. The density of the lubricating oil is basically affected by the addition of wear debris, addition of fuel and moisture [263]. It can be observed from the figure that, the density of the lubricating oil increases drastically during the initial engine run hour of 25 h and 50 h. This increase in density in the initial stage may be attributed to the higher wear of the engine components in the initial run hour due to frictional break-in. BUBDFM0.9/24.5/DEE6/18.5 gives a higher rate of increase in density of the lubricating oil than that of diesel throughout the test hour. This is because of the polymerization reaction of the lubricating oil by continuous heating and exposure to moisture, which increases the density. Also the lubricating oil density may also be increased by the sludge

formation in the oil, which is the mixture of oil, water, dust, dirt from different parts and carbon particles originates from the incomplete combustion of fuel [265].

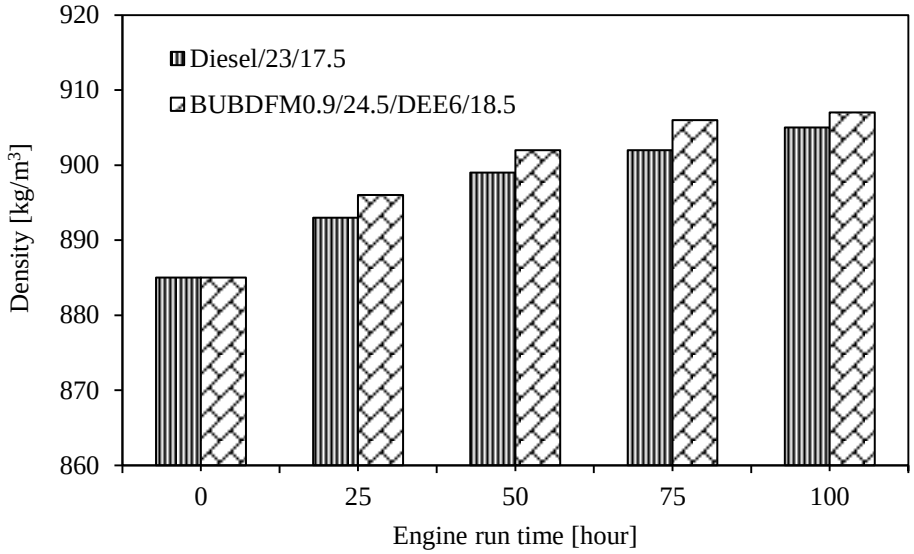

Figure 5.9.6 Variation of lubricating oil density with the variation in engine run time.

5.9.3.4 Moisture content

Figure 5.9.7 portrays the variation of moisture content in the lubricating oil with the variation in engine run time.

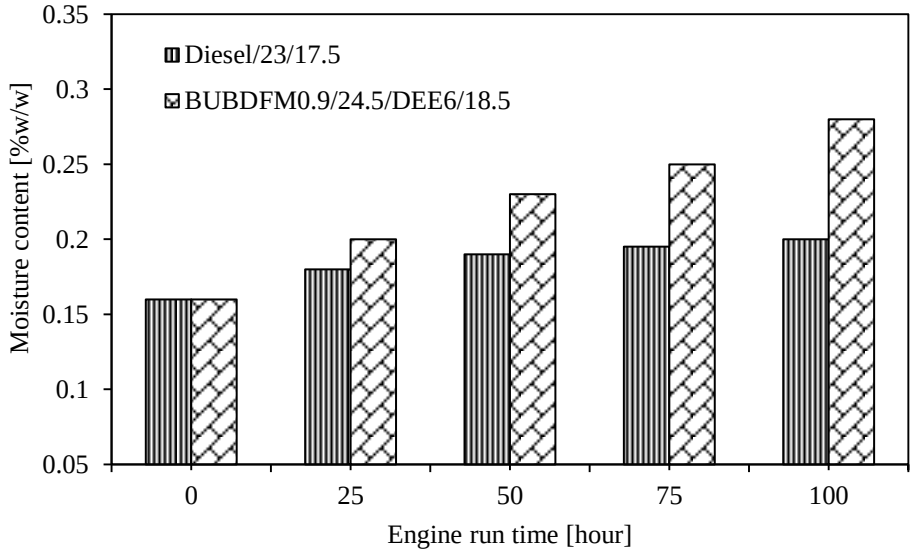

Figure 5.9.7 Variation of moisture content with the variation in engine run time.

Moisture content in the lubricating oil is a negative parameter which destroys the strength of the oil film. Moisture content in the oil will accelerate the oxidation reaction resulting in premature aging of oil. The moisture content in the lubricating oil oxidizes Fe^{2+} ion to Fe^{3+} ion and facilitates easy corrosion of the metallic components. Even a small trace of moisture in lubricating oil would increase the corrosion rate inside the engine. It can be observed from the figure that, the moisture content in the lubricating oil increases for both the fuels with respect to the increase in engine run time. This increase in moisture content of the lubricating oil is an indication of more fuel dilution and precipitation of additives [266]. BUBDFM0.9/24.5/DEE6/18.5 exhibits higher moisture content than that of diesel irrespective of the engine run time. This is due to the hygroscopic nature of Karanja biodiesel that leads to increase moisture percentage in the lubricating oil. High moisture content in the lubricating oil could destruct the sealing arrangement between piston rings-liner interfaces, and may lead compression leakage and over dilution [267].

5.9.3.5 Ash content

Ash content of lubricating oil is the percentage of mass of non-combustible residue that remains after the complete incineration of oil samples. Figure 5.9.8 portrays the variation of ash content of the lubricating oil with engine run time.

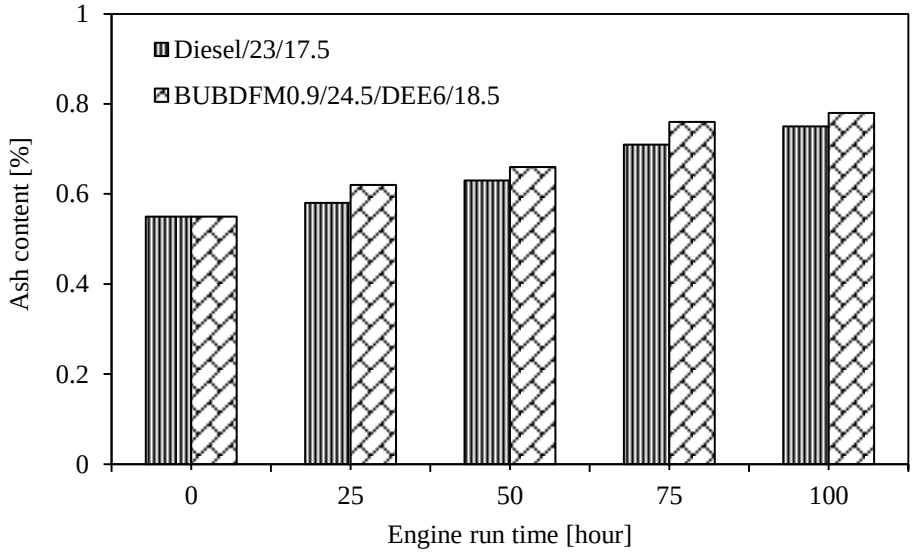

Figure 5.9.8 Variation of ash content of the lubricating oil with engine run time.

It can be observed from the figure that, the ash content for diesel and BUBDFM0.9/24.5/DEE6/18.5 increases gradually with the increase in engine run time. After

100 h run BUBDFM0.9/24.5/DEE6/18.5 gives 3.8% higher ash content than that of diesel. This is due to the higher polymerization of the lubricating oil because of the increasing content of non-combustible polymerized part of higher molecular weight based combustible product remains as carbon residue after combustion. Dhar and Agarwal [263] documented the similar results for the investigation of the tribological properties of Karanja biodiesel in a DI diesel engine.

5.9.3.6 Total base number

Total base number (TBN) is one of the neutralization number specifically used to measure the alkalinity reserve remaining in the lubricant. It is an indication of lubricant's ability to neutralize corrosive acids that formed during the engine operation [267]. Higher TBN value gives low concentration of free acids of lubricating oil. The variation of TBN with the variation in engine run hour is depicted in Figure 5.9.9.

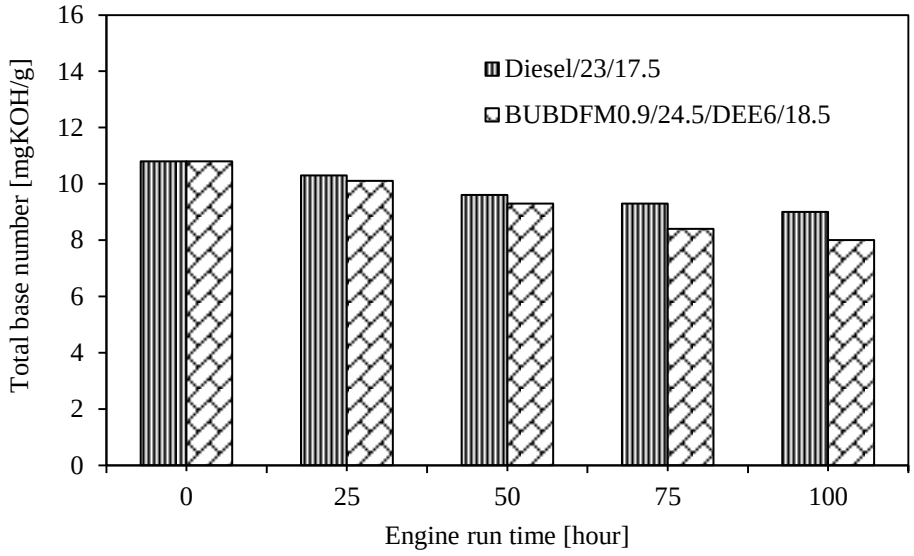

Figure 5.9.9 Variation of total base number with the variation in engine run time.

The TBN for the BUBDFM0.9/24.5/DEE6/18.5 is found to be lower than that of diesel throughout the endurance study. This is due to the higher formation of corrosive acids in case of Karanja biodiesel injection. It is also observed that the TBN for diesel and BUBDFM0.9/24.5/DEE6/18.5 is identical up to 50 h of run time. After 50 h the TBN for BUBDFM0.9/24.5/DEE6/18.5 decreases drastically at 75 h and 100 h. This may be due to relatively faster depletion of corrosion inhibitors (additives) in the lubricating oil, and possibly as a result of its interaction with Karanja biodiesel, which is chemically more active, compared to

that of diesel. Also the oxidation of diluted ester molecules of biodiesel in the lubricating oil encourages formation of organic acids, which reduce the reserve alkalinity of lubricating oil. This reason is well similar with the reason studied by Agarwal [268] in a biodiesel fueled CI engine.

5.9.4 Wear trace metals analysis

The determination of various wear metal elements in the lubricating oil samples were measured by atomic absorption spectroscopy (AAS). The spectrometer followed the ASTM 5185/13 test procedure. The possible wear elements like iron (Fe), copper (Cu), nickel (Ni), lead (Pb), aluminum (Al), chromium (Cr), zinc (Zn), and magnesium (Mg) were measured in the lubricating oil. Figure 5.9.10 Illustrates the variation of various wear trace metals in lubricating oil with engine run time.

5.9.4.1 Iron

Figure 5.9.10 (a) depicts the concentration of iron in the lubricating oil with the engine run time. The possible sources of iron element in diesel engine are the wear debris from piston, piston rings, cylinder head, valves, camshaft and crankshaft, cylinder block, valve guide, wrist pin, bearings and rust from the environment [263]. It is observed that, the concentration of iron is high for the BUBDFM0.9/24.5/DEE6/18.5 than that of diesel under all the operating conditions. This may be due to use of biogas as a fuel which reduces the lubricity, and results a higher frictional wear of the components. The concentration of iron for BUBDFM0.9/24.5/DEE6/18.5 in the lubricating oil after 100 h run time is 7.8% higher than that of diesel.

5.9.4.2 Copper

The concentration of copper in the lubricating oil is depicted in Figure 5.9.10 (b). Copper content in wear debris could originate from the injector shields, thrust washers, valve guides, connecting rod, piston rings and wear in bushings and bearings [262,263]. The copper concentration in the lubricating oil is higher for BUBDFM0.9/24.5/DEE6/18.5 than that of diesel. Mostly, wear in the piston and crank shaft may results in a larger concentration of copper. The use of biogas as a fuel provides a lower lubricity and hence the wear between the piston ring and cylinder increases. Also, the presence of abrasive and contamination in the oil causes excessive copper wear in the crank shaft.

5.9.4.3 Nickel

Figure 5.9.10 (c) depicts the concentration of nickel in the lubricating oil with the engine run time. Nickel added as an organometallic additive to the lubricating oil, in a very small quantity. The nickel concentration in the oil is both due to engine wear and the oil itself. The nickel is alloyed with iron for making high strength steel to increase the ductility of the material components and mostly used to make the cam, valve stem and valve guide. The wear of the piston, liners, bearings, valves, crank shafts and gear planting may give rise to nickel concentration in the lubricating oil. If the nickel concentration value is found to be higher than the expected value, then it may lead to rapid wear of the bearings.

5.9.4.4 Lead

The variation of the concentration of lead in the lubricating oil with the variation in engine run time is depicted in Figure 5.9.10 (d). Lead in the lubricating oil originates from wear of bearings, paints, grease, and fuel blow by, thrust bearings, bearing cages, bearing retainers, etc. [266]. The concentration of lead for BUBDFM0.9/24.5/DEE6/18.5 is 37% higher than that of diesel after 100 h of engine run time. This may be due to the reduced lubricity in the combustion chamber by the combustion of methane (about 90%) in the upgraded biogas.

5.9.4.5 Aluminum

The variation of the concentration of aluminum in the lubricating oil with time is depicted in Figure 5.9.10 (e). Aluminum in the lubricating oil originates from wear of piston, bearings, dirt, additives and thrust washers, push rods, oil pump, crank case oil paint etc. [266]. The concentration of aluminum in the lubricating oil is higher for BUBDFM0.9/24.5/DEE6/18.5 than that of diesel, irrespective of the engine time. The BUBDFM0.9/24.5/DEE6/18.5 gives a higher thermal stress on the piston and cylinder head. Also during the BUBDFM0.9/24.5/DEE6/18.5 operation, the cylinder peak pressure increases drastically, and allows more metal wear dissociation from piston. In a single cylinder CI engine the wear of aluminum is maximum from the wear of piston and bearings.

5.9.4.6 Chromium

The vitiation of the concentration of aluminum in the lubricating oil with time is depicted in Figure 5.9.10 (f). The components built for high pressure and temperature application like IC

engines are made up of special grade steel and alloys of aluminum, which contains chromium. The chromium increases the tensile and impact strength of the material [267]. Chromium in the lubricating oil could originate from the wear of cylinder liner, compression rings, gears, crankshaft and bearings. In BUBDFM0.9/24.5/DEE6/18.5 operation, the penalty of lubricity due to the induction of high methane fuel increases the wear, and results a higher degree of chromium in the lubricating oil. Also the presence of small percentage of H_2S (about 0.04%) in the upgraded biogas may lead to corrosion and give more chromium in lubricating oil.

5.9.4.7 Zinc

The variation of the concentration of zinc in the lubricating oil with time is depicted in Figure 5.9.10 (g). Zinc containing additive compound zinc di-alkyl-di-thio-phosphate (ZDDP) is added to the lubricating oil as multi-functional additives, which acts as antioxidant, anti-wear additive, detergent, and extreme pressure additive. Fresh lubricating oil contains a reasonable amount of zinc traces as an organo-metallic complex. The concentration of zinc in the BUBDFM0.9/24.5/DEE6/18.5 is found to be higher than that of diesel. This may be due to the additive depletion, wear of bearings due to low lubricity, and neoprene seals. Zinc in lubricating oil gives certain advantages over the engine components. It is an anti-wear additive, and also prevents the oxidation reaction of the lubricating oil. Of course, the zinc based additive is non-biodegradable, and aquatically toxic.

5.9.4.8 Magnesium

The vitiation of the concentration of magnesium in the lubricating oil with time is depicted in Figure 5.9.10 (h). Magnesium is added to the lubricating oil as detergent inhibitor additive. Magnesium in wear debris may originate from additive depletion, wear of cylinder liner surface, bearings, gear box housing etc. A small amount of magnesium is generally added to the lubricating oil for the reduction of component corrosion and wear. BUBDFM0.9/24.5/DEE6/18.5 gives a higher concentration of magnesium in the lubricating oil in comparison to the diesel throughout the engine run time. But, the change in magnesium concentration is quite high at 75 h and 100 h of engine run time. Magnesium in the lubricating oil gives advantage of clean and neutralizes the oil impurities which would normally cause deposits or oil sludge on the cam, cam shaft, valves and bearings. Also, it is an additive for corrosion and rust inhibitor. Magnesium in the lubricating oil retards the oxidation of metal and increases the engine durability.

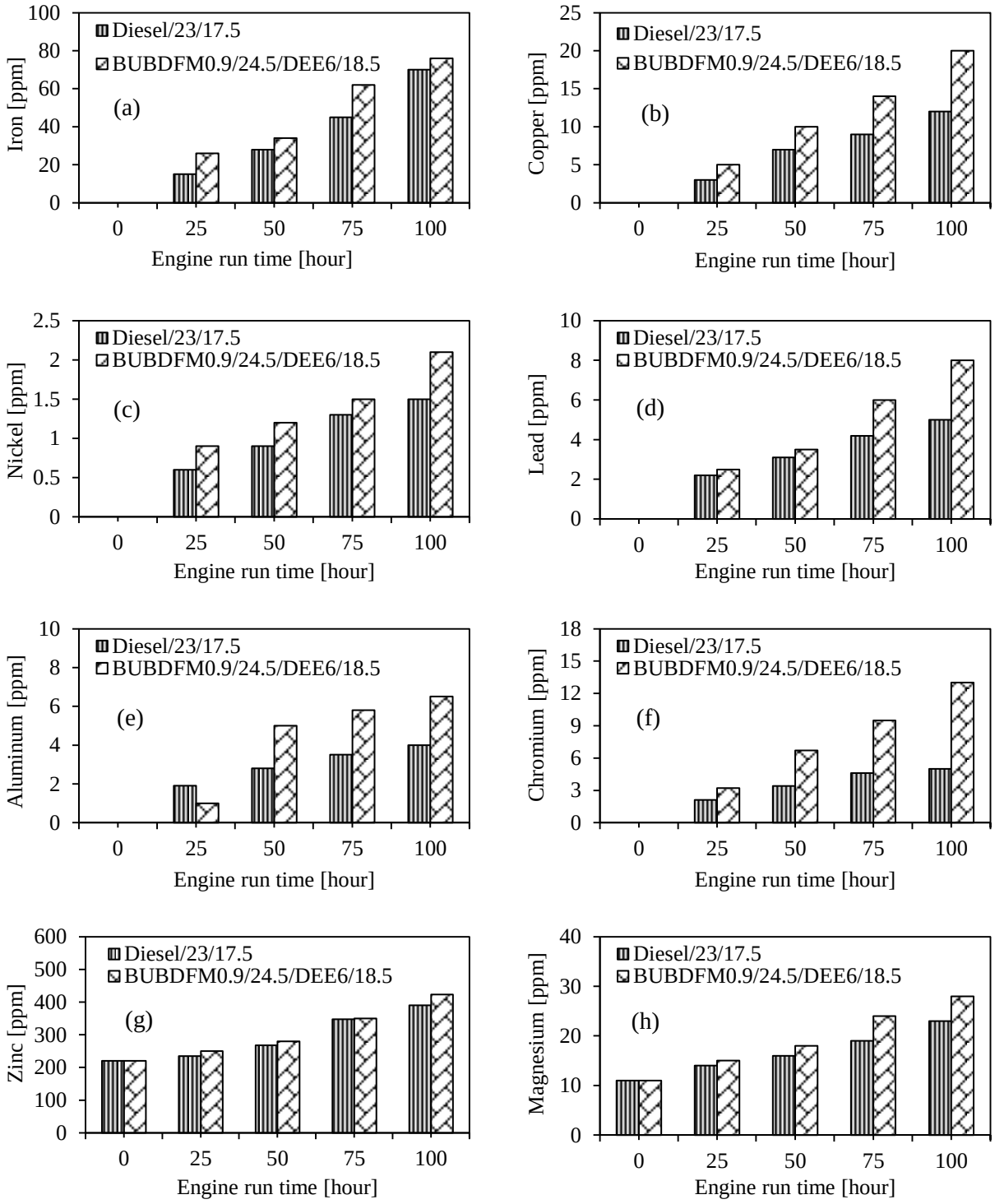

Figure 5.9.10 Variation of wear trace metals in lubricating oil with engine run time, (a) iron, (b) copper, (c) nickel, (d) lead, (e) aluminum, (f) chromium, (g) zinc, (h) magnesium.

5.9.5 Summary

After successfully running the engine with BUBDFM0.9/24.5/DEE6/18.5 for 100 h, a visual inspection was carried out for the wear analysis. The results of the visual inspection of carbon deposits on different engine components imply that there were traces of carbon deposits noticed in the cylinder head, piston crown, and injector nozzle tip of the engine fueled with the biodiesel-upgraded biogas dual fuel mode with minor engine and fuel modification. A marginal wear was also observed in the fuel injection pump. The lubricating oil properties were found to be deteriorated with the BUBDFM0.9/24.5/DEE6/18.5 operation. The concentrations of metals due to the wear of the engine components were observed to be high due to the lower lubricity offered by biogas during the dual fuel operation.

CHAPTER 6

CONCLUSIONS AND SCOPE FOR FURTHER RESEARCH

6.1 General

In this research work, biogas was produced from the co-digestion of Karanja seed cake a solid organic waste, obtained from biodiesel industries and cattle dung mixture in a large scale floating drum type digester. The generated biogas was further used as a fuel to run a single cylinder, four stroke, air cooled, DI diesel engine with a power of 4.4 kW at a constant speed of 1500 rpm, on dual fuel mode. Various fuel and engine modifications were carried out to run the diesel engine only on two different renewable fuels obtained from a single source (Karanja seed). The following conclusions can be drawn from each of the techniques employed in the investigation.

6.1.1 Validation of experimental results through mathematical model

- For the case of diesel, the simulated peak cylinder pressure is about 2.6% higher than that of the experimental result. But, for the case of KME, DBDFM0.9 and BBDFM0.9 the simulated peak cylinder pressure is about 1.5%, 1.9%, and 2.4% higher than that of the experimental result respectively.
- The deviation of ignition delay between the simulated and experimental results for the diesel operation is about 0.4 ^{o}CA, at full load. For the KME, DBDFM0.9, and BBDFM0.9 the deviation of ignition delay between simulation and experimental result is about 0.4 ^{o}CA, 0.3 ^{o}CA, and 0.2 ^{o}CA respectively, at full load.
- The deviation of NO emission between the simulation and experimental results is about 2.4%, 3.7%, 5.5%, and 5.4% for diesel, KME, DBDFM0.9 and BBDFM0.9 at full load.
- The deviation of smoke emission between the simulation and experimental results is about 1.4%, 2.2%, 2.9%, and 3% for diesel, KME, DBDFM0.9, and BBDFM0.9, at full load respectively.

6.1.2 Diesel-biogas dual fuel mode with different flow rates of biogas

The use of biogas with diesel in a CI engine seems to be desirable to reduce emissions, saving of conventional diesel and to utilize bioenergy from biomass.

- The diesel replacement of 0.263 kg/h was possible with DBDFM0.9 at full load.
- About 36% increase in the BSFC and 13.8% drop in BTE was noticed in the dual fuel operation of DBDFM0.9 in comparison with diesel, at full load.
- At full load, 23.3% and 30% increase in the CO and HC emissions were observed for DBDFM0.9, in comparison with diesel.
- A simultaneous reduction of 28% and 33% in NO and smoke emissions were observed for DBDFM0.9 in comparison with diesel, at full load respectively.

6.1.3 Diesel-biogas dual fuel mode with optimum biogas flow rate and different injection timings of pilot fuel

- The dual fuel operation of DBDFM0.9/26.0 gave an optimum result in terms of the combustion, performance and emission than those of other injection timings.
- The BSFC for DBDFM0.9/26.0 was found to be higher by about 25% than that of diesel operation, at full load.
- At full load, DBDFM0.9/26.0 gave a maximum BTE of 28.1%, which was higher than that of other injection timings.
- In the dual fuel operation, on advancing the pilot fuel injection to 3 ^{o}CA over that of normal injection timing, the BTE increased by about 4.7%, at full load.
- DBDFM0.9/26.0 gave lower BSCO and BSHC emissions of about 19% and 23%, than that of DBDFM0.9/23.0 but, the BSCO and BSHC emissions were higher by about 2% and 10% respectively, than that of diesel, at full load.
- The NO emission for DBDFM0.9/26.0 was higher by about 26% than that of DBDFM0.9/23.0 but, it was lower by about 3.8% than that of diesel, at full load.
- DBDFM0.9/26.0 gave a lower smoke emission of about 39% than that of diesel, at full load.

6.1.4 Biodiesel-biogas dual fuel mode with different flow rates of biogas

- In dual fuel operation BBDFM0.9 gave the optimum results, in terms of the performance, combustion and emission, than that of other flow rates, tested in this study.
- The BSFC for BBDFM0.9 was found to be higher by about 29% than that of KME at full load.
- BBDFM0.9 gave a drop in BTE of about 2.4% than that of KME at full load.

- The CO and HC emissions were found to be higher by about 28.5% and 37% for BBDFM0.9 in comparison with KME at full load.
- The NO and smoke emissions at full load were found to be lower by about 26% and 12.5% respectively, for BBDFM0.9, in comparison with KME.

6.1.5 Biodiesel-biogas dual fuel mode with optimum flow of biogas at different injection timings

- BBDFM0.9/24.5 gave an optimum result for the combustion, performance and emission characteristics, than those of other injection timing cases. The BSFC for BBDFM0.9/24.5 was found to be higher by about 23.9% than that of KME, but it is 5.1% lower than that of BBDFM0.9/23.0, at full load.
- About 6.6% increase in BTE was observed for BBDFM0.9/24.5 in comparison with the BBDFM0.9/23.0, at full load.
- BBDFM0.9/24.5 gave a reduction in CO, HC and smoke emissions of 17.1%, 18.2%, and 2.1%, in comparison with BBDFM0.9/23.0, at full load, respectively.
- The NO emission for BBDFM0.9/24.5 was marginally higher by about 5.5% than that of BBDFM0.9/23.0, at full load.

6.1.6 Biodiesel-biogas optimum flow rate + optimum injection timing + DEE injection

- BBDFM0.9/24.5/DEE4 gave the optimum results for the combustion, performance and emission characteristics of the engine, than those of other DEE injection quantities.
- BBDFM0.9/24.5/DEE4 gave an increase in BTE of 2.3% than that of BBDFM0.9/24.5 at full load.
- The BSFC for BBDFM0.924.5/DEE4 was found to be lower by about 5.8% than that of BBDFM0.9/24.5 at full load operation.
- BBDFM0.9/24.5/DEE4 gave a reduction in CO, HC and smoke emissions of 12.2%, 10.6% and 5.7% than that of BBDFM0.9/24.5, respectively at full load.
- The NO emission for the BBDFM0.9/24.5/DEE4 operation was 12.7% higher than that of BBDFM0.9/24.5, at full load. But it was found to be 10.9% lower than that of KME at full load.

6.1.7 Biodiesel-upgraded biogas optimum flow rate + optimum injection timing + DEE injection

- BUBDFM0.9/24.5/DEE6 gave optimum results for the combustion, performance and emission characteristics of the engine, than those of other dual fuel operations.
- BUBDFM0.9/24.5/DEE6 gave an increase in BTE of about 4.1%, and 5.8% than that of BBDFM0.9/24.5/DEE4, and BBDFM0.9/24.5/DEE6 at full load respectively.
- The BSFC for BUBDFM0.9/24.5/DEE6 was found to be lower by about 16.9%, and 21.1% than that of BBDFM0.9/24.5/DEE4, and BBDFM0.9/24.5/DEE6 at full load respectively.
- BUBDFM0.9/24.5/DEE6 gave a reduction in CO, HC and smoke emissions of 8.3%, 12.5% and 16.7% than that of BBDFM0.9/24.5/DEE4, at full load respectively.
- The NO emission for BUBDFM0.9/24.5/DEE6 is 4.9% higher than that of diesel at full load.

6.1.8 Biodiesel-upgraded biogas optimum flow rate + optimum injection timing + optimum DEE injection + compression ratio

- BUBDFM0.9/24.5/DEE6/18.5 gave optimum results for the combustion, performance and emission characteristics of the engine, than those of other compression ratios.
- BUBDFM0.9/24.5/DEE6/18.5 gave an increase in BTE of about 7.1% than that of KME at full load. But the BTE is found to be 0.6% lower than that of diesel, at full load.
- The BSFC for BUBDFM0.9/24.5/DEE6/18 was found to be lower by about 2.2% than that of KME at full load, but it was 13.3% higher than that of diesel at full load.
- BUBDFM0.9/24.5/DEE6/18 gave a reduction in CO, HC and smoke emissions of 44%, 42% and 42.8% than that of diesel, at full load respectively.
- The NO emission for the BUBDFM0.9/24.5/DEE6/18.5 was 7.6% higher than that of diesel, but 1.2% lower than that of KME, at full load.

6.1.9 Endurance test and lubrication oil analysis of the diesel engine fueled with BUBDFM0.9/24.5/DEE6/18.5

After successfully running of the engine with BUBDFM0.9/24.5/DEE6/18.5 for 100 h, a visual inspection was carried out for the wear analysis. The results of the visual inspection of carbon deposits on different engine components were carried out as follows;

- Traces of carbon deposits were noticed in the cylinder head, piston crown, and injector nozzle tip in the engine fueled with BUBDFM0.9/24.5/DEE6/18.5 in dual fuel mode.
- A marginal wear was also observed in the fuel injection pump.
- The lubricating oil properties were found to be deteriorated with BUBDFM0.9/24.5/DEE6/18.5 dual fuel mode in comparison to diesel.
- The concentrations of metals due to the wear of the engine components were observed to be high due to the lower lubricity offered by biogas during the dual fuel operation.

The adoption of this KME-biogas dual fuel technology will boost the proportion of the farms' renewable energy usage and can reduce the KME production cost. It is also a promising technique for on farm electricity generation. This biogas dual fuel engine, not only consumes a wide range of gaseous fuel resources effectively, but also has the potential to avoid much of the current and future problems facing diesel engines including a very significant reduction in its exhaust emission tradeoffs.

6.2 Scope for future work

The following points are suggested for future work, for the use of biogas in diesel engines on dual fuel mode:

- An improvement for the compression and storage stability of biogas can be carried out for its off-site application for heat and power generation.
- The performance of the biogas scrubber needs to be deeply analyzed to increase its efficiency.
- The regeneration stability of the solvent used in the scrubber need to be analyzed for reuse and recycle.
- CFD models can be used to predict the temperature distribution in the combustion chamber and flame propagation dynamics for indepth analysis of dual fuel combustion reaction.
- An improvement in the lubricity property of the engine oil for the biogas operated engine needs to be carried out for its long term use.

ANNEXURES

Annexure I

Test engine specification

Make/model	Kirloskar TAF 1
Engine type	Single cylinder, four strokes, CI, naturally aspirated
Injection type	Direct
Brake power, kW	4.4
Rated speed, rpm	1500
Cooling system	Air cooled with radial fan
Displacement volume, cm^3	662
Stroke, cm	11
Bore, cm	8.75
Combustion chamber shape	Hemispherical
TDC clearance, mm	1.1-1.2
Injection nozzle hole	3-hole
Injector nozzle hole diameter, mm	0.25
Nozzle opening pressure, bar	200
Injection timing, ^oCA bTDC	23
Compression ratio	17.5
Inlet valve open, ^oCA bTDC	4.5
Inlet valve close, ^oCA aBDC	35.5
Exhaust valve open, ^oCA bBDC	35.5
Exhaust valve close, ^oCA aTDC	4.5
Weight, kg	163
Type of fuel injection	Pump-line-nozzle injection system
Connecting rod length, mm	220

Annexure II

Specifications of the AVL 444 exhaust gas analyzer

Exhaust gas analyzer model	AVL 444DiGas
Dimension (W × D × H), mm^3	270 × 320 × 85
Weight, kg	4.5 (net weight without accessories)
Interfaces	RS 232 C, pick up, oil temperature probe
Power consumption and voltage supply, W and V-DC	25, 11-22
Response time, s	$t_{95} \leq 15$
Operating temperature, °C	5-45
Relative humidity, %	≤95, non-condensing
Connector CAL. Gas, l/h	60-140, max. overpressure 450 hPa
Connector Gas in, l/h	180, max. overpressure 450 hPa
Storage temperature, °C	0-50

Annexure III

Specification of the AVL 437C diesel smoke meter

Instrument model and company	AVL 437C smoke meter
Dimension (W × D × H), mm^3	600 × 260× 370
Weight, kg	24
Measuring range, % opacity	0-100
Accuracy and repeatability, % of full scale	±1
Resolution, %	0.1
Application	For free-acceleration test only
Linearity check, % or m^{-1}	48.4-53.1 or 1.54-1.76 of measurement range
Smoke inlet	Through a control valve
Smoke temperature at entrance, °C	250 (maximum)
Measuring chamber length and heating, mm	430±5 and thermostatically controlled
Light source (Halogen lamp), V and W	12 and 5
Sensor	Selenium photocell (diameter 45 mm)
Power supply, V-AC or V-DC, Hz, A	190-240 or 11.5-36, 50-60, 2.5
Ambient temperature, °C	0-50
Ambient humidity, % at 50 °C	90% (non-condensing)

Annexure IV

Specification of the Kistler piezo quartz pressure sensor

Make and model	Kistler and 5395A Piezotron® Quartz pressure sensor
Pressure range, bar	0-100
Type	Piezoelectric
Material	Quartz
Sensitivity, mV/bar	25
Cooling	Air cooled
Supply voltage, V DC	7-32
Supply current, mA	6
Output impedance, Ω	100
Operating temperature range, °C	-50-350

Annexure V

Range, accuracy, and uncertainty of the instruments used

Instruments used	Parameter measured with units	Range	Accuracy	Uncertainty, %
Load cell	Engine load, Watt	250-6000	±10	±0.2
Thermocouple	Temperature, ^{o}C	0-900	±1	±0.15
Burette	Fuel consumption, cm^3	1-30	±0.2	±0.5
Air flow meter	Air consumption, m^3/min	0.5-50	±0.1	±0.5
Biogas flow meter	Biogas consumption, m^3/min	0.1-25	±0.1	±0.02
Speed sensor	Engine speed, rpm	0-10,000	±10	±1
Charge amplifier	Amplifies input voltage, Volt	-	±1 %	±0.1
Pressure transducer	In-cylinder pressure, bar	0-110	±0.1	±0.15
Crank angle encoder	Crank position, ^{o}CA	0-720	±0.6	±0.01
Data acquisition system	Converts signal to digital values, bit	16	±0.1	±0.001
Smoke meter	Smoke opacity, %	0-100	±1	±1
Exhaust gas analyzer	Exhaust emission NO, ppm HC, ppm CO, % vol.	NO: 0-5,000	< 500 ppm vol: ± 50 ppm vol. ≥ 500 ppm vol: ± 10% of initial value.	±1
		HC: 0-20,000	< 200 ppm vol: ± 10 ppm vol. ≥ 200 ppm vol: ± 5% of initial value.	±0.5
		CO: 0-10	< 0.6% vol: ±0.03% vol. ≥ 0.6% vol: ± 5% of initial value.	±0.03
Overall uncertainty		-	-	±2.201

Annexure VI

Algorithm to operate DEE electronic injector

```
/*
  Program to control the amount of fuel injected into the air inlet.

 It uses a switch statement to interact with the computer through serial communication and
control the timing of injector relay.

The switch statement allows one to choose from among a set of discrete values of a variable.  It's
similar to a series of if statements.

  The circuit:
 * Input of a motor driver is attached to digital pin 3 of the microcontroller.

 Fuel motor pump is connected directly to the 12volt power supply.

 */
Int dutycycle =0;
Int dutycycle1 = 2;
Int dutycycle2 = 4;
Int dutycycle3 = 6;
void setup() {
  // initialize serial communication:
  Serial.begin(9600);
   // initialize the injector pin:
              pinMode(3, OUTPUT);
      }
}
void loop() {
  // read the sensor:
  if (Serial.available() > 0) {
    int inByte = Serial.read();
    // do something different depending on the character received.
    // The switch statement expects single number values for each case;
    // the controller to get the ASCII value for the character.  For
    // example 'a' = 97, 'b' = 98, and so forth:
    switch (inByte) {
    case 'a':
     dutycycle = dutycycle1;
      Serial.Println(" Duty cycle 2% initiated");
      break;
   case 'b':
      Serial.Println(" Duty cycle 4% initiated");
      dutycycle = dutycycle2;
      break;
    case 'c':
      Serial.Println(" Duty cycle 6% initiated");
      dutycycle = dutycycle3;
```

```
case 'd':
      Serial.Println(" Duty cycle 0% initiated");
      dutycycle = 0;
      break;
          default:
    }
      digitalWrite(3,HIGH);
      // Switch on the injector.
      delay(dutycycle);
      // give a suitable delay to keep the injector valve open for a
specified time period.
      digitalWrite(3,LOW);
      //turn off the injector valve.
      delay(100 - dutycycle);
      //adjust the time period of the wave
    Serial.Print(" Current Duty cycle:  ");
      Serial.Println(dutycycle);
      // give the feedback to the computer about the current dutycycle.

  }
}
```

Annexure VII

MATLAB Program for combustion and emission model

```
clear all
close all
clc
%Declaration of parameters
gamma = 1.35;               % gamma
gm = 0.35;                  % gamma - 1
Vcl = 0.0000401;            % clearance volume
D = 87.5e-3;                % cylinder bore diameter
a = 8;                      % connecting rod length (cm)
l = 2;                      % crank radius (cm)
aw = 3;                     % wiebe function constant
nw = 5;                     % wiebe function constant
Mf = 115;                   %
Ma = 103;                   %
Tw = 450;                   % temperature of cylinder wall (K)
R = 8.314;                  % universal gas constant
c = 3.4e-8;                 %
dmfb = 0.725986;            % at no load
lhc = 35.479e6;             % lower heat of combustion

ca=zeros(1,290); p=zeros(1,290); T=zeros(1,290); V=zeros(1,290);
E=zeros(1,290); dW=zeros(1,290); dQ=zeros(1,290); q=zeros(1,290);
k=zeros(1,290); ht=zeros(1,290); ddd=zeros(1,290);
tu=zeros(1,290); qq=zeros(1,290); bu=zeros(1,290); au=zeros(1,290);
bb=zeros(1,290); ab=zeros(1,290); Tb=zeros(1,290); bbmix=zeros(1,290);
Tbmix=zeros(1,290); wbmix=zeros(1,290); wb=zeros(1,290);
cau=zeros(123,290); W = zeros(1,290);

%IVC
ca(1) = -145;
p(1) = 1.85e5;
T(1) = 350;
V(1)=0.0000401+0.0003305*(1+4-cos(ca(1)*0.017453)-sqrt(16-
(sin(ca(1)*0.017444))^2));
injmf = 4.9e-5;
mfj = injmf/12;
Watot = (p(1)*V(1))/(R*T(1));       % ideal gas equation
afr = Watot/injmf;
maj = afr/mfj;
Wftot = Watot/afr;                  % global AFR=Watot/Wftot
E(1) = ienergy(T(1))*1000;          % calcualte E1

for i=1:123

        ca(i+1) = ca(i) + 1;
        V(i+1)=0.0000401+0.0003305*(1+4-cos(ca(i+1)*0.017453)-sqrt(16-
(sin(ca(i+1)*0.017444))^2));
        T(i+1)=T(i)*(V(i)/V(i+1))^gm;           % isentropic process
        b(i) = Watot;

        for it = 1:5
```

```
            p(i+1) = (V(i)*T(i+1)*p(i))/(V(i+1)*T(i));

            for j = 1:50
               [fe fed dq]=enerbal(p(i),p(i+1),T(i),T(i+1),V(i),V(i+1));
               tu(j+1)=tu(j+1) - fe/fed;        % newton raphson method
               ddd(j+1)=dq;
               ht(j+1)=-ddd(j+1);
            end

        end
        tu(j)=T(i);
end

%start of combustion
cau(123) = ca(123);
Tu(123) = T(123);
Tb(123) = T(123);
Vu(123) = V(123);
Vb(123) = 0;
bu(123) = b(123);
bb(123) = 0;

for ii=123:289

     qq(ii+1)=combsm2(ca(ii+1));
     q=qq(ii+1);
     ca(ii+1)=ca(ii)+1;
     cau(ii+1)=cau(ii+1);
     V(ii+1)=0.0000401+0.0003305*(1+4-cos(ca(ii+1)*0.017453)-sqrt(16-
sin(ca(ii+1)*0.017453)*sin(ca(ii+1)*0.017453)));
     T(ii+1)=T(ii)*(V(ii)/V(ii+1))^gm;           % gm=1.31

     W(ii) = 1 - exp(-3*(((ca(ii) - (-30))/71)^5));

     Tu(ii+1)=Tu(ii)*(V(ii)/V(ii+1))^gm;
     p(ii+1)=(p(ii)*V(ii)*T(ii+1))/(T(ii)*V(ii+1));

     bu(ii+1)= Watot - maj/Ma;
     wloss = bu(ii) - bu(ii+1);
     au(ii) = bu(ii);
     if ii<=136
        if ii==5
            au(ii) = bu(ii) - 0.21*wloss;
        elseif ii==6
            au(ii) = bu(ii) - 0.79*wloss;

        end

     Vu(ii+1) = (bu(ii+1)*R*Tu(ii+1))/p(ii+1);

     for j =1:50
        [fe fed]=enerbal2(p(ii),p(ii+1),T(ii),T(ii+1),Vu(ii),Vu(ii+1),q);
        if fed<eps
           T(ii+1)=T(ii);
        else
           T(ii+1)=T(ii+1)-fe/fed;   %newton raphson method
        end
```

```
     end
     end
      %burning zone
     bb(ii+1) = Watot + maj/Mf;
     wgmin = bb(ii+1) - bu(ii);

        if ii==5
            bbmix(ii) = bb(ii) + 0.21*wgmin;
        elseif ii==6
            bbmix(ii) = bb(ii) + 0.79*wgmin;
        elseif ii==7
            bbmix(ii) = bb(ii) + (mfb/Mf);
        else
            bbmix(ii) = bb(ii);
        end

     Tbmix(ii) = (bb(ii)*Tb(ii) + wgmin*Tu(ii))/(bb(ii) + wgmin);

     Tb(ii+1) = Tbmix(ii)*((p(ii+1)/p(ii))^(gm/gamma)) -
(dmfb*lhc*gm)/(bbmix(ii)*R);
     Vb(ii+1) = (wb(ii)*R*Tb(ii+1))/p(ii+1);

     for j = 1:50
           [fe fed dq]=enerbal(p(i),p(i+1),T(i),T(i+1),V(i),V(i+1));
           tu(j+1)=tu(j+1) - fe/fed;     %newton raphson method
           ddd(j+1)=dq;
           ht(j+1)=-ddd(j+1);
     end
     for j=1:50
        [fe fed dq]=enerbal2(p(ii),p(ii+1),T(ii),T(ii+1),V(ii),V(ii+1),q);
        T(ii+1)=T(ii+1)-fe/fed;          %newton raphson method
     end

     ddd(ii+1)=dq;
     ht(ii+1)=qq(ii+1)+ddd(ii+1);
end
%Fuel Injection alock

z=3; %numaer of nozzles
Mftot =1.18*2.8e-3/170;%input for total fuel input in the engine for 3
nozzles.
Matot = 14.2*Mftot/3; %mass of air
Mftot1= Mftot/z; %input for fuel injection per nozzle
Minjp =[0.1485136,  2.279569,  3.036051,3.42156,  3.741282, 3.908897,
12.11944,  25.21904,  38.43114,  51.38495,  62.85519,  72.4708, 80.32899,
86.64405, 91.58, 95.39, 98.39,  100 ];
N = 1500; %RPM
%value needs to be edited. Fuel injected in 24.5 CA
Dn= 0.25*10^-3;
densityL=809;
Uinja=zeros(20);
Pinj= zeros(20);
Utot=0;
for i=2:18
    Uinja(i) = ((Minjp(i)-Minjp(i-
1))*Mftot1*6*N/100)/((pi*Dn*Dn/4)*densityL);
    Utot=Utot + Uinja(i);
```

```
    Pinj(i)=power(Uinja(i)/.39,2)*densityL/2;
end

Uavg = Utot/18;
CA= zeros(400);
t=zeros(400);
p=zeros(400);
v=zeros(400);
  %defining initial temperature pressure and volume
rc=18.5; %compression ratio
R= 3.5;
Vc= 3.7*(10^-5);
CA(1)=-180;
t(1)=350;
p(1)=1.655e5;
v(1)=Vc*(1 + .5*(rc-1)*(R+1 - cos(3.14*CA(1)/180) - sqrt(R*R-
sin(3.14*CA(1)/180)*sin(3.14*CA(1)/180))));
densityA = 1.618;
E = zeros(400);
E(1) = Matot*1000*(.3 * ienergy(t(1), .446, .3098, -.123, .227, -.1552, -
.489) + .78*ienergy(t(1), .289, .1515, -.57235, .99807, -.6522, -.90586 ) +
.21*ienergy(t(1), .362, .736, -.196, .362, -.289, -.120));
%fuel break up time
Tbr = 28.61*densityL*Dn/sqrt(200*10^5*densityA);

%fuel spray angle
Ac=4.9;
theta = 2*atan((4*pi*sqrt(densityA/densityL)*sqrt(3))/(Ac*6));
gamma=1.35;
W=zeros(400);
E1=zeros(400);
hr=zeros(400); %heat release
for i=2: 157
    %Compression starts after suction
    CA(i)=CA(i-1)+1;
    v(i)=Vc*(1+.5*(rc-1)*(R+1 - cos(3.14*CA(i)/180) - sqrt(R*R-
sin(3.14*CA(i)/180)*sin(3.14*CA(i )/180))));
    c=power(v(i-1)/v(i),.35);
    t(i)= t(i-1)*c;
    p(i)=p(i-1)*(v(i-1)/v(i))*(t(i)/t(i-1));

   for j=1:10 %newton raphson method needs correction correct values not
shown.
    E(i) = Matot*1000*(.3 * ienergy(t(i), .446, .3098, -.123, .227, -.1552, -
.489) + .78*ienergy(t(i), .289, .1515, -.57235, .99807, -.6522, -.90586 ) +
.21*ienergy(t(i), .362, .736, -.196, .362, -.289, -.120));

    W(i)= 0.5*(p(i)+p(i-1))*(v(i)-v(i-1));
    Q=heatL(t(i));
    f= E(i)-E(i-1) + W(i) -Q;
    Q1=heatL1(t(i));
    E1(i) = Matot*1000*(.3 * ienergy1(t(i), .446, .3098, -.123, .227, -.1552)
+ .78*ienergy1(t(i), .289, .1515, -.57235, .99807, -.6522 ) +
.21*ienergy1(t(i), .362, .736, -.196, .362, -.289));
    E1(i-1) = Matot*1000*(.3 * ienergy1(t(i-1), .446, .3098, -.123, .227, -
.1552) + .78*ienergy1(t(i-1), .289, .1515, -.57235, .99807, -.6522 ) +
.21*ienergy1(t(i-1), .362, .736, -.196, .362, -.289));
```

```
    f1= E1(i)-E1(i-1) + W(i) - Q1;
    t(i)=t(i) - f/f1;
   end
    hr(i)=Q;
end

%Sauter Mean Diameter
vL=1.95*10^-2;
sig=0.02;
vA=20.76*10^-6;
Reinj = zeros(20);
Weinj=zeros(20);
Dsm1=zeros(20);
Dsm2=zeros(20);
Dsmm=zeros(20);
imax = 52;
jmax= 26;
jmid= 5;
Rmid =  zeros(20,20);
x= zeros(20,20,20);
y= zeros(20,20,20);
Umid = zeros(20,20);
thetaZ = zeros(20,20,20);
Uz = zeros(20,20,20);
Dsm = zeros(20,20,20);
Ndrop= zeros(20,20,20);
phi= zeros(20,20,20);
Maz= zeros(20,20,20);
thetaZS= zeros(20,20,20);
Rz=zeros(22,18,20);
Rzimp = zeros(20,20,20);
thetaZSimp=zeros(20,20,20);
thetaZROT = zeros(20,20,20);
xs=zeros(20,20);
ys=zeros(20,20);
cop=zeros(20,20);
sh=zeros(20);
rd=zeros(20);
vA=20.76*10^-6;
Mfz=zeros(20,20);
for k=2:18 %23 deg BTDC
for i=2:k

    %fuel development
     Reinj(k) = Uinja(k)*Dn/vL;
     Weinj(k) = Uinja(k)*Uinja(k)*Dn*densityL/sig;
     Dsm1(k) = 0.38*power(Reinj(k),0.25)*power(Weinj(i),-
.32)*power(vL/vA,0.37)*power(densityL/densityA,-.47)*Dn;%choose the maximum
of the 2 values
     Dsm2(k) = 0.38*power(Reinj(k),0.12)*power(Weinj(i),-
.75)*power(vL/vA,0.54)*power(densityL/densityA,.18)*Dn;

                    if(Dsm1(k)<Dsm2(k))
                        Dsmm(k)= Dsm2(k);
                    else
                        Dsmm(k) = Dsm1(k);
                    end
```

```
       Rmid(k,i)=sqrt(power(x(k,i,5),2)+ power(y(k,i,5),2));
       beta = .57;
       Umid(k,i) =
2.95*beta*power(Pinj(k)/densityA,0.25)*sqrt(Dn)/(power(i*1.11*(10^-4),1-
beta));%mid zone velocity
        Mfz(k) = (Minjp(i)-Minjp(i-1))*Mftot1/9;
                    for j=2:9

                        alpha=4.5*4.5;
                        thetaZ(k,i,j) = -(theta/2) + ((j-1)*theta/9) +
((theta)/(2*9));

                        Uz(k,i,j) = Umid(k,i)*(2.7^(-
alpha*thetaZ(k,i,j)*thetaZ(k,i,j)));

                        w=7.5; %assign w between 5-10
                        Dsm(k,i,j)= (1-1/w)*Dsmm(k)*(j-1)/(jmid-1);

                        Ndrop(k,i,j) =
Minjp(k)*Mftot1/((pi/6)*power(Dsm(k,i,j),3)*densityL);

                        Maz(k,i,j)= Minjp(k)*Mftot1*(Uinja(k) -
Uz(k,i,j)*cos(thetaZ(k,i,j)))/(Uz(k,i,j)*cos(thetaZ(k,i,j)));

                        %air equivalence ratio in each zone
                        phi(k,i,j) = (Minjp(k)*Mftot1/Maz(k,i,j))/(1/(14.2));

                        if(j<jmid)
                            thetaZS(k,i,j) = (thetaZ(k,i,j));
                        else if (j>jmid)
                            thetaZS(k,i,j)= thetaZ(k,i,j) +
thetaZS(k,i,jmid);
                        else
                            thetaZS(k,i,jmid)= 0.5*thetaZ(k,i,jmid) +
.5*thetaZS(k,i,jmid-1);

                            end
                        end


                        if(Rz(k-1,i,j)<40)

                                    x(k,i,j) = x(k-1,i,j) +
(Uz(k,i,j))*cos(thetaZS(k,i,j))/(6*N)*10^3;
                                    y(k,i,j) = y(k-1,i,j) +
(Uz(k,i,j)*sin(thetaZS(k,i,j)))/(6*N)*10^3;

                                    Rz(k,i,j) = sqrt(power(x(k,i,j),2)+
power(y(k,i,j),2));
                                    if (Rz(k,i,j)>40)

                                        x(k,i,j)=x(k-1,i,j);
                                        y(k,i,j) = y(k-1,i,j);
                                    end
```

```
                                RZimp = 46;
                                thetaZSimp= thetaZS(k,i,j);

                        end
                        if(Rz(k-1,i,j)>=40)
                                if (j<jmid)
                                thetaZROT(k,i,j) = thetaZROT(k,i,j) +
(Uz(k,i,j)*1000/(46*6*N));
                                end
                                if(j>=jmid)
                                thetaZROT(k,i,j) = thetaZROT(k,i,j) -
(Uz(k,i,j)*1000/(46*6*N));

                                end

                                thetaZS(k,i,j) = thetaZSimp +
thetaZROT(k,i,j);

                                x(k,i,j)=RZimp*cos(thetaZS(k,i,j));
                                if(j<jmid)
                                y(k,i,j) = -RZimp*sin(thetaZS(k,i,j));
                                end
                                if(j>=jmid)
                                y(k,i,j) = -RZimp*sin(thetaZS(k,i,j));
                                end

                        end
                        xs(i-1,j)= x(18,i,j);
                        ys(i-1,j)=y(18,i,j);
                        cop(19-i,j)=Uz(18,i,j);

                       %evaporation model
                       Ua(k,i,j) = (2*3.14*N/60)*Rz(k,i,j);
                       urel(k,i,j)=sqrt(Uz(k,i,j)^2 + Ua(k,i,j)^2);
                       Madrop= Maz(k,i,j)/Ndrop(k,i,j);
                       Re=Dsm(k,i,j)*Urel*vA;

                       Dfa = 8.1*(10^-
6)*power(t(157+k)/399),1.5)/(p(157+k)/101325);
                       Sc=vA,/Dfa;%database required
                       Sh=2 + .6*(Re^.5)*(Sc^.333);
                       Y= densityFV/densityA;
                       Ys = Mftot1/(Mftot1 + Matot*(p(157+k)/pv)-1);
                       B=(Ys-Y)/(1-Ys);
                       rd(k,i,j)= rd(k-1,i,j)-
((densityA/densityL)*(Dfa/Dsm)*Sh*log(1+B)*2.303;

                       Mev(i,j)=Mfz(i)*2*rd(18,i,j)/Dsm(18,i,j);
                       phiE(i,j) = (Mev(i,j)/Maz(18,i,j))/(i/14.2);

                       %ignition delay
                       I(k,i,j) = I(k-1,i,j)+ 1/(Kpr*power(p(k+157),-
.757)*exp(618840/(CN+25)*8.314*T(k+257)));
                       %enter CN and Kpr
                   end

end
```

```
end

T2u = T2;
T2k= T2;
V2u= v(157);
V2k=v(157);
bn1 = 6.1*10^-3);%CO
bn2 =5.7*(10^-1);%CO2
bn3 = 9.7*(10^-5);%H
bn4 = 1.5*(10^-4); %H2
bn5 = 1.0*(10^-1);%H2O
bn6 = 1*(10^-5);%N
bn7=5*(10^-6);%NO
bn8= 1.5*(10^-2);%NO
bn9 =6.9*(10^-1);%N2
bn10=8.6*(10^-1);%O
bn11 = 2.2*(10^-2);%OH
bn12 = 2.3*(10^-2);%O2
Tbulk1=0;
Tbulk2=0;
T1u=t(157);
T1k=t(157);
for i=157:360

    v(i)=Vc*(1+.5*(rc-1)*(R+1 - cos(3.14*CA(i)/180) - sqrt(R*R-
sin(3.14*CA(i)/180)*sin(3.14*CA(i )/180))));
    p(i)=p(i-1)*power(v(i-1)/v(i),1.35);


    Tbulk1= ((bn1 + bn2 +bn3 + bn4 +bn5 + bn6+bn7 + bn8 +bn9 + bn10 +bn11 +
bn12)*T1u +   (bn1k + bn2k +bn3k + bn4k +bn5k + bn6k+bn7k + bn8k +bn9k +
bn10k +bn11k + bn12k)*T1k)/((bn1 + bn2 +bn3 + bn4 +bn5 + bn6+bn7 + bn8 +bn9 +
bn10 +bn11 + bn12) + ((bn1k + bn2k +bn3k + bn4k +bn5k + bn6k+bn7k + bn8k
+bn9k + bn10k +bn11k + bn12k));
    Tbulk2=((an1 + an2 +an3 + an4 +an5 + an6+an7 + an8 +an9 + an10 +an11 +
an12)*T2u +   (an1k + an2k +an3k + an4k +an5k + an6k+an7k + an8k +an9k +
an10k +an11k + an12k)*T2k)/((an1 + an2 +an3 + an4 +an5 + an6+an7 + an8 +an9 +
an10 +an11 + an12) + ((an1k + an2k +an3k + an4k +an5k + an6k+an7k + an8k
+an9k + an10k +an11k + an12k));

    qu= heatLI((Tbulk1+Tbulk2)/2))*((bn1 + bn2 +bn3 + bn4 +bn5 + bn6 + bn7 +
bn8 +bn9 + bn10 +bn11 + bn12)*T1u + (an1 + an2 +an3 + an4 +an5 + an6+an7 +
an8 +an9 + an10 +an11 + an12)*T2u/((bn1 + bn2 +bn3 + bn4 +bn5 + bn6+bn7 + bn8
+bn9 + bn10 +bn11 + bn12)T1u + ((bn1k + bn2k +bn3k + bn4k +bn5k + bn6k+bn7k +
bn8k +bn9k + bn10k +bn11k + bn12k)*T1k + (an1 + an2 +an3 + an4 +an5 + an6+an7
+ an8 +an9 + an10 +an11 + an12)T12u + ((an1k + an2k +an3k + an4k +an5k +
an6k+an7k + an8k +an9k + an10k +an11k + an12k)*T2k);
    qk=heatLI((Tbulk1+Tbulk2)/2))*((bn1 + bn2 +bn3 + bn4 +bn5 + bn6 + bn7 +
bn8 +bn9 + bn10 +bn11 + bn12)*T1k + (an1 + an2 +an3 + an4 +an5 + an6+an7 +
an8 +an9 + an10 +an11 + an12)*T2k/((bn1 + bn2 +bn3 + bn4 +bn5 + bn6+bn7 + bn8
+bn9 + bn10 +bn11 + bn12)T1u + ((bn1k + bn2k +bn3k + bn4k +bn5k + bn6k+bn7k +
bn8k +bn9k + bn10k +bn11k + bn12k)*T1k + (an1 + an2 +an3 + an4 +an5 + an6+an7
+ an8 +an9 + an10 +an11 + an12)T12u + ((an1k + an2k +an3k + an4k +an5k +
an6k+an7k + an8k +an9k + an10k +an11k + an12k)*T2k);
    w1u=bn1 + bn2 +bn3 + bn4 +bn5 + bn6+bn7 + bn8 +bn9 + bn10 +bn11 + bn12;
    for k=1:18
```

```
        for j=1:9
            if (I(i-156,k,j)<1)%zone not burning

                E(i) = Matot*1000*(.3 * ienergy(T1u), .446, .3098, -.123,
.227, -.1552, -.489) + .78*ienergy(T1u), .289, .1515, -.57235, .99807, -
.6522, -.90586 ) + .21*ienergy(T1u), .362, .736, -.196, .362, -.289, -.120));

                W(i-1)= 0.5*(p(i-1)+p(i-2))*(v(i-1)-v(i-2));
                Q=heatL(T1u);
                f= E(i)-E(i-1) + W(i) -Q;
                V1u = Mftot*w1u*8.314*T1u/p(i-1);
                w2u= (Matot - (Maz(i-156,k,j)/Ma)/Mftot; %Ma molecular weight
of air
                wloss=w1u-w2u;
                an1=bn1;
                an2=bn2;
                an3=bn3;
                an4=bn4;
                an7=bn7;
                an8=bn8;
                an9=bn9;
                an10=bn10;
                an11=bn11;
                an12=bn12;
                an5=bn5-.21*wloss;
                an6=bn6 - .79*wloss;
                c=power(v(i-1)/v(i),.35);

                 T2u= T1u*c;
                 V2u= Mftot*W2u*8.314*T2u/p(i);
                 W(i)= 0.5*(p(i)+p(i-1))*(v(i)-v(i-1));
                 %newton Raphson to be applied

            else %zone burning

               wg= ((Maz(i-155)-Maz(i-156)/Ma)/Mftot;
               bn1km = bn1k;
               bn2km = bn2k;
               bn3km = bn3k;
               bn4km = bn4k;
               bn8km = bn8k;
               bn9km = bn9k;
               bn10km = bn10k;
               bn11km = bn11k;
               bn12km = bn12k;

               bn5km = bn5k + 0.21*wg;
               bn6km = bn6k + .79*wg;
               bn7km = bn7k + ((Mev(i-156,k,j)/Mf)/Mftot;

               w1km= bn1km + bn2km +bn3km +bn4km +bn5km +bn6km +bn7km +bn8km
+bn9km +bn10km +bn11km +bn12km ;
               po = p(i-1)*(b5km)/w1km;
               %enthalpy of 12 elements
               %enthalpy of air entered of wg
               T1km = (w1km*T1k + wg*T1u)/(w1km + wg);
               v1km = (w1km*v1k + wg*v1u)/(w1km + wg);
```

```
                if (Mev(i-156,k,j) - Mfb(i-156,k,j) < Maz(i-156,k,j) -
14.2*Mfb(i-156,k,j))
                dmfb = Kbu*(p(i-1)^.757)*((Mev(i-156,k,j) - Mfb(i-
156,k,j))*power(2.7,-5000/t(i-1));
                else
                     dmfb = Kbu*(p(i-1)^.757)*((Maz(i-156,k,j) - 14.2*Mfb(i-
156,k,j))*power(2.7,-5000/t(i-1));
                end
                Mfb(i-156,k,j) = Mfb(i-156,k,j)-dmfb;

                T2k = T1km*power(p(i)/p(i-1), (gamma-1/gamma))-
dfmb*Qc/(Mftot*w1km*Cv); ;
                V2k = Mftot*w1km*8.314*T2k/p(i);
                W1 = 0.5*(p(i-1) - p(i))*(V2k - V1k);

                %NO sub model
                k1f = 3.1*(10^10)*exp(-160/T2k);
                k2f =6.4*(10^6)*exp(-3125/T2k);
                k3f=4.2*(10^10);
                R1= k1f*bn6k*bn7k;
                R2= k2f*bn6k*bn12k;
                R3= k3f*bn6k*bn11k;
                alpha = bn7k/bn7;
                bn7k = 2*(i-alpha^2)*(R1/(1+ alpha/(R2+R3)));

                %soot submodel
                msf = power(Mev-Mfb, 0.8)*(p^0.5)*power(2.71,-Esf/8.314*t(i));
                msc= msn(i-1)*(Po(i)/p(i))*power(p,1.8)*power(2.71,-
Esc/8.314*t(i));
                msn(i)= msf - msc;


            end

        end
    end
end
```

REFERENCES

[1] https://en.wikipedia.org/wiki/Electricity_generation#cite_noteStatistics_and_Balances-14, 03 Oct, 2015.

[2] http://www.iea.org/publications/freepublications/. IEA. 2014. pp. 6,24,28.

[3] Nebojša N, Arnulf G. Alan MC. Global energy: perspectives. Cambridge, New York: Cambridge University Press. 1998, ISBN 0521642000.

[4] World Energy Assessment (WEA). UNDP, United Nations Department of Economic and Social Affairs, World Energy Council, New York 2014.

[5] Statistical Review of World Energy, Workbook (xlsx), London, 2013.

[6] Garg HP, Datta G. Global Status on Renewable Energy. International Workshop, Iran University of Science and Technology 1998; 19-20 May.

[7] Cuff DJ, Young WJ. US energy atlas. New York: Free Press/McMillan; 1980.

[8] Deeba F, Kumar V, Gautam K, Saxena RK, Sharma DK. Bioprocessing of Jatropha curcas seed oil and deoiled seed hulls for the production of biodiesel and biogas. Biomass and Bioenergy 2012; 40:13-18.

[9] Demirbas AH, Demirbas I. Importance of rural bioenergy for developing countries. Energy Conversion and Management 2007; 48:2386-2398.

[10] Balat M. Gasification of biomass to produce gaseous products. Energy Sources A 2009; 31:516-526.

[11] Sher E. Environmental Aspects of Air Pollution, In: Handbook of Air Pollution. Editor: E. Sher, Academic Press, Boston 1998, 27-41.

[12] Hei. Diesel Exhaust: A Critical Analysis of Emissions, Exposure, and Health Effects, Health Effects Institute, Cambridge, MA, April 1995.

[13] Demirbas A. Progress and recent trends in bio-fuels. Process in Energy and Combustion Science 2007; 33:1-18.

[14] Vivek, Gupta AK. Biodiesel production from karanja oil. Journal of Scientific and Industrial Research 2004; 63:39-47.

[15] Ma F, Hanna MA. Biodiesel production: A review. Bioresource Technology 1999; 70:1-15.

[16] Sinha S, Agarwal AK, Garg S. Biodiesel development from rice bran oil: transesterification process optimization and fuel characterization. Energy Conversion and Management 2008; 49:1248-1257.

[17] Sharma PK, Singh JK. Biodiesel-An Environment-friendly fuel for use in transportation as a substitute for diesel. Agricultural Engineering Today 2004; 28:1-8.

[18] Gupta KK, Rehman A, Sarviya RM. Evaluation of soya bio-diesel as a gas turbine fuel. In: 1st International conference on new frontiers in bio-fuels. New Delhi: Delhi Technical University 2010: p. 24-33.

[19] American Society for Testing of Materials (ASTM). Annual book of ASTM standards. Philadelphia: ASTM 19103; 1983.

[20] Barik D, Murugan S. Assessment of sustainable biogas production from de-oiled seed cake of karanja - an organic industrial waste from biodiesel industries. Fuel 2015; 148:25-31.

[21] Osman GA, Tinay AHE, Mohamed EF. Biogas production from agricultural wastes. Journal of Food Technology 2006; 4:37-39.

[22] Pike PW, Hertwig TA. Integrating biomass feedstocks into chemical production complexes using new and existing processes. Minerals Processing Research Institute, Louisiana State University, Baton Rouge, LA; November 3, 2008.

[23] Astbury GR. A review of the properties and hazards of some alternative fuels. Process Safety and Environment Protection 2008; 86:397-414.

[24] Technical Bulletin. Center for the Polyurethanes Industry. January 2008. Document AX-396.

[25] Demirbas A, Current technologies for the thermo-conversion of biomass into fuels and chemicals, Energy Source 2004; 26:715-730.

[26] Thamburaj R. Fast pyrolysis of biomass for green power generation. In: First world conference and exhibition on biomass for energy and industry, Sevilla, Spain; June 5-9, 2000.

[27] Fernando S, Adhikari S, Chandrapal C, Murali N. Biorefineries: current status challenges and future direction, Energy and Fuel 2006; 20:1727-1737.

[28] Jiang L, Zheng A, Zhao Z, He F, Li H, Wu N. The comparison of obtaining fermentable sugars from cellulose by enzymatic hydrolysis and fast pyrolysis. Bioresource Technology 2016; 200:8-13.

[29] Divakara BN, Upadhyaya HD, Wani SP, Gowda CLL. Biology and genetic improvement of Jatropha curcas: A review. Applied Energy 2010; 87:732-742.

[30] Mohanty P, Pant KK, Naik SN, Das LM, Vasudevan P. Fuel production from biomass: Indian prospective for pyrolysis oil. Journal of Scientific & Industrial Research 2011; 70:668-674.

[31] Ciferno JP, Marano JJ. Benchmarking Biomass Gasification Technologies for Fuels, Chemicals and Hydrogen Production. U.S. Department of Energy National Energy Technology Laboratory. June 2002.

[32] Demirbas MF, Balat M, Balat H. Potential contribution of biomass to the sustainable energy development. Energy Conversion and Management 2009; 50:1746-1760.

[33] Balat M, Kırtay E, Balat H. Main routes for the thermo-conversion of biomass into fuels and chemicals. Part 1: pyrolysis systems. Energy Conversion and Management 2009; 50:3147-3157.

[34] Demirbas MF. Biorefineries for biofuel upgrading: a critical review. Applied Energy 2009; 86:151-161.

[35] Raheman H, Ghadge SV. Performance of compression ignition engine with mahua (Madhuca indica) biodiesel. Fuel 2007; 86:2568-2573.

[36] Yetilmezsoy K, Sakar S. Improvement of COD and colour removal from UASB treated poultry manure wastewater using Fenton's oxidation. Journal of Hazardous Materials 2008; 151:547-558.

[37] Raheman H, Mondal S. Biogas production potential of Jatropha seed cake. Biomass and Bioenergy 2012; 37:25-30.

[38] Monlau F, Latrille E, Costa ACD, Jean-Philippe Steyer, Carrere H. Enhancement of methane production from sunflower oil cakes by dilute acid pre-treatment. Applied Energy 2012; 102:1105-1113.

[39] Budzianowski WM. Can 'negative net CO_2 emissions' from decarbonised biogas-to electricity contribute to solving Poland's carbon capture and sequestration dilemmas? Energy 2011; 36:6318-6325.

[40] Diesel Rodolf, Diesel engine, Patent number: 542846, 1895.

[41] Heywood JB. Internal Combustion Engine Fundamentals, New York 1988, McGraw- Hill Book Co.

[42] Lata DB, Mishra A. Analysis of ignition delay period of a dual fuel diesel engine with hydrogen and LPG as secondary fuels. International Journal of Hydrogen Energy 2011; 36:3746-3756.

[43] International Energy Agency (IEA) Statistics - CO_2 Emissions from Fuel Combustion-Highlights (2011). [Accessed 15/09/2012].

[44] Alkidas AC. Combustion-chamber crevices: the major source of engine-out hydrocarbon emissions under fully warmed conditions. Progress in Energy and Combustion Science, 1999; 25:253-273.

[45] Bagal NL, Rutland CJ, Foster DE, Narayanaswamy K, He Y. CO Emission Model for an Integrated Diesel Engine, Emissions, and Exhaust Aftertreatment System Level Model. SAE Paper. 2009-01-1511, 2009.

[46] Xinling L, Zhen H. Emission reduction potential of using gas-to-liquid and dimethyl ether fuels on a turbocharged diesel engine. Science of The Total Environment 2009; 407:2234-2244.

[47] Zhu R, Cheung CS, Huang Z, Wang X. Regulated and unregulated emissions from a diesel engine fueled with diesel fuel blended with diethyl adipate. Atmospheric Environment 2011; 45:2174-2181.

[48] Magnusson R, Nilsson C, Andersson B. Emissions of Aldehydes and Ketones from a Two-Stroke Engine Using Ethanol and Ethanol-Blended Gasoline as Fuel. Environmental Science and Technology 2002; 36:1656-1664.

[49] Takada K, Yoshimura F, Ohga Y, Kusaka J, Daisho Y. Experimental Study on Unregulated Emission Characteristics of Turbocharged DI Diesel Engine with Common Rail Fuel Injection System. SAE Paper 2003-01-3158; 2003.

[50] Turriobaldassarri L, Battistelli CL, Conti L, Crebelli R, Deberardis B, Iamiceli AL, Gambino M, Iannaccone S. Emission comparison of urban bus engine fueled with diesel oil and 'biodiesel' blend. Science of The Total Environment 2004; 327:147-162.

[51] Machado CS, Arbilla G. Carbonyl emissions in diesel and biodiesel exhaust. Atmospheric Environment 2008; 42:769-775.

[52] Krahl J, Munack A, Schroder O, Ruschel Y, Bünger J. Ultrafine Particles from a Heavy Duty Diesel Engine Running on Rapeseed Oil Methyl Ester. SAE International Journal of Fuels and Lubricants 2009; 2:132-146.

[53] Nelson PF, Tibbett AR, Day SJ. Effects of vehicle type and fuel quality on real world toxic emissions from diesel vehicles. Atmospheric Environment 2008; 42:5291-5303.

[54] Stanmore BR, Brilhac JF, Gilot P. The oxidation of soot: a review of experiments, mechanisms and models. Carbon 2001; 39:2247-2268.

[55] Kawano D, Naito H, Suzuki H, Ishii H, Hori S, Goto Y, Odaka M. Effects of Fuel Properties on Combustion and Exhaust Emissions of Homogeneous Charge Compression Ignition (HCCI) Engine. SAE Paper, 2004-01-1966; 2004.

[56] Lapuerta M, Armas O, Rodríguezfernández J. Effect of biodiesel fuels on diesel engine emissions. Progress in Energy and Combustion Science 2008; 34:198-223.

[57] Masi M. Experimental analysis on a spark ignition petrol engine fuelled with LPG (liquefied petroleum gas). Energy 2012; 41:252-260.

[58] Price P, Guo S, Hirschmann M. Performance of an evaporator for a LPG powered vehicle. Applied Thermal Engineering 2004; 24:1179-1194.

[59] Varshney Rajiv, Bhagoria JL, Mehta CR. Small scale biomass gasification technology in India-an overview. Journal of Engineering, Science & Management Education 2010; 3:33-40.

[60] Saravanan N, Nagarajan G. An insight on hydrogen fuel injection techniques with SCR system for NO_x reduction in a hydrogen-diesel dual fuel engine. International Journal of Hydrogen Energy 2009; 34:9019-9032.

[61] Sahoo BB, Sahoo N, Saha UK. Effect of engine parameters and type of gaseous fuel on the performance of dual-fuel gas diesel engines-A critical review. Renewable and Sustainable Energy Reviews 2009; 13:1151-1184.

[62] Poonia MP, Ramesh A, Gaur RR. Effect of Intake Air Temperature and Pilot Fuel Quantity on the Combustion Characteristics of a LPG Diesel Dual Fuel Engine. SAE Paper, 982455;1998.

[63] Raslavicius L, Kersys A, Mockus S, Kersiene N, Starevicius M, Liquefied petroleum gas (LPG) as a medium-term option in the transition to sustainable fuels and transport, Renewable and Sustainable Energy Review 2014; 32:513-525.

[64] Goldsworthy L. Combustion behavior of a heavy duty common rail marine diesel engine fumigated with propane. Experimental Thermal and Fluid Science 2012; 42:93-106.

[65] Johnson E. LPG: a secure, cleaner transport fuel? A policy recommendation for Europe. Energy Policy 2003; 31:1573-1577.

[66] Tira HS, Herreros JM, Tsolakis A, Wyszynski ML. Characteristics of LPG-diesel dual fuelled engine operated with rapeseed methyl ester and gas-to-liquid diesel fuels. Energy 2012; 47:620-629.

[67] Boretti A, Conversion of a heavy duty truck diesel engine with an innovative power turbine connected to the crankshaft through a continuously variable transmission to operate compression ignition dual fuel diesel-LPG. Fuel Processing Technology 2013; 113:97-108.

[68] Lata DB, Misra A, Medhekar S. Effect of hydrogen and LPG addition on the efficiency and emissions of a dual fuel diesel engine. International Journal of Hydrogen Energy 2012; 37:6084-6096.

[69] Kumaraswamy A, Prasad BD. Performance Analysis of a Dual Fuel Engine Using LPG and Diesel with EGR System. Procedia Engineering 2012; 38:2784-2792.

[70] Renald CJT, Somasundaram P. Experimental Investigation on Attenuation of Emission with Optimized LPG Jet Induction in a Dual Fuel Diesel Engine and Prediction by ANN Model. Energy Procedia 2012; 14:1427-1438.

[71] Selim MYE, Radwan MS, Saleh HE. Improving the performance of dual fuel engines running on natural gas/LPG by using pilot fuel derived from jojoba seeds. Renewable Energy 2008; 33:1173-1185.

[72] Elnajjar E, Hamdan MO, Selim MYE. Experimental investigation of dual engine performance using variable LPG composition fuel. Renewable Energy 2013; 56:110-116.

[73] Qi DH, Bian YZ, Ma ZY, Zhang CH, Liu SQ. Combustion and exhaust emission characteristics of a compression ignition engine using liquefied petroleum gas-Diesel blended fuel. Energy Conversion and Management 2007; 48:500-509.

[74] Jothi NKM, Nagarajan G, Renganarayanan S. LPG fueled diesel engine using diethyl ether with exhaust gas recirculation. International Journal of Thermal Sciences 2008; 47:450-457.

[75] Vijayabalan P, Nagarajan G. Performance, Emission and Combustion of LPG Diesel Dual Fuel Engine using Glow Plug. Jordan Journal of Mechanical and Industrial Engineering 2009; 3:105-110.

[76] Lata DB, Misra A, Medhekar S. Investigations on the combustion parameters of a dual fuel diesel engine with hydrogen and LPG as secondary fuels. International Journal of Hydrogen Energy 2011; 36:13808-13819.

[77] Surawski NC, Miljevic B, Bodisco TA, Situ R, Brown RJ, Ristovski ZD. Performance and gaseous and particle emissions from a liquefied petroleum gas (LPG) fumigated compression ignition engine. Fuel 2014; 133:17-25.

[78] Selim MYE, Pressure-time characteristics in diesel engine fueled with natural gas, Renew. Energy 2001; 22:473-489.

[79] Abdelaal MM, Hegab AH, Combustion and emission characteristics of a natural gas-fueled diesel engine with EGR, Energy Conversion and Management 2012; 64:301-312.

[80] Liu SH, Wang ZY, Ren J. Development of compressed natural gas/diesel dual-fuel turbocharged compression ignition engine, Proceedings of the Institution of Mechanical Engineers Part D: Journal of Automobile Engineering 2003; 217:839-845.

[81] Papagiannakis RG, Hountalas DT. Experimental investigation concerning the effect of natural gas percentage on performance and emissions of a DI dual fuel diesel engine, Applied Thermal Engineering 2003; 23:353-365.

[82] Papagiannakis RG, Rakopoulos CD, Hountalas DT, Rakopoulos DC. Emission characteristics of high speed, dual fuel, compression ignition engine operating in a wide range of natural gas/diesel fuel proportions. Fuel 2010; 89:1397-1406.

[83] Carlucci AP, Risi AD, Laforgia D, Naccarato F. Experimental investigation and combustion analysis of a direct injection dual-fuel diesel-natural gas engine. Energy 2008; 33:256-263.

[84] Liu J, Yang F, Wang H, Ouyang M, Hao S. Effects of pilot fuel quantity on the emissions characteristics of a CNG/diesel dual fuel engine with optimized pilot injection timing. Applied Energy 2013; 110:201-206.

[85] Paul A, Panua RS, Debroy D, Bose PK. An experimental study of the performance, combustion and emission characteristics of a CI engine under dual fuel mode using CNG and oxygenated pilot fuel blends. Energy 2015; 86:560-573.

[86] Paul A, Bose PK, Panua RS, Banerjee R. An experimental investigation of performance-emission trade off of a CI engine fueled by diesel-compressed natural gas (CNG) combination and diesel-ethanol blends with CNG enrichment. Energy 2013; 55:787-802.

[87] Gharehghani A, Hosseini R, Mirsalim M, Jazayeri AS, Yusaf T. An experimental study on reactivity controlled compression ignition engine fueled with biodiesel/natural gas. Energy 2015; 89:558-567.

[88] Paul A, Panua RS, Debroy D, Bose PK. Effect of compressed natural gas dual fuel operation with diesel and Pongamia pinnata methyl ester (PPME) as pilot fuels on performance and emission characteristics of a CI (compression ignition) engine. Energy 2014; 68:495-509.

[89] Cheenkachorn K, Poompipatpong C, Ho CG. Performance and emissions of a heavy-duty diesel engine fuelled with diesel and LNG (liquid natural gas). Energy 2013; 53:52-57.

[90] Papagiannakis RG, Kotsiopoulos PN, Zannis TC, Yfantis EA, Hountalas DT, Rakopoulos CD. Theoretical study of the effects of engine parameters on performance and emissions of a pilot ignited natural gas diesel engine. Energy 2010; 35:1129-1138.

[91] Papagiannakis RG, Hountalas DT. Combustion and exhaust emission characteristics of a dual fuel compression ignition engine operated with pilot Diesel fuel and natural gas. Energy Conversion and Management 2004; 45:2971-2987.

[92] Ryu K. Effects of pilot injection timing on the combustion and emissions characteristics in a diesel engine using biodiesel-CNG dual fuel. Applied Energy 2013; 111:721-730.

[93] Ryu K. Effects of pilot injection pressure on the combustion and emissions characteristics in a diesel engine using biodiesel-CNG dual fuel. Energy Conversion and Management 2013; 76:506-516.

[94] Lantz M, Svensson M, Björnsson L, Börjesson P. The prospects for an expansion of biogas systems in Sweden-Incentives, barriers and potentials. Energy Policy 2007; 35:1830-1843.

[95] Corbo P, Gambino M, Iannaccone S, Unich A. Comparison Between Lean-Burn and Stoichiometric Technologies for CNG Heavy-Duty Engines. SAE Paper 950057;1995.

[96] Roubaud A, Favrat D. Improving performances of a lean burn cogeneration biogas engine equipped with combustion pre-chambers. Fuel 2005; 84:2001-2007.

[97] Bedoya ID, Arrieta AA, Cadavid FJ. Effects of mixing system and pilot fuel quality on diesel–biogas dual fuel engine performance. Bioresource Technology 2009; 100:6624-6629.

[98] Duc PM, Wattanavichien K. Study on biogas premixed charge diesel dual fuelled engine. Energy Conversion and Management 2007; 48:2286-2308.

[99] Makareviciene V, Sendzikiene E, Pukalskas S, Rimkus A, Vegneris R. Performance and emission characteristics of biogas used in diesel engine. Energy Conversion and Management 2013; 75:224-233.

[100] Chandra R, Vijay VK, Subbarao PMV, Khura TK. Performance evaluation of a constant speed IC engine on CNG, methane enriched biogas and biogas. Applied Energy 2011; 88:3969-3977.

[101] Cacua K, Amell A, Cadavid F. Effects of oxygen enriched air on the operation and performance of a diesel-biogas dual fuel engine. Biomass and Bioenergy 2012; 45:159-167.

[102] Bora BJ, Saha UK, Chatterjee S, Veer V. Effect of compression ratio on performance, combustion and emission characteristics of a dual fuel diesel engine run on raw biogas. Energy Conversion and Management 2014; 87:1000-1009.

[103] Yoon SH, Lee CS. Experimental investigation on the combustion and exhaust emission characteristics of biogas-biodiesel dual-fuel combustion in a CI engine. Fuel Processing Technology 2011; 92:992-1000.

[104] Luijten CCM, Kerkhof E. Jatropha oil and biogas in a dual fuel CI engine for rural electrification. Energy Conversion and Management 2011; 52:1426-1438.

[105] Mustafi NN, Raine RR, Verhelst S. Combustion and emissions characteristics of a dual fuel engine operated on alternative gaseous fuels. Fuel 2013; 109: 669-678.

[106] Bari S. Effect of carbon dioxide on the performance of biogas/diesel dual-fuel engine. Renewable Energy 1996; 9:1007-1010.

[107] Tippayawong N, Promwungkwa A, Rerkkriangkrai P. Long-term operation of a small biogas/diesel dual-fuel engine for on-farm electricity generation. Biosystems Engineering 2007; 98:26-32.

[108] Banapurmath NR, Tewari PG, Hosmath RS. Experimental investigations of a four-stroke single cylinder direct injection diesel engine operated on dual fuel mode with producer

gas as inducted fuel and Honge oil and its methyl ester (HOME) as injected fuels. Renewable Energy 2008; 33:2007-2018.

[109] Roy MM, Tomita E, Kawahara N, Harada Y, Sakane A. Performance and emission comparison of a supercharged dual-fuel engine fueled by producer gases with varying hydrogen content. International Journal of Hydrogen Energy 2009; 34:7811-7822.

[110] Devakumar MLS, Reddy KVK. Effect of fuel injection pressure on full load performance of diesel-producer gas dual fuel engine. Indian Journal of Science and Technology 2010; 3:1056-1061.

[111] Parikh PP, Bhave AG, Shashikantha. Performance evaluation of a diesel engine dual-fueled on producer-gas and diesel. In: Proceedings of the tenth national conference on IC engines and combustion. Rajkot, India. AF179-AF186; 1987.

[112] Sombatwong P, Thaiyasuit P, Pianthong K. Effect of Pilot Fuel Quantity on the Performance and Emission of a Dual Producer Gas-Diesel Engine. Energy Procedia 2013; 34:218-227.

[113] Arunachalam A, Olsen DB. Experimental evaluation of knock characteristics of producer gas. Biomass and Bioenergy 2012; 37:169-176.

[114] Kapdi SS, Vijay VK, Rajesh SK, Prasad R. Upgrading biogas for utilization as a vehicle fuel, Asian Journal on Energy and Environment 2006; 7:387-393.

[115] http://www.energy.ca.gov/research/renewable/biomass/anaerobic_digestion/index.html.

[116] Semblante GU, Hai FI, Huang X, Ball AS, Price WE, Nghiem LD. Trace organic contaminants in biosolids: Impact of conventional wastewater and sludge processing technologies and emerging alternatives. Journal of Hazardous Materials 2015; 300:1-17.

[117] Rao PV, Baral SS, Dey R, Mutnuri S. Biogas generation potential by anaerobic digestion for sustainable energy development in India. Renewable and Sustainable Energy Reviews 2010; 14:2086-2094.

[118] Yadvika, Santosh, Sreekrishnan TR, Kohli S, Rana V. Enhancement of biogas production from solid substrates using different techniques-A review. Bioresource Technology 2004; 95:1-10.

[119] Zheng Y, Pan Z, Zhang R, Mashad HME, Pan J, Jenkins BM. Anaerobic digestion of saline creeping wild ryegrass for biogas production and pretreatment of particleboard material. Bioresource Technology 2009; 100:1582-1588.

[120] Kalia AK, Singh SP. Performance evaluation of Pragati and KVIC biogas plant in hilly regions. Biogas Forum 1996; 64:6-10.

[121] Dermott BLM, Chalmers AD, Goodwin JAS. Ultrasonification as pre-treatment method for the enhancement of the psychrophilic anaerobic digestion of aquaculture effluents. Environment Technology 2001; 22:823-830.

[122] Farland MJM, Biosolids engineering, McGraw Hill Professional, 2000.

[123] Deublein D, Steinhauser A. Biogas from waste and renewable resources, Dieter doublein, Wiley-VCH, 2008.

[124] Weiland P. Biogas production: current state and perspectives. Applied Microbiology and Biotechnology 2010; 85:849-860.

[125] Saxena RC, Adhikari DK, Goyal HB. Biomass-based energy fuel through biochemical routes: A review. Renewable and Sustainable Energy Reviews 2009; 13:167-178.

[126] Balat M, Demirbas MF. Bio-oil from Pyrolysis of Black Alder Wood. Energy Sources, Part A: Recovery, Utilization, and Environmental Effects 2009; 31:1719-1727.

[127] Lux Research, Waste to energy, <http://www.luxresearchinc.com/pdf/08CTR_ tech_profile> [accessed February 2010].

[128] Wright JD. Ethanol from lignocellulosics: an overview. Energy Progress 1988; 84:71-80.

[129] Mosier N, Wyman C, Dale B, Elander R, Lee YY, Holtzapple M, Ladisch M. Features of promising technologies for pretreatment of lignocellulosic biomass. Bioresource Technology 2005; 96:673-686.

[130] Kumar P, Barrett DM, Delwiche MJ, Stroeve P. Methods for pretreatment of lignocellulosic biomass for efficient hydrolysis and biofuel production. Industrial & Engineering Chemistry Research 2009; 48:3713–3729.

[131] Zheng Y, Zhao J, Xu F, Li Y. Pretreatment of lignocellulosic biomass for enhanced biogas production. Progress in Energy and Combustion Science 2014; 42:35-53.

[132] Hashem A, Akasha A, Ghith A, Hussein DA. Adsorbent based on agricultural wastes for heavy metal and dye removal: A review. Energy Education Science and Technology 2007; 19:69-86.

[133] Demirbas A. Pyrolysis of biomass for fuels and chemicals. Energy Sources, Part A: Recovery, Utilization, and Environmental Effects 2009; 31:1028-1037.

[134] Mel M, Yong ASH, Avicenna, Ihsan SI, Setyobudi RH. Simulation Study for Economic Analysis of Biogas Production from Agricultural Biomass. Energy Procedia 2015; 65:204-214.

[135] Takizawa N, Umetsu K, Takahata H, Hoshiba H. Temperature effects on continuously expanding anaerobic digester with dairy manure slurry. Research Bulletin of Obihiro University, Natural Science 1994; 19:31-36.

[136] Markowski M, Białobrzewski I, Zieliński M, Dębowski M, Krzemieniewski M. Optimizing low-temperature biogas production from biomass by anaerobic digestion. Renewable Energy 2014; 69:219-225.

[137] Ostrem KM, Millrath K, Themelis NJ. Combining anaerobic digestion and waste-to-energy, 12th North American Waste to Energy Conference, Savannah, Georgia, May 2004; 17-19.

[138] Angelidaki I, Ahring BK. Thermophilic anaerobic digestion of livestock waste: the effect of ammonia. Applied Microbiology and Biotechnology 1993; 38:560-564.

[139] Garba B. Effect of temperature and retention period on biogas production from ligrocellulosic material. Renewable Energy 1996; 9:938-941.

[140] Dar GH, Tandon SM. Biogas production from pretreated wheat straw, lantana residue, apple and peach leaf litter with cattle dung. Biological Wastes 1987; 21:75-83.

[141] Singh R, Jain MK, Tauro P. Pre-digestion to improve production of biogas from cattle waste. Agricultural Wastes 1983; 6:167-174.

[142] Wang Q, Kuninobu M, Kakimoto K, Ogawa HI, Kato Y. Upgrading of anaerobic digestion of waste activated sludge by ultrasonic pretreatment. Bioresource Technology 1999; 68:309-313.

[143] Klassen V, Klassen OB, Hoekzema Y, Mussgnug JH, Kruse O. A novel one-stage cultivation/fermentation strategy for improved biogas production with microalgal biomass. Journal of Biotechnology 2015; 215:44-51.

[144] Verma S. Anaerobic digestion of biodegradable organics in municipal solid wastes. M.S. Thesis, Columbia University; 2002.

[145] Chandra R. Studies on production of enriched biogas using jatropha and pongamia de-oiled seed cakes and its utilization in I.C. Engines. PhD Thesis. Centre for Rural Development and Technology, IIT Delhi; 2009.

[146] Gupta A, Kumar A, Sharma S, Vijay VK. Comparative evaluation of raw and detoxified mahua seed cake for biogas production. Applied Energy 2013; 102:1514-1521.

[147] Desai M, Madamwar D. Anaerobic digestion of a mixture of cheese whey, poultry waste and cattle dung: a study of the use of adsorbents to improve digester performance. Environment and Pollution 1994; 86:337-340.

[148] Baserja U. Biogas production from cowdung: influence of time and fresh liquid manure. Swiss-Biotechnology 1984; 2:19-24.

[149] Rubia MADL, Cegrí VF, Raposo F, Borja R. Influence of particle size and chemical composition on the performance and kinetics of anaerobic digestion process of sunflower oil cake in batch mode. Biochemical Engineering Journal 2011; 58-59:162-167.

[150] Gollakota KG, Meher KK. Effect of particle size, temperature, loading rate and stirring on biogas production from castor cake. Biological Wastes 1988; 24:243-249.

[151] Gunaseelan VN. Parthenium as an additive with cattle manure in biogas production. Biological Wastes 1987; 21:195-202.

[152] Vervaeren H, Hostyn K, Ghekiere G, Willems B. Biological ensilage additives as pretreatment for maize to increase the biogas production. Renewable Energy 2010; 35 2089-2093.

[153] Tirumale S, Nand K. Influence of Anaerobic cellulolytic bacterial consortia in the anaerobic digesters on biogas production. Biogas Forum III 1994; 58:12-15.

[154] Geeta GS, Jagadeesh KS, Reddy TKR. Nickel as an accelerator of biogas production in water hyacinth (Eichornia crassipes solms) Biomass 1990; 21:157-161.

[155] Sichuan PR, Spobd. Biogas technology and utilization. Sichuan provincial office of biogas development. Chengdu seminar, China, 1979.

[156] Chowdhury SDR, Gupta SK, Banerjee SK. Evaluation of the potentiality of tree leaves for biogas production. Indian Forester 1994; 120:720-728.

[157] Kalia AK, Kanwar SS. Anaerobic fermentation of ageratum for biogas production. Biological Wastes 1989; 32:155-158.

[158] Malik RK, Dahiya DS. Biogas production from cattle waste by recycling of filtered liquid of digested slurry. Urja 1990; 28:30-35.

[159] Kanwar SS, Guleri RL. Effect of recycling of digested slurry on biogas production. Biogas Forum IV 1994; 59:12-13.

[160] Santosh, Vasudevan P, Chanel S. Studies on developing a model for water conservation in biogas system. Project sponsored by DST, CRDT, IIT, Delhi, India, (1999).

[161] Teghammara A, Karimia K, Horvath IS, Taherzadeh MJ. Enhanced biogas production from rice straw, triticale straw and softwood spruce by NMMO pre-treatment. Biomass and Bioenergy 2012; 36:116-120.

[162] Thorin E, Lindmark J, Nordlander E, Odlare M, Dahlquist E, Kastensson J, Leksel N, Pettersson CM. Performance optimization of the Växtkraft biogas production plant. Applied Energy 2012; 97:503-508.

[163] Kana EBG, Oloke JK, Lateef A, Adesiyan MO. Modeling and optimization of biogas production on saw dust and other co-substrates using Artificial Neural network and Genetic Algorithm. Renewable Energy 2012; 46:276-281.

[164] Comino E, Riggio VA, Rosso M. Biogas production by anaerobic co-digestion of cattle slurry and cheese whey. Bioresource Technology 2012; 114:46-53.

[165] Liu X, Gao X, Wang W, Zheng L, Zhou Y, Sun Y. Pilot-scale anaerobic co-digestion of municipal biomass waste: Focusing on biogas production and GHG reduction. Renewable Energy 2012; 44:463-468.

[166] Juntarasiri P, Nijsunkij S, Buatick T, Jamkrajang E, Wacharawichanant S, Seadan M, Wasantakorn A, Suttiruengwong S. Enhancing Biogas Production from Padauk Angsana Leave and Wastewater Feedstock through Alkaline and Enzyme Pretreatment. Energy Procedia 2011; 9:207-215.

[167] Castrillón L, Fernández-Nava Y, Ormaechea P, Marañón E. Optimization of biogas production from cattle manure by pre-treatment with ultrasound and co-digestion with crude glycerine. Bioresource Technology 2011; 102:7845-7849.

[168] Zhong W, Zhang Z, Luo Y, Sun S, Qiao W, Xiao M. Effect of biological pretreatments in enhancing corn straw biogas production. Bioresource Technology 2011; 102:11177-11182.

[169] Dahrieh JA, Orozco A, Groom E, Rooney D. Batch and continuous biogas production from grass silage liquor. Bioresource Technology 2011; 102:10922-10928.

[170] Rajesh JB, Kaliappan S, Rajkumar M, Beck D. Treatment of spent wash in anaerobic mesophilic suspended growth reactor (AMSGR). Journal of Envirromental Biology 2006; 27:111-117.

[171] Martinez E, Marcos A, Kassir AA, Jaramilloo MA, Mohamad AA. Mathematical model of a laboratory-scale plant for slaughterhouse effluents bio digestion for biogas production. Apllid Energy 2012; 95:210-219.

[172] Qiao W, Yan X, Ye J, Sun Y, Wang W, Zhang Z. Evaluation of biogas production from different biomass wastes with/without hydrothermal pretreatment. Renewable Energy 2011; 36:3313-3318.

[173] Bhattacharya TK, Mishra TN, Singh B. Techniques for removal of CO_2 and H_2S from biogas. Paper presented at XXIV annual convention of ISAE, held at PKV, Akola, 1988.

[174] Vijay VK. Studies on utilization of biogas for improved performance of dual fuel engine. ME (Ag.) Thesis, CTAE, Udaipur; 1989.

[175] Khapre UL. Studies on biogas utilization for domestic cooking. Paper presented at XXV annual convention of ISAE, held at CTAE, Udaipur; 1989.

[176] Dubey AK. Wet scrubbing of carbon dioxide. Annual report of CIAE, Bhopal (India); 2000.

[177] Tippayawong N, Thanompongchart P. Biogas quality upgrade by simultaneous removal of CO_2 and H_2S in a packed column reactor. Energy 2010; 35:4531-4535.

[178] Biswas TD, Kartha ARS, Pundarikakhadu R. Removal of carbon dioxide from biogas. Proceedings of national symposium on biogas technology and uses. New Delhi: IARI; 1977.

[179] Baciocchi R, Carnevale E, Corti A, Costa G, Lombardi L, Olivieri T, Zanchi L, Zingaretti D. Innovative process for biogas upgrading with CO_2 storage: Results from pilot plant operation. Biomass and Bioenergy 2013; 53:128-137.

[180] Savery WC, Cruzon DC. Methane recovery from chicken manure. Journal of the Water Pollution Control Federation 1972; 44:2349-2354.

[181] Wise DL. Analysis of systems for purification of fuel gas. Fuel gas production from biomass, vol 2. Boca Raton, FL: CRC Press; 1981.

[182] Schomaker IT, Boerboom AHHM, Vissel A, Pfeifer AE. Technical summary on gas treatment. Anaerobic digestion of agro industrial wastes: information network project FAIR-CT96-2083; 2000.

[183] Pandey DR, Fabian C. Feasibility studies on the use of naturally accruing molecular sieves for methane enrichment from biogas. Gas Separation and Purification 1989; 3:143-147.

[184] Hagen M, Polman E. Adding gas from biomass to the gas grid. Final report submitted to Danish Gas Agency; 2001:26-47.

[185] Wellinger A, Lindeberg A. Biogas upgrading and utilization. Task 24: energy from biological conversion of organic wastes 1999: 1-19.

[186] Deng L, Hägg MB. Techno-economic evaluation of biogas upgrading process using CO_2 facilitated transport membrane. International Journal of Greenhouse Gas Control 2010; 4: 638-646.

[187] Rautenbach R, Ethresmann E, Wayer H. Removal of carbon dioxide from fermentation gas by membrane separation. Chemical Abstracts 1987; 107(14):154.

[188] Glub JC, Diaz LF. Biogas purification process. Biogas and alcohol fuels production, vol II.: The JP Press Inc; 1991.

[189] Stern SA, Krishnakumar B, Charati SG, Amato WS, Friedman AA, Fuess DJ. Performance of a bench-scale membrane pilot plant for the upgrading of biogas in a wastewater treatment plant. Journal of Membrane Science 1998; 151:63-74.

[190] Chandra R, Vijay VK, Subbarao PMV, Khura TK. Production of methane from anaerobic digestion of jatropha and pongamia oil cakes. Applied Energy 2012; 93:148-159.

[191] Okeh CO, Chukwudi OO, Frederick JCO. Biogas production from rice husks generated from various rice mills in Ebonyi State, Nigeria. Renewable Energy 2014; 62:204-208.

[192] Demirel B, Scherer Paul. Bio-methanization of energy crops through mono-digestion for continuous production of renewable biogas. Renewable Energy 2009; 34:2940-2945.

[193] Havukainen J, Uusitalo V, Niskanen A, Kapustina V, Horttanainen M. Evaluation of methods for estimating energy performance of biogas production. Renewable Energy 2014; 66:232-240.

[194] Martin A, Borja R, Garcia I, Fiestas JA. Kinetics methane production from olive mill waste water. Process Biochemistry 1991; 26:101-107.

[195] Athanasoulia E, Melidis P, Aivasidis A. Optimization of biogas production from waste activated sludge through serial digestion. Renewable Energy 2012; 47:147-151.

[196] Demirbas A. Biogas production from the organic fraction of municipal solid waste. Energy Sources part A. 2006; 28:1127-1134.

[197] Nathan SS, Mallikarjuna JM, Ramesh A. An experimental study of the biogas-diesel HCCI mode of engine operation. Energy Conversion and Management 2010; 51:1347-1353.

[198] Barik D, Murugan S. Simultaneous reduction of NO_x and smoke in a dual fuel DI diesel engine, Energy Conversion and Management 2014; 84:217-226.

[199] Barik D, Murugan S. Experimental investigation on the behavior of a DI diesel engine fueled with raw biogas-diesel dual fuel at different injection timing, Journal of the Energy Institute (2015), http://dx.doi.org/10.1016/j.joei.2015.03.002.

[200] Tan Q, Tang L, Yang M, Xue C, Zhang W, Liu J, Xiong J. Three-gas detection system with IR optical sensor based on NDIR technology. Optics and Lasers in Engineering 2015; 74:103-108.

[201] Sklorz A, Schafer A, Lang W. Merging ethylene NDIR gas sensors with preconcentrator-devices for sensitivity enhancement. Sensors and Actuators B 2012; 170:21-27.

[202] Jones M. Advanced opacity meters: their potential role in future emission testing legislation for Diesel vehicles. Proc. of the 6th ETH Conference on Nanoparticle Measurement, Zurich, August 2002.

[203] Finesso R, Spessa E. Ignition delay prediction of multiple injections in diesel engines. Fuel 2014; 119:170-190.

[204] Rabl S, Davies TJ, McDougall AP, Cracknell RF. Understanding the relationship between ignition delay and burn duration in a constant volume vessel at diesel engine conditions. Proceedings of the Combustion Institute 2015; 35:2967-2974.

[205] Prakash G, Shaik AB, Ramesh A. An approach for estimation of ignition delay in a dual fuel engine. 1999; SAE paper No 990232.

[206] Prakash R, Singh RK, Murugan S. Experimental investigation on a diesel engine fueled with bio-oil derived from waste wood-biodiesel emulsions. Energy 2013; 55:610-618.

[207] Rakopoulos DC. Heat release analysis of combustion in heavy-duty turbocharged diesel engine operating on blends of diesel fuel with cottonseed or sunflower oils and their biodiesel. Fuel 2012; 96:524-534.

[208] Lakshmanan T, Nagarajan G. Experimental investigation of timed manifold injection of acetylene in direct injection diesel engine in dual fuel mode. Energy 2010; 35:3172-3178.

[209] Coleman HW, Steele Jr WG. Experimentation and uncertainty analysis for engineers. New York: John Wiley & Sons; 1989.

[210] Ramadhas AS, Jayaraj S, Muraleedharan C. Theoretical modeling and experimental studies on biodiesel-fueled engine- Technical note. Renewable Energy 2006; 31:1813-1826.

[211] Annand WJD. Heat transfer in the cylinders of reciprocating internal combustion engines. Proceedings of Institue of Mechanical Engineering 1963; 177:973-990.

[212] Gogoi TK, Baruah DC. A cycle simulation model for predicting the performance of a diesel engine fuelled by diesel and biodiesel blends. Energy 2010; 35:1317-1323.

[213] World fuel ethanol production, renewable fuels association. http://ethanolrfa.org /pages/World-Fuel-Ethanol-Production [accessed on 5.9.2015].

[214] Way RJB. Methods for determination of composition and thermodynamic properties of combustion products for internal combustion engine calculations. Proceedings of Institue of Mechanical Engineering 1977; 190:687-697.

[215] Lavoie GA, Heywood JB, Keck JC. Experimental and theoretical study of nitric oxide formation in internal combustion engines. Combustion Science and Technology 1970; 1:313-26.

[216] Hiroyasu H, Kadota T, Arai M. Development and use of a spray combustion modeling to predict Diesel engine efficiency and pollutant emissions. Bull Japan Society of Mechanical Engineers 1983; 26(214): 569.

[217] Dhar A, Agarwal AK. Effect of Karanja biodiesel blend on engine wear in a diesel engine. Fuel 2014; 134:81-89.

[218] Muralidharan K, Vasudevan D, Sheeba KN. Performance, emission and combustion characteristics of biodiesel fuelled variable compression ratio engine. Energy 2011; 36:5385-5393.

[219] Park SH, Yoon SH, Cha J, Lee CS. Mixing effects of biogas and dimethyl ether (DME) on combustion and emission characteristics of DME fueled high-speed diesel engine. Energy 2014; 66:413-422.

[220] Karim GA. Combustion in gas fueled compression ignition engines of the dual fuel type. ASME Journal of Engineering for Gas Turbines and Power 2003; 125:827-836.

[221] Ekrem B. Effects of biodiesel on a diesel engine performance emission and combustion characteristics. Fuel 2010; 89:3099-4005.

[222] Devan PK, Mahalakshmi NV. Study of the performance, emission and combustion characteristics of a diesel engine using poon oil-based fuels. Fuel Processing Technology 2009; 90:513-519.

[223] Lounici MS, Loubar K, Tarabet L, Balistrou M, Niculescu DC, Tazerout M. Towards improvement of natural gas-diesel dual fuel mode: An experimental investigation on performance and exhaust emissions. Energy 2014; 64:200-211.

[224] Abdelaal MM, Rabee BA, Hegab AH. Effect of adding oxygen to the intake air on a dual-fuel engine performance, emissions, and knock tendency. Energy 2013; 61:612-620.

[225] Mustafi NN, Raine RR. A study of the emissions of a dual fuel engine operating with alternative gaseous fuels. 2008; SAE paper 1394.

[226] Karim GA. A review of combustion processes in the dual fuel engine-the gas diesel engine. Progress in Energy and Combustion Science 1980; 6:277-285.

[227] Saravanan S, Nagarajan G, Anand S, Sampath S. Correlation for thermal NO_x formation in compression ignition (CI) engine fuelled with diesel and biodiesel. Energy 2012; 42:401-410.

[228] Al-Dawody MF, Bhatti SK. Optimization strategies to reduce the biodiesel NO_x effect in diesel engine with experimental verification. Energy Convers Manage 2013; 68:96-104.

[229] Nagarajan G, Renganayanan S, Rao AN. Emission and performance characteristics of neat ethanol fuelled DI diesel engine. International Journal of Ambient Energy 2002; 23:149-158.

[230] Karthikeyana R, Mahalakshmi NV. Performance and emission characteristics of a turpentine-diesel dual fuel engine. Energy 2007; 32:1202-1209.

[231] Behera P, Murugan S, Nagarajan G. Dual fuel operation of used transformer oil with acetylene in a DI diesel engine. Energy Conversion and Management 2014; 87:840-847.

[232] Agarwal AK, Srivastava DK, Dhar A, Maurya RK, Shukla PC, Singh AP. Effect of fuel injection timing and pressure on combustion, emissions and performance characteristics of a single cylinder diesel engine. Fuel 2013; 111:374-383.

[233] Nwafor OMI. Effect of advanced injection timing on emission characteristics of diesel engine running on natural gas. Renewable Energy 2007; 32:2361-2368.

[234] Satyanarayana M, Muraleedharan C. A comparative study of vegetable oil methyl esters (biodiesels). Energy 2011; 36:2129-2137.

[235] Park SH, Yoon SH, Lee CS. Effects of multiple-injection strategies on overall spray behavior, combustion, and emissions reduction characteristics of biodiesel fuel. Applied Energy 2011; 88:88-98.

[236] Donateo T, Tornese F, Laforgia D. Computer-aided conversion of an engine from diesel to methane. Applied Energy 2013; 108:8-23.

[237] Papagiannakis RG, Hountalas DT, Rakopoulos CD. Theoretical study of the effects of pilot fuel quantity and its injection timing on the performance and emissions of a dual fuel diesel engine. Energy Conversion and Management 2007; 48:2951-2961.

[238] Jingura RM, Matengaifa R. Optimization of biogas production by anaerobic digestion for sustainable energy development in Zimbabwe. Renewable and Sustainable Energy Review 2009; 13:1116-1120.

[239] Yang B, Wei X, Xi C, Liu Y, Zeng K, Lai MC. Experimental study of the effects of natural gas injection timing on the combustion performance and emissions of a turbocharged common rail dual-fuel engine. Energy Conversion and Management 2014; 87:297-304.

[240] Krishnan SR, Srinivasan KK, Singh S, Bell SR, Midkiff KC, Gong W, Fiveland SB, Willi M. Strategies for reduced NO_x emissions in pilot-ignited natural gas engines. ASME J. Eng. Gas Turbines Power 2004; 126:665-671.

[241] Bedoya ID, Saxena S, Cadavid FJ, Dibble RW, Wissink M. Experimental study of biogas combustion in a HCCI engine for power generation with high indicated efficiency and ultra-low NO_x emissions. Energy Conversion and Management 2012; 53:154-162.

[242] Alla GHA, Soliman HA, Badr OA, Rabbo MFA. Effect of injection timing on the performance of a dual fuel engine. Energy Conversion and Management 2002; 43:269-277.

[243] Tonkunya N, Wongwuttanasatian T. Utilization of biogas-diesel mixture as fuel in a fertilizer pelletising machine for reduction of greenhouse gas emission in small farms. Energy for Sustainable Development 2013; 17:240-244.

[244] Patterson J, Clarke A, Chen R. Experimental study of the performance and emissions characteristics of a small diesel Genset operating in dual-fuel mode with three different primary fuels. SAE Paper 2006-01-0050; 2006.

[245] Selim MYE. Sensitivity of dual fuel engine combustion and knocking limits to gaseous fuel composition. Energy Conversion and Management 2004; 45:411-425.

[246] Sayin C, Canakci M, Effects of injection timing on the engine performance and exhaust emissions of a dual-fuel diesel engine, Energy Conversion and Management 2009; 50:203-213.

[247] Bora BJ, Saha UK. Improving the Performance of a Biogas Powered Dual Fuel Diesel Engine Using Emulsified Rice Bran Biodiesel as Pilot Fuel Through Adjustment of Compression Ratio and Injection Timing. ASME J Eng Gas Turb Power 2015; 137:1-14.

[248] Geo VE, Nagarajan G, Nagalingam B. Studies on improving the performance of rubber seed oil fuel for diesel engine with DEE port injection. Fuel 2010; 89:3559-3567.

[289] Hansdah D, Murugan S. Bioethanol fumigation in a DI diesel engine. Fuel 2014; 130:324-333.

[250] Imtenan S, Masjuki HH, Varman M, Fattah IMR, Sajjad H, Arbab MI. Effect of n-butanol and diethyl ether as oxygenated additives on combustion-emission-performance characteristics of a multiple cylinder diesel engine fuelled with diesel-jatropha biodiesel blend. Energy Conversion and Management 2015; 94:84-94.

[251] Hariharan S, Murugan S, Nagarajan G. Effect of diethyl ether on Tyre pyrolysis oil fueled diesel engine. Fuel 2013; 104:109-115.

[252] Sudheesh K, Mallikarjuna JM. Diethyl ether as an ignition improver for biogas homogeneous charge compression ignition (HCCI) operation-An experimental investigation. Energy 2010; 35:3614-3622.

[253] Swaminathan C, Sarangan J. Performance and exhaust emission characteristics of a CI engine fueled with biodiesel (fish oil) with DEE as additive. Biomass and Bioenergy 2012; 39:168-174.

[254] Qi DH, Chen H, Geng LM, Bian YZ. Effect of diethyl ether and ethanol additives on the combustion and emission characteristics of biodiesel-diesel blended fuel engine. Renewable Energy 2011; 36:1252-1258.

[255] Sivalakshmi S, Balusamy T. Effect of biodiesel and its blends with diethyl ether on the combustion, performance and emissions from a diesel engine. Fuel 2013; 106:106-110.

[256] Tangoz S, Akansu SO, Kahraman N, Malkoc Y. Effects of compression ratio on performance and emissions of a modified diesel engine fueled by HCNG. International Journal of Hydrogen Energy 2015; 40:15374-15380.

[257] Ibrahim MM, Narasimhan JV, Ramesh A. Comparison of the predominantly premixed charge compression ignition and the dual fuel modes of operation with biogas and diesel as fuels. Energy 2015; 89:990-1000.

[258] Bora BJ, Saha UK. Optimisation of injection timing and compression ratio of a raw biogas powered dual fuel diesel engine. Applied Thermal Engineering 2016; 92:111-121.

[259] Guerry ES, Raihan MS, Srinivasan KK, Krishnan SR, Sohail A. Injection timing effects on partially premixed diesel-methane dual fuel low temperature combustion. Applied Energy 2016; 162:99-113.

[260] Chintala V, Subramanian KA. Experimental investigations on effect of different compression ratios on enhancement of maximum hydrogen energy share in a compression ignition engine under dual-fuel mode. Energy 2015; 87:448-462.

[261] Sayin C, Gumus M. Impact of compression ratio and injection parameters on the performance and emissions of a DI diesel engine fueled with biodiesel-blended diesel fuel. Applied Thermal Engineering 2011; 31:3182-3188.

[262] Gopal KN, Raj RTK. Effect of pongamia oil methyl ester-diesel blend on lubricating oil degradation of di compression ignition engine. Fuel 2016; 165:105-114.

[263] Dhar A, Agarwal AK. Experimental investigations of effect of Karanja biodiesel on tribological properties of lubricating oil in a compression ignition engine. Fuel 2014; 130;112-119.

[264] Lin YC, Lee WJ, Wu TS, Wang CT. Comparison of PAH and regulated harmful matter emissions from biodiesel blends and paraffinic fuel blends on engine accumulated mileage test. Fuel 2006; 85:2516-2523.

[265] Stanislav P, Marta S, Marko K, Breda K. Biodiesel influence on tribology characteristics of a diesel engine. Fuel 2009; 88:970-979.

[266] Agarwal AK. Experimental investigations of the effect of biodiesel utilization on lubricating oil tribology in diesel engine. Proceedings of the Institution of Mechanical Engineers, Part D: Journal of Automobile Engineering 2005; 219:703-713.

[267] Sinha S, Agarwal AK. Experimental Investigations of the effect of biodiesel utilization on lubricating oil degradation and wear of transportation CIDI engine. ASME J Eng Gas Turbines power 2010; 132:042801-042809.

[268] Agarwal AK. Lubrication oil tribology of a biodiesel–fuelled CI engine. J Automob Eng Proc IMechE Part D 2005; 219:703-713.

LIST OF PUBLICATIONS

(i) INTERNATIONAL JOURNALS

1. Debabrata Barik, S. Murugan. Investigation on combustion performance and emission characteristics of a DI (direct injection) diesel engine fueled with biogas-diesel in dual fuel mode, **Energy** 2014; 72:760-771.

2. Debabrata Barik, S. Murugan. Simultaneous reduction of NO_x and smoke in a dual fuel DI diesel engine, **Energy Conversion and Management** 2014; 84:217-226.

3. Debabrata Barik, S. Murugan. Assessment of sustainable biogas production from de-oiled seed cake of karanja-an organic industrial waste from biodiesel industries. **Fuel** 2015; 148:25-31.

4. Debabrata Barik, S. Murugan. Effects of diethyl ether (DEE) injection on combustion performance and emission characteristics of Karanja methyl ester (KME) -biogas fueled dual fuel diesel engine. **Fuel** 2016; 164:286-296.

5. Debabrata Barik, S. Murugan. Experimental investigation on the behavior of a DI diesel engine fueled with raw biogas-diesel dual fuel at different injection timing. **Journal of the Energy Institute** 2016; 89:373-388.

6. Debabrata Barik, S. Murugan. An artificial neural network and genetic algorithm optimized model for biogas production from co-digestion of seed cake of Karanja and cattle dung. **Waste and Biomass Valorization** 2015; 6:1015-1027.

7. Debabrata Barik, S. Murugan. Effects of pilot fuel injection timing on the performance and emission characteristics of a diesel engine fueled with biogas. **International Journal of Oil, Gas and Coal Technology** 2016; 13:407-427.

8. Debabrata Barik, S. Murugan. Combustion analysis of diesel-biogas dual fuel direct injection diesel engine- the gas diesel engine. **International Journal of Ambient Energy** (2015). DOI: 10.1080/01430750.2015.1086681. (Accepted, in press).

9. Debabrata Barik, Sudhir Sah, S. Murugan. Effects of varying injection timing on performance and emission characteristics of dual fuel engine fueled with biogas, International Journal of Scientific & Engineering Research 2013; 4:97-103.

10. Debabrata Barik, Sudhir Sah, S. Murugan, "Biogas Production and Storage for Fueling Internal Combustion Engines" International Journal of Emerging Technology and Advanced Engineering 2013; 3:193-202.

11. Debabrata Barik, S. Murugan. Production and Application of Biogas as a Gaseous Fuel for Internal Combustion Engines, International Journal of Engineering Research & Technology 2013; 1:1-5.

12. Debabrata Barik, S. Murugan. Experimental investigation on the behavior of a direct injection diesel engine fueled with Karanja methyl ester-biogas dual fuel at different injection timings. Energy. (Under review).

(ii) <u>CONFERENCE PUBLICATIONS</u>

1. Debabrata Barik, Murugan Sivalingam, Investigation on Performance and Exhaust Emissions Characteristics of a DI Diesel Engine Fueled with Karanja Methyl Ester and Biogas in Dual Fuel Mode, SAE Technical Paper; Paper number: 2014-01-1311, 2014, doi:10.4271/2014-01-1311, South Korea.

2. Debabrata Barik, Murugan Sivalingam, Performance and Emission Characteristics of a Biogas Fueled DI Diesel Engine, SAE Technical Paper; Paper number: 2013-01-2507, 2013, doi:10.4271/2013-01-2507, USA Detriot.

3. Debabrata Barik, S. Murugan, Review on parameters affecting optimum biogas production, International Conference on Alternative Fuels for I.C. Engines, MNIT, Jaipur, 6-8 Feb, 2013.

4. Debabrata Barik, S. Murugan, Experimental investigation on combustion characteristics of a dual fuel direct injection diesel engine-the gas diesel engine, International conference on Environment and Energy, Jawaharlal Nehru Technological University, Hyderabad, December 15^{th}-17^{th}, 2014.

5. Debabrata Barik, Sudhir Sah, S. Murugan, Biogas Production and Storage for Fueling Internal Combustion Engines, International Conference on Energy Resources and Technologies for Sustainable Development, Bengal Engineering and Science University, Shibpur, India, Vol-3, 07-09 Feb 2013. ISSN 2250-2459.

6. Debabrata Barik, Sudhir Sah, S. Murugan, Effects of Varying Injection Timing on Performance and Emission Characteristics of Dual Fuel Engine Fueled with Biogas, International Conference on Emerging Trends in Renewable Energy, C V Raman college of engineering, Bhubaneswar, India, 27-28 December, 2013.

7. Debabrata Barik, S. Murugan, Design and development of floating type biogas digester for power generation, International Conference on Advancement of Engineering, Mount Abu, India, Vol-1, 08-09 August 2012. ISSN 2278-2540.

8. Susmita Samal, Debabrata Barik, Sudhir Sah, Intelligent Management of Distribution Management System in Automation Industries, International Conference on Innovation in Design, Manufacturing and Concurrent Engineering, National Institute of Technology, Rourkela, India, 1-10;1-3 March 2014.

9. Kosish Gaihre, Debabrata Barik, S. Murugan. Production and utilization of biogas for automotive application. National Conference on automotive engineering, Karpakam College of engineering, Coimbatore, 7th September. 2012.

BIODATA

DEBABRATA BARIK

E-mail: debabrata93@gmail.com
Mobile: +91-8895197745

PERSONAL DETAILS

Date of birth: 15/04/1986
Fathers Name: Charchil Kumar Barik
Mothers Name: Urmila Barik
Permanent address: Karanjapada, Khuntapal, Morada,
Mayurbhanj - 757020, Odisha, India.

EXPERIENCE

- Worked as Assistant Professor in Ajay Binay Institute of Technology, Cuttack, Odisha, Affiliated to Biju Patnaik University of Technology, Rourkela from 13th August 2008 to 31st December 2011.

- Worked as Assistant Professor in Dhaneswar Rath Institute of Engineering and Management Studies, Cuttack, Odisha, Affiliated to Biju Patnaik University of Technology, Rourkela from 01 January 2016 to 30 September 2016.

- Working as Associate Professor in Karpagam University, Coimbatore, Tamil Nadu from 5th October 2016 to still date.

EDUCATIONAL QUALIFICATION

- Completed B. Tech. (Mechanical Engineering) degree with First Class from Biju Patnaik University of Technology, Rourkela in the year 2008.

- Completed M. Tech. (Thermal Engineering) degree with First Class from Siksha O Anusandhan University, Bhubaneswar in the year 2011.